ABSTRACT

LOU, XINHUI. Atom Transfer Radical Polymerization (ATRP) in Amplification-by-Polymerization for DNA Sensing. (Under the direction of Lin He.)

DNA sensing has attracted a lot of attention due to its importance in biological and medical fields. Numerous methods have been developed to amplify DNA hybridization signals to meet different needs. The purpose of this research was to develop a simple yet efficient method to detect sequence specific DNA in a home testing kit format according to the concept of amplification-by-polymerization.

This dissertation reports the development of an atom transfer radical polymerization (ATRP)-based DNA detection method. The background knowledge on current DNA sensing methods and the applications of polymers in DNA sensing technologies are described in Chapter 1. Chapter 2 describes the proof-of-concept experiments of this DNA detection method. In this method, DNA hybridization and ligation reactions led to the attachment of ATRP initiators on gold surface where specific DNA sequences located. These initiators subsequently triggered the growth of polymer at the end of DNA molecules. Only the perfectly matched targets were distinctively observed by the naked eye due to the formation of polymer that altered the substrate opacity. The demonstrated capability to detect DNA with direct visualization laid the groundwork for the future development of detector-free testing kits in DNA sensing.

Chapter 3 describes the two strategies to further improve the sensitivity of this detection method: by formation of branched polymer through repetitive ATRP and by minimization of the background noise through optimization of the passivation layer in DNA monolayers.

Chapter 4 describes the kinetics of DNA/polymer formation using different catalyst systems. The effects of the composition and concentration of the catalysts used during DNA-accelerated ATRP reaction were evaluated. The results showed a strong correlation between polymer formation and the reaction conditions. The results also showed that the presence of DNA molecules significantly fastened the growth rates of both PHEMA and POEGMA in ATRP. This accelerating effect was suspected as a combined result of the highly charged DNA backbones and the unique chemical structure of DNA molecules.

Chapter 5 describes the two applications of this ATRP-based detector-free DNA detection method: in single nucleotide polymorphism (SNP) detection and in human gender determination.

Chapter 6 describes a colorimetric ATRP-based DNA detection method based on the increased stability of polymer coated gold nanoparticles (GNPs). In this method, hybridizations, ligation and ATRP were conducted on ssDNA labeled GNPs. GNPs remained red color or aggregated after ATRP at the presence or absence of complementary target DNA in the hybridization step, respectively. The reported method provides a generic approach for biomolecular hybrid formation on a solid surface and could open up new possibilities in the applications of DNA detection and gene delivery.

Chapter 7 describes a direct comparison between CNBr chemical ligation and T4 ligation. Much higher ligation efficiency and specificity of CNBr ligation was found compared to T4 ligation, which renders the potential applications of CNBr ligation in DNA sensing to replace enzymatic ligation.

ATOM TRANSFER RADICAL POLYMERIZATION (ATRP)
in AMPLIFICATION-by-POLYMERIZATION for DNA SENSING

by

XINHUI LOU

A dissertation submitted to the Graduate Faculty of

North Carolina State University

In partial fulfillment of the

Requirements for the degree of

Doctor of Philosophy

CHEMISTRY

Raleigh

2006

APPROVED BY:

Chair of Advisory Committee

DEDICATION

To my husband Wensheng, my parents Helin and Fenglan, my parents-in-law Zhendong and Lianhua, and my sisters and brother Zhongying, Yuwan, Zhongjv, and Wenwei,

I appreciate all of your love, encouragement, patience, and support.

BIOGRAPHY

Born: Septemper 23, 1973, Xinxiang, Henan province, China

Parents: Fenglan Guo and Helin Lou

Siblings: Yuwan Lou and Zhongying Lou

Married: September 29, 1998

Spouse: Wensheng Wang

Son: Harrison Lou Wang

Parents-in-law: Lianhua Duan and Zhendong Wang

Siblings-in-law: Wenwei Wang and Zhongjv Hao

High School: HuiXian First High School, graduated 1991

Undergraduate: Beijing University of Technology,

B.E. Inorganic Material Science, graduated 1996

Minor in Computer Science

Graduate: Beijing University of Technology,

M.S. Chemistry, graduated 1999

ACKNOWLEDGMENTS

My advisor, Professor Lin He, provided guidance, patience, and financial support during my graduate studies. North Carolina State University Department of Chemistry also provided financial support. My former advisor, Professor Binghe Wang, also provided guidance during the first one and a half year of my graduate study.

Geoffrey Okelo, Mark Eckert and Peng He also worked on the DNA sensing project. Matthew S. Lewis did AFM measurements related to that project. Dr. Simon Lappi helped with FTIR and PM-IRRAS experiments. Rafaelo Galvao and Tim L. Sit helped with PCR experiments and PAGE gel electrophoresis.

Matthew S. Lewis also gave me a lot of valuable suggestions for the dissertation preparation.

I also thank the other former and current members of the He group and the Wang group, especially Dr. Xingming Gao, Dr. Yanling Zhang, Dr. Eric Ballard, Dr. Cuiying Wang, Dr. Zhong Guo, and Nancy Finkel.

The members of my committee made suggestions and comments during my graduate studies. These faculty members are Professors Daniel L. Feldheim, Morteza G. Khaledi and Bruce Novak. The graduate school representative is Professor Aziz Amoozegar from the Department of Soil Science.

I thank Profs. Jan Genzer, Stefan Franzen, Harold Ade and Wendy Boss for the use of their ellipsometer, FT-IR, contact angle meter and thermocycler, respectively.

I am grateful to my fellow graduate students and postdocs within the department, especially the Feldheim, Franzen and Novak group. I'd like to thank Dr. Dage Liu,

Dr.Feng Lv, Yanli Liu, Selina J. Anthireya, Michael Davis, Crissy Rhodes and Li Na Loo for the helpful discussion and technical support.

Members of the support staff provided prompt assistance with regard to equipment repairs and administrative matters. These persons include Mr. Leonard Page, Mr. Eddie Barefoot, Mr. Tony Radford, Mr. Glenn Hennessee, Mr. Jeff Cable, Ms.Crissy Williams Brown, Ms. Cynthia Waltz, Ms. Brenda Burgess and Ms. Michelle Clark.

I am very fortunate to have known several close friends at NCSU. Their friendship is one of the most important parts in my life. I'd to give my special thank to my roommates Yuee Feng, Shufen Cao and my first friend in US, Lan Tu Quan. We are more like four sisters and I am the eldest one. I will always remember the precious time we spent together. I'd like to give my sincere thank to my former lab mate Haibo Li. I can't remember how many kind helps Haibo has given to me since I came to US. I also sincerely thank Yujie Lv for his considerate help. You are always ready to help other people whenever they need.

I'd like to thank is Showyi Ju. You are a successful mom with a heart filled with love, not just for your family, but also for all others. I'll always remember the thanksgiving party at your lovely house and the delicious cookie you put onto my desk.

Finally, I'd like to sincerely thank my mother-in-law, Ms. Lianhua Duan. She has been taking care of my son since he was eight month old with her love and patience. Without the support and love from her, I would not have been able to successfully finish the Ph.D. program. I will always remember the sleepless night I and my mother-in-law spent in the emergency room with my infant son when he was sick.

Best wishes to all.

TABLE OF CONTENTS

Page

LIST OF SCHEMES x

LIST OF TABLES xi

LIST OF FIGURES xii

CHAPTER 1: Introduction 1

1.1 DNA Sensing and Current Methods 1

1.1.1 Enzyme-Facilitated Signal Amplification 2
1.1.2 Highly Responsive Detection Tags in Signal Amplification 3
1.1.2.1 Radioactive Labels 3
1.1.2.2 Fluorescent Labels 3
1.1.2.3 Nanomaterial Labels 4
1.1.3 Conclusions 10

1.2 Polymeric Material in Biosensing 11
1.2.1 Polymer as Biomolecular Receptors (Molecular Imprinted Polymers) 11
1.2.2 Polymer in Electrochemical Sensing 15
1.2.3 Polymers in Fluorescent Sensing 16
1.2.4 Polymers in Chromic Sensing 21
1.2.5 Volumetric Measurements 22
1.2.6 Low Young's modulus 23
1.2.7 Mass Measurement 23

1.3 ATRP in Amplification –by-Polymerization for Detector-Free DNA Sensing 24
1.4 Atom Transfer Radical Polymerization (ATRP) 26
References 33

CHAPTER 2: Concept Proof of Atom Transfer Radical Polymerization (ATRP) in DNA Detection 38

2.1 Introduction 38
2.2 Experimental Section 40
2.2.1 Materials 40
2.2.2 Capture Probe Immobilization 40

Page

2.2.3 Synthesis of Bromoisobutyryl -N-hydroxysuccinimide (NHS) Ester 41
2.2.4 Initiator Coupling to Detection Probe (D) 42
2.2.5 Three-strand DNA Hybridization 42
2.2.6 DNA Ligation 43
2.2.7 ATRP Reaction for DNA Detection 43
2.2.8 SPR Real-Time Hybridizations and T4 Ligation....44
2.2.9 Instrumentation 45

2.3 Results and Discussion 47
2.4 Conclusions....52
References....61

CHAPTER 3 Reaction Optimization of ATRP-Based DNA Sensing....62

3.1 Introduction....62
3.1.1 Increasing the Amount of Polymer....62
3.1.2 Minimization of the Nonspecific Absorption 63

3.2 Experimental Section....65
3.2.1 Materials 65
3.2.2 DNA Sensing Using Multi-Initiator Labeled Detector Probes....66
3.2.3 DNA Sensing by Formation of Branched Polymer 69
3.2.4 Minimization of Background Noise....70
3.2.5 Instrumentation 71

3.3 Results and Discussion 72
3.3.1 ATRP-Based DNA Sensing Using Multi-Initiator Labeled Detector Probes....72
3.3.2 DNA Sensing by Formation of Branched Polymer 73
3.3.3 Reduction of Background Noise....76

3.4 Conclusions....81
References....99

CHAPTER 4 Kinetic Studies of DNA-Accelerated Atom-Transfer Radical Polymerization on a Gold Surface 100
4.1 Introduction....100
4.2 Experimental Section....102
4.2.1 Materials 102
4.2.2 Immobilization of Initiator-Coupled ssDNA on Gold....103
4.2.3 Immobilization of Initiator-Coupled Small Molecules on Gold...104

Page

4.2.4 Surface-Initiated ATRP Polymerization 105
4.2.5 Synthesis of Ethyl α-Bromoisobutylamide 106
4.2.6 Solution ATRP Polymerization 106
4.2.7 Instrumentation 107

4.3 Results and Discussion 109
4.3.1 Surface-Initiated Polymer Formation in ATRP 109
4.3.2 The Effect of Surface-Anchored DNA in ATRP Reaction 111
4.3.3 Optimization of the ATRP Reaction on Surface-Anchored DNA 116

4.4 Conclusions 118
References 130

CHAPTER 5 Applications of ATRP-Based DNA Detection In Single Nucleotide Polymorphisms (SNPs) Detection and Human Gender Determination ... 132

5.1 Introduction 132
5.1.1 Single Nucleotide Polymorphisms (SNPs) Detection 132
5.1.2 Human Gender Determination 134

5.2 Experimental Section 135
5.2.1 Materials 135
5.2.2 Single Nucleotide Polymorphisms (SNPs) Detection 136
5.2.3 Human Gender Determination 138

5.3 Results and Discussion 144
5.3.1 Single Nucleotide Polymorphisms (SNPs) Detection 144
5.3.2 Human Gender Determination 146

5.4 Conclusions 149
References 164

CHAPTER 6 Ultrasensitive DNA Detection Using Polymer-Coated Core-shell Nanoparticles 165

6.1 Introduction 165
6.2 Experimental Section 167
6.2.1 Materials 167
6.2.2 Preparation of Au Nanoparticle Conjugates Prior to ATRP Reactions 168
6.2.3 Au Nanoparticle Conjugates during ATRP Reactions 171

Page

6.2.4 Instrumentation 171

6.3 Results and Discussion 174
6.3.1 Polymer Growth on DNA-coated Nanoparticles 174
6.3.2 Polymer-DNA-Coated GNPs in DNA Detection 178

6.4 Conclusions....182
References....198

CHAPTER 7 Comparison Between CNBr Chemial Ligation And T4 Enzymic Ligation 199

7.1 Introduction....199
7.2 Experimental Section....203
7.2.1 Materials 203
7.2.2 Initiator Coupling to Detection Probe (D) 204
7.2.3 T4 DNA Ligation....205
7.2.4 CNBr Chemical Ligation 205
7.2.5 Gel Electrophoresis Analysis of Ligation Products 205
7.2.6 MALDI-TOF Mass Spectrometer Analysis of Ligation Products....206

7.3 Results and Discussion 207
7.3.1 Optimization of T4 ligation 207
7.3.2 Optimization of CNBr Chemical Ligation....211

7.4 Conclusions....215
References....230

LIST OF SCHEMES

Page

Scheme 1.1 Schematic Drawing of ATRP-Assisted DNA Detection.....30
Scheme 1.2 The General Mechanism of ATRP.....31
Scheme 2.1 Chemical Formation of PHEMA in DNA Detection 54
Scheme 3.1 Schematic Drawing of Initiator labeled GNP-Based DNA Detection 83
Scheme 3.2 Chemical Formation of PHEMA in DNA Detection 84
Scheme 4.1 Model Molecules in the Study of Polymer Growth in ATRP.....120
Scheme 4.2 PHEMA and POEGMA Formation in ATRP 121
Scheme 6.1 Colorimetric DNA Sensing Using Core-Shell Particles Formed in ATRP 184
Scheme 6.2 PHEMA and POEGMA Formation in ATRP 185
Scheme 7.1 T4 Ligation Mechanism 217
Scheme 7.2 CNBr Ligation Mechanism 218

LIST OF TABLES

Page

Table 1.1 Detection Limits of Current Hybridization Based DNA Detection Assays-Methods Using Highly Responsive Non-enzyme Detection Tags.....32

Table 2.1 Summary of the DNA Sequences Used in This Chapter.....55

Table 2.2 Ellipsometric and Contact Angle Measurements of PHEMA Formation in ATRP-Assisted DNA Detection.....56

Table 3.1 Summary of the DNA Sequences Used in This Chapter.....85

Table 5.1 DNA Sequences Used in SNPs Detection.....151

Table 5.2 Primers and Probes for Human Gender Determination Assay.....152

Table 5.3 Ellipsometric and Contact Angle Measurements in SNPs by ATRP-Assisted DNA Detection.....153

Table 5.4 Optimization of PCR Using TaqDNA Polymerase.....154

Table 5.5 SPR Intensity Changes From Hybridization.....155

Table 6.1 Summary of the DNA Sequences Used.....186

Table 6.2 NaCl Titration of Citrate-capped GNP(13nm).....187

Table 6.3 NaCl Titration of BSPP-capped GNP(13nm).....188

Table 7.1 Oligonucleotides Used in This Report.....219

Table 7.2 The Effect of DTT Concentrations on Ligation Efficiency.....220

LIST OF FIGURES

Page

Figure 2.1 The PM-IRRAS spectra of (a) capture-DNA probes on the Au surface; (b) initiator-coupled DNA duplex on the surface after hybridization; and (c) a reflectance FT-IR spectrum of the formation of PHEMA atop DNA molecules on the surface 57

Figure 2.2 MALDI spectra of detection probe D (a) before and (b) after the coupling of the ATRP initiator (ΔMW=149).....58

Figure 2.3 (Top)Real-time SPR monitoring of DNA hybridizations and T4 ligation (Bottom) SPR images before (left) and after (right) hybridization and ligation 59

Figure 2.4 A photograph of 0.1μM target DNA C'D' detected after the ATRP Reaction 60

Figure 3.1 Photo after 5hr ATRP amplification of (A)10nM target DNA using multiple initiator-labeled detector probes and (B) 1μM target DNA using single initiator-labeled detector probes.....86

Figure 3.2 The increased visibility of films: A) ssDNA (1.6nm); B) PHEMA (16nm); C)PHEMA after acetylation; D) Branched PHEMA 87

Figure 3.3 Reflective FTIR spectra of (a) a DNA and MCH mixed monolayer after DNA ligation, (b) a grafted PHEMA layer (7nm), (c) an opaque PHEMA layer after 2nd ATRP, and (d) opaque PHEMA film derivatized with Bromoisobutyryl bromide.....88

Figure 3.4 Representative AFM 2D images of (A) PHEMA layer (1μm x 1μm) and (B)branched-PHEMA layer (30μm x 30μm) prepared by ATRP 89

Figure 3.5 (A) The concept of a two-stage ATRP reaction to form branched polymers and (B) A photograph of 1nM target DNA C'D' detected after the two-stage ATRP reaction.....90

Figure 3.6 AFM images of PHEMA films grown on DNA-coated Au substrates (A) after a 5hr ATRP reaction and (B) after two 30min ATRP reaction.....91

Figure 3.7 (Top) OEG7 monolayers preparation on SPR substrates and (bottom) SPR sensorgrams of BSA (1mg/mL) absorbed onto bare gold surface (blue lines) and OEG7-SAMs prepared from 1mM OEG7 aqueous solution for different incubation time 92

Page

Figure 3.8 The percentage amount of BSA absorbed onto the surface as a function of incubation time in 1mM OEG7 aqueous solution.....93

Figure 3.9 SPR sensorgrams of BSA (1mg/mL) absorbed onto (a) MCH monolayer and OEG7-SAMs prepared from different solvents: (b) H_2O, (c) 95% ethanol, and (d) THF.....94

Figure 3.10 SPR sensorgrams of lysozyme (1mg/mL), 50%HEMA and 15%PEG 8000 absorbed onto OEG7-SAMs prepared from THF.....95

Figure 3.11 Ellipsometric measurements of different SAMs for comparison of their abilities of nonspecific absorption resistance 96

Figure 3.12 Reflectance FTIR spectra of OEG7, from 900 to 1400 cm^{-1}, at different times: 2h (black lines) and 1day (red lines).....97

Figure 3.13 Kinetics of hybridization on (A)ssDNA /MCH and (B) ssDNA /OEG7 mixed monolayer 98

Figure 4.1 The H^1(Top) and C^{13}(Bottom) NMR spectra of $[Br(CH_3)_2CCO]_2O$ (carboxylic anhydride) formed using the old synthetic route 122

Figure 4.2 (A) Chemical pathway to prepare initiator-coupled ssDNA molecules to be used as the model molecule in the study; (B) MALDI spectra of (a)ssDNA, (b) initiator-coupled ssDNA, and (c) initiator-coupled ssDNA after DTT reduction 123

Figure 4.3 (Top) The PM-IRRAS spectra of (a) initiator-coupled ssDNA on the Au surface and (b) the formation of POEGMA atop DNA molecules on the surface. (Bottom) The PM-IRRAS spectra of initiator-coupled ssDNA on the Au surface and (b) a reflectance FT-IR spectrum of the formation of PHEMA atop DNA molecules on the surface 124

Figure 4.4 (A) Plots of PHEMA film thicknesses as a function of polymerization time from **4**-coated substrates at full coverage (■), **1**-coated substrates (●), and **4**-coated substrates but at the same initiator density as for **1**-coated substrates (▲). (B) Enlarged view of panel A to illustrate the detail of polymer growth from the substrates of lower initiators densities.....125

Figure 4.5 Plots of POEGMA film thicknesses as a function of polymerization time from **1**-coated substrates (■) and **4/6**-coated substrates at the same initiator density as for the **1**-coated surface(●).....126

Page

Figure 4.6 Plots of PHEMA film thicknesses as a function of polymerization time from **1**-coated substrates using different halide catalyst systems 127

Figure 4.7 (A) Plots of PHEMA film thicknesses on ssDNA-coated surfaces as a function of polymerization time using 5 mM (●) and 69 mM (■) of CuCl/30%$CuBr_2$ as the catalyst mixture. (B) Plots of PHEMA thicknesses as a function of CuCl concentration in a 5-h reaction 128

Figure 4.8 A photograph showing two substrates in which PHEMA was formed atop ssDNA molecules using (A) CuBr/bpy = 1:2.2 and [CuBr] = 69mM and (B) CuCl/$CuBr_2$/bpy = 1:0.3:2.9 and [CuCl] = 23mM.....129

Figure 5.1 A) Sequence alignment of a portion of the homologous region of the human sex chromosomes. B) Probe design of gender determination. C) Gender determination assay 156

Figure 5.2 Photos of ATRP-assisted DNA amplification in DNA point mutation detection 157

Figure 5.3 Hybridization and salt stringency wash for C'D' complementary DNA and C1'D' one mismatched DNA on the same surface 158

Figure 5.4 Photos of ATRP-assisted DNA amplification in DNA point mutation detection 159

Figure 5.5 15% denatured PAGE gel image of PCR amplification of human genomic DNA 160

Figure 5.6 15% non-denatured PAGE gel image of hybrid PCR amplification of human genomic DNA and ssDNA preparation by exonuclease reaction after PCR amplification 161

Figure 5.7 MALDI spectra of detection probe **D** (**a**) before and (**b**) after the coupling of the ATRP initiator (ΔMW=148.6).....162

Figure 5.8 Photos of ATRP-assisted DNA amplification in human gender determination 163

Figure 6.1 *Polymer-coated particle characterization:* UV-Vis spectra of (a) citrate-coated 13nm Au nanoparticles (520nm), (b) BSPP-coated Au nanoparticles(523nm), (c) DNA (Nano-A-IN)-coated Au nanoparticles (523nm), (d) PHEMA-DNA-coated Au nanoparticles after 1.5hr ATRP

(535nm) and (e) DNA (Nano-A)-coated Au nanoparticles after 1.5hr ATRP (551nm).....189

Figure 6.2 *TEM images of Gold particle conjugates:* (A) citrate-coated Au nanoparticles, (B) BSPP-coated Au nanoparticles, (C) DNA-coated Au nanoparticles, (D) and (E) DNA-coated Au nanoparticles after a 1.5hr ATRP reaction using HEMA as the monomers, and (F) DNA-coated Au nanoparticles after 7hr ATRP reaction using OEGMA as the monomers....190

Figure 6.3 *Au particle conjugates characterization:* Nondenaturing 1% agarose gel of gold nanoparticles: (a) and (g) citrate-coated Au nanoparticles (13 nm), (b) and (h) BSPP-coated Au nanoparticles, (c) DNA (Nano-B)-coated Au nanoparticles, (d) DNA duplex (Nano-B-B'D'-D-IN)-coated Au nanoparticles, (e) DNA (Nano-B)-coated Au nanoparticles after mixing with non-B'D' and D-IN, followed by ligation, (f) DNA duplex (Nano-B-B'D'-D-IN)-coated Au nanoparticles after 1hr ATRP, (i) DNA (Nano-A-IN)-coated Au nanoparticles and (j) DNA (Nano-A-IN)-coated Au nanoparticles after 3hr ATRP 191

Figure 6.4 (A) Chemical pathway to prepare initiator-coupled ssDNA(Nano-A-IN) molecules to be used as the model molecule in the study; (B) MALDI spectra of (a) Nano-A, (b) initiator-coupled Nano-A, and (c) initiator-coupled Nano-A after DTT reduction 192

Figure 6.5 UV-vis spectra and photo images of DNA conjugates (Nano-A red line and Nano-A-IN black line) immediately after 1.5hr ATRP when (A) OEGMA and (B) HEMA used as monomers, and (C) overnight after 1.5hr ATRP when HEMA used as monomers.....193

Figure 6.6 Light scattering measurements of DNA (Nano-A-IN) GNP conjugates (A) before and (B) after 1.5hr ATRP.....194

Figure 6.7 *Concept-proof in DNA sensing* (Top) UV-vis spectra of Au nanoparticles in the detection of 1 μM complementary DNA (B'D') and the detection of 1 μM non-complementary DNA (Non-B'D') in the control experiment (b) after an 1.5-hr ATRP reaction using OEGMA as the monomers. (Bottom) The corresponding photo image of Au nanoparticle solution for the detection of 1 μM complementary DNA (B'D') (a) and the control experiment (b).....195

Figure 6.8 *Concept-proof in DNA sensing:* (Top)The photo image of the Au nanoparticle solutions for the detection of complementary DNA (0-1μM)

after 1.5hr ATRP reaction using OEGMA as the monomers. (Bottom) AFM height measurements of Au particles.....196

Figure 6.9 *DNA detection of increasing ATRP times* (Top) UV-vis spectra of Au nanoparticles in ATRP after a 1.5hr (a) and a 12hr (b) ATRP reaction using HEMA as the monomers. (Bottom) The photo image of the Au nanoparticle solutions for the detection of complementary DNA (0-1nM) after 2hr ATRP.....197

Figure 7.1 MALDI-TOF mass spectrum of T4 ligation product 221

Figure 7.2 Effect of NaCl on T4 ligation efficiency.....222

Figure 7.3 Effect of template length on T4 ligation efficiency.....223

Figure 7.4 Effect of the amount of T4 ligase on T4 ligation efficiency 224

Figure 7.5 CNBr chemical ligation at 0°C and 25°C.....225

Figure 7.6 CNBr chemical ligation at different $MgCl_2$ concentrations 226

Figure 7.7 CNBr chemical ligation at different buffer pH.....227

Figure 7.8 CNBr chemical ligation at the presence of templates with different length.....228

Figure 7.9 CNBr chemical ligation at different types of nicks.....229

.

CHAPTER 1 Introduction

1.1 DNA Sensing and Current Methods

DNA sequences are unique to all biological units such as bacterium, virus, and pathogen. Sequence specific DNA sensing techniques are key tools in many fields including biological evolution research,[1] pharmacology,[2] and disease diagnosis.

Hybridization based DNA detection methods have been conveniently used in sequence-specific DNA detection, which is critical to the diagnosis of genetic and pathogenic diseases. This strategy involves annealing a labeled unknown DNA fragment to a sequence-specific oligonucleotide probe pre-immobilized on a solid surface and deciphering the unknown sequence from the hybridization pattern.

Polymerase chain reaction (PCR) coupled with molecular fluorophore assays has been the dominant method in sequence specific DNA sensing field.[3, 4] PCR technology provides unlimited amplification of interested DNA sequences and ultimate detection sensitivity.[5] However, the complexity, sensitivity to contamination, and high cost of PCR along with the need of sophisticated fluorescence microscopy/scanners hamper the applications in point-of-care settings. There is a need for methodologies that can rapidly, simply, and accurately determine specific sequences of DNA at low cost in a simple fashion.

A large variety of different techniques have been developed for DNA analysis with the aim to simplify detection methods and lower detection limits. Two general approaches have been widely adapted to improve the detection sensitivity and fidelity of DNA mutation detection and are explained in more detail below.

1.1.1 Enzyme-Facilitated Signal Amplification

The first set of existing methods utilizes sequence-specific enzymatic reactions, such as cleavage, ligation, and replication, to recognize allele-specific sequences and amplify the recognition events, or uses enzyme as labels to amplify hybridization signals.[6] A prominent example is the use of Rolling Circle Amplification (RCA) in which a short DNA primer is attached at the end of a detection probe.[7, 8] Upon DNA hybridization, that brings the detection probe close to the surface, an excess amount of DNA repeating units was generated by replication for detection. Coupled with an invader technique, as few as 1,000 DNA molecules in the biological matrix have been successfully detected.[9, 10] Another example is taking advantage of enzyme-specific RNA digestion upon the formation of RNA-DNA heteroduplexes.[11] Specifically, surface immobilized RNA probes are efficiently removed by enzyme RNase H. after DNA hybridization that forms RNA-DNA duplexes. The then-released DNA binds to the next available RNA probe until there is a complete consumption of particular RNA probes on the surface. A detection limit of 1fM has been achieved, corresponding to a remarkable 10^6 enhancement to conventional detection sensitivity. A highly sensitive amperometric DNA detection method with a detection limit down to 5zmol was developed by Heller's group by coupling a horseradish-peroxidase onto the target and using an electron-conducting redox polymer.[6]

1.1.2 Highly Responsive Detection Tags in Signal Amplification

The other set of approaches to improve DNA detection employs highly responsive non-enzyme detection tags to amplify transducer signals. Radioactive labels, fluorescent labels and all kinds of nanomaterial labels have been widely used in DNA detection assays and are described in detail below.

1.1.2.1 Radioactive Labels

Radioactive ^{32}P or ^{35}S labels in polynucleotide detection offer exquisite sensitivity and are commonly used to follow hybridization.[12-15] However, radioactive probes create disposal problems, require specially trained personnel, and have a short shelf life. Increasingly, radioactive atoms are being replaced by non-radioactive reporter groups, which are detected by their colors, fluorescence, or luminescence.

1.1.2.2 Fluorescent Labels

Fluorescent detection method eliminates many of the problems associated with radiochemical labeling methods. There are many fluorescent compounds with different characteristic excitation and emission spectra commercially available for use in fluorescent labeling. Fluorescent labels can be easily coupled onto modified oligonucleotides by reacting with amines, sulfhydryls, aldehyde/ketones, cytidine and other functional groups. The detection limits of molecular fluorophore-based DNA assays are typically in the picomolar range,[16] with best reported value of 600fM.[17] The matured commercial instruments and detectors, such as fluorescence plate scanners and DNA

microarray readers, also fulfill the need of high throughput and automation in genotyping and gene expression studies. Indeed, fluorescent labels have become the most widely used labels in DNA detection.

However, low fluorescent intensities, non-uniform fluorophore photo-bleaching rates and overlapping spectral features lead to several potential complications when multiple fluorescent labels are needed.

1.1.2.3 Nanomaterial Labels

1.1.2.3.1 Gold Nanoparticles Labels

With the advances in nanotechnology, many nanomaterials including nanoparticles, nanowires, nanotubes and quantum dots have been utilized as detection tags to enhance the signal transduction in DNA sensing due to their unique optical and electrical properties. Among those nanomaterials, gold nanoparticles have been first reported in the application of signal amplification in DNA sensing by Chad Mirkin's group.[18, 19] In this pioneer method, two different sets of target capture ssDNA-13nm gold nanoparticle hybrids were prepared. They all had sequence complementary to the target DNA. Hybridization with the target resulted in the formation of a polymeric network of nanoparticles and the solution color changed from red to purple. The color change is due to the red shift in the surface plasmon resonance of the gold nanoparticles. Exhibiting a very narrow transition temperature range, this method is highly sensitive to differentiate single base mismatch detection. In addition, this method is very fast, easy and there is no

need of any instrument for signal read-out. The major limitation of this approach is its high detection of limit, which is in 1-10nM range.

The detection limit has been further improved to 50pM using larger nanoparticles (50nm) in the consecutive reports by the same group.[14] With silver amplification the detection limits have been dramatically improved to 50fM for ssDNA and 100aM for PCR products.[20] Specifically, thiol modified capture oligonucleotides were immobilized to the surface of float glass microscope slides. Then nanoparticle labeled probes and synthetic oligonucleotide target were cohybridized to the probe on the surface (three-component system). The reduction of silver onto the gold nanoparticle surfaces amplified the hybridization signal by a factor of 10^5. The detection limit of this scanometric approach was further pushed down to 500zM (10strands in solution) by coupling bio-bar-code amplification (BCA) strategy into the detection process.[14] There are two components in this assay: target capture probe functionalized magnetic micropaticles and gold nanopaticles coated with another target capture strands and bar-code capture DNA, which hybridized to bar-code DNA. At the presence of target DNA, the magnetic microparticle, the target DNA and the gold nanoparticles form a complex that can be isolated from the solution magnetically and washed with water to collect the dehybridized bar-code DNA. The bar-code DNAs are then detected by the scanometric approach. This ultrasensitive detection method allows the fast detection of genomic DNA without PCR.[21] In addition, a new type of probes consisting of 13nm gold nanoparticles functionalized with Raman dye-labeled oligonucleotide were introduced into the detection system and allowed the multiplexed detection of analytes.[15]

While Mirkin *et al* are at the frontier of gold nanoparticles facilitated DNA sensing, others groups have also demonstrated some interesting gold nanoparticle based sensing methods. One major group of these methods is based on the stability of gold nanoparticles under different conditions similarly to the colorimetric method developed by Mirkin. Those methods typically have high detection limits (10-500nM).[22-24] A more detail review of those stability based sensing methods is described in Chapter 5. Gold nanoparticles were also coupled with some well developed DNA assays to significantly improve the assay sensitivity. For example, gold nanoparticle labled detector probes were used in surface plasmon resonance (SPR) to detect the target DNA hybridization in a sandwich format. The typical SPR detection limit is around 150nM. By using gold nanoparticles, the detection limit was improved approximately 1000-fold to 10pM.[25] Gold nanoparticle labeled target probes are also used to replace conventional fluorescent markers to enhance the DNA detection sensitivity of the quartz crystal microbalance (QCM). Using this method 1fM detection limit can be achieved.[26]

Another prominent example is the application of gold nanoparticles in molecular beacon DNA assay. In the typical molecular beacon DNA assay, the hairpin-shaped molecular beacon probe has a fluorophore and non-fluorescent quencher pair attached to each end and the middle part sequence complementary to a specific target. In the absence of the target, the fluorophore is held close to the quencher and fluorescence doesn't occur. Only when the probe binds to its target, the greater stability of the probe-target helix forces the stem to unwind, resulting in a fluorescence output. One drawback of traditional molecular beacons is the low quenching efficiency of the molecular

quencher.[27] The replacement of molecular quencher by gold nanoparticles provides much better sensitivity since gold nanopartilces can quench fluorescence more than 100 times better than the molecular quencher when the emission wavelength is close to the absorption wavelength of gold nanoparticles- 520nm. Dubertret, *et al* took advantage of this property and developed a hybrid material for single-mismatch DNA detection. This hybrid is composed of a single- stranded DNA with hairpin structure, a 1.4nm gold nanoparticle at one end and a fluorophore at other end. The fluorescence is highly quenched by the nanoparticle through a distance dependent process. Upon hybridization the fluorescence of this hybrid molecule increased by a factor of 10^3.[27] Besides the improved sensitivity, molecular beacon structure also improves the specificity of the recognition of DNA targets from the formation of thermodynamically more favorable conformation upon target binding. Based on the similar concept, Nie *et al* also developed a molecular beacon DNA assay using gold nanoparticles as quenchers.[12] Unlike conventional molecular beacons with a stem-and-loop structure, the nanoparticle probes in their method do not require a stem.

Like other nanoparticles,[28] gold nanopraticles have unique light-scattering properties. Taking advantage of this property, Yguerabide *et al* first demonstrated the application of resonance light-scattering (RLS) gold particles to replace molecular fluorophores in typical cDNA microarray.[29-31] In their method, anti-biotin-labeled RLS gold particles bind to the biotinylated probe DNA on the specific regions of the cDNA microarrays and signal the presence specific probe DNA sequences. They reported that the light scattering power of a single 80nm gold nanopartilce was 10^6 times stronger than

that of conventional fluorophores. Using this method they detected about 300 times more genes than Cy3, a commonly used molecular fluorophore at the low probe DNA concentrations.[29] In addition, RLS particles are quench resistant. The shortcoming of this method is the difficulty in calibration due to the light scattering sensitivity of nanoparticles to a lot of factors including particle size, shape, orientation on surface, and self-interactions. Storhoff *et al* monitored scattered light instead of reflective light from gold nanoparticles in the homogeneous colorimetric detection of DNA and significantly improved the detection limit to the zeptomole range, which is four orders of magnitude improvement of previously reported absorbance-based method.[19, 32]

1.1.2.3.2 Quantum Dots Labels

Semiconductor quantum dots are nanometer-sized particles with bright, photostable fluorescence, broad excitation spectra and narrow tunable emission bands from blue to red brought about by changing the size of the particles. Quantum dots have attracted extensive attentions for their potentical to replace conventional fluorescent markers *in vivo* biological targeting and imaging field due to their exceptional optical features.[33-39] Quantum dots also found their applications in biodetection assays. Nie and co-workers have used a mixture of CdSe/ZnS quantum dots in polymeric microbeads as detection tags for multiplexed DNA detection.[40] In their method, ssDNA probes with different sequences are uniquely labeled with polymeric microbeads containing different ratios of quantum dots. After hybridization with fluorophore labeled target DNA, single-bead spectroscopy measurements revealed the presence and sequence information of the

analyte. Theoretically, one million DNA sequences can be coded by using a combination of 10 intensity levels and 6 colors of quantum dots. Quantum dots were also successfully used in chip-based single nucleotide polymorphism DNA detection with the detection limit about 2nM.[41] Even through quantum dots labels have obvious advantages in the application of multicomplexed biological detection, the sensitivity and specificity of those detection methods need to be improved to be comparable with other detection methods. The cytotoxicity of those quantum dots is another problem that has yet to be solved.[42]

1.1.2.3.3 Other Nano-material Labels

Among nano-materials, nanowires and nanotubes have attracted a lot of attention in electrochemical-based DNA detections due to their unique electronic, chemical and mechanical properties.[43-47] In most applications, nanowires or nanotubes are used as a part of the nanosensors, such as nanoelectrodes,[45, 47] nanocircuit,[46] or nano-AFM-tips.[44] In very few examples those nano-materials are used as detection tags. Wang *et al* used alkaline phosphatase enzymes –coated nanotubes as labels in a DNA detection assay to remarkably improve the detection limit to 54aM. The assay consists of three components: (1) magnetic particle labeled probe DNA with sequence complementary to half of the target DNA, (2) alkaline phosphatase enzymes –coated nanotubes that were labeled with probe DNA with sequences complementary to the other half of the target DNA, and (3) target DNA. After hybridization between these three components, a magnetic separation is conducted to separate the three-component complexes and free magnetic particle

labeled probe DNA from the assay solution. Then an enzymatic amplification is carried out by adding the substrate of enzyme, α-naphthyl phosphate, into the mixture. Finally the product, α-naphthol is detected by a carbon nanotube-modified electrode through chronopotentiometric stripping. The low detection limit results from the high amount of enzyme labeled on the nanotubes and subsequently high amount of product of the enzymatic reaction.

Magnetic particles are not just used in DNA detection assays for product separation,[14, 48] they are also used as detection tags in solution-based assay for DNA. Perez *et al* found a unique magnetic phenomenon resulting from the self-assembly of nano-magnetic particles. Specifically, the aggregate of individual magnetic iron oxide particles can more efficiently diphase the spins of surrounding water protons and enhance spin-spin relaxation time compared to individual particles. Based on this observation, they exploited a general assay for molecular interaction detection including DNA-DNA interaction. At the presence of target DNA, DNA probe labeled iron oxide particles aggregate and the relaxation time of the surrounding water accordingly increases. Utilizing this method, Perez *et al* was able to detect DNA at the 20pM concentration.

1.1.3 Conclusions

Many methods have been developed for sensitive DNA sensing. Some of these methods have been summarized into **Table 1.1** with respect to their sensitivities. In general, all these methods depend on the unique properties of the reporter group used. While most methodologies to date have significantly improved detection sensitivity and

specificity in DNA genotyping, very few reported protocols are amenable for clinical settings. The main obstacle lies in the requirements for special laboratory skills in detection label preparation and/or for the complex instruments in signal readout. A new approach that enables sensitive detection of DNA with off-shelf chemistry in an instrument-free detection fashion is desirable for the development of any portable screening devices.

1.2 Polymeric Material in Biosensing

Polymer plays an increasingly important role in improving sensing performance. Polymer has extended its applications from enhancing specific binding, reducing nonspecific absorption, improving bio-stability of the sensing moiety or increasing probe density to direct participation in detection. Depending on the chemical or physical properties of the polymers utilized, they have been used either as the detection probes in analyte recognition or as the signal transducers to report the occurrence of such binding events.

1.2.1 Polymer as Biomolecular Receptors (Molecular Imprinted Polymers)

One attractive property of polymer is its stability. Compared to natural entities such as enzymes and antibodies, synthetic polymer has much better stability, and therefore can be stored for years without losing affinity for target analytes. In addition to its stability, synthetic polymer also has other valuable advantages such as ease of fabrication, low cost, multiple functionalities, and versatile formats available (bead/block

/thin film) following the need of applications. Taking advantage of these properties, molecularly imprinted polymers (MIPs) as synthetic receptors in sensor technology have attracted an increasing attention in the past decade. Several reviews have been published on the field of molecularly imprinting technology with different focuses.[49-51]

MIP is prepared by radical polymerization in the presence of a template molecule. The crosslink of monomers surrounding the template leads to replication of the structural information in a "lock-and key" model.[49] The release of the template leaves a cavity that is later recognizable by the template. Compared to the natural receptors, such as substrate-specific enzymes and antibodies, MIP exhibits the benefits of enhanced structural stability, improved protease digestion, and lower preparation cost. Improved assay performance in both sensitivity and selectivity has been reported for selected systems.[52]

Molecularly imprinting technology has been successfully used to detect a broad range of molecules including small molecules (carbohydrates, drug molecules, amino acids, etc), proteins, DNA and cells.[53] The choices of monomers and template molecules with different structures determine the application in biosensing devices. Piletsky and his coworkers prepared methacrylic polymers on a series of template molecules to build up a new imprinted polymer system for creating sensors selectively for nucleotides, amino acids and herbicids.[54] Chou and his coworkers synthesized a thin-film molecular imprint polymer using a pentameric protein as the template, which is a viable means of forming biosensors for the detection and quantification of relatively large proteins.[55] Particularly, Husson and his coworkers combined the use of molecular imprint technique and ATRP to

grow uniform imprint polymer films with adjustable thicknesses for the molecular recognition in biological systems.

However, to date, this method has been used primarily for the preparation of polymers that selectively bind to relatively low molecular weight molecules. The methodology of molecularly imprinting requires that the templates used have certain rigidity, which limits its dominate applications to smaller template molecules. The well-defined cavities in polymer can't be easily formed because the secondary and tertiary structures of large biomolecules such as proteins are labile and sensitive to the chemical and physical environment involved in the fabrication of molecularly imprinting polymers. Rebinding to the recognition sits in the network of polymer is also quite difficult due to the large size of these molecules.

The inherent problem for large biomolecules could be circumnavigated by several strategies. Rachkov *et al* developed the epitope approach to extend the applicability of molecular imprinting to peptides and proteins.[52] Instead of using a whole protein or antibody as the template, a short peptide that represents only part of the protein or antibody has been used as the template. It has been found that the imprinted polymer can successfully recognize both the short peptide template and large peptides which contains the same characteristic substructure as the template. The proof of concept for the application of this approach was described in their paper. A polymer was imprinted using a tertapeptide residue as the template. Oxytocin that possesses the same C-terminal part of the structure was effectively recognized by the imprinted polymer. Another very promising approach for large biomolecules-proteins is radio-frequency glow-discharge

plasma deposition (RFGD) method developed by Ratner *et al*.[56] In their method, template proteins were dropped onto hydrophilic, negatively charged mica surface and then coated by disaccharide that formed precise position fixed hydrogen bonds with imbedded proteins. In this way the surface structure information of the template proteins was transferred to the disaccharide surface. On the top of the sugar shell was a polymer layer formed by RFGD and covalently jointed with the sugar shell. After peeling off the mica substrate and removing protein, the protein imprinted nanocavities were created. Highly selective recognition for four different template proteins including I-labelled BSA, immunoglobulin G, lysozome and ribonuclease as templates has been demonstrated.

To develop MIPs –based sensors one of the most challenging tasks is how to transform binding events into measurable signals. Extensive work has been done on this subject and been reviewed.[57] All kinds of optical techniques such as fluorescence spectroscopy, UV-vis absorption spectroscopy, infrared spectroscopy, chemiluminescence, surface plasmon resonance and surface enhanced raman scattering have been reported for signal transformation in MIPs-based sensors. All those techniques can only be used for certain types of analytes and have specific requirements for MIPs or templates. Although significant improvement has been achieved, compared to natural receptors MIPs still have a lot of problems to overcome, such as heterogeneous pore size and its distribution, low mass transfer rate, low specificity and sensitivity. The applications of MIPs-based sensors are still immature and further studies and better understandings are required to bring molecular imprinting into a generic recognition technology.

1.2.2 Polymer in Electrochemical Sensing

There is a unique class of synthetic polymers known as conducting polymers. Conducting polymers have an extended π electron conjugated system, has dramatic affect on their special electrical properties such as conductivity. Those electrical properties response to the outside chemical and physical stimuli and can also be modulated by modifying the functionalities of polymer side chains or its counter ions. The major function of conducting polymer in biosensors is to enhance signal transduction speed and increase detection sensitivity and versatility. An abundance of literature has been published on the applications of conducting polymer in biosensing including DNA detection, protein detection, and all kinds of small molecules detection. Readers can find useful information from this area in several recent reviews.[58-60]

Not limited to the use as transducers conducting polymers were also used as the part of detection probes. Gibbs and Mirkin *et al* developed a new approach for preparing polymer DNA hybrids as electrochemical probes for DNA detection.[61] In their method, multiple DNA stands and electrochemical active moieties such as ferrocenyl or dibromoferrocenyl groups were attached to the backbone of polymer DNA hybrids. This polymer DNA hybrid based DNA detection method has many advantages over molecular probe systems. The redox properties of these hybrids can be tailored by varying the types and ratio of electrochemical active moieties in the hybrids. Theoretically unlimited probes with different electrochemical properties could be prepared only using a few electrochemical tags, which made this method suitable in multiplexing assays. In addition, the higher selectivity was also expected to achieve using polymer hybrids as

detection probes due to its higher melting temperatures and sharper melting profiles than oligonucleotides without polymer backbones. A proof-of-concept experiment has been reported in their paper to detect single-base mismatches using two distinct hybrids as dual-channel detection probes.

1.2.3 Polymers in Fluorescent Sensing

1.2.3.1 Fluorescence from the Fluorophores on the Side Chains of Polymers

Take advantage of unique optical properties of all kinds of novel materials, various detection methods have been developed in the last decade. The most straightforward method is direct conjugation of fluorophores onto the side chains of polymers in which the polymers behave as a dye carrier to increase detection sensitivity significantly by simultaneously accruing multiple tags in one macromolecule. Alternatively, fluorescent monomers have been directly incorporated into the polymer structure and made the polymer itself a gigantic sensing tag. Pitschke *et al* reported decades ago that the incorporation of fluorescent dyes into the monomer units increased the sensitivity of fluorescent labeling 40 fold compared to the use of monomeric dyes alone.[62] Kanekiyo *et al* synthesized several copolymers containing boronic acid and fluorescent units. Saccharide was detected by monitoring the fluorescence signal changes induced by conformational changes of polymers due to the binding with saccharides.[63]

1.2.3.2 Fluorescence from the Conjugated Polymers

In addition to directly monitoring the fluorescent moiety itself, the change in fluorescence wavelength changes or fluorescence intensity changes, can also be detected as sensing signals. Conjugated polymers are prominent examples in the fluorescence-based sensing methods because of their strong absorption (and often emission) in the UV-vis region. Absorption (and sometimes emission) wavelengths and intensities of conjugated polymers are sensitive to various factors including temperature, pressure, solvent, and additives. Those changes can be used to detect different analytes. One interesting research study conducted by Bunz *et al* was to use biotin-substitued poly(*para*phenyleneethynylene)s (PPE) as a model compound and streptavidin coated polystyrene bead as primitive cell/bacterium model to study their interactions.[64] The emission spectrum of biotin modified PPE was significantly changed when it binds to the streptavidin coated polystyrene bead surface. This simple system has the potential application for pathogen and toxins detection. Disney *et al* extended the applications of conjugated fluorescent polymer to detect real bacteria cells.[65] They coupled carbohydrate units to the polymer backbones after polymerization. The glycosides attached on the surface of polymer still retain their activity to carbohydrate-binding lectins. After incubation the polymer with *E. coli* bright fluorescent cell clusters were formed due to the multivalent interactions between the mannosylated polymer and mannose receptors located on the bacterial pili. This was the first reported application in cell detection.

1.2.3.3 Quenched or Enhanced Fluorescence from Fluorescence Resonance Energy Transfer between Conjugated Polymers and Quencher

Under most conditions, fluorescence intensity changes due to the conformation changes are within one order of magnitude and wavelength shifts are within narrow range. Spectral overlaps are quite commonly observed due to usually broad absorption and emission peaks. One method to effectively improve detection is called as the fluorescence resonance energy transfer (FRET). Compared to direct excitation, the fluorescent emission intensities of acceptor fluorescent molecules increase significantly when excitation energy is absorbed and transferred effectively from a donor which has large absorption coefficient. Due to their conjugated electron systems, conjugated polymers are very good light-harvesting materials with molar coefficient as high as 10^6 $M^{-1}cm^{-1}$. When the emission regions of conjugated polymers partially overlap the absorption regions of the acceptors, the excitation energy of polymer can effectively transfer to the nearby fluorescent acceptors along the conjugated backbone of the polymer.

All kinds of conjugated polymer based biosensors have been designed after Swager and coworker first developed a series of chemosensors based on this phenomenon.[66] Chen *et al* has found that the fluorescence of a polyanionic conjugated polymer can be quenched by extremely low concentrations of cationic electron acceptors in aqueous solutions. The corresponding quenching constant is nearly four orders of magnitude greater than that for stilbene in micelles and six orders of magnitude greater than that for dilute stilbene solutions. Their findings set the basis for a new class of

highly sensitive biological and chemical sensors.[67] Kumaraswamy *et al* developed a new strategy to detect the activity of proteolytic enzymes. A protein substrate containing proteolytic enzyme reactive sequence was coupled with a fluorescent polymer and a quencher at the two ends, resulting in a strong quenching of polymer fluorescence. The reversal of polymer fluorescence was observed when the peptide was cleaved by the protease.[68] Similar methods have been developed to detect several types of biological analytes including DNA, ions, glucose, viruses and cells.

Bazan *et al* has developed a fluorescence based DNA hybridization detection sensor.[69] Cationic water soluble conjugated polymer, poly [(9,9-bis (6'-N,N,N-trimethylammonium)-hexyl)-fluorene phenylene], and a ssDNA labeled with a dye (fluorescein) was mixed together at optimized ratio in favor of FRET. When the solution was excited at the excitation wavelength of polymer (λ_{max}=380nm), the fluorescence emission from the dye on ssDNA was 3 times more intense at the presence of complementary stand than was observed at the presence of noncomplementary ssDNA. This difference in FRET efficiency is due to a closer proximity between the polymer and the dye when more negatively charged dsDNA was formed through hybridization. Based on a similar concept, a method suitable for DNA chips has been reported by the same group by replacing the dye labeled ssDNA with neutral peptide nucleic acid (PNAs) and attached onto solid surface.[70] This method has also been used for neurodegenerative disease related single base mismatch detection.[71] Not just for DNA detection, Bazan and coworkers have also extended their methods to detect HIV viruses by using cationically

charged HIV- related tat peptide labeled with fluorescein and anionic specific TAR RNA.[72]

Taking advantage of the FRET phenomenon, Zhu *et al* developed a new homogenous detection method of potassium. In their method the FRET efficiency was enhanced by stronger electrostatic interactions between the cationic conjugated polymers and the more condensed G-quadruplexes whose formation were promoted by the presence of potassium ios.[73]

Other methods which can be utilized to enhance fluorescence detection of analyst are available and are based on specific binding interactions. One example is to use a new type of polyamide in sequence specific detection of DNA. It is well known that all kinds of cationic organic dyes such as ethidium bromide, SYBR green, and thiazole orange are widely used to visualize the presence of DNA. Those dyes usually lack of specificity and send out enhanced fluorescence when binding or intercalating onto DNAs or oligonucleotides. Dervan *et al* has found a new type of DNA minor groove-binding molecules, pyrrole imidazole polyamide that can be desigened to recognize specific DNA sequences.[74-77] The fluorescent dye, such as thiazole orange, was coupled to polyamides. The fluorescence was significantly enhanced when matched DNA was added into solution while only slight enhancement was observed when mismatched DNA was present. One advantage of this class of detection methods is no need of denaturation of DNA sequences.

1.2.4 Polymers in Chromic Sensing

Instead of monitoring fluorescent emission, visible chromic changes can also be used in detection. The UV-vis absorbance wavelength of a conjugated polymer is sensitive to its sensing environment. The fluctuation in temperature, solvent, pressure or more importantly bio-molecular binding interactions can lead to the microscopic environmental changes in polymers; subsequently a noticeable change in absorption profile of the polymer. As an example, in 1993 Charych and coworkers developed a direct colorimetric detection method of influenza virus hemagglutinin.[78]A polydiacetylene bilayer composed of a self-assembled monolayer of octadecylsilane and a Langmuir-Blodgett monolayer of polydiacetylene was assembled on glass microscope slides. An analog of sialic acid, the receptor-specific ligand for the influenza virus hemagglutinin was coupled at the end of polydiacetylene as a molecular recognition element. Upon the virus binding to the surface, the surface color changed dramatically from blue to red.

Asher *et al* developed a novel colorimetric glucose detection strategy using crystalline colloidal array embedded within a polymer network of a polyacrylamide-poly (ethylene glycol) (PEG) hydrogel, or a polyacrylamide-15-crown-5 hydrogel with pendent phenylboronic acid groups.[79] The hydrogel hybrid consists of a crystalline colloidal array embedded within the hydrogel that was pre-modified with glucose recognition agent, such as phenylboronic acid. The diffracted wavelength of crystalline colloidal array was determined by the lattice constant and could be monitored directly. The binding of glucose with the boronic acids on the hydrogel increased the hydrogel

cross-linking and contracted the volume, resulting in the decrease of lattic constant changes and subsequently the change of diffraction colors.

1.2.5 Volumetric Measurements

The volume of a hydrogel changes in response to different external stimuli such as pH, temperature, solvent composition, electrofields and more importantly biomolecules including DNA, antigen and saccharides when the hydrogel has had "receptors" prior grafted on its network. In 1999, Uragami *et al* reported an antigen responsive hydrogel that swelled when a specific antigen was present.[80] The crosslinks in the hydrogel network are formed by the interactions between the grafted antigen and corresponding antibody. When free antigen gets into this network antigen competitively binds to the antibody and the number of crosslinks in the hydrogel decreases, accordingly, the volume of hydrogel increases.

Based on the similar strategy, Maeda and Murakami developed a novel DNA responsive hydrogel that can either shrink or swell in responses to specific ssDNA samples.[81] Specifically, a ssDNA with stem-loop like a "molecular beacon" and ssDNA without intramolecular base pair are grafted onto a hydrogel framework as the crosslinking reagents. Upon hybridization of ssDNA targets to the stem-loop ssDNA or ssDNA without intramolecular base pair the overall hydrogel swells or shrinks, respectively. The method is shown to be sufficiently selective to differentiate single base mismatch.

1.2.6 Low Young's modulus

Fritz *et al* first reported the direct and specific transduction of surface stress changes induced by biomolecular interactions, such as DNA hybridization, into nano-mechanical response of microfabricated cantilevers.[82] The differential deflection of the cantilevers was found to be related to a true molecular recognition signal. Zhang and Xu used polymer microcantilevers to replace silicon cantilevers.[83] Polymers usually have lower Young's modulus than silicon and consequently offer better sensitivity of deflection measurements. They have demonstrated that as little as 0.01μM of 12 base oligonucleotides was detected successfully. Similarly, Calleja *et al* has used a novel polymer SU-8 to fabricate cantilevers and sensitivity is enhanced by a factor of six compared to that of commercial silicon nitride cantilevers.[84]

1.2.7 Mass Measurement

In addition to the volume changes, the apparent molecular weight change of polymer materials during polymerization can also be used directly in mass-sensitive biosensors. One incomparable advantage of polymer is its multiple functional groups on the side chains. Taking advantage of the high density of functional groups, polymers have been widely used in sensors to increase probe densities or itself used as probes. Wang *et al* has synthesized dentritic nucleic acid probes for DNA biosensors to significantly improve the detection sensitivity of QCM around 10 fold.[85] Polymeric nanoparticles have also been used as the detection tags in a prostate-specific antigen (PSA) assay in which the binding event was monitored by Surface Plasmon Resonance (SPR).[86]

1.3 Atom Transfer Radical Polymerization in Amplification –by-Polymerization for Detector-Free DNA Sensing

As summarized in the previous sections, polymer in a pre-formed macromolecular form has been widely used in all kinds of sensing technologies to significantly enhancing sensitivity and specificity.[69, 87, 88] However, most of those polymer-based sensing methods could not detect analyst without the help of the appropriate instruments, such as UV-vis, SPR or QCM. A sensing method that can directly detect analytes without the need of any instrument, as one of the basic requirements of home-testing-kit format detection is highly desired. In order to meet this requirement, it is necessary to significantly amplify sensing signals to make them visible to the naked eye, either by direct color change or by increasing the visibility.

The dynamic growing process of macromolecules has yet to be exploited as an amplification tool. We note that polymerization is essentially a highly efficient signal amplification process with an enhancement power controllable at will. Similar to RCA but using chemical reaction in the place of enzyme replication, connecting the same small monomers in a head-to-tail fashion forms a long polymer chain that contains hundreds to millions of repeating units. Consequently, the detection signal kept in one small monomer is amplified hundreds to millions of times through the chain propagation.

The research focus of this Ph.D. work is to develop a detector-free sequence specific DNA detection method according to the concept of amplification-by-polymerization. Taking advantage of this monomer-replicating concept, the detection of

specific DNA sequences is accomplished by the formation of polymer brushes on the surface at ambient temperature.

Chapter 2 describes the proof-of-concept experiments of this atom transfer radical polymerization (ATRP)-based DNA detection method (**Scheme 1.1**).[89] In this method, DNA hybridization and ligation reactions led to the attachment of ATRP initiators on gold surface where specific DNA sequences located. These initiators subsequently triggered the growth of polyhydroxyethylmethacrylate (PHEMA) at the end of immobilized DNA molecules and formed polymer brushes. The formation of PHEMA altered substrate opacity, rendering the corresponding spots readily distinguishable to the naked eye. The perfectly matched DNA targets were distinctively differentiated from those with single mutations. The demonstrated capability to detect DNA with direct visualization laid the groundwork for the future development of detector-free testing kits in DNA sensing. For the first time, the in-situ formed polymer was used as detection tags.

Chapter 3 describes the two strategies to further improve the sensitivity of this detection method: by formation of branched polymer through repetitive ATRP and by minimization of the background noise through optimization of the passivation layer in DNA monolayers.

Chapter 4 describes the kinetics of DNA/polymer formation using different catalyst systems. The effects of the composition and concentration of the catalysts used during DNA-accelerated ATRP reaction were evaluated. The results illustrated a strong correlation between polymer formation and the reaction conditions. The results also demonstrated that the presence of DNA molecules significantly increased the growth

rates of both PHEMA and POEGMA in ATRP. This accelerating effect was suspected as a combined result of the highly charged DNA backbones and the unique chemical structure of DNA molecules.

Chapter 5 describes the two applications of this ATRP-based detector-free DNA detection method: in single nucleotide polymorphism (SNP) detection and in human gender determination.

Chapter 6 describes a colorimetric ATRP-based DNA detection method based on the increased stability of polymer coated gold nanoparticles (GNPs). Hybridizations, ligation and ATRP were conducted on ssDNA labeled GNPs. GNPs retained their red color or aggregated after ATRP at the presence or absence of complementary target DNA in the hybridization step, respectively. The reported method provides a generic approach for biomolecular hybrid formation on a solid surface and also opens up new possibilities in the applications of DNA detection and gene delivery.

Chapter 7 describes a direct comparison between CNBr chemical ligation and T4 ligation. Much higher ligation efficiency and specificity of CNBr ligation was found compared to T4 ligation, which renders the potential applications of CNBr ligation in DNA sensing to replace enzymatic ligation.

1.4 Atom Transfer Radical Polymerization (ATRP)

The three most common methods in controlled/"living" radical polymerization are atom transfer radical polymerization (ATRP), reversible addition fragmentation chain transfer polymerization (RAFT), and nitroxide mediated polymerization (NMP). Among

these three methods, ATRP is the most popular polymerization reaction in sensing for its ease of handling and mild reaction conditions.[90,91] One example was used surface-initiated ATRP to covalently immobilize biomolecules, such as glucose oxidase, on poly(glycidylmethacrylate) (PGMA) brushes on Silicon.[92]

ATRP is a new class of controlled/"living" radical polymerization that was first reported by the groups of Sawamoto[93] and Matyjaszewski.[94, 95] ATRP employs atom transfer from an organic halide to a transition-metal complex to generate the reacting radicals, followed by back transfer from the transition metal to a product radical to form the final product (**Scheme 1.2**).[96] The deactivation rate constant being bigger than that of activation, the majority of radical initiators at any given time stays in a dormant form to allow the polymer chain's growth to be in a slow and continuous fashion.

ATRP has been a popular means to graft polymer brushes on a solid support because of the broad selection of monomers, good control over the product molecular weight and dispersity, and high tolerance of surrounding functional groups.[97-100] The demonstration of surface-initiated ATRP in aqueous media at room temperature further renders it feasible to be used as a signal amplification method in biosensing.[101-104]

An ATRP system consists of an initiator, a metal halide complexed with ligand(s), and monomers. In general, any alkyl halide with an activating subunit on the α-carbon, such as aryl, carbonyl, and allyl groups, can potentially be used as ATRP initiators. Polyhalogenated compounds (CCl_4 and $CHCl_3$) and compounds with a weak R-X bond, such as N-X, S-X, and O-X, can also presumably be used as ATRP initiators. The list of

potential ATRP initiators includes not only small molecules but also macromolecular species that can be used to synthesize block/graft copolymers.

As for metal catalysts, a complex of a copper (I) halide and 2,2'-bipyridyl is the most widely used catalyst.[104, 105] The catalyst undergoes a one-electron oxidation with concomitant abstraction of a halogen atom from a substrate. Ni,[106] Pd,[107] Ru,[108] Fe,[109]and other metals[110] have been used as well. So far, the copper-based ATRP system has been adapted successfully for the controlled/living polymerization of styrenes, acrylates, methacrylates, acrylonitrile, and other monomers. The current generation of catalyst systems is not sufficiently efficient to polymerize less reactive monomers, such as ethylene, a-olefins, vinyl chloride, and vinyl acetate, which produce non-stabilized, highly reactive radicals. Acrylic and methacrylic acid cannot be polymerized with currently available ATRP catalysts, because these monomers react rapidly with the metal complexes to form metal carboxylates which are inefficient deactivators and cannot be reduced to active ATRP catalysts.

ATRP has been carried out both in solution, neat or diluted, and on a solid surface at room temperature or higher temperature. Recently, several researches have conducted ATRP in an aqueous media at ambient temperature.[111, 112] Water plays an important role in promoting rapid ATRP at room temperature with narrow polydispersities ($M_w/M_n<1.30$) and high conversion. It also makes ATRP amenable for biomolecular copolymer formation where an aqueous reaction environment is a prerequisite for maintaining the biological function of final products.

The combination of synthetic versatility and simplicity makes ATRP a powerful technique for the design and synthesis of new polymeric materials with novel structures. ATRP can be used to polymerize and copolymerize a wide variety of monomers with accurate control over the molecular weight and molecular weight distribution of the final polymer. Many types of functional groups and polymerization additives can be tolerated. The composition, functionality, and architecture of the final polymer all can be controlled through variations in the side groups, end groups, and initiator structure.

Schemes

Scheme 1.1: Schematic Drawing of ATRP-Assisted DNA Detection.

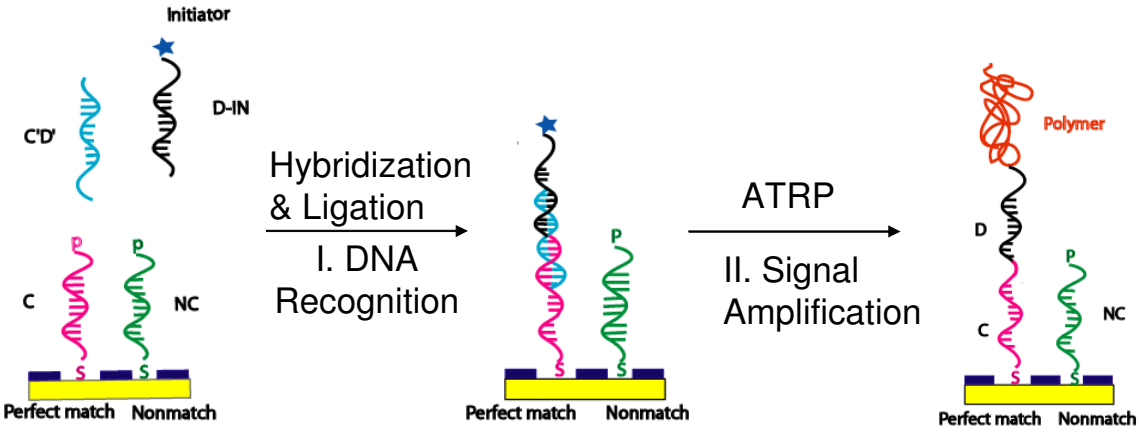

Scheme 1.2: The General Mechanism of ATRP.

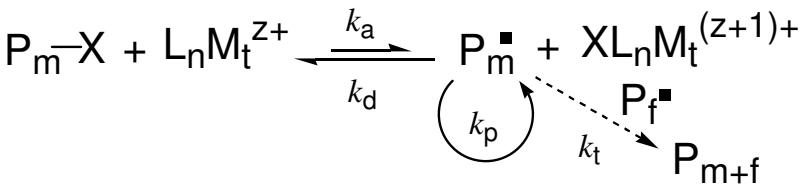

k_a activation rate constant of the initiator

k_d deactivation rate constant of the initiator

k_p chain propagation rate constant

k_t chain termination rate constant

X leaving groups in the initiator

L catalyst ligand

M transition metal

Z charge

P_m, P_f, P_{m+f} polymer

n,t,m,f,m+f the nubmers of units

Tables

Table 1.1 Detection Limits of Current Hybridization Based DNA Detection Assays-Methods Using Highly Responsive Non-enzyme Detection Tags.

Detection Assays	Reporter Group	Detection Limit	Year	Refs
Radioactive labels	^{32}P or ^{35}S	1amol	1975	[113]
Fluorescent labels	Fluorescent dyes	600fM	2001	[17]
Colorimetric detection	Gold nanoparticles	10nM	1997	[19]
Scannometric	Gold nanoparticles with Ag amplification	50fM	2000	[20]
Roman spectroscopy	Gold nanoparticles with Ag amplification	1fM	2002	[15]
Bio-bar-code	Gold nanoparticles with Ag amplification	500zM	2004	[14]
Quantum dots	ZnS/CdSe quantum dots	2nM	2003	[41]
Au-amplified SPR	Gold nanoparticles	10pM	2000	[25]
Quartz crystal microbalance	Gold nanoparticles	1fM	2001	[26]
Molecular beacon	Fluorophore	10nM	2001	[27]
ATRP-based detection	Polymer	1nM	2005	[89]

References

(1) Schmidt, P. S.; Duvernell, D. D.; Eanes, W. F. *Proc. Natl. Acad. Sci. U. S. A.* **2000**, *97*, 10861-10865.
(2) Marsh, S.; Kwok, P.; McLeod, H. L. *Hum. Mut.* **2002**, *20*, 174-179.
(3) Fang, X. H.; Tan, W. H. *Anal. Chem.* **1999**, *71*, 3101-3105.
(4) Weiss, S. *Science* **1999**, *283*, 1676-1683.
(5) Saiki, R. K.; Scharf, S.; Faloona, F.; Mullis, K. B.; Horn, G. T.; Erlich, H. A.; Arnheim, N. *Science* **1985**, *230*, 1350-1354.
(6) Caruana, D. J.; Heller, A. *J. Am. Chem. Soc* **1999**, *121*, 769-774.
(7) Qi, X.; Bakht, S.; Devos, K. M.; Gale, M. D.; Osbourn, A. *Nucleic Acids Res.* **2001**, *29*, e116/111-e116/117.
(8) Hatch, A.; Sano, T.; Misasi, J.; Smith, C. L. *Genet. Anal.* **1999**, *15*, 35-40.
(9) Lyamichev, V.; Neri, B. *Meth. Mol. Biol.* **2003**, *212*, 229-240.
(10) Achyuthan, K. E.; Bergstedt, T. S.; Chen, L.; Jones, R. M.; Kumaraswamy, S.; Kushon, S. A.; Ley, K. D.; Lu, L.; McBranch, D.; Mukundan, H.; Rininsland, F.; Shi, X.; Xia, W.; Whitten, D. G. *J. Mater. Chem.* **2005**, *15*, 2648-2656.
(11) Goodrich, T. T.; Lee, H. J.; Corn, R. M. *J. Am. Chem. Soc.* **2004**, *126*, 4086-4087.
(12) Maxwell, D. J.; Taylor, J. R.; Nie, S. *J. Am. Chem. Soc.* **2002**, *124*, 9606-9612.
(13) Wang, J.; Liu, G.; Merkoci, A. *J. Am. Chem. Soc.* **2003**, *125*, 3214-3215.
(14) Nam, J.-M.; Stoeva, S. I.; Mirkin, C. A. *J. Am. Chem. Soc.* **2004**, *126*, 5932-5933.
(15) Cao, Y. C.; Jin, R.; Mirkin, C. A. *Science* **2002**, *297*, 1536-1540.
(16) Storhoff, J. J.; Marla, S. S.; Garimella, V.; Mirkin, C. A. *Labels and Detection Methods. Microarray Technology and its Applications* **2004**, 147-174.
(17) Cao, Y. W.; Jin, R.; Mirkin, C. A. *J. Am. Chem. Soc.* **2001**, *123*, 7961-7962.
(18) Mirkin, C. A.; Letsinger, R. L.; Mucic, R. C.; Storhoff, J. J. *Nature* **1996**, *382*, 607-609.
(19) Elghanian, R.; Storhoff, J. J.; Mucic, R. C.; Letsinger, R. L.; Mirkin, C. A. *Science* **1997**, *277*, 1078-1081.
(20) Taton, T. A.; Mirkin, C. A.; Letsinger, R. L. *Science* **2000**, *289*, 1757-1760.
(21) Storhoff, J. J.; Marla, S. S.; Bao, P.; Hagenow, S.; Mehta, H.; Lucas, A.; Garimella, V.; Patno, T.; Buckingham, W.; Cork, W.; Muller, U. R. *Biosens. Bioelectron.* **2004**, *19*, 875-883.
(22) Chakrabarti, R.; Klibanov, A. M. *J. Am. Chem. Soc.* **2003**, *125*, 12531-12540.
(23) Sato, K.; Hosokawa, K.; Maeda, M. *J. Am. Chem. Soc.* **2003**, *125*, 8102-8103.
(24) Li, H. X.; Rothberg, L. *Proc. Natl. Acad. Sci. U. S. A.* **2004**, *101*, 14036-14039.
(25) He, L.; Musick, M. D.; Nicewarner, S. R.; Salinas, F. G.; Benkovic, S. J.; Natan, M. J.; Keating, C. D. *J. Am. Chem. Soc.* **2000**, *122*, 9071-9077.
(26) Weizmann, Y.; Patolsky, F.; Willner, I. *Analyst* **2001**, *126*, 1502-1504.
(27) Dubertret, B.; Calame, M.; Libchaber, A. J. *Nat. Biotechnol.* **2001**, *19*, 365-370.
(28) Stimpson, D. I.; Hoijer, J. V.; Hsieh, W. T.; Jou, C.; Gordon, J.; Theriault, T.; Gamble, R.; Baldeschwieler, J. D. *Proc. Natl. Acad. Sci. U. S. A.* **1995**, *92*, 6379-6383.

(29) Yguerabide, J.; E., Y. E. *J. Cell. Biochem. Suppl.* **2001**, *37*, 71-81.
(30) Yguerabide, J.; Yguerabide, E. E. *Anal. Biochem.* **1998**, *262*, 157-176.
(31) Yguerabide, J.; Yguerabide, E. E. *Anal. Biochem.* **1998**, *262*, 137-156.
(32) Storhoff, J. J.; Lucas, A. D.; Garimella, V.; Bao, Y. P.; Muller, U. R. *Nat. Biotechnol.* **2004**, *22*, 883-887.
(33) Gao, X. H.; Cui, Y. Y.; Levenson, R. M.; Chung, L. W. K.; Nie, S. M. *Nat. Biotechnol.* **2004**, *22*, 969-976.
(34) Dahan, M.; Levi, S.; Luccardini, C.; Rostaing, P.; Riveau, B.; Triller, A. *Science* **2003**, *302*, 442-445.
(35) Dubertret, B.; Skourides, P.; Norris, D. J.; Noireaux, V.; Brivanlou, A. H.; Libchaber, A. *Science* **2002**, *298*, 1759-1762.
(36) Chan, W. C. W.; Nie, S. M. *Science* **1998**, *281*, 2016-2018.
(37) Bruchez, M.; Moronne, M.; Gin, P.; Weiss, S.; Alivisatos, A. P. *Science* **1998**, *281*, 2013-2016.
(38) Gao, X.; Yang, L.; Petros, J. A.; Marshall, F. F.; Simons, J. W.; Nie, S. *Curr. Opin. Biotechol.* **2005**, *16*, 63-72.
(39) Chan, W. C. W.; Maxwell, D. J.; Gao, X.; Bailey, R. E.; Han, M.; Nie, S. *Curr. Opin. Biotechol.* **2002**, *13*, 40-46.
(40) Han, M. Y.; Gao, X. H.; Su, J. Z.; Nie, S. *Nat. Biotechnol.* **2001**, *19*, 631-635.
(41) Gerion, D.; Chen, F. Q.; Kannan, B.; Fu, A. H.; Parak, W. J.; Chen, D. J.; Majumdar, A.; Alivisatos, A. P. *Anal. Chem.* **2003**, *75*, 4766-4772.
(42) Derfus, A. M.; Chan, W. C. W.; Bhatia, S. N. *Nano Lett.* **2004**, *4*, 11-18.
(43) Chen, L. W.; Cheung, C. L.; Ashby, P. D.; Lieber, C. M. *Nano Lett.* **2004**, *4*, 1725-1731.
(44) Woolley, A. T.; Guillemette, C.; Cheung, C. L.; Housman, D. E.; Lieber, C. M. *Nat. Biotechnol.* **2000**, *18*, 760-763.
(45) Wang, J.; Kawde, A. N.; Musameh, M. *Analyst* **2003**, *128*, 912-916.
(46) Hahm, J.; Lieber, C. M. *Nano Lett.* **2004**, *4*, 51-54.
(47) Li, J.; Ng, H. T.; Cassell, A.; Fan, W.; Chen, H.; Ye, Q.; Koehne, J.; Han, J.; Meyyappan, M. *Nano Lett.* **2003**, *3*, 597-602.
(48) Wang, J.; Liu, G. D.; Jan, M. R. *J. Am. Chem. Soc.* **2004**, *126*, 3010-3011.
(49) Mahony, J. O.; Nolan, K.; Smyth, M. R.; Mizaikoff, B. *Anal. Chim. Acta* **2005**, *534*, 31-39.
(50) Haupt, K. *Anal. Chem.* **2003**, *75*, 376A-383A.
(51) Wulff, G. *Chem. Rev.* **2002**, *102*, 1-27.
(52) Rachkov, A.; Minoura, N. *Biochim. Biophys. Acta-Protein Struct. Molec. Enzym.* **2001**, *1544*, 255-266.
(53) Zhong, X.; Yuan, R.; Chai, Y.; Liu, Y.; Dai, J.; Tang, D. *Sens. Actuator B-Chem.* **2005**, *B104*, 191-198.
(54) Piletska, E. V.; Romero-Guerra, M.; Chianella, I.; Karim, K.; Turner, A. P. F.; Piletsky, S. A. *Anal. Chim. Acta* **2005**, *542*, 111-117.
(55) Chou, P.-C.; Rick, J.; Chou, T.-C. *Anal. Chim. Acta* **2005**, *542*, 20-25.
(56) Shi, H. Q.; Tsai, W. B.; Garrison, M. D.; Ferrari, S.; Ratner, B. D. *Nature* **1999**, *398*, 593-597.

(57) Henry, O. Y. F.; Cullen, D. C.; Piletsky, S. A. *Anal. Bioanal. Chem.* **2005**, *382*, 947-956.
(58) Adeloju, S. B.; Wallace, G. G. *Analyst* **1996**, *121*, 699-703.
(59) Ramanaviciene, A.; Ramanavicius, A. *Crit. Rev. Anal. Chem.* **2002**, *32*, 245-252.
(60) Gerard, M.; Chaubey, A.; Malhotra, B. D. *Biosens. Bioelectron.* **2002**, *17*, 345-359.
(61) Gibbs, J. M.; Park, S. J.; Anderson, D. R.; Watson, K. J.; Mirkin, C. A.; Nguyen, S. T. *J. Am. Chem. Soc.* **2005**, *127*, 1170-1178.
(62) Pitschke, M.; Fels, A.; Schmidt, B.; Heiliger, L.; Kuckert, E.; Riesner, D. *Colloid Polym. Sci.* **1995**, *273*, 740-752.
(63) Kanekiyo, Y.; Sato, H.; Tao, H. *Macromol. Rapid Commun.* **2005**, *26*, 1542-1546.
(64) Wilson, J. N.; Wang, Y.; Lavigne, J. J.; Bunz, U. H. F. *Chem. Commun.* **2003**, *14*, 1626-1627.
(65) Disney, M. D.; Zheng, J.; Swager, T. M.; Seeberger, P. H. *J. Am. Chem. Soc.* **2004**, *126*, 13343-13346.
(66) Swager, T. M. *Acc. Chem. Res* **1998**, *31*, 201-207.
(67) Chen, L. H.; McBranch, D. W.; Wang, H. L.; Helgeson, R.; Wudl, F.; Whitten, D. G. *Proc. Natl. Acad. Sci. U. S. A.* **1999**, *96*, 12287-12292.
(68) Kumaraswamy, S.; Bergstedt, T.; Shi, X.; Rininsland, F.; Kushon, S.; Xia, W.; Ley, K.; Achyuthan, K.; McBranch, D.; Whitten, D. *Proc. Natl. Acad. Sci. U. S. A.* **2004**, *101*, 7511-7515.
(69) Gaylord, B. S.; Heeger, A. J.; Bazan, G. C. *J. Am. Chem. Soc.* **2003**, *125*, 896-900.
(70) Liu, B.; Bazan, G. C. *Proc. Natl. Acad. Sci. U. S. A.* **2005**, *102*, 589-593.
(71) Gaylord, B. S.; Massie, M. R.; Feinstein, S. C.; Bazan, G. C. *Proc. Natl. Acad. Sci. U. S. A.* **2005**, *102*, 34-39.
(72) Wang, S.; Bazan, G. C. *Adv. Mater.* **2003**, *15*, 1425-1428.
(73) He, F.; Tang, Y. L.; Wang, S.; Li, Y. L.; Zhu, D. B. *J. Am. Chem. Soc.* **2005**, *127*, 12343-12346.
(74) White, S.; Szewczyk, J. W.; Turner, J. M.; Baird, E. E.; Dervan, P. B. *Nature* **1998**, *391*, 468-471.
(75) Dervan, P. B.; Burli, R. W. *Curr. Opin. Chem. Bio.* **1999**, *3*, 688-693.
(76) Fechter, E. J.; Olenyuk, B.; Dervan, P. B. *Angew. Chem. Int. Ed.* **2004**, *43*, 3591-3594.
(77) Fechter, E. J.; Olenyuk, B.; Dervan, P. B. *J. Am. Chem. Soc.* **2005**, *127*, 16685-16691.
(78) Charych, D. H.; Nagy, J. O.; Spevak, W.; Bednarski, M. D. *Science* **1993**, *261*, 585-588.
(79) Alexeev, V. L.; Sharma, A. C.; Goponenko, A. V.; Das, S.; Lednev, I. K.; Wilcox, C. S.; Finegold, D. N.; Asher, S. A. *Anal. Chem.* **2003**, *12775*, 2316-2323.
(80) Miyata, T.; Asami, N.; Uragami, T. *Nature* **1999**, *399*, 766-769.
(81) Murakami, Y.; Maeda, M. *Biomacromolecules* **2005**, *6*, 2927-2929.

(82) Fritz, J.; Baller, M. K.; Lang, H. P.; Rothuizen, H.; Vettiger, P.; Meyer, E.; Guntherodt, H. J.; Gerber, C.; Gimzewski, J. K. *Science* **2000**, *288*, 316-318.
(83) Zhang, X. R.; Xu, X. *Appl. Phys. Lett.* **2004**, *85*, 2423-2425.
(84) Calleja, M.; Nordstroem, M.; Alvarez, M.; Tamayo, J.; Lechuga, L. M.; Boisen, A. *Ultramicroscopy* **2005**, *105*, 215-222.
(85) Wang, J.; Jiang, M.; Nilsen, T. W.; Getts, R. C. *J. Am. Chem. Soc.* **1998**, *120*, 8281-8282.
(86) Besselink, G. A. J.; Kooyman, R. P. H.; van Os, P.; Engbers, G. H. M.; Schasfoort, R. B. M. *Anal. Biochem.* **2004**, *333*, 165-173.
(87) Gaylord, B. S.; Heeger, A. J.; Bazan, G. C. *Proc. Natl. Acad. Sci. U. S. A.* **2002**, *99*, 10954-10957.
(88) Kim, W. J.; Sato, Y.; Akaike, T.; Maruyama, A. *Nat. Mater.* **2003**, *2*, 815-820.
(89) Lou, X.; Lewis, M. S.; Gorman, C. B.; He, L. *Anal. Chem.* **2005**, *77*, 4698-4705.
(90) Kamigaito, M.; Ando, T.; Sawamoto, M. *Chem. Rev.* **2001**, *101*, 3689-3745.
(91) Matyjaszewski, K.; Beers, K. L.; Woodworth, B.; Metzner, Z. *J. Chem. Educ.* **2001**, *78*, 547-550.
(92) Xu, F. J.; Cai, Q. J.; Li, Y. L.; Kang, E. T.; Neoh, K. G. *Biomacromolecules* **2005**, *6*, 1012-1020.
(93) Sawamoto, M.; Kamigaito, M. *Trends Polymer Sci.* **1996**, *4*, 371-377.
(94) Matyjaszewski, K.; Patten, T. E.; Xia, J. *J. Am. Chem. Soc.* **1997**, *119*, 674-680.
(95) Wang, J.-S.; Matyjaszewski, K. *Macromolecules* **1995**, *28*, 7572-7573.
(96) Patten, T. E.; Matyjaszewski, K. *Adv. Mater.* **1998**, *10*, 901-915.
(97) Matyjaszewski, K.; Xia, J. *Chem. Rev.* **2001**, *101*, 2921-2990.
(98) Jeyaprakash, J. D.; Samuel, S.; Dhamodharan, R.; Ruhe, J. *Macromol. Rapid Commun.* **2002**, *23*, 277-281.
(99) Zheng, G.; Stoever, H. D. H. *Macromolecules* **2002**, *35*, 6828-6834.
(100) Chen, X.; Randall, D. P.; Perruchot, C.; Watts, J. F.; Patten, T. E.; von Werne, T.; Armes, S. P. *J. Colloid Interface Sci.* **2003**, *257*, 56-64.
(101) Coullerez, G.; Carlmark, A.; Malmstroem, E.; Jonsson, M. *J. Phys. Chem. A* **2004**, *108*, 7129-7131.
(102) Huang, W.; Kim, J.-B.; Bruening, M. L.; Baker, G. L. *Macromolecules* **2002**, *35*, 1175-1179.
(103) Wang, X. S.; Armes, S. P. *Macromolecules* **2000**, *33*, 6640-6647.
(104) Huang, W.; Baker, G. L.; Bruening, M. L. *Angew. Chem. Int. Ed.* **2001**, *40*, 1510-1512.
(105) Ma, Y. H.; Tang, Y. Q.; Billingham, N. C.; Armes, S. P.; Lewis, A. L.; Lloyd, A. W.; Salvage, J. P. *Macromolecules* **2003**, *36*, 3475-3484.
(106) Grove, D. M.; Vankoten, G.; Verschuuren, A. H. M. *J. Mol. Cata.* **1988**, *45*, 169-174.
(107) Tsuji, J.; Sato, K.; Nagashima, H. *Chem. Lett.* **1981**, 1169-1170.
(108) Nagashima, H.; Wakamatsu, H.; Ozaki, N.; Ishii, T.; Watanabe, M.; Tajima, T.; Itoh, K. *J. Org. Chem.* **1992**, *57*, 1682-1689.
(109) Minisci, F. *Acc. Chem. Res* **1975**, *8*, 165-171.
(110) Iqbal, J.; Bhatia, B.; Nayyar, N. K. *Chem. Rev.* **1994**, *94*, 2549-2549.

(111) Wang, X. S.; Jackson, R. A.; Armes, S. P. *Macromolecules* **2000**, *33*, 255-257.
(112) Ramakrishnan, A.; Dhamodharan, R.; Ruhe, J. *Macromol. Rapid Commun.* **2002**, *23*, 612-616.
(113) Rihn, B.; Coulais, C.; Bottin, M. C.; Martinet, N. *J. Biochem. Biophys. Methods* **1995**, *30*, 91-102.

CHAPTER 2 Concept Proof of Atom Transfer Radical Polymerization (ATRP) in DNA Detection

2.1 Introduction

While numerous methodologies to date have significantly improved detection sensitivity and specificity in DNA sensing (see Chapter 1), the reported protocols are yet to be amenable for clinical settings. The main obstacle lies in the requirements for special laboratory skills in detection label preparation and/or for the complex instruments in signal readout. A new approach that enables sensitive DNA detection with off-shelf chemistry in an instrument-free detection fashion is desirable for the development of any portable screening devices.

Polymers have long been used in biological applications as blocking reagents to reduce nonspecific adsorption and as scaffolding frames to support immobilization of biomolecules. There are a few reports in which polymers of unique electrical or optical properties have been used in a pre-formed macromolecular form for DNA detection. For example, the DNA polymer hybrid was formed by electrostatically attracting cationic polymers to highly negatively charged DNA or by chemical coupling to attach DNA on the polymer side chains.[1-4] However, the dynamic growing process of macromolecules has yet to be exploited as an amplification tool. Polymerization is essentially a highly efficient signal amplification process with an enhancement power controllable at will. Using chemical reaction in the place of enzyme replication, polymerization connects the same small monomers in a head-to-tail fashion to form a long-chain polymer that contains hundreds to millions of repeating units. Consequently, the detection signal kept

in one small monomer is amplified hundreds to millions of times through the chain propagation.

Atom transfer radical polymerization (ATRP) is a new class of controlled/"living" radical polymerization that was first reported by the groups of Sawamoto[5,6] and Matyjaszewski.[7,8] Compared with other living polymerization techniques, ATRP is based on the repetitive addition of monomers to radicals that are generated from dormant alkyl halides in a reversible redox process.[9] ATRP has become a popular method that is used to graft polymer brushes on a solid support because of the broad selection of monomers, good control over the product molecular weight and polydispersity, and high tolerance of surrounding functional groups.[9-12] The demonstration of surface-initiated ATRP in aqueous media at room temperature further renders it feasible to be used as a signal amplification method in biosensing.[13-16]

In this chapter, a simple polymerization-facilitated detection strategy to amplify DNA hybridization events using an ATRP reaction is described. Taking advantage of this monomer-replicating concept, the detection of specific DNA sequences is accomplished by the formation of polymer brushes on the surface at ambient temperature (**Scheme 1.1**). Because the formed polymers change the refractive index near the surface and subsequently affect surface opacity, the spots where DNA hybridization occurred are directly visible.

To our knowledge, this is the first time dynamic molecular growth has been used as amplification means in bioanalytical detection. The demonstrated direct visualization

of DNA hybridization also marks a promising step towards the development of portable DNA detection device.

2.2 Experimental Section

2.2.1 Materials

Au substrates (50Å chrome followed by 1000Å gold evaporated on float glass slides) were purchased from Evaporated Metal Films (Ithaca, NY). Gold chips for surface plasmon resonance measurements were prepared in house by evaporation 20Å chrome at a rate of 0.2Å/sec followed by 480Å gold at a rate of 2Å/sec on BK7 glass. Dithiothreitol (DTT), triethylamine (TEA), mercaptohexanol (MCH), bromoisobutyryl bromide, N-Hydroxysuccinimide (NHS), 2-hydroxyethyl methacrylate (HEMA), CuCl, $CuBr_2$ and 2, 2'-bipyridyl (bpy) were purchased from Sigma-Aldrich (St. Louis, MO). All oligonucleotides were purchased from Integrated DNA Technologies (Coralville, IA). The sequences of DNA used in this chapter are listed in **Table 2.1**. T4 DNA ligase was purchased from Stratagene (La Jolla, CA). A NAP^{TM}-5 column from Amersham Pharmacia Biotech was used for DNA purification.

2.2.2 Capture Probe Immobilization

The gold substrates were cleaned in a piranha solution (70% in volume of 18.4M H_2SO_4, 30% in volume of 30% H_2O_2 aqueous solution) prior to the use. The oligonucleotide probes, **C** and **NC** (**Table 2.1**), had disulfide bonds at the 3'-terminus for surface attachment. The generation of free thiol groups for surface immobilization was

acquired via the mixing of 100µL stock oligonucleotide solution (**C** or **NC**) at 100µM and 100µL stock DTT solution at 0.1M along with 4µL TEA at room temperature for 20min. A Voyager DE STR MALDI-TOF mass spectrometer (Applied Biosystems) was used to confirm the successful reduction of disulfide bonds. After reduction, the excess amount of DTT was removed using a NAP^{TM}-5 column. The concentrations of the reduced oligonucleotides were determined by the UV absorbance at 260nm. Freshly reduced capture probes at 1µM in a KH_2PO_4 buffer (1M, pH4.4) were spotted onto Au substrates at room temperature and incubated in a humid chamber for 16-20hr. The surfaces were then incubated with 1mM MCH aqueous solution for 1hr, followed by copious rinsing with DI water and dried under Ar.[17, 18]

2.2.3 Synthesis of Bromoisobutyryl -N-hydroxysuccinimide (NHS) Ester

The previously reported procedure was used.[19] Briefly, a solution of bromoisobutyryl bromide (0.217M) in diethyl ether (50mL) was cooled in an ice bath, and a solution of N-hydroxysuccinimide acid (0.434M) and TEA (0.652M) in dioxane (25mL) was added drop-wise. When the addition was completed, the reaction mixture was stirred at room temperature for 1hr, followed by the filtration to remove any precipitates. The solution was washed with saturated $NaHCO_3$ (25mL) and then water (25mL) and dried over $MgSO_4$. Evaporation *in vaco* resulted in 2.2g white crude solid product (yield 77%). The NMR spectrum showed the formation of the expected product. ^{1}H NMR (in CD_3Cl, 300MHz): δ=2.8(s, 4H), 2.1(s, 6H). ^{13}C NMR (in CD_3Cl, 300MHz):

δ=25.9, 30.9, 51.4, 166.2, 168.9. No further purification was required. This crude product was directly used in the next step.

2.2.4 Initiator Coupling to Detection Probe (D)

Initiator-coupled DNA detection probe was prepared as previously described.[19] Briefly, 70μL of oligonucleotide **D** solution at 100μM and 10μL of 10 x conjugation buffer (1.0M $NaHCO_3/Na_2CO_3$, pH9.0) were added into a 1.5mL centrifuge tube, followed by the addition of freshly prepared bromoisobutyryl NHS ester solution (10 mg/mL in DMF, 20μL). After 30min reaction at room temperature, un-reacted NHS ester was removed by gel filtration. MALDI-TOF MS was again used to monitor the coupling efficiency by measuring the amount of oligonucleotides before and after the coupling reaction.

2.2.5 Three-strand DNA Hybridization

Probe **C** and **NC**-attached Au surface was incubated with 1.5μL target oligonucleotides, **C'D'**, at various concentrations in a humidity chamber at room temperature. 1M NaCl in the Tris-EDTA (TE) buffer was used as the hybridization buffer. After 1-6hr hybridization, the surface was briefly rinsed with water. An additional hybridization with 1μM initiator-modified detection probes, **D-IN**, was conducted for 1hr in 1M NaCl/TE buffer afterwards. After hybridization, the surface was rinsed with a ligation buffer containing 50mM Tris-HCl (pH7.5) and 7mM $MgCl_2$ (at the absence of DTT to eliminate possible replacement of thiol-labeled DNA probes).

2.2.6 DNA Ligation

After hybridization, the surface was then reacted with 20μL of a solution containing 4U T4 DNA ligase and 15% PEG 8000 in a 1 x T4 DNA ligation buffer without DTT. The reaction was allowed to proceed for 2hr at room temperature before rinsing with 5% SDS and subsequently with 1% SDS in 40mM K_2HPO_4/KH_2PO_4 at 45ºC.

2.2.7 ATRP Reaction for DNA Detection

In a typical surface-initiated ATRP reaction, a mixed solution of HEMA (16mL) and DI water (16mL) was degassed with Ar for 30min to reduce the amount of O_2 present in the reaction system, followed by another 15min degassing upon the addition of the catalyst mixture of CuCl (220mg, 2.2mmol), $CuBr_2$ (144mg, 0.64mmol) and 2,2'-bipyridyl (976mg, 1.56mmol). The flask containing the DNA-immobilized substrate was also purged with Ar for 15min. The monomer/catalyst solution was then injected into the flask containing substrate. The polymerization was quenched by the removal of the substrate, followed by the subsequent rinse with methanol. Direct coupling of 2-bromoisobutyryl bromide to the hydroxyl groups on the PHEMA side chains was achieved by immersing the PHEMA-coated substrate in 10mL DMF containing 99μL 2-bromoisobutyryl bromide (0.08M) and 139μL TEA (0.1M) for 20min. The polymer film formed was characterized using PM-IRRAS, ellipsometry, and contact angle measurements.

2.2.8 SPR Real-Time Hybridizations and T4 Ligation

Probe **C** and **NC**-attached SPR surface was installed into the SPR sample cell and incubated with 1M NaCl until baseline was stable. After baseline was stabilized, the real-time SPR hybridization and ligation experiment started (**Figure 2.3**). Firstly, the surface was continuously washed with 1M NaCl TE buffer for 2min, then an aqueous solution of 1μM target DNA **C'D'** in 1M NaCl TE buffer was passed through the cell for 5min (step A), followed by the wash step using 1M NaCl TE buffer for 2min. Secondly, 8M urea aqueous solution was flowed through the cell for 10min (step B) to denature the duplex formed in the first step, then the surface was again washed with 1M NaCl TE buffer until the SPR signal was stable. Thirdly, 1μM target DNA **C'D'** in human gene mixture (20ng/μL) in1M NaCl TE buffer (step C) and 1μM detector DNA **D-IN** in 1M NaCl TE buffer (step D) was subsequently passed through the SPR sample cell. The surface was washed with 1M NaCl TE buffer until the SPR signal stable after each hybridization-step. Subsequently, the surface was briefly washed with 1x ligation T4 ligation buffer without DTT for 1min, followed by an injection of 30μL ligation reaction mixture containing 50mM Tris-HCl (pH7.5), 7mM $MgCl_2$, 1mM DTT, 15% PEG 8000, 1mM rATP and 6U T4 ligase. After 20min incubation (step E), the surface was washed with 1x ligation buffer lacking DTT for 1min and 1M NaCl TE buffer, followed by incubation in 8M urea for 15min (step F). The surface was finally washed and incubated in 1M NaCl TE buffer.

2.2.9 Instrumentation

A Voyager^{TM} DE-STR matrix-assisted laser desorption/ionization mass spectrometry (MALDI-MS) was used to monitor the coupling reaction between amino-labeled DNA and bromoisobutyryl NHS ester and the reduction of disulfide bonds on DNA. 35mg/mL 3-hydroxypicolinic acid (3-HPA) in 7mg/mL diammonium citrate and 10% acetonitrile in water was used as the MALDI matrix. DNA solutions were desalted using C_{18}ZipTip^{TM} column (Millipore).

The polarization modulation-infrared reflection-adsorption spectroscopic (PM-IRRAS) spectra were recorded on a Digilab FTS 7000 (Randolph, MA) spectrometer.[20] Reflectance FTIR spectroscopy was performed using a Digilab spectrometer containing a PIKE grazing angle (70º) attachment. The spectra were typically collected with 256 scans using a MCT detector.

The hybridization and ligation conditions were confirmed and optimized by surface plasmon resonance measurements using the SPRimager® from GWC Technologies Inc. (Madison, WI). All the kinetic curves were collected at a fixed optimized angle of the prism to achieve the best sensitivity and linearity of the detections. This angle position usually corresponds to one third of the difference between the minimum and the maximum reflectivity of the surface. The angle of the prism was optimized in the experimental buffer for each experiment by adjusting the incident light angle through rotating the angle adjustment knob. The line profile function of the V+ + software provided by GWC was used to monitor the SPR intensity changes corresponding to the angle change. The angle adjustment knob was turned until the pixel

value reached a minimum. Then the angle adjustment knob was counter-clockwise turned until the pixel value typically reached 70-80. Once the angle was optimized, the specific regions of interest (ROIs) on the surface were selected and a reference image was taken before the surface was exposed to the analyte. For the regions with same molecules attached at least two ROIs were selected. The kinetic experiments were then started after Microsoft Excel was launched and the V+ + "TimeSeries" Macro was activated. Typically, the computer took time-course measurements every 4 seconds by averaging 30 images and subtracting the reference image from average images to obtain "difference images", which represented the SPR responses. At the same time the SPR response of each ROI as a function of the time plotted in the Excel spreadsheet.

The film thickness was measured with a VB-250 VASE Ellipsometer. The instrument was equipped with a 633nm He/Ne laser that provided an irradiation source at 70° incident angle. Commercial WVASE software was used for surface thickness calculation. The reflective index values of the polymer films and DNA were taken from the literature and are 1.5 and 1.46, respectively.[21] A three-layer model was used to fit the experimental data.

Contact angle measurements were obtained using a CAM 200 optical contact angle meter (KSV instrument LTD). HPLC grade water was used for measurement. The contact angle was determined by using the Young/Laplace fitting method. Three replicates were measured for each substrate to calculate the standard deviation of the measurements.

All surface measurements were conducted with dried samples.

2.4 Results and Discussion

As shown in **Scheme 1.1**, using ATRP to augment the presence of specific DNA sequences was separated into two consecutive yet independent stages: specific DNA recognition and signal amplification. DNA hybridization and ligation were used to differentiate target DNA sequences from mismatches. Since ATRP initiators attached on the detection probes had negligible impacts on either DNA duplex formation or DNA ligation, standard DNA handling protocols that have been well documented in the literature were directly adapted to maximize sequence recognition specificity.

A 3-strand synthetic oligonucleotide system was used in the proof of concept experiment. DNA capture probes of complementary (**C**) and noncomplementary (**NC**) sequences to the target DNAs were first immobilized on a Au substrate (**Scheme 1.1**). To ensure a consistent surface coverage, the thiol groups at the 3'-end of both probes were freshly reduced.[17] Subsequent surface blocking with mercaptohexanol (MCH) for 1hr was conducted to passivate the surface and remove any physically adsorbed oligonucleotides. The successful immobilization of probes **C** and **NC** on the surface was confirmed in a polarization modulation-infrared reflection-adsorption spectroscopy (PM-IRRAS) spectrum: a small peak near 1700cm^{-1} was observed from the carbonyl stretching and exocyclic $-NH_2$ bending vibrations of DNA bases. Additional peaks around 1500 cm^{-1} from the purine and pyrimidine rings, and peaks in the region of 1000-1300cm^{-1} from DNA phosphodiester backbones were also observed (**Figure 2.1a**).[20] Note that no absorption was observed using traditional reflectance FT-IR measurements due to the limited amount of materials attached on the surface.

Following surface immobilization, incubating the capture probe-coated substrates with the target DNA sequence (**C'D'**) and then the initiator-labeled detection probes (**D-IN**) in the hybridization buffer led to the formation of DNA duplex at the desired location. The detection probes, **D,** were coupled with ATRP initiators (NHS ester of bromoisobutyroyl bromide) before hybridization. MALDI-MS was used to examine the coupling efficiency (**Figure 2.2**). A mass increase of 149 was clearly observed, corresponding to the addition of bromoisobutyroyl group at the end of probe **D**. The negligible residual peak at the original position confirmed the coupling reaction was near completion in less than 30min. Upon the hybridization of **C'D'** and **D-IN** on the surface, a slight increase in carbonyl stretching was observed in the corresponding PM-IRRAS spectrum (**Figure 2.1b**), supporting the successful hybridization of DNA and the initiator-coupled detection probes. A T4 ligase was subsequently used to connect the nicks between **C** and **D-IN** probes to permanently affix the detection probes on the surface, along with the ATRP initiators.

Traditionally, the hybridization and ligation efficiency on surface was measured by radioactive labeled DNA strands. As one of the most powerful label-free surface interaction analysis technologies, SPR has great advantages for applications in molecular biology. SPR was conveniently used here to monitor the two-step hybridization and T4 ligation steps involved in this ATRP-based DNA detection assay.

Figure 2.3 (Top) is the kinetic curve of in situ hybridizations and ligation. The horizontal scale is the time scale of this kinetic experiment and the vertical scale is the SPR intensity changes for each reaction step. The stepwise kinetic experiment (step A-F)

was conducted continuously by flowing in or injecting in appropriate buffers or reagents. Buffer wash was conducted between each step as indicated in the experimental part. As shown in **Figure 2.3**, the SPR intensity change difference (ICD) after the hybridizations of synthetic target ssDNA **C'D'** to complementary probes **C** and to non-complementary probes **NC** was 14.6± 1.0pixels (step A). The ssDNA surface was regenerated by incubating the surface in 8M urea for 15-20min. The regenerated surface was then hybridized with a mixture containing 20ng/mL human genomic DNA and 1μM **C'D'** (step B)**.** The presence of complex genetic background didn't interfere the hybridization between **C'D'** and complementary probe **C**. In the standard deviation range of the SPR system, the observed SPR ICD (14.9± 1.5pixels) was similar to what previously obtained when the DNA array hybridized with target **C'D'** without the human genomic DNA background.

Followed the first hybridization with **C'D'**, the surface was subsequently hybridized with ATRP initiator-coupled detector DNA **D-IN**. The observed SPR ICD between probe **C** and **NC** was 25.2±1.3pixels, which was more than 10pixels higher than the ICD of the first step hybridization. The increase of the ICD value corresponded to the successful hybridization between target DNA **C'D'** and detector **D-IN** on probe **C** attached positions.

The 20min T4 ligation at room temperature was conducted after the two step hybridizations to seal the gaps in the three component-duplexes on the surface. The ICD value of 13.8pixels was observed after incubated the surface in dehybridization reagent

Urea, which clearly confirmed the success of the ligation step. If the ligation step was failed, the expected value of ICD would be zero.

The success of hybridization and ligation was also confirmed by the difference between SPR images collected before and after hybridization and ligation. As shown in **Figure 2.3** (Bottom), two probe C attached spots and two probe NC attached spots showed similar gray scale before hybridization and ligation since similar amount of DNA molecules were immobilized on the gold surface under the same surface immobilization conditions. After hybridization and ligation, compared to the previous image the two spots corresponding to probe C became significantly whiter due to the local mass increase and the two spots corresponding to probe NC retained about the same gray scale.

After ligation, the substrate was then immersed in an ATRP reaction mixture containing 2-hydroxyethyl methacrylate (HEMA) as the monomer. HEMA was chosen in our study for its good water solubility and rapid polymer growth.[14] It also offers an additional benefit in multi-stage ATRP reactions, which will be discussed later. The reaction catalyst was a mixture of CuCl, $CuBr_2$ and 2, 2'-bipyridyl. $CuBr_2$ was used as a deactivator to control the polymer growth rate and ensure the formation of thick polymer films.[29] Immersion of the initiator-attached Au substrate into this mixture immediately triggered ATRP (**Scheme 2.1, A**). After a 5hr reaction, a layer of polyhydroxyethylmethacrylate (PHEMA) film was formed on the surface at where the capture probes **C** were located. The formed thick polymer film altered surface reflectivity, changed surface opacity, and rendered the spots directly visible to the naked eye. The film visibility further enhanced by transforming the free hydroxyl groups in

PHEMA into secondary initiators to intensify the contrast (**Scheme 2.1, B**) (**Figure 2.4**). Similar color change was observed from the other nearby spot, prepared as the reaction replicate. The control spots where the capture probes **NC** were immobilized, however, remained unchanged. The reflectance FT-IR measurement of the polymer-occupied spots illustrated the formation of a new peak between 3000cm^{-1} and 3500cm^{-1} (hydroxyl stretching), accompanied with a significant absorption increase of carbonyl content near 1700cm^{-1} (**Figure 2.1c**). Both changes confirmed the formation of PHEMA on the surface. No reflectance FT-IR signal was observed from the control spots where few HEMA molecules adsorbed non-specifically.

Contact angle measurements were also conducted to monitor surface hydrophobicity changes as surface chemistry varied (**Table 2.2**). The bare gold substrate exhibited a highly hydrophobic surface with a contact angle of ~89°. The assembly of negatively charged DNA onto the surface greatly altered its interfacial properties and significantly reduced this contact angle to ~31°. After DNA hybridization the contact angle further decreased to ~26°. Since both HEMA and PHEMA are more hydrophobic than DNA molecules, an increase in the contact angle was observed after exposing the surface to the ATRP reaction solution. The measured contact angle (~44°) was similar to our previous measurement of PHEMA film grown atop ω-mercaptoundecyl bromoisobutyrate. The contact angle of the control spots also increased after exposure to the ATRP mixture. Note that the contact angle measurements alone could not be used to differentiate the formation of PHEMA from the nonspecifically adsorbed HEMA monomers due to their similar hydrophobicity.

To clearly distinguish the growth of PHEMA atop DNA from the nonspecifically adsorbed HEMA on the control spots, an ellipsometer was used to measure the film thickness changes after ATRP. Using a bare gold substrate as the reference point, the immobilization of DNA capture probes resulted in a film growth of 16.4±0.5Å (**Table 2.2**). Hybridization with the target and detection probes only slightly increased the film thickness due to the limited hybridization efficiency. The ATRP reaction, however, significantly increased the film thickness to 100.1±0.7Å. While the molecular weight of PHEMA can not be directly measured, due to the limited amount of materials formed on the surface, at least several hundred repeating units were suspected in the formed polymer chains.[22] On the control spot, on the other hand, the film thickness increased less than 20Å from the nonspecific adsorption of monomers on the surface. It is interesting to note that the **NC** spots exhibited less background signal, comparing to the surrounding areas where MCH was used as blocking reagent. Using DNA and other reagents as the blocking reagents, along with more stringent surface washes, are under investigation to further reduce the background. Nevertheless, this background adsorption did not interfere with DNA detection from a direct inspection of the substrate (**Figure 2.4**).

2.5 Conclusions

In conclusion, a signal amplification technique has been developed for the detection of specific DNA sequences based on controlled/"living" radical polymerization, ATRP. It is the first time that a small molecule-initiated chain growth was used as an amplification method for bio-molecular interaction detection. It offers three advantages

over current DNA detection techniques: 1) small initiators instead of bulky detection tags are pre-labeled onto DNA probes that introduce minimal interference to DNA sequence recognition; 2) detection amplification is independently conducted *after* DNA recognition. Consequently, numerous well-established DNA hybridization and ligation protocols can be used to improve single mismatch detection fidelity. Meanwhile, various chemical procedures can be used to optimize polymerization reaction without the concerns over detection tag or DNA duplex stabilities; 3) the growth of high MW polymers eliminates the needs of sophisticated detectors to visualize target DNA in the sample. Together, the demonstration of the instrument-free ATRP-assisted DNA detection simplifies the future sensor construction and opens up the opportunities for the development of point-of-care diagnostic devices.

Schemes

Scheme 2.1: Chemical Formation of PHEMA in DNA Detection.

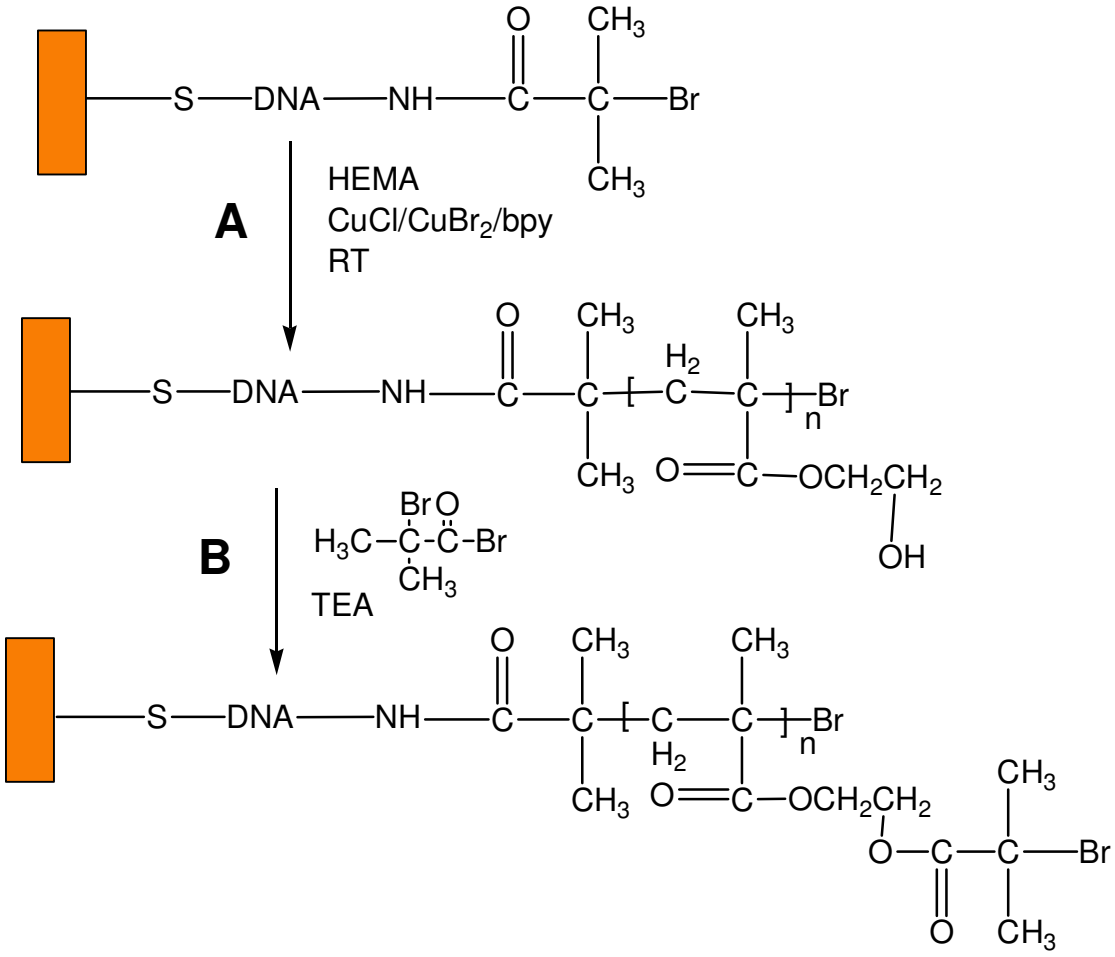

Tables

Table 2.1 Summary of the DNA Sequences Used in This Chapter.

Name	Sequence	Description
C	5'-pTAA CAA TAA TCC CTC AA A_{18}-C_3-S-S-C_3	Capture probe partially complementary to **C'** portion of target **C'D'**
D	5'-NH_2-C_6-A_{18} AAA TCC TTA TCA ATA TT	Detection probe partially complementary to **D'** portion of target **C'D'**
D-IN	5'-Br$(CH_3)_2$CCONH-C_6-A_{18} AAA TCC TTA TCA ATA TT	Initiator-coupled **D**
NC	5'-pGGC AGC TCG TGG TGA AA A_{18}-C_3-S-S-C_3	Non-complementary capture probes to target **C'D'**
C'D'	5'-GAG GGA TTA TTG TTA AAT ATT GAT AAG GAT	Perfectly matched target DNA complementary to probes **C** and **D**.

Table 2.2 Ellipsometric and Contact Angle Measurements of PHEMA Formation in ATRP-Assisted DNA Detection.[a]

Films	**Film Thickness (Å)**	**Contact Angle (˚)**
Bare Gold Surface	0[b]	89.0± 0.5
ssDNA-coated Surface	16.4± 0.5	31.0± 0.0[c]
dsDNA-coated Surface	18.8±0.5	26.0±0.2
PHEMA Formation on the Surface	100.1± 0.7	44± 2
Control after ATRP	36.2± 0.7	49 ± 2

[a]: Two replicates were measured in ellipsometry and three replicates for contact angle measurements. The average of the measurements were calculated, and the standard variation was shown.

[b]: the bare Au substrate was used as the reference point. No measurement was made at this point.

[c]: in this experiment, three measurements yielded the same readouts, with the standard variation of zero.

Figures

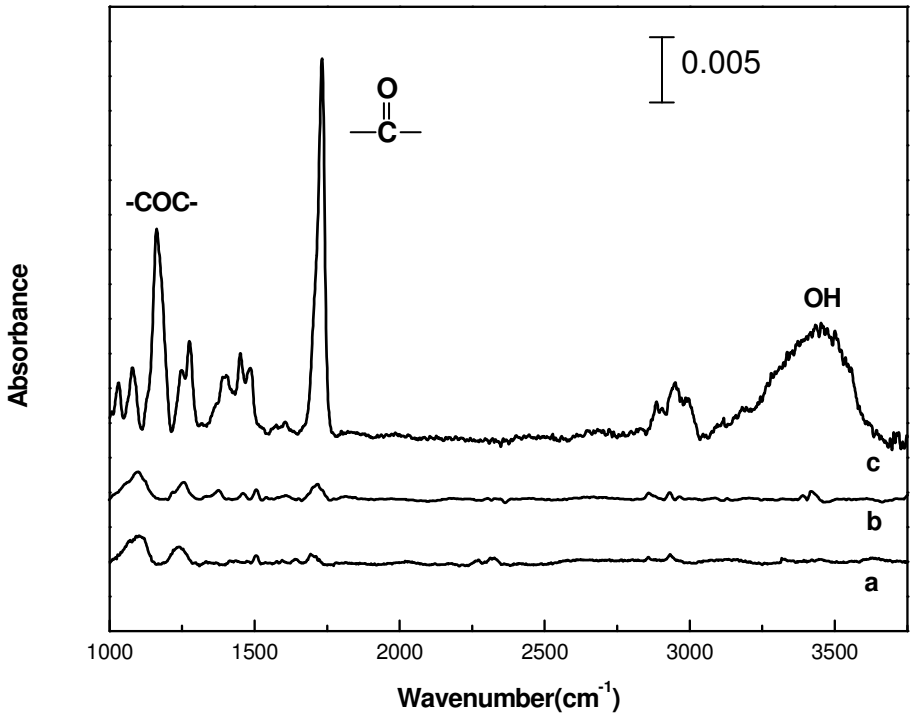

Figure 2.1 The PM-IRRAS spectra of (**a**) capture-DNA probes on the Au surface; (**b**) initiator-coupled DNA duplex on the surface after hybridization; and (**c**) a reflectance FT-IR spectrum of the formation of PHEMA atop DNA molecules on the surface. The scale bar is shown at the up-right corner. Note that the reflectance FT-IR system used there is approximately 10 x less sensitive than PM-IRRAS.

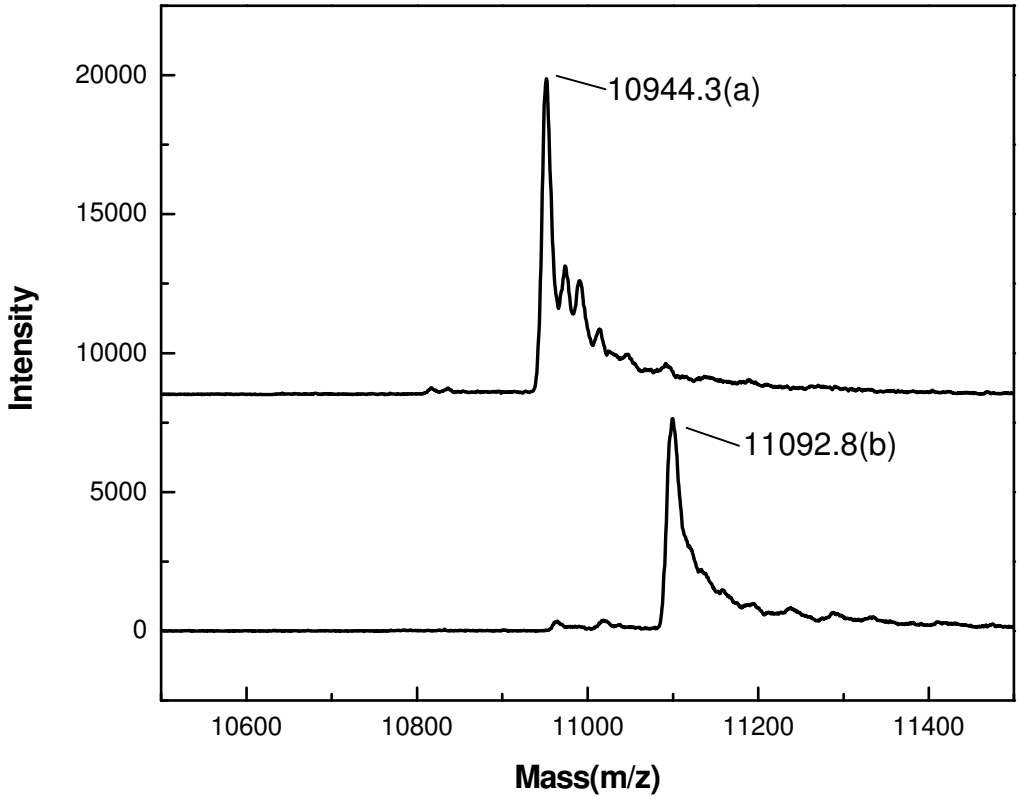

Figure 2.2 MALDI spectra of detection probe **D** (**a**) before and (**b**) after the coupling of the ATRP initiator (ΔMW=149). MALDI-MS conditions: accelerating voltage 25kV, grid voltage 90%, positive mode detection, delay time 300ns, and 100 laser shots collected per spectrum, 35mg/mL 3-HPA as the matrix.

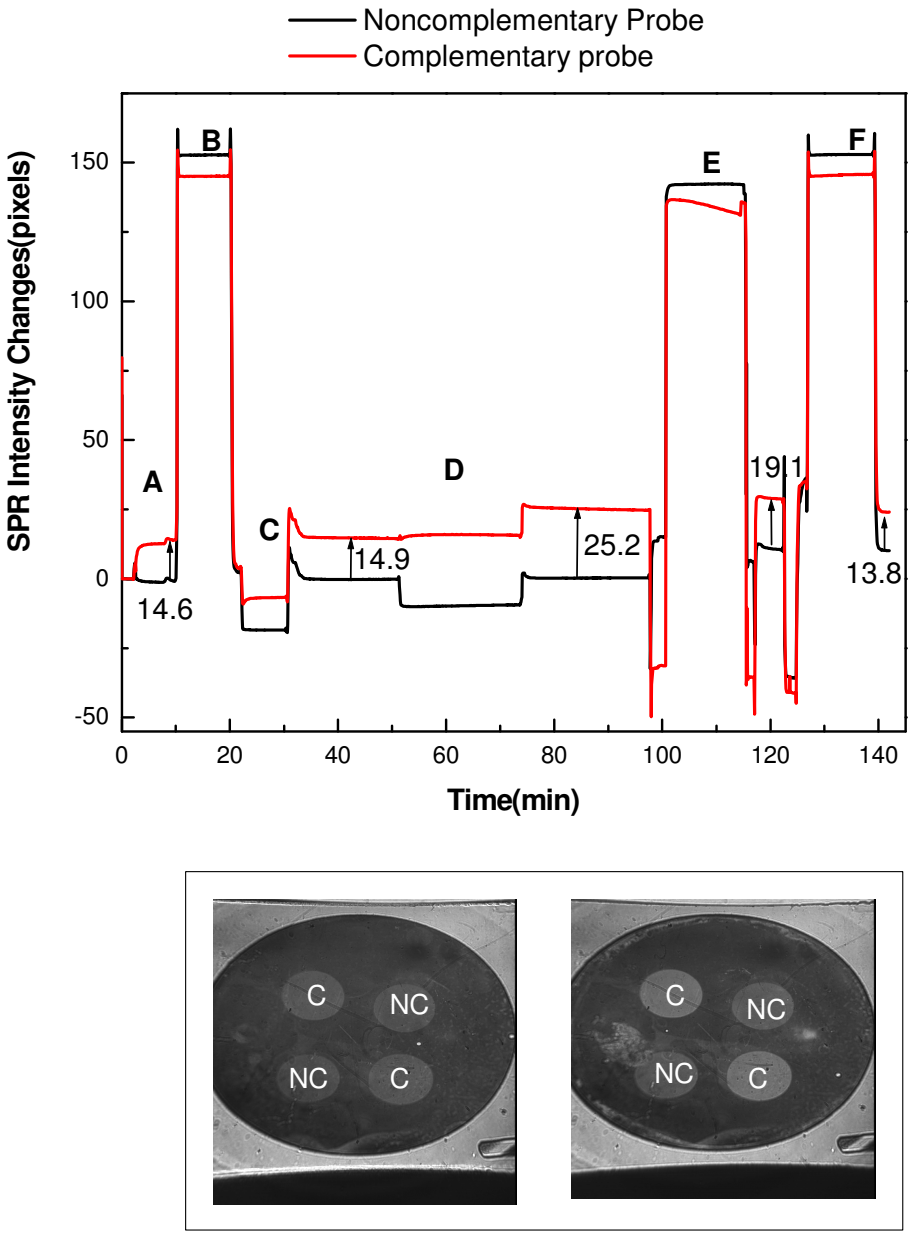

Figure 2.3 (Top) Real-time SPR monitoring of DNA hybridizations and T4 ligation. A: hybridization with target DNA C'D'; B: Urea dehybridization; C: hybridization with target DNA C'D' under 20ng/mL human genomic DNA environment; D: hybridization with detector D-IN; E: T4 ligation; F: Urea dehybridization. Buffer wash was conducted between each step. The numbers shown in the graph are values of SPR intensity change difference (ICD) between the complementary probe C and the noncomplementary probe NC. (Bottom) SPR images before (left) and after (right) hybridization and ligation.

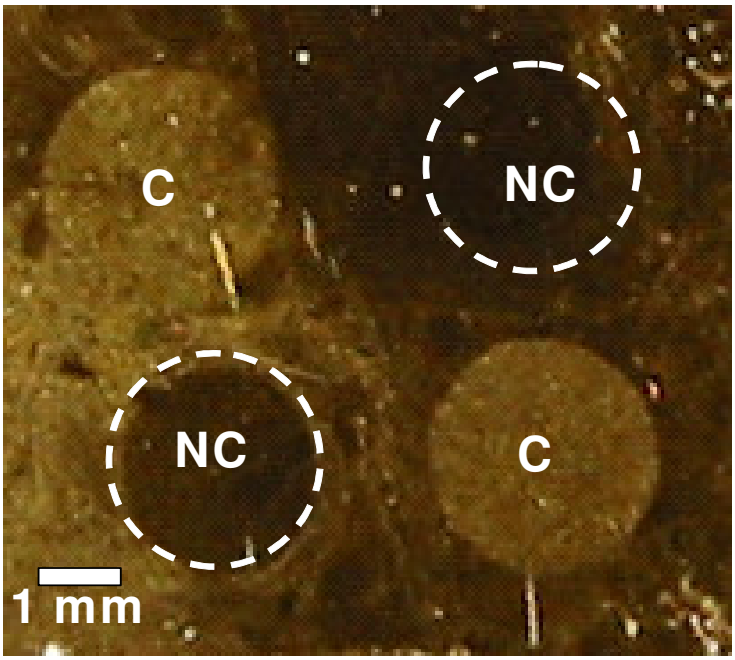

Figure 2.4 A photograph of 1μM target DNA **C'D'** detected after the ATRP reaction. The growth of the polymer film results in the directly observable opaque spots (**C**), whereas the control spots remain transparent (**NC**). The dotted circles are merely guides to the eye. Detailed ATRP reaction conditions see the text.

References

(1) Liu, B.; Bazan, G. C. *J. Am. Chem. Soc.* **2004**, *126*, 1942-1943.
(2) Gaylord, B. S.; Heeger, A. J.; Bazan, G. C. *J. Am. Chem. Soc.* **2003**, *125*, 896-900.
(3) Gaylord, B. S.; Heeger, A. J.; Bazan, G. C. *Proc. Natl. Acad. Sci. U. S. A.* **2002**, *99*, 10954-10957.
(4) Kim, W. J.; Sato, Y.; Akaike, T.; Maruyama, A. *Nat. Mater.* **2003**, *2*, 815-820.
(5) Sawamoto, M.; Kamigaito, M. *Trends Polymer Sci.* **1996**, *4*, 371-377.
(6) Sawamoto, M.; Kamigaito, M. *J. Macromol. Sci.* **1997**, *A34*, 1803-1814.
(7) Matyjaszewski, K.; Patten, T. E.; Xia, J. *J. Am. Chem. Soc.* **1997**, *119*, 674-680.
(8) Wang, J.-S.; Matyjaszewski, K. *Macromolecules* **1995**, *28*, 7572-7573.
(9) Matyjaszewski, K.; Xia, J. *Chem. Rev.* **2001**, *101*, 2921-2990.
(10) Jeyaprakash, J. D.; Samuel, S.; Dhamodharan, R.; Ruhe, J. *Macromol. Rapid Commun.* **2002**, *23*, 277-281.
(11) Zheng, G.; Stoever, H. D. H. *Macromolecules* **2002**, *35*, 6828-6834.
(12) Chen, X.; Randall, D. P.; Perruchot, C.; Watts, J. F.; Patten, T. E.; von Werne, T.; Armes, S. P. *J. Colloid Interface Sci.* **2003**, *257*, 56-64.
(13) Coullerez, G.; Carlmark, A.; Malmstroem, E.; Jonsson, M. *J. Phys. Chem. A* **2004**, *108*, 7129-7131.
(14) Huang, W.; Kim, J.-B.; Bruening, M. L.; Baker, G. L. *Macromolecules* **2002**, *35*, 1175-1179.
(15) Wang, X. S.; Armes, S. P. *Macromolecules* **2000**, *33*, 6640-6647.
(16) Huang, W.; Baker, G. L.; Bruening, M. L. *Angew. Chem. Int. Ed.* **2001**, *40*, 1510-1512.
(17) Herne, T. M.; Tarlov, M. J. *J. Am. Chem. Soc.* **1997**, *119*, 8916-8920.
(18) Peterlinz, K. A.; Georgiadis, R. M.; Herne, T. M.; Tarlov, M. J. *J. Am. Chem. Soc.* **1997**, *119*, 3401-3402.
(19) Lou, X.; He, L. *Polymer Preprint* **2004**, *45*, 455-456.
(20) Brewer, S. H.; Anthireya, S. J.; Lappi, S. E.; Drapcho, D. L.; Franzen, S. *Langmuir* **2002**, *18*, 4460-4464.
(21) Elhadj, S.; Singh, G.; Saraf, R. F. *Langmuir* **2004**, *20*, 5539-5543.
(22) Wang, J.; Xu, D.; Kawde, A. N.; Polsky, R. *Anal. Chem.* **2001**, *73*, 5576-5581.

CHAPTER 3 Reaction Optimization of ATRP-Based DNA Sensing

3.1 Introduction

After the concept proof experiment of ATRP based DNA detection (see Chapter 2) was achieved, the next goal was to further improve the sensitivity of this DNA detection method. There were two strategies to obtain this aim: increasing the amount of polymer formed on the surface and decreasing the nonspecific absorption.

3.1.1 Increasing the Amount of Polymer

The sensitivity of this polymerization-assisted DNA detection directly depends on two factors: 1) the number of the polymer chains formed, i.e. the density of the reaction initiators available on the surface; and 2) the final molecular weight (MW) of each individual polymer molecule formed. In DNA detection, the electrostatic repulsion of highly charged DNA backbones limits the maximum amount of capture DNA probes immobilized to ~10^{13} molecules/cm^2.[1] The low concentration of target DNAs obtainable for detection along with lower than 100% hybridization and ligation efficiencies further reduce the amount of immobilized initiators available. Therefore, the increase of initiator density or the formation of high molecular weight polymer becomes the two logical choices for the improvement of DNA detection limit.

One straightforward way to increase the initiator density on surface is to use multiple-initiator labeled detection probes. Only one initiator (IN) was coupled with each detection probe (D) in the proof-of-concept experiment (see Chapter 2). In this approach, a multiple initiator-labeled 13nm gold nanoparticle was coupled to the detector probe

replace the single initiator and to significantly increase the initiator density on the surface (**Scheme 3.1).** As the result, the amount of target DNA detectable decreased two order magnitudes (**Figure 3.1**).

Alternatively, the formation of branched polymer molecules can be used as a more efficient means to grow substantial materials in a reasonable reaction period.[2] Taking advantage of the additional hydroxyl groups available on HEMA, a secondary ATRP reaction was performed to form branched PHEMA to dramatize DNA detection. With this method, 1nM target DNA was readily discernable to the naked eye. In addition, it is worth pointing out that the reaction time was also significantly shortened from 5hrs in linear polymer formation to 2 x 30min in the formation of branched polymers.

3.1.2 Minimization of the Nonspecific Absorption

Reduction of background noise including nonspecific absorption is another important strategy to improve the detection sensitivity. Passivation layers play a key role in the minimization of background noise in many biosensors. In DNA sensors, mercaptohexanol (MCH) is often used to block the bare gold surface after DNA immobilization. Three benefits makes MCH one of the most popular passivation molecules for DNA sensors: (1) MCH reduces nonspecific absorption of DNA on the gold surface by replacing loosely absorbed DNA molecules through the bases with stronger thiol-Au interaction; (2) MCH is water-soluble, which eliminates the needs for non-polar solvent exchange that can cause reduced solubility of DNA molecules; (3) The methylene spacer between the thiol groups and the ssDNA is of the similar length of

MCH; thus little steric interfere from MCH is expected in DNA hybridization on the sensor surface. In fact, the presence of MCH has been shown to significantly improve the hybridization efficiency.[1]

Despite its popularity, MCH has limited roles in our sensing platform, mainly for its chain-end hydroxyl group that interferes with secondary ATRP reactions in the formation of branched polymer. The hydrophobic alkyl chains are also less efficient in blocking nonspecific absorptions of the proteins used in DNA ligation.

A number of self-assembled monolayers (SAMs) with oligo (ethylene glycol) (OEG),[3] carboxylic anhydride,[4] phosphorylcholine[5-7] motifs have been found to be more efficient in resisting protein nonspecific absorption than alkyl chains. Among them, oligo (ethylene glycol)-terminated alkane thiol SAMs, $HS(CH_2)m(OCH_2CH_2)nOR$ (R=H, CH_3), have attracted the most attention based on the pioneer work of Whitesides'group.[3,8,9] The chain length, chain density, and chain conformation of OEG molecules were recognized as important factors that affect the interaction between SAMs and proteins at the solid-liquid interface.[10]

Vanderah *et al* found found that-$S(CH_2)_2(OCH_2CH_2)_5OCH_3$ SAM layer was less ordered when it was prepared from dry THF, compared to the SAM prepared from more polar solvent, 95%ethanol.[11-13] This less ordered film exhibited better protein inhibition. They also found that -$S(CH_2)_3(OCH_2CH_2)_5OCH_3$ SAM layer at 60-80% surface coverage prepared from aqueous solution exhibited best protein resistance. A commercial available -$S(CH_2)_2(OCH_2CH_2)_6OCH3$ (OEG7) molecule was therefore chosen to be used in our

study with the expectation of similar protein resistant ability since only small structural difference existed between OEG7 and $HS(CH_2)_{2-3}(OCH_2CH_2)_5OCH_3$.

In the second section of this chapter, OEG7 was used as the passivation molecule to investigate its protein resistance ability with the aim to minimize the non-specific absorptions during ATRP-based DNA sensing process. Different SAM immobilization conditions were tested to optimize the surface protein resistant ability. In addition, the hybridization efficiencies of the DNA assay with OEG7 and MCH as passivation layers were compared via real time surface plasmon resonance measurements.

3.2 Experimental Section

3.2.1 Materials

Single-stranded DNA (ssDNA) used in this chapter was purchased from Integrated DNA Technologies, Inc. (Coralville, IA) (**Table 3.1**). 2-Hydroxyethyl methacrylate (HEMA, 98%) was purchased from Sigma-Aldrich and was purified using an inhibitor remover column to remove methyl hydroquinone inhibitor. The inhibitor remover was purchased from Aldrich (cat. no. 31,134-0), and the column was packed in house. 3-Hydroxypicolinic acid (3-HPA), diammonium citrate, dioxane, dithiothreitol (DTT), triethylamine (TEA), mercaptohexanol (MCH), bromoisobutyryl bromide, N-Hydroxysuccinimide (NHS), 6-mercapto-1-hexanol (MCH), and 1-octadecanethiol (ODT), CuCl, $CuBr_2$, 2, 2'-bipyridyl (bpy), trissodium citrate dihydrate, $HAuCl_4 \cdot 3H_2O$ and diethyl ether were purchased from Sigma-Aldrich (St. Louis, MO) and used as received. Bis(p-sulfonatophenyl)phenylphosphine dihydrate dipotassium (BSPP) was

purchased from Strem Chemicals Inc. (Newburyport, MA). Methoxyoligoethyleneglycol, $[CH_3(OCH_2CH_2)_7S]_2$ (OEG7) was purchased from Bio Vectra (Prince Edward Island, Canada). Micro Bio-Spin® 30 Columns were bought from Bio-Rad Laboratories, Inc. for ssDNA purification. C_{18}ZipTip™ was bought from Millipore for DNA desalting before MALDI measurements. Gold substrates (50Å Chromium followed by 1000Å gold on a float glass) were purchased from Evaporated Metal Films (Ithaca, NY). Gold chips for surface plasmon resonance measurements were prepared in house by evaporation 20Å chrome at a rate of 0.2Å/sec, followed by 480Å gold at a rate of 2Å/sec on BK7 glass.

3.2.2 DNA Sensing Using Multi-Initiator Labeled Detector Probes

Preparation of Citrate-Coated Au Nanoparticles. All glassware and stir bar were cleaned in aqua regia (3:1 HCl:HNO_3), rinsed with Millipore water, and then oven dried before use. Through the whole synthesis process the solution was vigorously stirred to keep the homogeneity of the solution. An aqueous solution of $HAuCl_4$ (1mM, 250ml) was heated in a sand bath and refluxed for 10min. Then a trisodium citrate solution (38.8mM, 25ml) was quickly mixed with the refluxed $HAuCl_4$ solution. A rapid color change from pale yellow to deep red indicated the formation of gold nanoparticles. After the color change the solution was refluxed for an additional 15min and allowed to slowly cool down to room temperature in the sand bath. The deep red solution was finally filtered through a 0.22μm cellulose nitrate filter.

Preparation of BSPP-Coated Au Nanoparticles. The citrate to BSPP substitution reaction was carried out in a round bottom flask equipped with a magnetic stir bar. An aqueous solution of citrate-coated nanoparticles (10mL) were added to the flask and stirred. Then a large excess of BSPP (25mg) was added to the flask while the colloidal suspension was stirred vigorously. The mixture was allowed to react overnight under constant stirring. The colloidal particles were precipitated by adding sodium chloride powder to the stirred solution until the colloidal suspension turned gray/brown. The gray/brown solution was centrifuged for 15min at 13,000rpm until a black pellet was formed at the bottom. The pellet was resuspended in 1mL 250mg/mL BSPP solution and the final solution was stored at 4°C in an eppendorf tube.

Preparation of Multi-Initiator Labeled Detector Probes. Before synthesis of DNA gold nanoparticle conjugates, the single stranded oligonucletide **Nano-A-IN-SH** (**Table 3.1**) with free thiol and initiator of ATRP reaction was prepared as following. The coupling of the initiator to DNA **Nano-A** was conducted using the following protocol: 40µL 10 x conjugation buffer (1.0M $NaHCO_3$ / Na_2CO_3, pH9.0), 280µL 100µM disulfide bond protected single strand oligonucleotide aqueous stock solution and 80µL of freshly prepared NHS active ester DMF solution (10mg/mL) were added into a 1.5mL eppendorf tube and stirred well for 0.5hr at room temperature. The coupling reaction was near completion within 0.5hr according to MALDI-TOF data. Then 480µL 0.1M DTT stock solution and 19.2µL triethylamine (TEA) were added into the tube containing DNA **Nano-A-IN** and stirred well at room temperature for 20min to cleave the mixed disulfide.

The reaction mixture of DNA **Nano-A-IN-SH** was purified into 10mM phosphate buffer through a desalting NAP^{TM}-10 column. The oligonucleotide was reduced completely as observed via MALDI-TOF. The concentration of purified DNA concentration was determined by UV-vis absorption at 260nm. The single strand oligonucleotide **Nano-D-SH** was prepared by mixing 100μL ssDNA **Nano-D** 100μL 0.1M DTT, 5μL TEA and 45μL water together for 20min, followed by filtration purification and UV-vis quantization.

Oligonucleotide gold nanoparticle bioconjugates were then synthesized by mixing aqueous 13nm diameter BSPP-coated Au nanoparticle solution (=122nM) with an oligonucleotide mixture of two ssDNAs (**Nano-D-SH** and **Nano-A-IN-SH,** at the molar ratio of 1 to 8, 5-15μM) in 10mM phosphate buffer at the molar ratio 1 to 500. The final volume was adjusted to 900μL using 10mM phosphate buffer. After standing for 16hr, the solution was stepwise mixed with 100μL 1 M NaCl, 10mM phosphate buffer (pH7) (10μL/30min) and allowed to stand for 2 days, followed by centrifugation for at least 30min at 13000rpm to remove excess reagents. Following removal of the supernatant, the red precipitate was washed with 200μL of stock 0.1M NaCl, 10mM phosphate buffer (pH7) solution, centrifuged, and redispersed in 0.5mL of DI water.

Capture Probe Immobilization. Complementary capture probe **Nano-C** and noncomplementary capture probe **Nano-NC** were immobilized onto gold surface according to previous published protocol.[14] Briefly, probe **Nano-C** and **Nano-NC** were

reduced by DTT and purified by column filtration, followed by spotting onto the gold surface and incubation in a humid chamber 3hr.

Three-strand DNA Hybridization and Ligation. Probe **Nano-C** and **Nano-NC** immobilized substrate was incubated with 10nM target DNA **C'D'** in 8 x PBS for 2.5hr, followed by incubation with 5nM nanoparticle detector in 2 x PBS for 1hr. After the two –step hybridization CNBr chemical ligation was conducted by dipping the substrate into a solution containing 0.25M MES and 0.5M CNBr at 0°C for 1min.

ATRP Reaction for DNA Detection. ATRP amplification was subsequently carried out for 5hr at optimized catalyst concentration (23mM CuCl/30%$CuBr_2$ /bpy). The substrate was subsequently immersed into 10mL DMF containing 2-bromoisobutyryl bromide (0.08M) and TEA (0.1M) for 20min.

3.2.3 Formation of Branched Polymer

*Capture Probe Immobilization; Initiator Coupling to Detection Probe (**D**); Three-strand DNA Hybridization; DNA Ligation and ATRP Reaction for DNA Detection* were done as described in Chapter 2 including all the ssDNA used. A second-stage 30min ATRP reaction was conducted following the subsequent anchoring of additional initiators on the PHEMA that was formed during the first-stage polymerization. The branched polymer was also formed on the top of **Nano-A-IN-SH** that was pre-immobilized on the gold surface to mimic the ligation product.

3.2.4 Minimization of Background Noise by Optimization of Surface Passivation Layer

SPR Measurements. Most monolayers were prepared by immersing the regular gold substrates or the SPR gold substrates into 1mM SAM molecules (6-mercaptohexanol in H_2O, or 1-octadecanethiol (ODT) in absolute ethanol, or OEG7 in H_2O/95% ethanol/dry THF). The OEG7 monolayers were also prepared by time-sequentially spotting 2μl/spot of 1mM OEG7 in H_2O onto the same SPR substrate at different period of time (from 1s to 3days) in a humid chamber. 2μL 1mM 6-mercaptohexanol in H_2O with incubation time 1hr was spotted onto the same surface as reference.

In protein absorption experiments, the baseline of the SPR signal intensity was stabilized in 10mM PBS buffer (pH7.4) first. After baseline stabilization, the surface was continuously washed with 10mM PBS buffer for 3min, then an aqueous solution of protein (1mg/mL BSA, or lysozyme in 10mM PBS) or 50%HEMA or 15%PEG 8000 was passed through the SPR sample cell for 10min. Finally the surface was washed with 10mM PBS buffer until the SPR signal was stable.

SPR Real-Time Hybridizations. The SPR surface coated with ssDNA probes was prepared according to our published protocol with minor modifications.[15] Briefly, the oligonucleotide capture probes **C** and **NC**, were reduced by DTT at the presence of TEA to generate free thiol groups for surface immobilization. After reduction, the excess amount of DTT was removed using a NAP^{TM}-5 column. The concentrations of the reduced oligonucleotides were determined by the UV absorbance at 260nm. Freshly reduced capture probes at 1μM in a KH_2PO_4 buffer (1M, pH4.4) were spotted onto Au

substrates at room temperature and incubated in a humid chamber for 16-20hr. The surfaces were then incubated with 1mM OEG7 95% ethanol solution (or 1mM MCH in H_2O) for 1hr, followed by copious rinsing with 95% ethanol (or H_2O) and dried under compressed air.

Probe **C** and **NC**-attached SPR surface was installed into the SPR sample cell and incubated with 1M NaCl TE buffer until baseline was stable. After baseline was stabilized, the real-time SPR hybridization experiment started. Firstly, the surface was continuously washed with 1M NaCl TE buffer for 2min, then an aqueous solution of 1μM target DNA **C'D'** in 1M NaCl TE buffer was passed through the cell for 5min, followed by the wash step using 1M NaCl TE buffer for 2min.

3.2.5 Instrumentation

The use of Voyager^{TM} DE-STR matrix-assisted laser desorption/ionization mass spectrometry (MALDI-MS), SPRimager®, VB-250 VASE ellipsometer, and CAM 200 optical contact angle meter was described in Chapter 2.

Reflectance FTIR spectroscopy was performed using a Digilab spectrometer containing a PIKE grazing angle (85º) attachment. The spectra were typically collected with 128 scans using a MCT detector.

The topology and roughness measurements of polymer film formed on the substrates were measured using a Digital Instruments Nanoscope IIIa (Digital Instruments, Inc.) AFM microscope images were collected in tapping mode. The scan resolution was set at 512 points/line, the scan rate at 1Hz, and the scan area of 2.5μm x

2.5μm. The scale bar of z-values was adjusted depending on surface roughness, and was placed besides the images. The RMS values were calculated with the vendor-provided software.

All surface measurements were conducted with dried samples.

3.3 Results and Discussion

3.3.1 Multi-Initiator Labeled Detector Probes in DNA Sensing

In the ATRP-based DNA detection method described in Chapter 2, one initiator was attached at one detector DNA probe and the polymer growing from this initiator contributed to hybridization signal amplification.[14] Under non-optimized conditions, 1μM target DNA can be detected by the naked eye after 5hr ATRP, followed by 20min initiator coupling. One strategy to detect lower concentration of target DNA is to increase the number of initiators per target DNA on the surface after hybridization and ligation. A straightforward way to increase the amount of initiators is to couple multiple initiators at the end of each detector DNA probe. Taking advantage of larger surface areas provided by Au nanoparticles (GNPs), multiple initiators were attached to each gold nanoparticle and the particle was used to replace the original a single initiator at the end of each detector probe. Subsequent ATRP reaction resulted in the growth of multiple polymer chains from each DNA binding site, as illustrated in **Scheme 3.1.**

Two ssDNAs of 35mer in length (**Nano-D-SH** and **Nano-A-IN-SH**) were coated on 13nm BSPP-coated GNPs. The number of ATRP initiators per GNP was determined by the size of GNP, the size of ssDNAs, and the ratio between the two ssDNAs.

According to literature, the saturated number of ssDNA per 13nm particle is 120±20 and 90±10 stands per particle for 12 and 25 base thiol labeled ssDNA, respectively.[16] Thus, it was estimated ~60 copies of 35mer ssDNAs on Au surface. Given the mixing ratio of **Nano-D-SH : Nano-A-IN-SH** at 1 : 8, an approximated ~ 50 ATRP initiators were expected to present an each particle. A 10nM target DNA **C'D'** was introduced and hybridized with the complementary probes **Nano-C** on the surface. The multiple initiator-coated GNP detector probes were subsequently attached to the complementary probe positions through the hybridization between **Nano-D-SH** and target DNA **C'D'**.

After ligation, 5hr ATRP was conducted and the substrate was subsequently incubated in initiator coupling solution for 20min. The two white spots at the complementary positions were visible to the naked eye (**Figure 3.1**), which was not detectable with single ATRP initiator detection. In comparison, the panel B in **Figure 3.1** showed the detection of 1μM target DNA using the old single initiator reaction. The less discernable spots suggested an around 50x improvement in detection sensitivity was achieved. The method illustrated here is just to show the potential improvement of the detection sensitivity of the ATRP based DNA detection method by using multiple initiator labeled detector tags.

3.3.2 Formation of Branched Polymer in DNA Sensing

Alternatively, the linear PHEMA grown atop DNA molecules in the first 30min ATRP reaction was used as an anchor layer to provide multiple initiators for polymer growth (**Scheme 3.2, A**). Additional 2-bromoisobutyryl bromide initiators were coupled

to the hydroxyl groups on the side chains of the anchor PHEMA. These initiators were subsequently used in the second round of 30min ATRP reaction to form branched PHEMA (**Figure 3.2, left**). This concept was first demonstrated on a ssDNA model using **Nano-A-IN-SH** to mimic the ligation product. Direct surface inspection after each surface modification step illustrated the formation of a much thicker layer of polymeric material as the optical clarity of the surface drastically changed (**Figure 3.2**). The stepwise changes of surface were also evidenced by FTIR measurements in **Figure 3.3**. The FTIR signal intensities significantly increased after linear polymer formations and subsequent modifications. The successful acetylation was indicated by the apparent decrease of the absorption peak of hydroxyl groups (3500-3300cm^{-1}) and a large increase of carbonyl peak around 1700cm^{-1} in the FTIR measurements. The acetylation and branched polymer formation significantly changed the reflective index of the surface, which rendered the visibility of those films. This visibility by naked eyes sets the foundation for its applications in detector-free sensing technologies.

Atom force microscopy (AFM) was performed to examine the nanoscale surface topography of linear PHEMA and branched-PHEMA layers, and understand the dramatically improved visibility. **Figure 3.4, A** shows a typical phase and topographic scan of the linear PHEMA layer. It reveals that the surface had a root-mean-square roughness, RMS= 0.8 nm. Compared to linear PHEMA film, the branched-PHEMA film was much rougher and isolated domains were visible (**Figure 3.4, B**). An average RMA of 12nm was measured. This roughness could be the main reason of improved visibility as the increased scattering occurs.

The formation of branched polymer was successfully used in DNA sensing. 1nM target DNA was readily discernable to the naked eye (**Figure 3.5**) after two-time ATRP. Considering the small volume of the hybridization solution used (1.5μL), this change corresponded to the detection of 1.5femtomole of 30-mer oligonucleotide without the aid of any detectors. Note that the irregularity in the spots was not from surface chemistry heterogeneity. Rather, it was from the physical scratches of the surfaces during substrate handlings.

Similarly, the formation of an ultra-thick film using this two-stage ATRP DNA sensing strategy was also evidenced during surface characterization. The ellipsometer was used in previous studies failed to give an accurate readout because the film thickness had exceeded the measurable range of the instrument and surface roughness. A local examination of the surface using an atomic force microscope (AFM) revealed the formation of polymer islands on the surface with feature heights exceeding 200nm (**Figure 3.6**). These large individual features were attributed to the formation of branched polymers. The AFM images again revealed a pronounced difference in surface roughness between the substrates prepared from the two-stage ATRP as compared to the one-time ATRP reaction. The root-mean-square (RMS) roughness was 37.2nm and 1.81nm for the substrates prepared from two-stage and one-time ATRP, respectively. In addition, it is worth pointing out that the reaction time was also significantly shortened from a 5-hr linear reaction to 2 x 30min reactions in the formation of branched polymers.

3.3.3 Reduction of Background Noise

Detection sensitivity of any sensors in is decided by its signal output and the background noise level, i.e. the S/N ratio. Therefore, it is critical for all sensing technologies to minimize non-specific absorptions and increase signal noise ratio in order to achieve better sensitivity. Surface passivation is one of the key approaches used to reduce the non-specific absorptions during DNA sensing process. In the ATRP-based DNA sensing method, one of the major nonspecific absorptions was found in the ligation step, where DNA enzymes nonspecifically absorbed on the surface.

Due to its commercial availability, low cost, and most importantly, its potential in protein resistance, $[CH_3(OCH_2CH_2)_7S]_2$ (OEG7) was selected to replace MCH. $[CH_3(OCH_2CH_2)_7S]_2$ (OEG7) was used here also because of its better storage stability compared to the corresponding free thiol molecule to improve reproducibility of SAM preparations. Another advantage of using disulfide OEG7 is its relative small immobilization kinetic rate, which helps us to control the surface coverage simply by shortening/lengthening the incubation time.

Surface Coverage of OEG7 in Protein Resistance. In this study, BSA (MW = 67kDa, pI = 4.7) was used as the model protein to study the protein rejection ability of a surface. SPR, with great sensitivity to surface binding, was used for real-time detection of protein adsorption on gold surfaces. To minimize the experimental errors introduced by the use of different SPR substrates, the OEG7 coatings of different incubation time were prepared on the same SPR surface in an array as shown in **Figure 3.7** (top). The amount

of BSA adsorbed on different surfaces were shown in **Figure 3.7** (bottom). An increase in SPR intensity after the introduction of 1mg/mL BSA solution was attributed to the non-specific adsorption of protein molecules on the surface, with higher changes the more bound protein molecules. As expected, a significant amount of BSA was adsorbed on the bare gold surface. A continuous decrease in nonspecific protein binding was observed with an increased OEG7 incubation time. Eventually, the amount of BSA adsorbed on a substrate pre-incubated with 1mM OEG7 for one day was less than 0.7% of what was adsorbed on the bare gold surface (**Figure 3.8**). To quantitatively evaluate the surface resistance to proteins, **Figure 3.8** shows the plotting of the relative percentage of BSA nonspecifically absorbed on the surfaces to that on an uncoated gold surface as a function of the substrate incubation time in OEG7. The absorption of BSA decreased rapidly within the first hour of the incubation, with ~50% decrease in the first 5min (**Figure 3.8** inset). After approximately 15hr incubation in 1mM OEG7, the amount of OEG7 absorbed and the molecular conformation on the SPR surface reached equilibrium, evidenced by the negligible changes in protein adsorption.

Solvent Effects in OEG7 Immobilization and Protein Resistance. It is known that the solvent used in surface preparation also has a determining impact on the molecular conformation formed, and subsequently the anti-fouling property of the surface. Considering a less polar solvent would advance the formation of less-ordered OEG-terminated coatings, a less ordered molecular conformation was expected when the surface was prepared in dry THF verse 95% ethanol. In-situ real time SPR was again

used to measure the ability of OEG7-based SAMs to prevent surface nonspecific adsorption. All the surfaces with OEG7 coatings prepared from different solvents (water, 95% ethanol or THF) showed better protein resistance, albeit to different degrees, than those with MCH coatings (**Figure 3.9**). Among the three solvents used, the surface prepared in THF showed the best resistance to BSA. Lysozyme, 15% PEG8000, and 50% 2-hydroxyethyl methacrylate in water were also tested in addition to BSA for OEG7/THF-caoted surface to mimic the chemical environment during DNA ligation and ATRP amplification. The resistance to nonspecific adsorptions was found to be universal, with negligible bindings of lysozyme, 50% HEMA and 15% PEG8000 on the surface (**Figure 3.10**). The observation was confirmed in the ellipsometric measurements to quantify the amount of nonspecific adsorption on various chemically protected surfaces (**Figure 3.11**). Compared to the most popular used SAMs (MCH or ODT), the surfaces with OEG7 coatings illustrated better nonspecific absorption resistance throughout. Especially for the sample prepared in 1mM THF solution of OEG7 for 1hr with no measurable changes in film thicknesses after incubation in 1mg/mL BSA.

Proposed Mechanism of OEG7-coated Surface in Protein Resistance. Extensive theoretical and experimental studies have been conducted to understand the mechanism for OEG-based SAMs to resist protein nonspecific absorption. Several models have been suggested in the development of a global mechanism to explain the experimental data reported to date. For example, De Gennes *et al* have postulated that the protein resistance of PEG terminated surfaces results from the disfavored energy consumption in order to

release the water molecules in the hydrated PEG chains when proteins approach the surface.[19,20] The model explains well the observation where the longer chain lengths and higher surface densities provided better protein resistance, but failed in understanding the presence of the optimized surface density to resist the nonspecific absorption of proteins for several PEG- and OEG-terminated molecules. Szleifer has improved De Gennes' model by adapting the single-chain mean-field (SCMF) theory to calculate the effective size of the polymer chain. The calculation illustrated that the most important parameter in preventing protein absorption by grafted polymer was the surface density only, whereas the polymer chain length had a weak impack.[21, 22]

While Szleifer's model was able to explain experimental results for short oligo(ethylene glycol) (OEG) terminated SAMs, both De Gennes and Szleifer's models provide no molecular-level information regarding the mechanism of protein resistance. Whitesides *et al* have concluded four common features of optimal SAMs to resist protein nonspecific absorption: hydrophilic, electrically neutral, being hydrogen bond acceptors but not donors.[23] Jiang's and Grunze's groups pointed out the importance of the surface density of hydrogen bonds by molecular simulation studies.[24,25] The ability of OEG surface resistance of protein was correlated with the surface chain density of OEG, the amount of water tightly bound to OEG chains and the flexibility of the chains. They found that the OEG-based SAMs with highly hydrated chains and larger mobility contained a large amount of hydrogen bonds with water, leading to better protein resistance. Similarly, Vanderah *et al* found that BSA only absorbed onto the most ordered

helical $HS(OCH_2CH_2)_6CH_3$ SAMs, but not onto the disordered ones, as a result of low mobility of the SAMs of ordered SAMs.[11]

Experimental results have shown the presence of an optimal surface coverage of $HSCH_2CH_2CH_2O(CH_2CH_2O)_5CH_3$ prepared from aqueous solution at 60-80% to inhibit protein absorption.[12] Zheng *et al* have also reported the presence of an optimized surface coverage range (60-80%) of $HS(CH_2)_{11}O(CH2CH2O)_4CH_3$ for protein resistance.[18] Similarly, Brash *et al* has found that 750 and 2000 MW Polyethyleneglycol layers were most resistant to fibrinogen absorption (80% decrease in absorption compared to the bare gold surface) when surface density was 0.5chain /nm^2. Deviation from this optimal surface density in either direction resulted in increased nonspecific absorption.[10]

In our study, the performance of the disordered OEG7 monolayers prepared from dry THF behaved as expected according to Vanderah's findings. On the other hand, a closely packed, ordered OEG7 SAM formed in aqueous solution also efficiently prevents the non-specific protein absorption as well. Indeed, a monotonic improvement in protein resistance with increasing surface coverage of OEG7 was observed in our experiment. Reflectance FTIR was used to examine the molecular confirmation of OEG7 on the surfaces (**Figure 3.12**). Sharper vibration bands at 964, 1118, 1245 and 1348cm^{-1} in spectrum A were characteristic bands for the OEG segments in a 7/2 helical conformation, confirming our speculation that an ordered SAM layer was formed after allowing the molecules to undergo an extensive local rearrangement (1day incubation).[13] On the other hand, the shoulder band at 1142cm^{-1} and the weak band at 1323cm^{-1} in spectrum B suggested the presence of some all-trans conformation of a less ordered

structure after a merely 2hr incubation.[13] This finding contradicts to what reported by Vanderah *et al*. The rationale behind this phenomenon was not fully understood.

Impact of OEG7 Coating in DNA Hybridization. As our experimental results have shown, OEG7 SAMs prepared from 95% ethanol or THF are much better than MCH for preventing the nonspecific absorption of molecules used in ATRP-based DNA detection such as protein (BSA as model), 15% PEG8000 and 50% HEMA. More importantly, the absence of active functional groups in OEG7 molecules eliminated possible interference in the initiator coupling step and secondary ATRP. Another critical requirement in the selection of a proper passivation layer is that the molecules used should not significantly hinder the hybridization steps that are the base of most DNA technologies. In order to test the performance of OEG7 in DNA hybridization assay, two simple real-time SPR experiments were conducted on MCH and OEG7 passivated DNA monolayers, respectively. As shown in **Figure 3.13**, similar hybridization signal changes were observed from OEG7 and MCH monolayer protected surfaces. In addition, the OEG7 monolayer prevented the nonspecific absorption of non-complementary ssDNA as well.

3.4 Conclusions

The detection limit of ATRP-based DNA detection assay was improved about two orders of magnitude by using multiple initiator labeled detector probes to increase the initiator surface density. The formation of branched polymers in multistage ATRP

reaction also improved the detection limit (< 1nM) and significantly reduced the assay turn-over rate.

Oligo(ethylene oxide) ($[CH_3(OCH_2CH_2)_7S]_2$, OEG) monolayer has been formed on Au from different solvents including water, 95%ethanol and dry THF. Ellipsometric, contact angle and Surface Plasmon Resonance (SPR) measurements have been conducted to examine their abilities to prevent nonspecific absorption of proteins (BSA), synthetic polymers (PEG 8000) and small organic molecules (2-hydroxyethylmethacrylate). It was found that longer incubation time with thiolated OEGs resulted in better prevention of protein absorption when the monolayer was prepared from water. For the OEG monolayers prepared for 1hr, the monolayer formed from 95% ethanol exhibited better protein resistance compared to the monolayer prepared from water. No detectable BSA absorption was observed when the monolayer was formed from dry THF. The finding was applied in a two-step surface modification procedure for the creation of DNA arrays on the gold surface. The ssDNA/OEG7 mixed monolayer mainteined the hybridization efficiency to the level similar to ssDNA/MCH mixed monolayer.

Schemes

Scheme 3.1: Schematic Drawing of Initiator labeled GNP-Based DNA Detection.

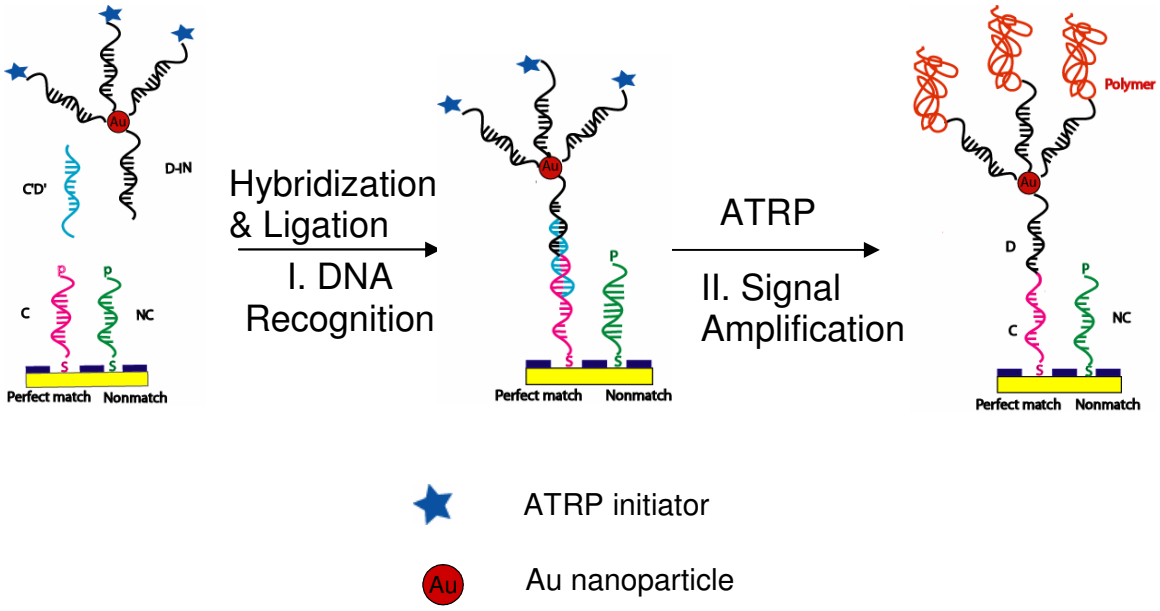

Scheme 3.2: Chemical Formation of PHEMA in DNA Detection.

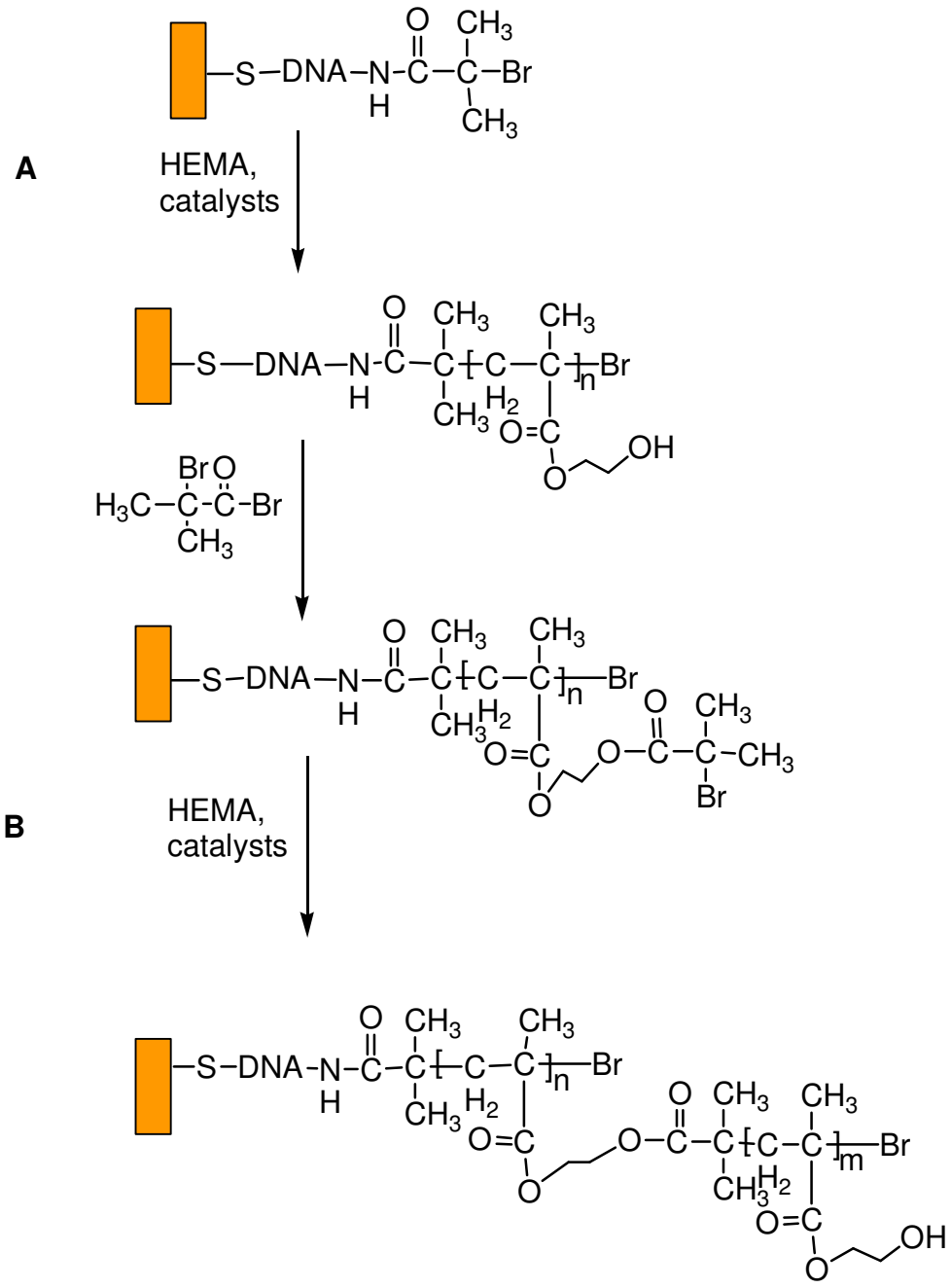

Tables

Table 3.1 Summary of the DNA Sequences Used in This Chapter.

Name	Sequence	Description
Nano-C	5'-TAA CAA TAA TCC CTC AA A_{18}-C_3-S-S-C_3	Capture probe partially complementary to **C'** portion of target **C'D'**
Nano-NC	5'-GGC AGC TCG TGG TGA AA A_{18}- C_3-S-S-C_3	Non-complementary capture probes to target **C'D'**
C'D'	5'-GAG GGA TTA TTG TTA AAT ATT GAT AAG GAT	Perfectly matched target DNA complementary to probes **Nano-C** and **Nano-D**.
Nano-D	5'C6-S-S-A_{21} TCC TTA TCA ATA TTp	Detector probe partially complementary to **D'** portion of target **C'D'**
Nano-D-SH	5'-HS-A_{21} TCC TTA TCA ATA TTp	Free thiol detector probe partially complementary to **D'** portion of target **C'D'**
Nano-A	5'-NH_2-C_6-TAA CAA TAA TCC CTC A_{20}- C_3-S-S-C_3	Initiator anchor on gold nanoparticles
Nano-A-IN	5'-Br$(CH_3)_2$CCONH-C_6-TAA CAA TAA TCC CTC AA A_{18}- C_3-S-S-C3-OH	Initiator-coupled **Nano-A**
Nano-A-IN-SH	5'-Br$(CH_3)_2$CCONH-C_6-TAA CAA TAA TCC CTC AA A_{18}- C_3-SH	Initiator and free thiol-coupled **Nano-A**
C	5'-pTAA CAA TAA TCC CTC AA A_{18}-C_3-S-S-C_3	Capture probe partially complementary to **C'** portion of target **C'D'**
D	5'-NH_2-C_6-A_{18} AAA TCC TTA TCA ATA TT	Detection probe partially complementary to **D'** portion of target **C'D'**
D-IN	5'-Br$(CH_3)_2$CCONH -C_6-A_{18} AAA TCC TTA TCA ATA TT	Initiator-coupled **D**
NC	5'-pGGC AGC TCG TGG TGA AA A_{18}- C_3-S-S-C_3	Non-complementary capture probes to target **C'D'**

Figures

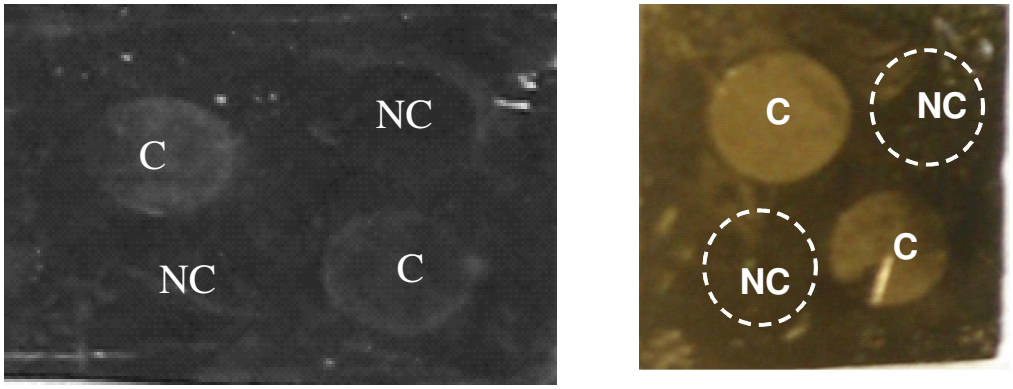

(A) (B)

Figure 3.1 Photo after 5hr ATRP amplification of (A)10nM target DNA using multiple initiator-labeled detector probes and (B) 1μM target DNA using single initiator-labeled detector probes.

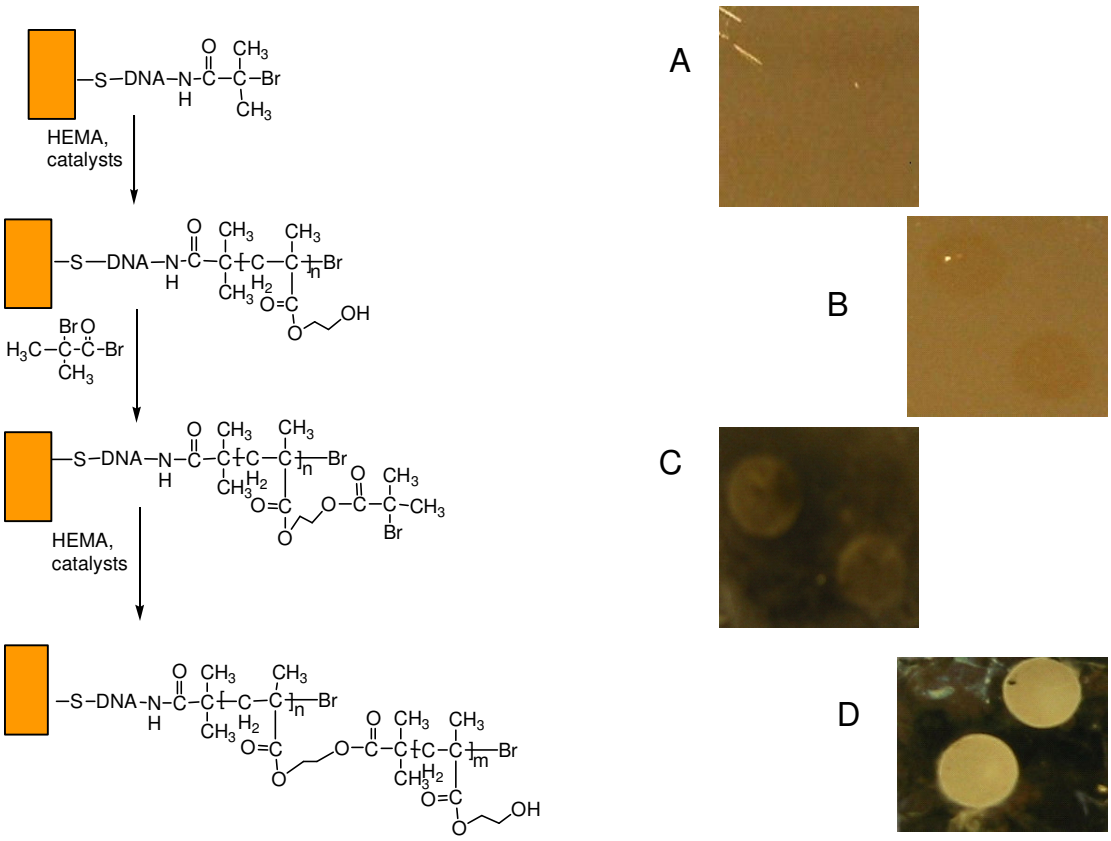

Figure 3.2 The increased visibility of films: A) ssDNA (1.6nm); B) PHEMA (16nm); C) PHEMA after acetylation; D) Branched PHEMA.

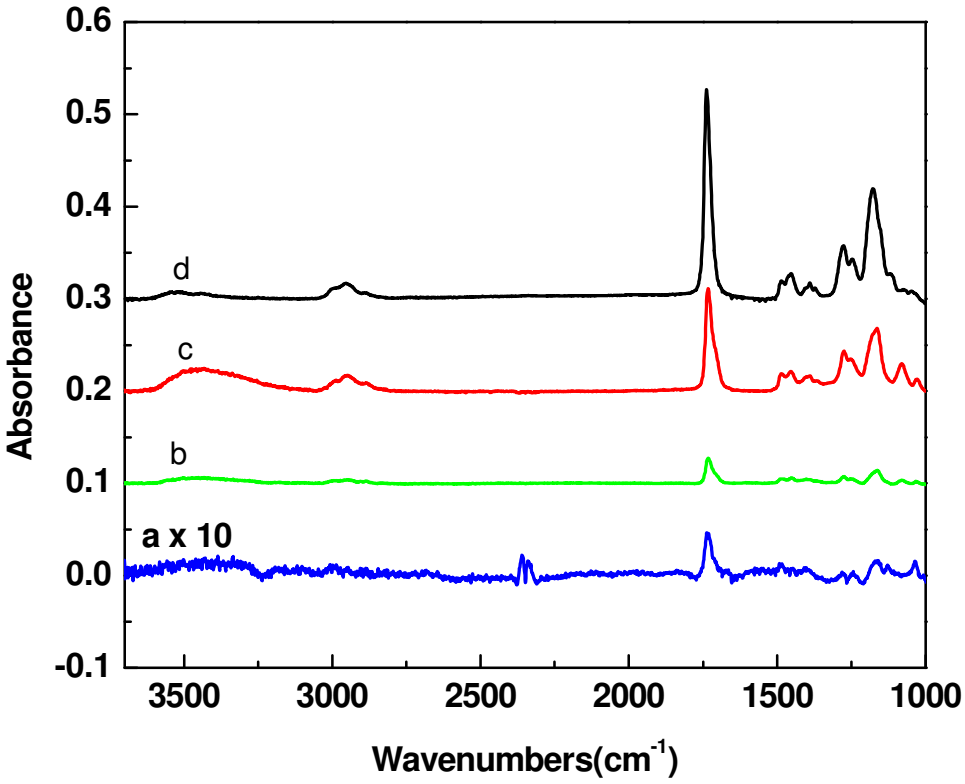

Figure 3.3 Reflective FTIR spectra of (a) a DNA and MCH mixed monolayer after DNA ligation, (b) a grafted PHEMA layer (7nm), (c) an opaque PHEMA layer after 2nd ATRP, and (d) opaque PHEMA film derivatized with Bromoisobutyryl bromide.

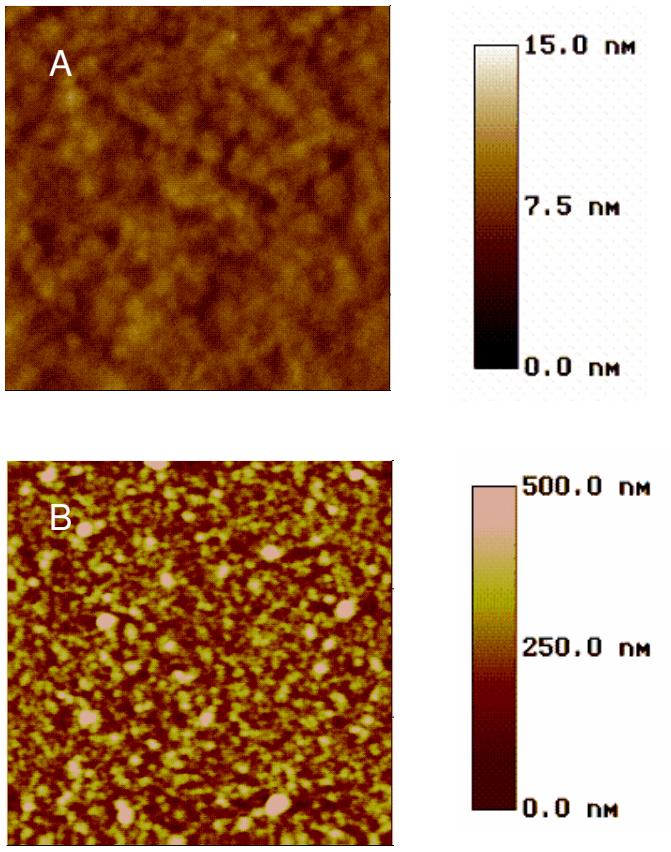

Figure 3.4 Representative AFM 2D images of (A) linear PHEMA layer (1μm x 1μm) and (B) branched-PHEMA layer (30μm x 30μm) prepared by ATRP. The scale bars showing surface roughness are placed on the side of the images.

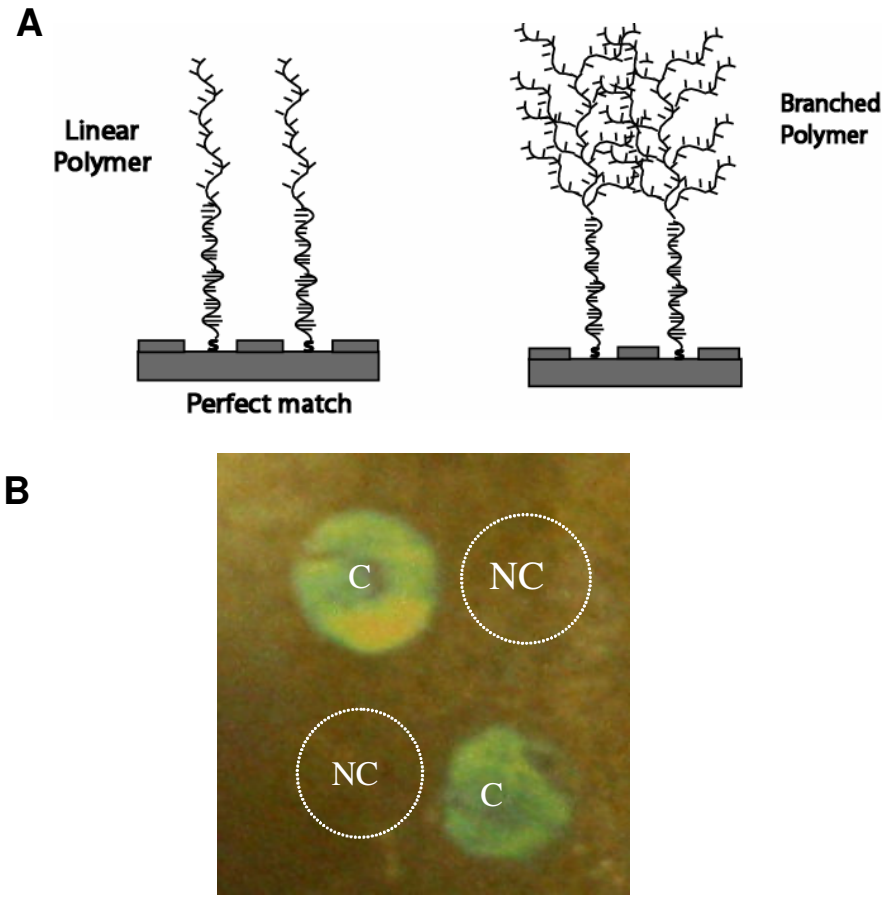

Figure 3.5 (**A**) The concept of a two-stage ATRP reaction to form branched polymers. Note that the polymer structure was significantly simplified and no unique conformation of linear/branched polymers was suggested in this scheme. (**B**) A photograph of 1nM target DNA **C'D'** detected after the two-stage ATRP reaction. The spots immobilized with the complementary probes showed significant color change (**C**), whereas the control spots remain unchanged (**NC**). The dotted circles are guides to the eye. Detailed ATRP reaction conditions see the text.

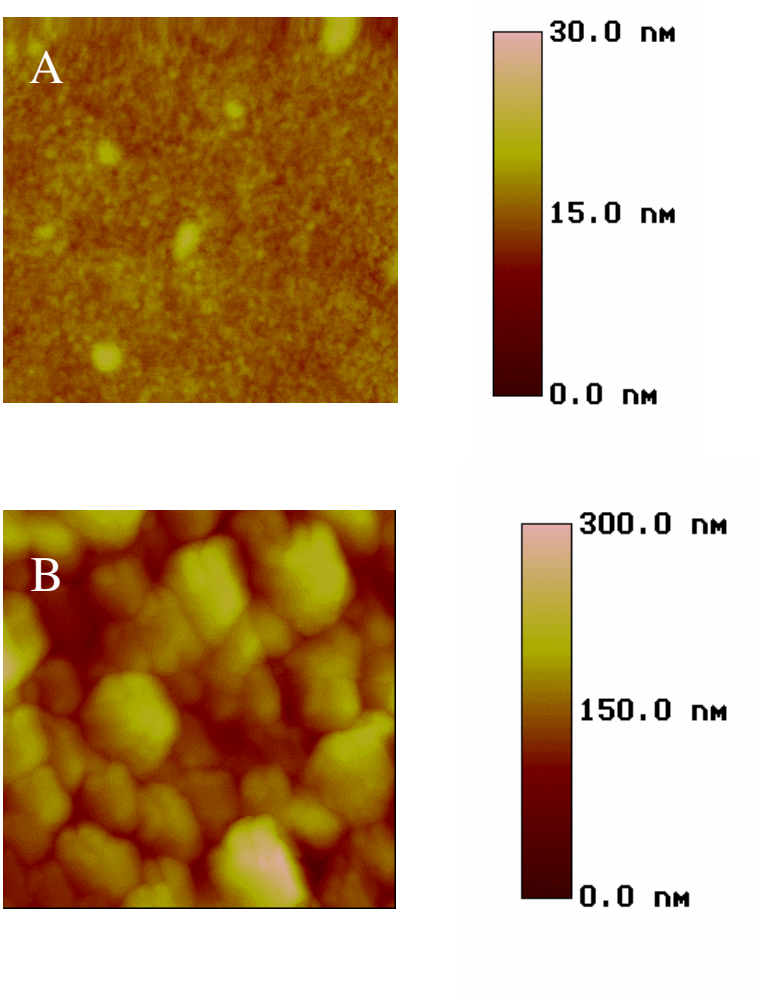

Figure 3.6 AFM images of PHEMA films grown on DNA-coated Au substrate after hybridization, ligation and (**A**) a 5hr ATRP reaction and (**B**) after two 30-min ATRP reaction. The images are 2.5µm x 2.5µm. The scale bars showing surface roughness are placed on the side of the images.

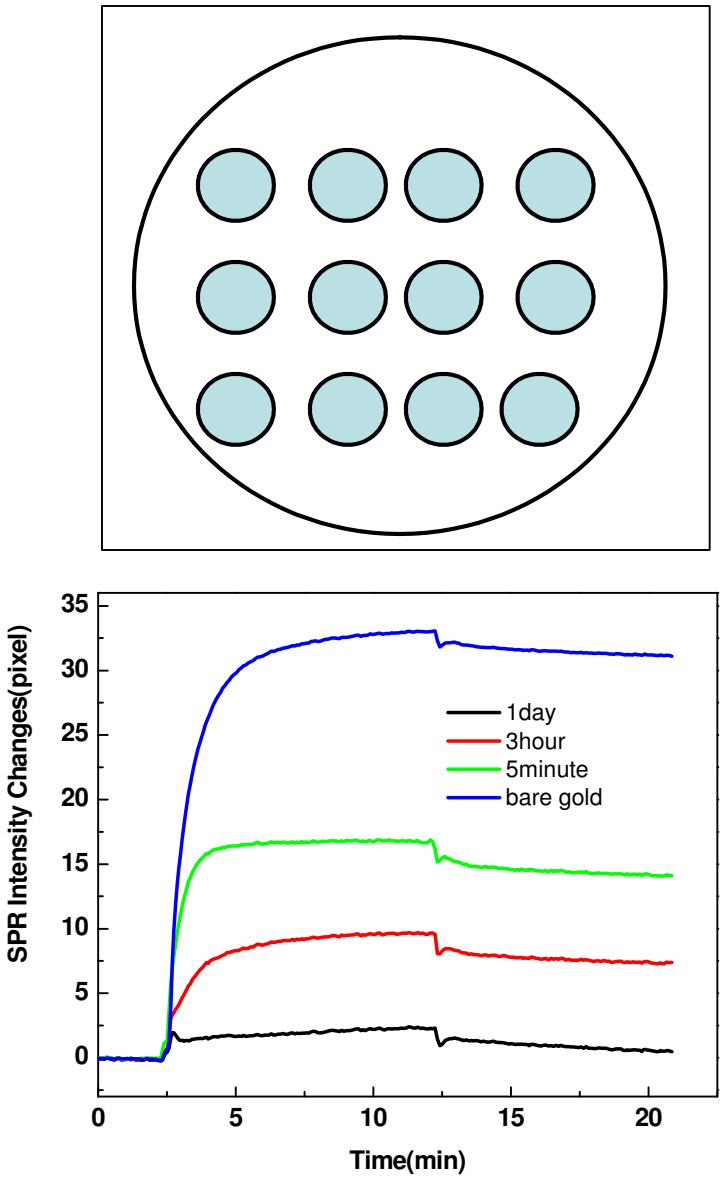

Figure 3.7 (Top) OEG7 monolayers preparation on SPR substrates and (bottom)SPR sensorgrams of BSA(1mg/mL) absorbed onto bare gold surface (blue lines) and OEG7-SAMs prepared from 1mM OEG7 aqueous solution for different incubation time: 1day (black lines), 3hr (red lines) and 5min (green lines).

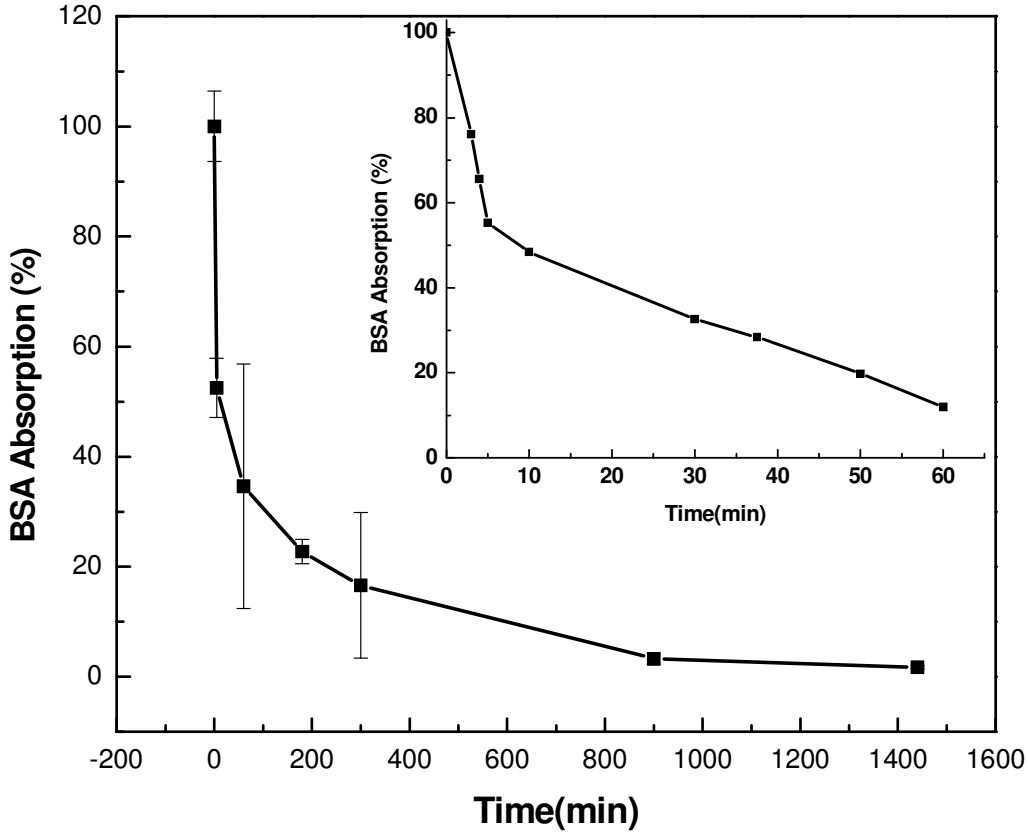

Figure 3.8 The percentage amount of BSA absorbed onto the surface as a function of incubation time in 1mM OEG7 aqueous solution.

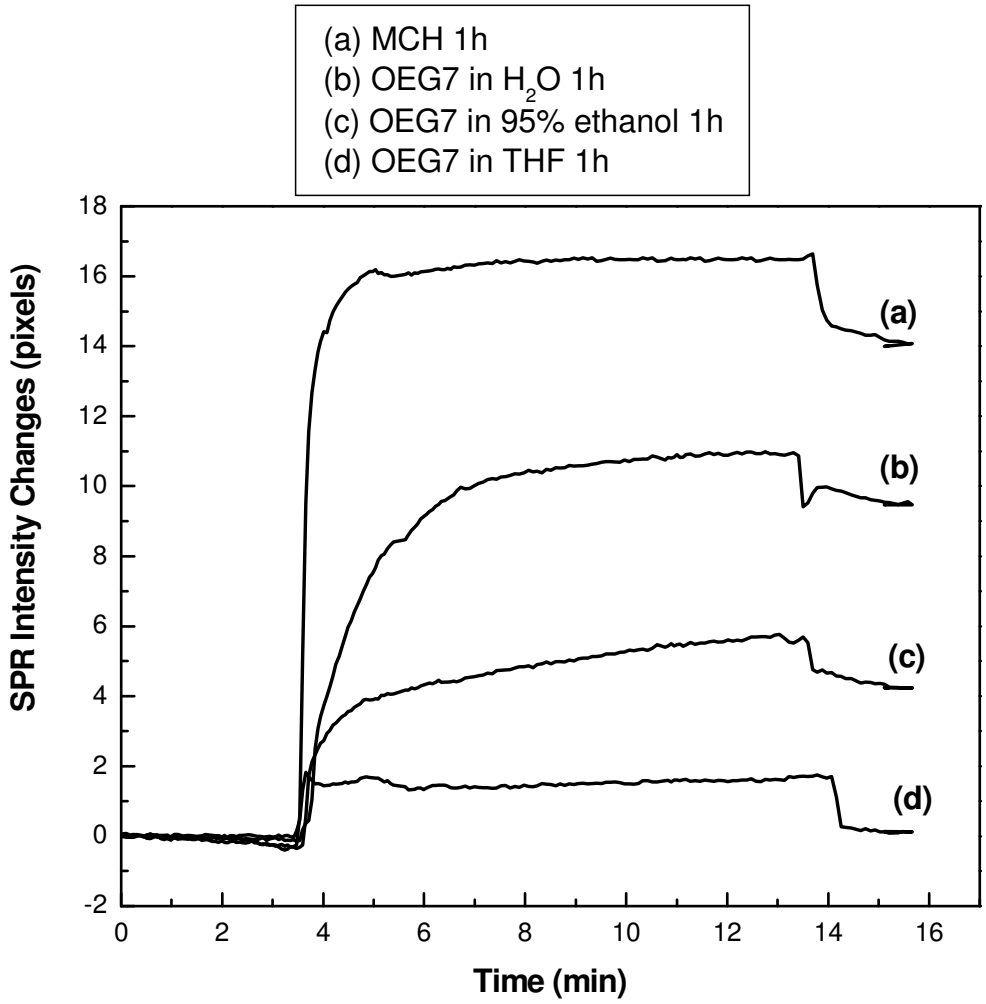

Figure 3.9 SPR sensorgrams of BSA (1mg/mL) absorbed onto (a) MCH monolayer and OEG7-SAMs prepared from different solvents: (b) H_2O, (c) 95% ethanol, and (d) THF.

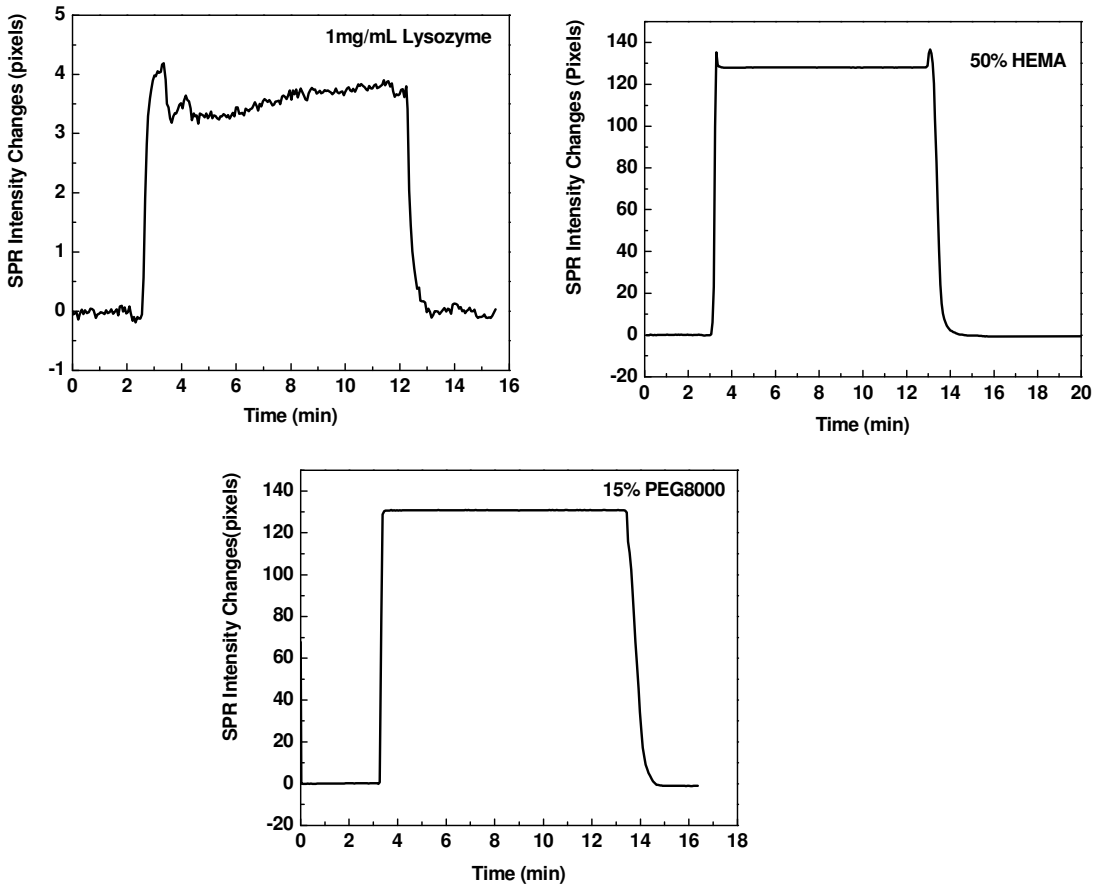

Figure 3.10 SPR sensorgrams of lysozyme (1mg/mL), 50%HEMA and 15%PEG 8000 absorbed onto OEG7-SAMs prepared from THF.

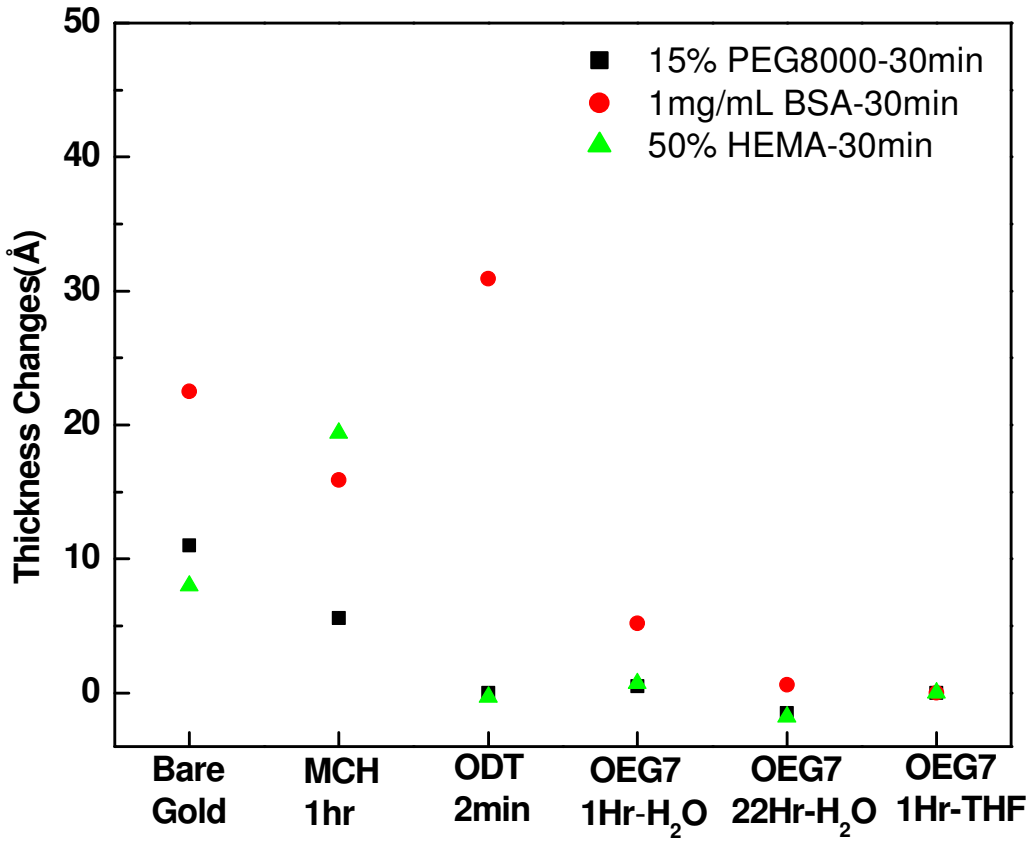

Figure 3.11 Ellipsometric measurements of different SAMs for comparison of their abilities of nonspecific absorption resistance.

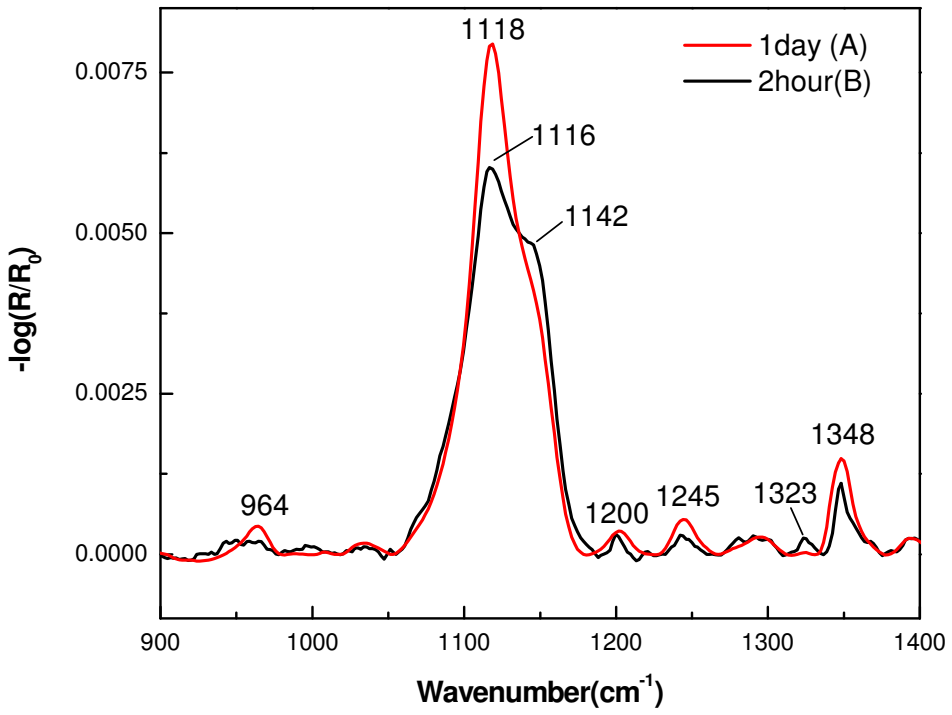

Figure 3.12 Reflectance FTIR spectra of OEG7, from 900 to 1400cm^{-1}, at different times: 2hr (black lines) and 1day (red lines).

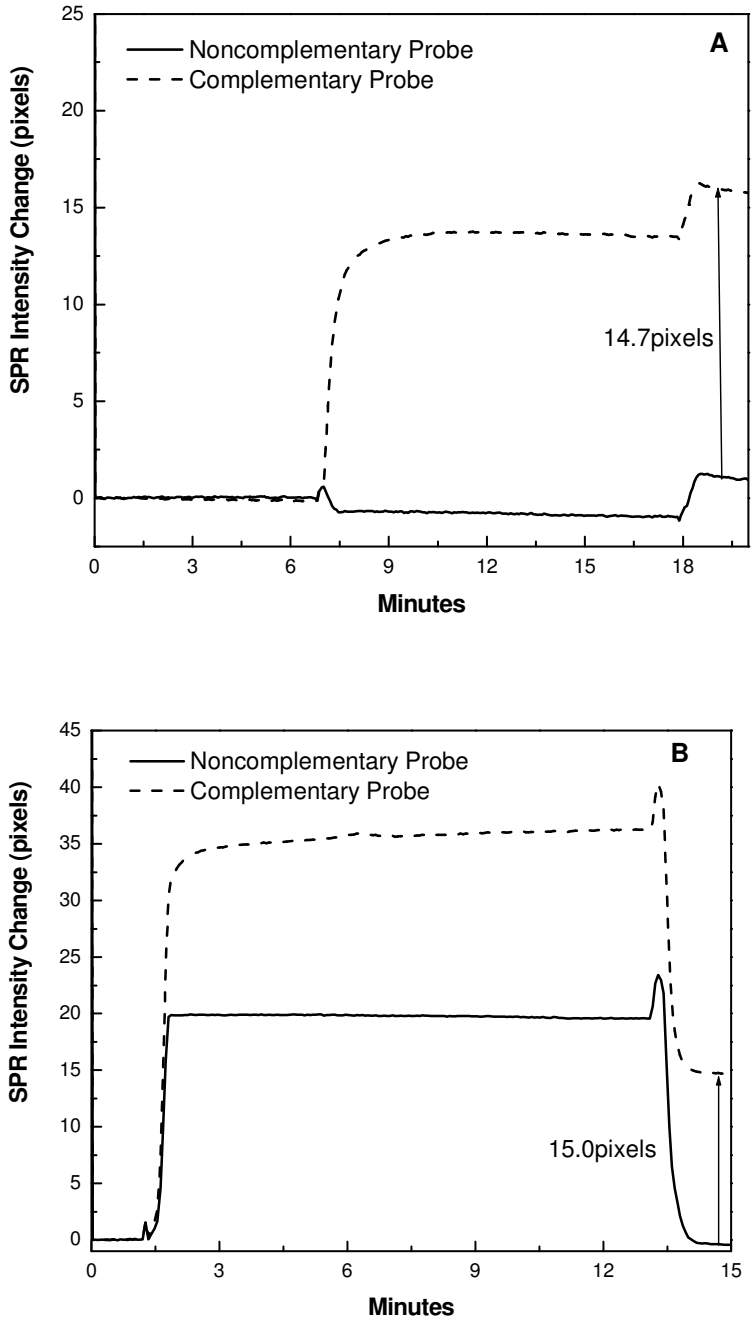

Figure 3.13 Kinetics of hybridization on (A)ssDNA /MCH and (B) ssDNA /OEG7 mixed monolayer. 1μM complementary ssDNA **C'D'** in 1M NaCl TE was flowed in.

References

(1) Herne, T. M.; Tarlov, M. J. *J. Am. Chem. Soc.* **1997**, *119*, 8916-8920.
(2) Narain, R.; Armes, S. P. *Biomacromolecules* **2003**, *4*, 1746-1758.
(3) Prime, K. L.; Whitesides, G. M. *Science* **1991**, *252*, 1164-1167.
(4) Chapman, R. G.; Ostuni, E.; Takayama, S.; Holmlin, R. E.; Yan, L.; Whitesides, G. M. *J. Am. Chem. Soc.* **2000**, *122*, 8303-8304.
(5) Murphy, E. F.; Lu, J. R.; Brewer, J.; Russell, J.; Penfold, J. *Langmuir* **1999**, *15*, 1313-1322.
(6) Chen, S.; Liu, L.; Jiang, S. *Langmuir* **2006**, *22*, 2418-2421.
(7) Chen, S.; Zheng, J.; Li, L.; Jiang, S. *J. Am. Chem. Soc.* **2005**, *127*, 14473-14478.
(8) Palegrosdemange, C.; Simon, E. S.; Prime, K. L.; Whitesides, G. M. *J. Am. Chem. Soc.* **1991**, *113*, 12-20.
(9) Prime, K. L.; Whitesides, G. M. *J. Am. Chem. Soc.* **1993**, *115*, 10714-10721.
(10) Unsworth, L. D.; Sheardown, H.; Brash, J. L. *Langmuir* **2005**, *21*, 1036-1041.
(11) Vanderah, D. J.; Valincius, G.; Meuse, C. W. *Langmuir* **2002**, *18*, 4674-4680.
(12) Vanderah, D. J.; La, H. L.; Naff, J.; Silin, V.; Rubinson, K. A. *J. Am. Chem. Soc.* **2004**, *126*, 13639-13641.
(13) Vanderah, D. J.; Arsenault, J.; La, H.; Gates, R. S.; Silin, V.; Meuse, C. W.; Valincius, G. *Langmuir* **2003**, *19*, 3752-3756.
(14) Lou, X.; Lewis, M. S.; Gorman, C. B.; He, L. *Anal. Chem.* **2005**, *77*, 4698-4705.
(15) Elhadj, S.; Singh, G.; Saraf, R. F. *Langmuir* **2004**, *20*, 5539-5543.
(16) Sandstrom, P.; Boncheva, M.; Akerman, B. *Langmuir* **2003**, *19*, 7537-7543.
(17) Narain, R.; Armes, S. P. *Chem. Commun.* **2002**, 2776-2777.
(18) Zheng, J.; Li, L. Y.; Chen, S. F.; Jiang, S. Y. *Langmuir* **2004**, *20*, 8931-8938.
(19) Jeon, S. I.; Andrade, J. D. *J. Colloid Interface Sci.* **1991**, *142*, 159-166.
(20) Jeon, S. I.; Lee, J. H.; Andrade, J. D.; Degennes, P. G. *J. Colloid Interface Sci.* **1991**, *142*, 149-158.
(21) McPherson, T.; Kidane, A.; Szleifer, I.; Park, K. *Langmuir* **1998**, *14*, 176-186.
(22) Szleifer, I. *Curr. Opin. Solid State Mat. Sci.* **1997**, *2*, 337-344.
(23) Ostuni, E.; Chapman, R. G.; Holmlin, R. E.; Takayama, S.; Whitesides, G. M. *Langmuir* **2001**, *17*, 5605-5620.
(24) Li, L.; Chen, S.; Zheng, J.; Ratner, B. D.; Jiang, S. *J. Phys. Chem. B* **2005**, *109*, 2934-2941.
(25) Pertsin, A. J.; Grunze, M. *Langmuir* **2000**, *16*, 8829-8841.

CHAPTER 4 Kinetic Studies of DNA-Accelerated Atom Transfer Radical Polymerization on a Gold Surface

4.1 Introduction

Significant advances in controlled/"living" radical polymerization, such as atom transfer radical polymerization (ATRP), have allowed us to construct well-defined polymer structures with a variety of monomers.[1-3] The tolerance towards functional groups in biomolecules and the mild reaction conditions have also rendered ATRP an ideal choice for the formation of biomolecule-containing block copolymers.[4-7] The applications of such polymer materials have been demonstrated in gene therapy, bio-implantation, and biomolecule-directed self assembly.[8-10]

We have recently described an *amplification-by-polymerization* approach in biosensing in which ATRP is used to facilitate the detection of single point mutations in DNA sequences.[11] Specifically, DNA duplexes containing surface-immobilized capture probes, DNA targets, and detection probes are formed after DNA hybridization. Subsequent ligation leads to the permanent attachment of the detection probes on the surface. Since these detection probes are pre-coupled with the ATRP initiators, the initiators are fixed on the surface simultaneously at the locations where specific DNA sequences are present. Under the proper conditions, these initiators prompt the growth of polymer brushes on the surface. The reaction results in a layer of densely packed polymer chains that changes surface opacity and enables direct visualization of the locations where DNA hybridization and ligation occurred. While our preliminary experiments have demonstrated that ATRP is inert to the multitude of functionality in

nucleotides, little is known on how the presence of DNA molecules on the sensing substrate affects the reaction kinetics. Yet, understanding such reaction characteristics directly relates to efficient optimization of ATRP reaction conditions and formation of polymers in a controllable fashion for semi-quantitative DNA detection.

The reaction kinetics for traditional ATRP reactions at the absence of DNA has been extensively studied in the past.[12-18] For example, the polarity of the reaction environment, including both surface polarity and the solvent used, has been found to affect the growth rates. Bontempo *et al.* have reported that the use of hydrophobic surfaces reduced polymer growth by limiting the diffusion of catalyst-containing polar solution towards the surface-bound initiators.[19] Several groups have reported the use of polar solvents to accelerate reaction rates.[15,19-22] The addition of a small amount of water in the reaction mixture has since been used to prepare various block copolymers.[23] The density of the initiators on surface also influences the polymer growth on a solid support. Jones *et al.* have shown a near linear correlation of PMMA film thickness with respect to surface initiator density during the first 60min ATRP reaction.[18,24] For an extended reaction (>10hr), radical termination has been suggested to occur more frequently with the increasing radius of gyration of the polymer chains formed, leading to significant observed deviation from the linear polymer growth.[15,17, 25] Studies of additional factors affecting polymer growth in ATRP, such as catalyst composition, catalyst concentration, and the choice of monomer, have all been reported.[15]

Given the significant differences in surface polarity and the initiator density in the presence of DNA molecules in our system, a departure of polymer growth kinetics

from any previously reported studies is expected. Because of the unique chemical structure of DNA molecules, the possibility of influencing the ATRP reaction kinetics by DNA participating as one of the reaction components (e.g., the nucleotide bases acting as Schiff base ligands to compete for Cu ions) also arises. This report describes our preliminary investigation of the reaction characteristics of surface-initiated ATRP at the presence of DNA molecules.

4.2 Experimental Section

4.2.1 Materials

A single stranded DNA (ssDNA), 5' NH_2-C_6-AAA AAA AAA AAA AAA AAA AAA TCC TTA TCA ATA TT-C_3-S-S-C_3-OH, was purchased from Integrated DNA Technologies, Inc. (Coralville, IA). Monomethoxy-capped oligo (ethylene glycol) methacrylate (OEGMA, mean degree of polymerization of 7-8) was a gift from Laporte Specialties (Hythe, UK). 2-hydroxyethyl methacrylate (HEMA, 98%) was purchased from Sigma-Aldrich. OEGMA and HEMA were both purified using an inhibitor remover column to remove methyl hydroquinone inhibitor. The inhibitor remover was purchased from Aldrich (cat. no. 31,134-0), and the column was packed in house. N-hydroxysuccinimide acid (NHS), bromoisobutyryl bromide, 3- hydroxypicolinic acid (3-HPA), diammonium citrate, dioxane, dithiothreitol (DTT), triethylamine (TEA), 6-mercapto-1-hexanol (MCH), 1-ethyl-3-(dimethylaminopropyl) carbodiimide hydrochloride (EDC), copper (I) bromide (CuBr), copper (I) chloride (CuCl), copper (II) bromide ($CuBr_2$), 2,2'-bipyridine (bpy), 1-undecanethiol and diethyl ether were

purchased from Sigma-Aldrich and used as received. Gold substrates (50Å Chromium followed by 1000Å gold on a float glass) were purchased from Evaporated Metal Films (Ithaca, NY). 11-Amino-1-undecanethiol was purchased from Dojindo (Kumaoto, Japan). A NAP^{TM}-5 column was purchased from Amersham Pharmacia Biotech for DNA purification. C_{18}ZipTip^{TM} was bought from Millipore for DNA desalting before MALDI measurements.

4.2.2 Immobilization of Initiator-Coupled ssDNA on Gold

The previously reported procedure was followed in the preparation of initiator-coupled ssDNA (**1**, **Scheme 4.1, D**).[11,26] Briefly, a solution of bromoisobutyryl bromide (0.22M) in diethyl ether (50mL) was cooled in an ice bath, and a solution of N-hydroxysuccinimide acid (0.43M) and TEA (0.65M) in dioxane (25mL) was added drop-wise. When the addition was completed, the reaction mixture was stirred at room temperature for 1hr, followed by the filtration to remove any precipitates. The solution was washed with saturated $NaHCO_3$ and then water and dried over $MgSO_4$. Evaporation *in vaco* resulted in 2.2g white crude solid product (yield 77%). ^{1}H NMR (in CD_3Cl, 300MHz): δ=2.8(s, 4H), 2.1(s, 6H). ^{13}C NMR (in CD_3Cl, 300MHz): δ=25.9, 30.9, 51.4, 166.2, 168.9. No further purification was required. This crude NHS active ester was directly used in the next step.

Next, 70μL of ssDNA aqueous solution at 100μM and 10μL of 10 x conjugation buffer (1.0M $NaHCO_3$ /Na_2CO_3, pH9.0) were added into a 1.5mL eppendorf tube equipped with a stir bar. Freshly prepared NHS active ester solution (10mg/mL in DMF,

20μL) was added to the aforementioned reaction mixture. The coupling reaction was finished in 30min. at room temperature with 100% coupling efficiency. Without further purification, 100μL DTT stock solution (0.1M) and 4μL TEA were added into the coupling reaction mixture to cleave the disulfide bond at the 3' end of ssDNA and generate free thiol group for surface immobilization. The reducing reaction was completed in 20min. The modified ssDNA was purified by gel filtration (NAP^{TM} -5 column). The final concentration of purified ssDNA was determined by the UV-vis absorption measurement at 260nm.

The Au substrate was cleaned in a piranha solution (70% H_2SO_4, 30% H_2O_2) prior to the use. *Caution: piranha solution is hazardous and corrosive. Handle with care!* Freshly reduced initiator-coupled ssDNA at 1μM in KH_2PO_4 (1M, pH4.5) was spotted onto the Au surface at room temperature and incubated in a humid chamber for 16hr. Typically 5μL of ssDNA solution was spotted per spot and the resulted spot size was 3-4 mm^2. Freshly reduced ssDNA of the same sequence without the initiator (**2**) was spotted nearby and used as the control. The surface was then immersed into 1mM MCH (**3**) solution for 1hr to block any unoccupied Au surface and to remove nonspecifically adsorbed DNA molecules.[27-29] Copious rinses with DI water were subsequently conducted and the substrate was dried under Ar.

4.2.3 Immobilization of Initiator-Coupled Small Molecules on Gold

Initiator-coupled small molecule, HS-$(CH_2)_{11}NHCOC(CH_3)_2Br$ (**4**), was prepared via direct coupling of HS-$(CH_2)_{11}NH_2$ with N-hydroxysuccinmidyl bromoisobutyrate.

The Au substrate was then immersed in 1mM **4** in 95% ethanolic solution for 48hr. The same molecule without the initiator (**5**) was used as the control for background subtraction. 1-Undecanethiol (**6**) was used as the surface diluting reagent.

4.2.4 Surface-Initiated ATRP Polymerization

A typical surface-initiated ATRP was performed as what has been described previously:[11,26] the reaction container was purged with Ar for 15min to reduce the amount of O_2 present in the reaction system. The monomer solution of HEMA or OEGMA (monomer: H_2O =1:1, volume ratio) was also degassed by purging Ar for 30min. The catalyst mixture was mixed in the solid state and added to the monomer solution, followed by an additional 30min degassing. The monomer/catalyst solution was then transferred into the flask where the substrate was located through a syringe. The reaction flask was kept under Ar purging during polymerization. For the kinetics studies, multiple substrates of the same surface chemistry were placed in separate reaction flasks and the reactions were conducted in parallel. One substrate was removed from the reaction flask at each time point, whereas the rest of substrates were not disturbed for continuous polymer growth. The substrate that had been taken out of the reaction flask was thoroughly rinsed and bathed in methanol overnight to remove nonspecific adsorbed monomers. The film formed was then characterized by polarization modulation-infrared reflection-adsorption spectroscopy (PM-IRRAS) and reflectance FT-IR to confirm the growth of polymer film. Meanwhile, ellipsometry was used to measure corresponding

film thicknesses to correlate polymer growth to the reaction time. The experiments were repeated twice to reduce random reaction variations.

4.2.5 Synthesis of Ethyl α-Bromoisobutylamide[30]

To a solution of α-Bromoisobutyric acid (2g, 12mmol), EDC (2.76g, 14.4mmol), and ethylamine hydrochloride (0.98g, 12mmol) in the 50mL of water at room temperature, was dropwise added 99.5% triethylamine to adjust the pH to 9-10. The reaction finished within 40min from the TLC in 10:1 DCM/methanol. The reaction mixture was worked up by adding DCM (30mL) to extract the aqueous solution and washed the organic layer with saturated NaCl aqueous solution. Then the organic layer was dried over $MgSO_4$, filtered. The DCM was evaporated, and the crude product was purified by a silica column resulting in 0.8g pure white solid (30%). The elution solution used was from 1:1=hexanes: DCM to DCM. ^{1}HNMR (in CD_3Cl, 300MHz) confirmed the result: δ=6.7(broad, 1H), 3.3(m, 2H), 1.9(s, 6H), 1.2ppm (t, 3H).

4.2.6 Solution ATRP Polymerization

For the comparison purpose, solution ATRP was carried out in deionized water at room temperature under a nitrogen atmosphere.[21] The reaction initiator ethyl α-bromoisobutylamide (0.72mmol, 1 equiv), water (10mL), monomer OEGMA (10g, 23.92mmol) and other components were added in a flask. The water solution was degassed by purging with N_2 for 15min. CuCl (71.3mg, 0.72mmol) and 2,2'-bipyridyl (224.9mg, 1.44mmol) were mixed in 2mL degassed DI water to form copper (I)

complexes. The dark brown colored mixture was then added into the degassed monomer solution. The reaction solution was kept under purging during the reaction, but the viscosity of the solution increased over time. After the reaction was terminated, the catalyst was removed through a silica column to yield a colorless polymer product. The dried polymer was characterized by ^{1}H NMR.

4.2.7 Instrumentation

^{1}H and ^{13}C NMR spectra were collected on a Mercury 300MHz spectrometer. Using ^{1}H NMR spectroscopy, the monomer vinyl signals of OEGMA were detected at δ5.6 and 6.0ppm and their intensities decreased with time. As POEGMA formation preceded, the relative intensity of the ethylene oxide proton signal at δ4.0ppm increased, so did the methacrylate backbone signals at δ0.8-2.0ppm, suggesting the formation of polymer materials. The conversion efficiency of monomers was calculated by comparing the signal intensities at δ6.0 and 4.0ppm of the respective monomer and polymer peaks, following the literature report.[31]

A Voyager DE-STR matrix-assisted laser desorption ionization mass spectrometer (MALDI-TOF) was used to monitor the coupling efficiency between ssDNA and NHS-bromoisobutyrate, and the reduction efficiency of disulfide bonds of ssDNA. A linear positive detection mode was used; each spectrum was collected by averaging 100 laser shots. The best detection was achieved at 90% grid voltage of 25,000V and 300ns delay time. The MALDI matrix solution contained 35mg/mL 3-HPA, 7mg/mL diammonium

citrate, and 10% acetonitrile. DNA solutions were desalted using C_{18} ZipTips (Millipore) before the MALDI measurements.

Reflectance FT-IR spectroscopy was performed using a Digilab spectrometer containing a PIKE grazing angle (70º) attachment. The spectra were typically collected with 256 scans using a MCT detector at a resolution of $4cm^{-1}$. The PM-IRRAS spectra were recorded on a Digilab FTS 7000 spectrometer (Randolph, MA) at room temperature at a resolution of $4cm^{-1}$. A step scan interferometer, a liquid nitrogen-cooled narrow-band MCT detector, a globar source and a UDR-8 filter were included. Stepping at 0.5-2.5Hz, the IR radiation was typically phase modulated at frequencies of 400 or 800Hz.[32]

The polymer film thickness was measured using a VB-250 VASE Ellipsometer (J. A. Woollam) at 70° incident angle. The wavelength for the measurements was from 400nm to 700nm at 10nm/step. The reflective indexes of 1.5 and 1.46 were used for the polymer films and ssDNA, respectively, according to the literature.[33] A three-layer model was used to fit the experimental data.[34] All measurements were conducted on dried samples. For each sample three measurements were conducted and averaged.

Contact angle measurements were obtained using the CAM 200 optical contact angle meter (KSV instrument LTD). HPLC grade water was used for measurement. The contact angle was determined by using the Young/Laplace fitting method.

The topology and roughness measurements of polymer surface were obtained using A Digital Instruments Nanoscope IIIa (Digital Instruments, Inc.) in tapping mode.

All measurements were conducted after drying the samples.

4.3 Results and Discussion

4.3.1 Surface-Initiated Polymer Formation in ATRP

Two independent steps are involved in ATRP-assisted DNA detection:[11] (a) sequence-specific hybridization and ligation, and (b) signal amplification by polymerization. To simplify the investigation of ATRP reaction kinetics in the presence of DNA molecules, single-stranded DNAs (ssDNAs) were used as the model system to mimic the ligation products that formed during actual DNA detection (**Scheme 4.1, A**). In particular, ssDNA molecule **1** used in this report had dual functional groups with a 5'-end amino group for initiator coupling and a 3'-end thiol group for surface immobilization. Early attempts to prepare initiator-coupled ssDNA were conducted using the traditional carbodiimide coupling to join α-bromoisobutyric acid to the reactive amines at the 5' ends of ssDNA molecules. However, the strong electron withdrawing nature of bromine makes α-bromoisobutyric acid a strong nucleophilic reagent that reacted with the carbonyl groups in a competitive fashion. Carboxylic anhydride was subsequently formed in solution instead, as confirmed by NMR (**Figure 4.1**). The failure to observe the mass spectrometric peak of the DNA molecules shifting to a higher *m/z* position that corresponded to the initiator-coupled product also confirmed our speculation. A modified coupling pathway was therefore developed in which N-hydroxysuccinmidyl bromoisobutyrate was used as a more active electrophile to react with the primary amine groups on ssDNAs and form the amide products that permanently attached ATRP initiators at the 5' end of DNA molecules.

It has been reported that the formation of an amide bond near bromine in the ATRP initiator slowed down polymer growth in ATRP. In particular, Matyjaszewski and his coworkers have reported that the polymerization of methacrylamide was slower than that of methacrylate.[35] They have attributed the observation to slower activation of the initiators because the C-Br bond in methacrylamide was more difficult to break at the presence of the free electron pair on the nearby nitrogen atom. A quantitative measurement of the initiation activity of α-bromoisobutylamide in solution ATRP showed ~90% monomer conversion efficiency comparing to that of 2-bromoisobutyrate during a 30min reaction (calculated based on the changes in the peak integrations at δ6.0 and 4.0ppm in the ^{1}H NMR spectra of monomer and polymer solutions, respectively). Although less ideal, this straightforward synthetic route to prepare DNA-initiator complexes was chosen to be used in our subsequent studies.

The successful preparation of initiator-coupled DNA molecules was routinely monitored using MALDI-MS (**Figure 4.2**). A single MS peak at *m/z* 11189.6 was observed before the coupling reaction, corresponding to the molecular ion peak of unmodified ssDNAs. The MS peak shifted to *m/z* 11338.7 upon coupling of bromoisobutyryl group. The observed mass increase of Δ*m/z* =149.1 corresponded well to the expected structural addition of the bromoisobutyryl moiety (theoretical Δ*m/z* =148.9). The disappearance of the *m/z* 11189.6 peak suggested that the coupling reaction was close to completion in 30min. A subsequent reduction of disulfide bonds at the 3'-end of ssDNAs led to the back shift of the MS peak to *m/z* 11248.6, along with the disappearance of the MS peak at *m/z* 11338.7.

Upon 3'-terminal reduction, a submonolayer of initiator-coupled ssDNAs was formed on the gold surface through Au-thiolinteraction. 6-Mercapto-1-hexanol (MCH) was subsequently used to passivate the gold surface and to reduce nonspecific adsorption of ssDNA.[27] **Scheme 4.2** outlines the chemical pathways for the formation of poly (2-hydroxyethyl methacrylate) (PHEMA) and poly(oligoethylene glycol methacrylate) (POEGMA) on the gold surface. The formation of PHEMA and POEGMA was confirmed using Reflectance FT-IR spectroscopy and PM-IRRAS, in which the increases of C=O stretching at 1700cm^{-1} and C-O stretching at ~1100cm^{-1} were evident in both cases (**Figure 4.3**).

4.3.2 The Effect of Surface-Anchored DNA in ATRP Reaction

To investigate the effect of highly charged DNA molecules on polymer grafting, a small molecule, $HS(CH_2)_{11}NHCOC(CH_3)_2Br$ (**4**) was used in place of DNA molecules to provide a less-polar coating on the Au surface for comparison (**Scheme 4.1**). The thicknesses of the polymer films formed on both surfaces were measured using ellipsometry and plotted as a function of the reaction time. For each experiment, multiple reaction flasks with one substrate in each were run in parallel under the same conditions. The flasks were opened one at a time at different time points. The same ssDNAs and small molecules without the initiators (**2** and **5)** were used as control molecules to allow background measurements because of the nonspecific adsorption of monomers or polymer products on the surface. Small alkanethiol molecules, MCH (**3**) or 1-

undecanethiol (**6**), were used as the diluting reagents to control surface density (**Scheme 4.1**).

Near-linear polymer growth was observed for PHEMA formation from the surface coated with the small molecules **4** (**Figure 4.4,** Top) over the course of the 10hr reaction. The polymer growth rate from the DNA-coated substrate, however, showed a gradual decrease in the growth rate during the first 2hr reaction period till it reached a slower but steady rate after 2hr (**Figure 4.4,** Bottom). Considering the exact same reaction conditions were applied in both systems except for the difference in the initial surface chemistry (surface polarity and initiator density), it was reasonable to suspect that this nonlinear deviation in polymer growth was due to the presence of DNA molecules.

The question then arose on whether the DNA molecules "accelerated" the film growth at the beginning of ATRP reaction or "decelerated" the growth at the later stage – both could lead to the observed deviation from the classic linear polymer growth in ATRP. To eliminate any ambiguity caused by the variation in surface initiator densities, a surface immobilized with a less polar molecule **4** but at the surface density similar to that of the DNA **1**-coated substrate was prepared (**Scheme 4.1, C**) on the basis of the following calculations: It has been reported that a complete coverage of HS-$(CH_2)_{11}COC(CH_3)_2Br$ on the surface yields a surface density of 4.8×10^{14}molecules/cm^2.[15] Because **4** has the same alkyl chain length and a similar headgroup to HS-$(CH_2)_{11}COC(CH_3)_2Br$; it is therefore approximated that full surface coverage would yield a density at 4.8×10^{14}molecules of **4**/cm^2.[36] For the surface coated with DNA molecules, an initiator density of ~1.0×10^{12} DNA molecules/cm^2 was typically achieved for 35-mer

oligonucleotides because of electrostatic repulsion between DNA molecules.[27,37] By diluting **4** on the surface using **6** of similar chain length in a ratio of 1:480 (i.e. **4/6** = 1.0×10^{12} : (4.8×10^{14}-1.0×10^{12}) = 1:480), an ATRP initiator density for **4** of 1.0×10^{12} initiators/cm^2 was subsequently estimated.[38-40] Substrates immobilized with a mixture of **5** and **6** at the same ratio were used as the control to monitor any background signals from nonspecific adsorption. Upon surface preparation with **1** or **4/6**, ATRP was carried out under the same reaction conditions. No measurable polymer growth was found from the substrates immobilized with **4/6** after the background subtraction because of the detection limit of the ellipsometer (**Figure 4.4,** Bottom). However, approximately 2.7 **+/-** 0.2nm PHEMA from the DNA-anchored substrate was clearly observed in 2hr, qualitatively suggesting more efficient polymer growth at the presence of DNA molecules. The decrease in the polymer growth rate on the DNA-anchored surface beyond 2hr was probably the result of the formation of thick polymer film that reduced the impacts of the surface-anchored DNA molecules. It is important to note that, although reduced, the polymer growth rate from DNA-coated surfaces was still much higher than that from **4/6**-coated ones.

A similar phenomenon was also observed for POEGMA formation (**Figure 4.5**). A POEGMA layer with noticeable film thickness was observed from the ssDNA **1-**coated surface during a 4hr reaction. In contrast, from the substrate coated with molecule **4/6** only (of the same initiator density as for the DNA-coated substrates) no polymer growth was measured, confirming the generality of DNA-accelerated ATRP reactions.

To semiquantitate the accelerating factor induced by the presence of DNA molecules, the substrates with a full-coverage of molecule **4** were again used to compare with DNA **1**-coated substrates (**Figure 4.4,** Top). The use of the substrates with higher initiator densities ensured considerable polymer growth that was capable of being measured by our ellipsometer. In addition, it has been shown that for ATRP reaction <40min there exists a linear relationship between the polymer film thickness and the active initiator density on the surface (after radical self-quenching at high density was taken into consideration).[15,17] Therefore solely on the basis of the ratio of the surface initiator densities, the expected difference in the film thickness from **4**- or **1**-coated substrates could be estimated.[17,18] Any discrepancy between the estimation and the actual measurements would be the result of the growth accelerating effect from the DNA molecules. In **Figure 4.4,** Top, polymer growth of 9.7±1.2nm for the first 30min was measured for the **4-**coated surface. For the DNA-attached substrates, the polymer growth on the surface was measured at 0.8**+/-**0.2nm for the first 30min. Considering that the ratio of the initiator density of the **1**-coated surface to the **4**-coated one was <1%, the amount of polymer growth from the DNA-coated surface well exceeded expectation.

The final but crucial piece of evidence of DNA-accelerated polymerization came from a solution-based ATRP reaction. In a 30min ATRP reaction in which the monomers and the ATRP initiators (i.e. OEGMA and ethyl α-bromoisobutylamide) were mixed at 33:1 v/v ratio, POEGMA remained dissolved in solution, suggesting a product of relative low molecular weight and short chains. In comparison, upon the addition of 2'-deoxyadenosine 5'-monophosphate (dA), one of the four basic nucleotides, to the same

ATRP reaction mixture to mimic the chemical environment of a DNA-immobilized surface, the reaction solution rapidly changed into an insoluble product in less than 10 min. This observation suggested that POEGMA was formed at a much faster rate and with a much higher molecular weight at the presence of dAs.

The acceleration effects from the use of polar-solvents or polar-additives in ATRP have been reported previously, albeit at a much smaller scale.[19, 22, 23, 41, 42] It has been argued that an improvement in the radical activation rate and a decrease in radical recombination rate collectively led to the observed phenomena in those cases. Matyjaszewski, for example, proposed that highly polarized species could stabilize free ion formed in the ATRP transition state.[23] In addition, a recent report has shown that a highly negatively charged surface could concentrate positively charged catalysts (i.e. Cu ions) and subsequently enhance the chain growth rate.[43] We postulate that a similar mechanism applies to the DNA-facilitated polymer reaction, considering the highly charged sugar-phosphate backbones of DNA molecules. Additional features brought about by the unique structure of DNA molecules could also play an important role. For example, the rigid structure of DNA molecules could slow down radial termination with neighbor radicals by reducing polymer chain bending. The bases in the DNA sequence could also participate in chelating with copper ions in place of the bipyridines and play a role in halogen-water exchange on the Cu center.[44] These effects collectively could lead to a faster polymer growth rate but still maintain the linear characteristic of a well-controlled ATRP system. An in-depth investigation is needed to discern the contribution of each factor to understand the underlying reaction mechanism fully.

4.3.3 Optimization of the ATRP Reaction on Surface-Anchored DNA

The catalyst mixture used in ATRP reaction is an important factor that affects the overall polymer chain growth by controlling the number of radicals generated to reduce chain termination and ensure sufficient chain growth.[2] Using an oxidation reagent as a radical deactivator to reduce the free radical concentration and using CuCl in the place of CuBr to provide a stronger R-X interaction that slows down free radical generation have both been proven to be effective in obtaining polymers of high molecular weights for the DNA-absent coated systems.[13,15]

As we expected, similar phenomena were also observed from DNA-anchored surfaces (**Figure 4.6**). When CuBr was used as the catalyst alone, a rapid increase in the polymer film thickness was observed initially, but the growth rate slowed down over time and eventually reached a growth plateau in 2hr. The addition of $CuBr_2$ as an oxidation reagent helped to increase the final film thickness slightly by decreasing the radical density and reducing radical self-termination. A more drastic improvement was brought out by replacing CuBr with CuCl, in which a steady growth of polymer was achieved after initial DNA-assisted acceleration. Despite the initial growth rate being smaller than the reactions using CuBr or CuBr/$CuBr_2$ as the catalyst, the system using CuCl/$CuBr_2$ as the catalyst mixture exhibited a better overall growth rate over the 10hr reaction period with a much thicker polymer film. The observed similarity in the catalyst effects to that of the DNA-absent systems suggests that regardless the presence of DNA molecules the reaction still follows the basic rules of ATRP.[15]

Reducing the concentration of the Cu (I) catalyst also helps to reduce radical quenching by decreasing the amount of radicals formed in the first place (**Figure 4.7,** Top). But an over-diluted catalyst solution would decrease the polymer growth rate to the point of being impractical. In addition, without a sufficient amount of Cu (I) ions in solution to quench residual O_2, the activity of O_2 could no longer be neglected and multiple side reactions could become more prominent. For example, we noticed that an in-solution polymerization became dominant when the concentration of the catalyst in the system was lower than 1mM. The formation of gel-like PHEMA was observed in solution within 2hr using 0.1mM CuCl/$CuBr_2$ (1:0.3) as the catalyst mixture and within 1.5hr using 0.01mM CuCl/$CuBr_2$ (1:0.3), regardless the fact that the initiators were immobilized on the surface exclusively. Air-triggered reverse ATRP was suspected as the culprit, as in the previously reported methacrylate polymerization in the absence of ATRP initiators.[45, 46]

To identify the suitable catalyst concentration for the reaction, we varied the concentration of CuCl in the catalyst mixture from 0.1mM to 69mM while kept $CuBr_2$ at a fixed 30% molar ratio with respect to CuCl (**Figure 4.7,** Bottom). For 5hr, the thickest film formed was from the reaction using 23mM CuCl/6.9mM $CuBr_2$, whereas both higher and lower catalyst concentrations showed the formation of thinner films. It is important to note that this optimal catalyst concentration is closely related to other reaction conditions such as the initiator density on the surface and the reaction time.[16]

The benefit of such study was clearly revealed in **Figure 4.8** in which PHEMA was formed using the old (**Figure 4.8, A**) and newly optimized reaction conditions

(**Figure 4.8, B**). A sufficient amount of PHEMA was formed under the optimized ATRP reaction conditions that enabled direct visualization of the spots where the ssDNA-initiators were immobilized. However, no discernable features were observed on the surface exposed to less-than-optimal ATRP reaction conditions. Longer reaction times or additional reaction amplification steps would have to be applied to effectively report the presence of DNA on the surface.[11]

4.4 Conclusions

We described here an observation of accelerated ATRP reactions in the presence of DNA molecules. To investigate this phenomenon, thiolated single-stranded DNA molecules (ssDNAs) with ATRP initiators coupled at the distal point were used as the model molecule in the study. In comparison, a small molecule, HS-$(CH_2)_{11}NHCOC(CH_3)_2Br$, was used to provide a less-polar surface coating for polymer grafting. 2-Hydroxyethyl methacrylate (HEMA) and monomethoxy-capped oligo(ethylene glycol) methacrylate (OEGMA) were used as the ATRP monomers. The polymer growth rates were monitored by measuring the thickness of the polymer films formed at different times. Our results show that the presence of DNA molecules, although at a less than 1% surface coverage, significantly accelerated the growth rates of both poly(2-hydroxyethyl methacrylate)(PHEMA) and poly(oligoethylene glycol methacrylate) (POEGMA) at the beginning of the ATRP reactions. This accelerating effect was suspected to be a combined result of the highly charged sugar-phosphate backbones of DNA molecules and the formation of Cu complexes with DNA bases. After

the initial polymer growth, a smaller yet constant polymer growth rate was observed, suggesting the reduced influence of DNA molecules as the ATRP reaction centers moved farther away from the surface. Similar to conventional ATRP reactions, the polymer growth from surface-anchored DNA molecules was found to be strongly dependent on the composition and the concentration of the catalysts used. Specifically, a catalyst mixture of CuCl/30% CuBr/bpy with 23mM CuCl was found to provide the optimal reaction condition to yield the fastest polymer film growth among the conditions tested.

It is important to point out that regardless of the limited knowledge of the reaction mechanism this rate-enhancement phenomenon is greatly beneficial for any DNA-sensing applications, considering that fast reactions are always desirable for practical reasons. Furthermore, we envision that such a phenomenon may also find applications in the field of material synthesis, in which DNA molecules could be used as biocatalysts to expedite polymer grafting efficiency.

Schemes

Scheme 4.1: Model Molecules in the Study of Polymer Growth in ATRP.

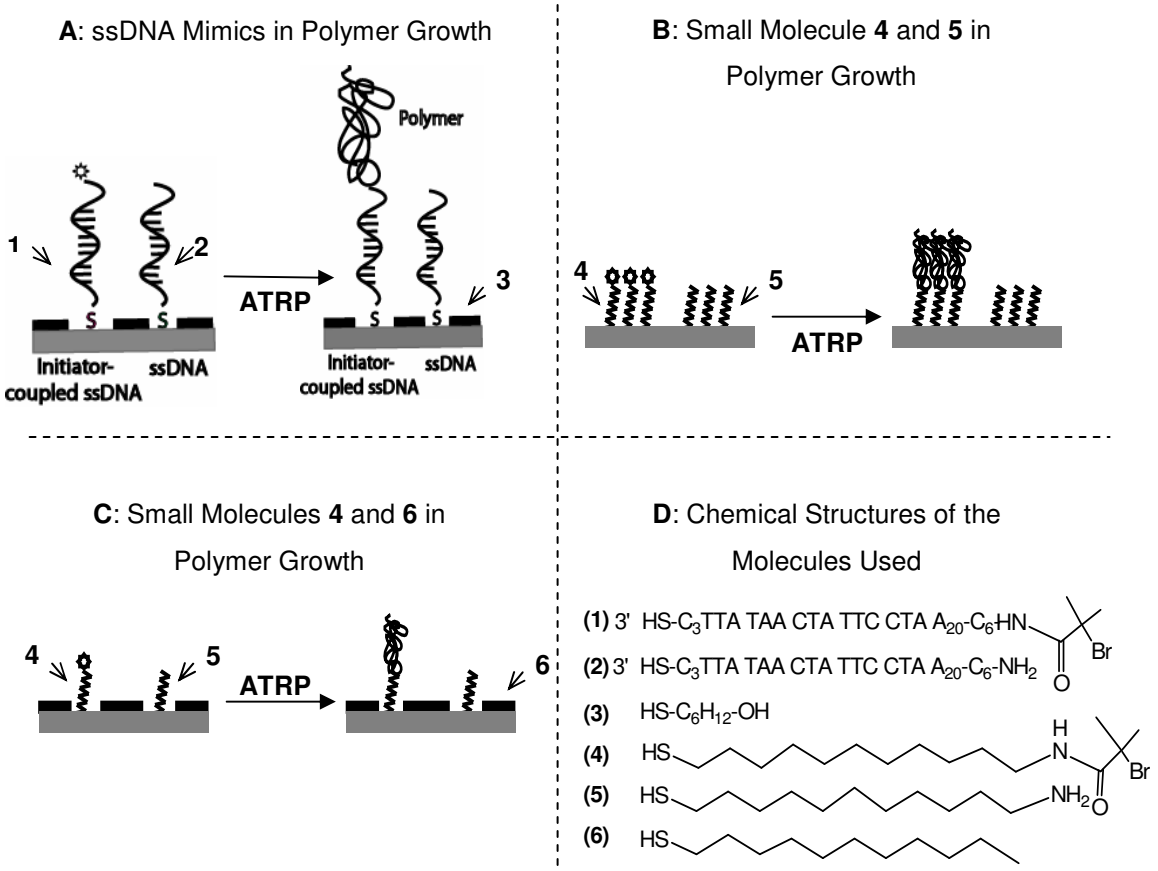

Scheme 4.2: PHEMA and POEGMA Formation in ATRP.

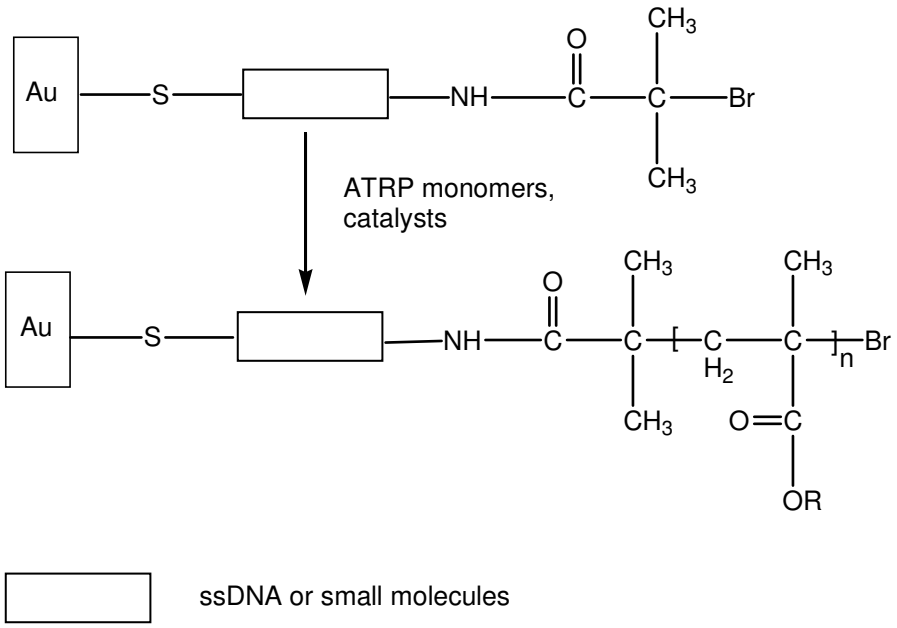

ssDNA or small molecules

R= CH_2CH_2OH (as in PHEMA)
or = $(CH_2CH_2O)_7CH_3$ (as in POEGMA)

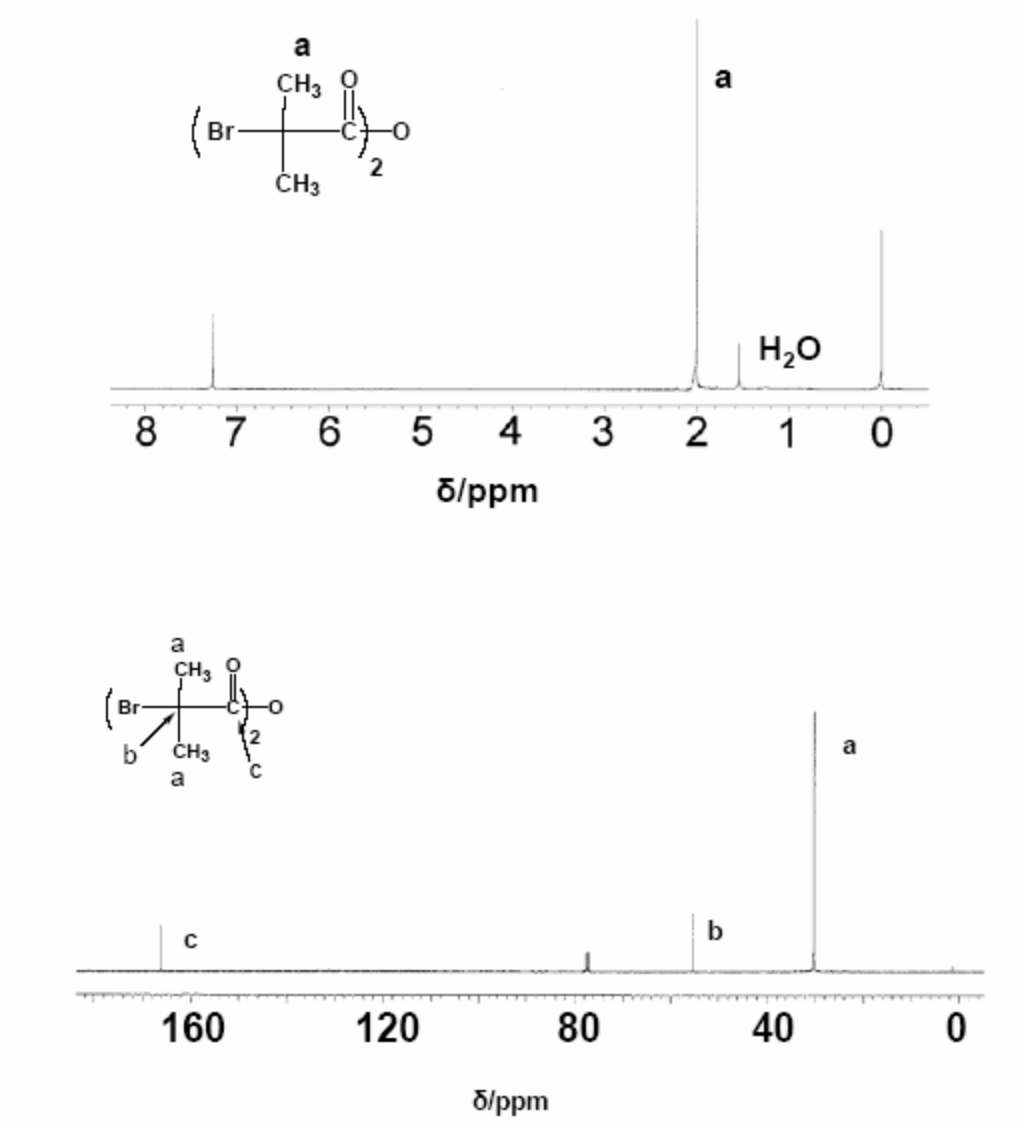

Figure 4.1 The H^1 (Top) and C^{13} (Bottom) NMR spectra of $[Br(CH_3)_2CCO]_2O$ (carboxylic anhydride) formed using the old synthetic route. The synthesis was then modified to generate N-hydroxysuccinmidyl bromoisobutyrate to be coupled with amino-labeled ssDNA. CD_3Cl was used as solvent.

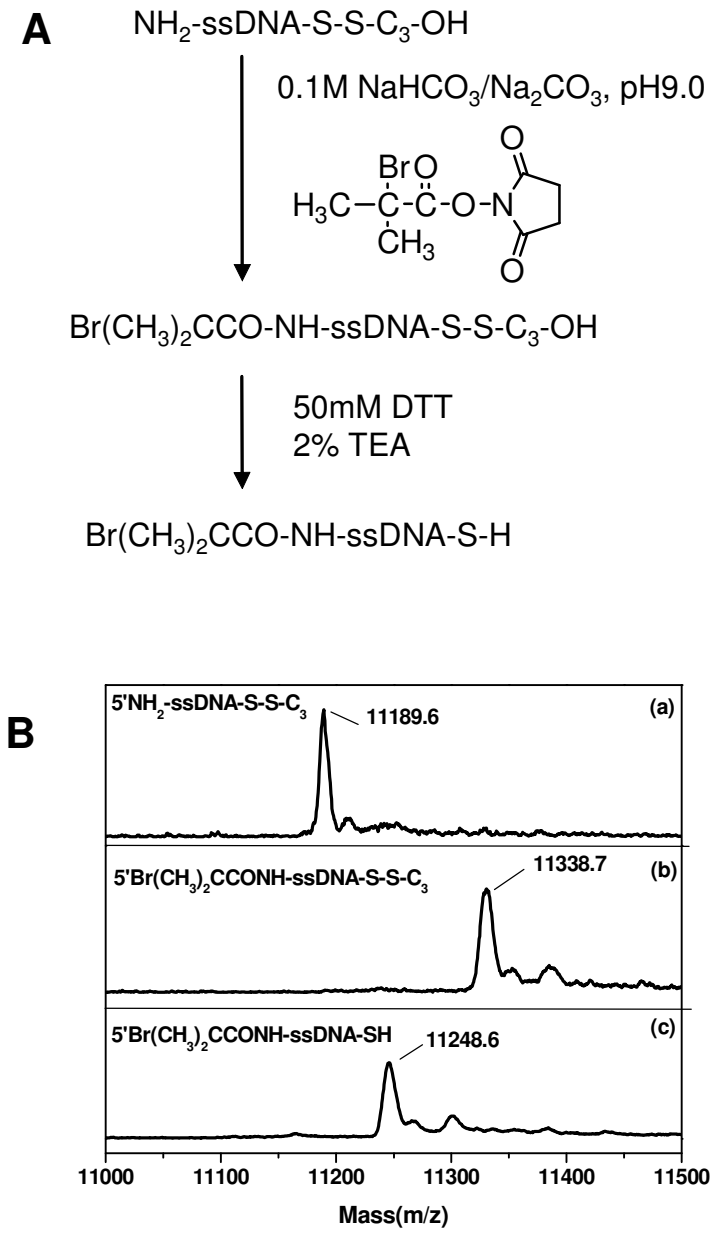

Figure 4.2 (A) Chemical pathway to prepare initiator-coupled ssDNA molecules to be used as the model molecule in the study; (B) MALDI spectra of (a) ssDNA, (b) initiator-coupled ssDNA, and (c) initiator-coupled ssDNA after DTT reduction. Details of the measurements see the Experimental Section.

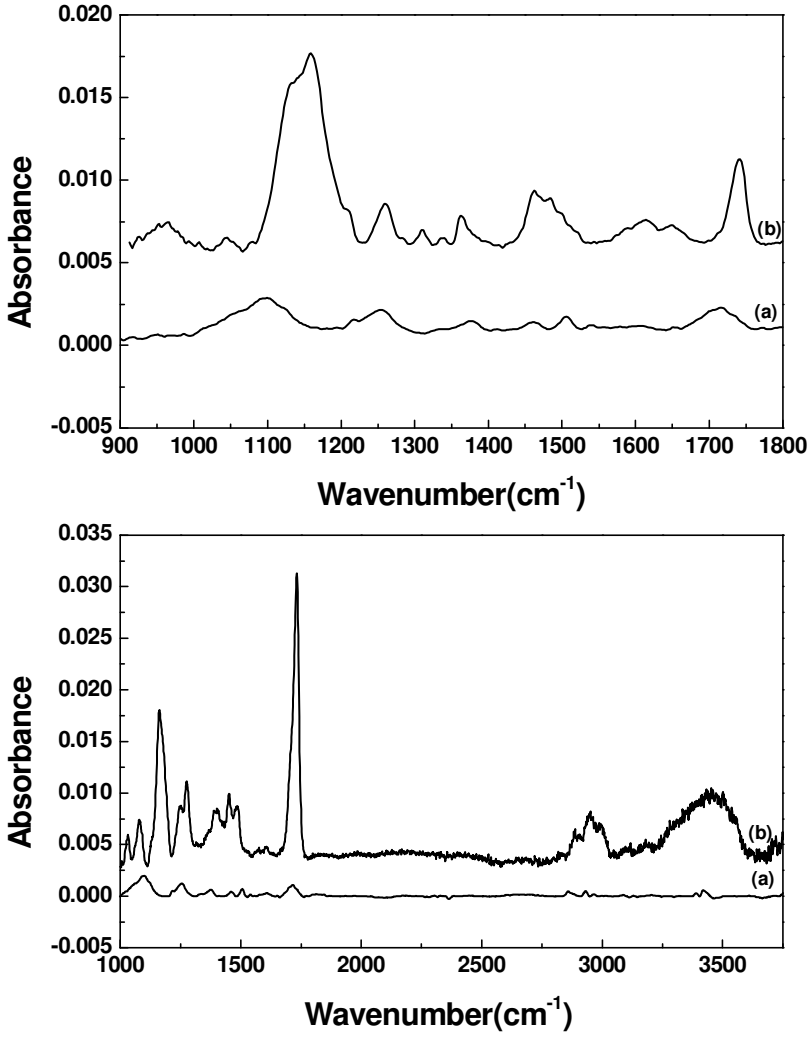

Figure 4.3 (Top) The PM-IRRAS spectra of (**a**) initiator-coupled ssDNA on the Au surface and (**b**) the formation of POEGMA atop DNA molecules on the surface. (Bottom) The PM-IRRAS spectra of (**a**) initiator-coupled ssDNA on the Au surface and (**b**) a reflectance FT-IR spectrum of the formation of PHEMA atop DNA molecules on the surface.

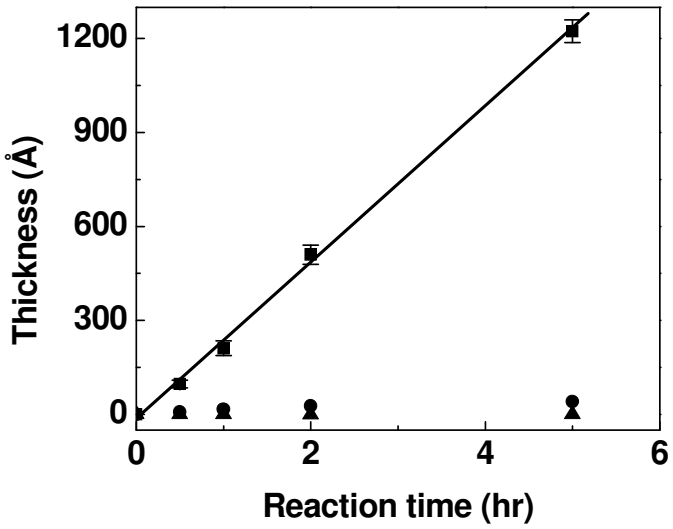

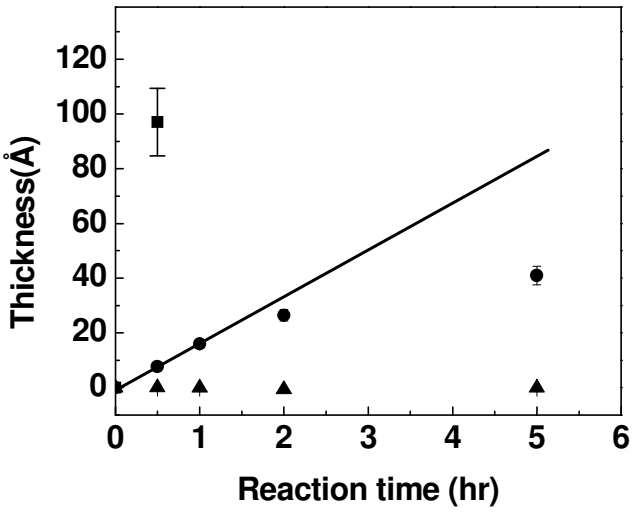

Figure 4.4 (Top) Plots of PHEMA film thicknesses as a function of polymerization time from **4**-coated substrates at full coverage (■), **1**-coated substrates (●), and **4**-coated substrates but at the same initiator density as for **1**-coated substrates (▲). (Bottom) Enlarged view of panel A to illustrate the detail of polymer growth from the substrates of lower initiators densities. The straight lines in both panels are merely guides of the eye**.** The nonspecific absorption background was subtracted. The error bars corresponded to the standard deviations of three measurements at each time point. Note that at several points the error bars were too small to be seen. The reaction conditions are CuCl:$CuBr_2$:bpy = 1:0.3:2.9 (molar ratio), [CuCl] = 69mM, HEMA: H_2O = 1:1 (v/v), and room temperature.

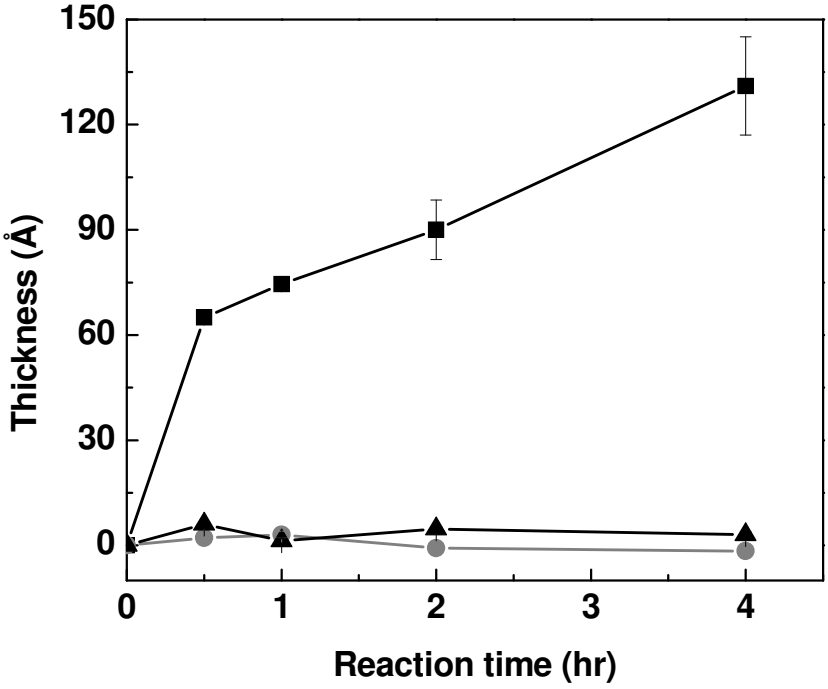

Figure 4.5 Plots of POEGMA film thicknesses as a function of polymerization time from **1**-coated substrates (■) and **4/6**-coated substrates at the same initiator density as for the **1**-coated surface (●). The control substrates coated with molecule **6** only was also plotted to show the negligible nonspecific adsorption occurred (▲). The error bars corresponded to the standard deviations of three measurements at each time point. For several points the error bars were too small to be seen. The reaction conditions are CuCl:$CuBr_2$:bpy=1:0.3:2.9 molar ratio, [CuCl]=69mM, OEGMA: H_2O=8:15 (v/v), and room temperature.

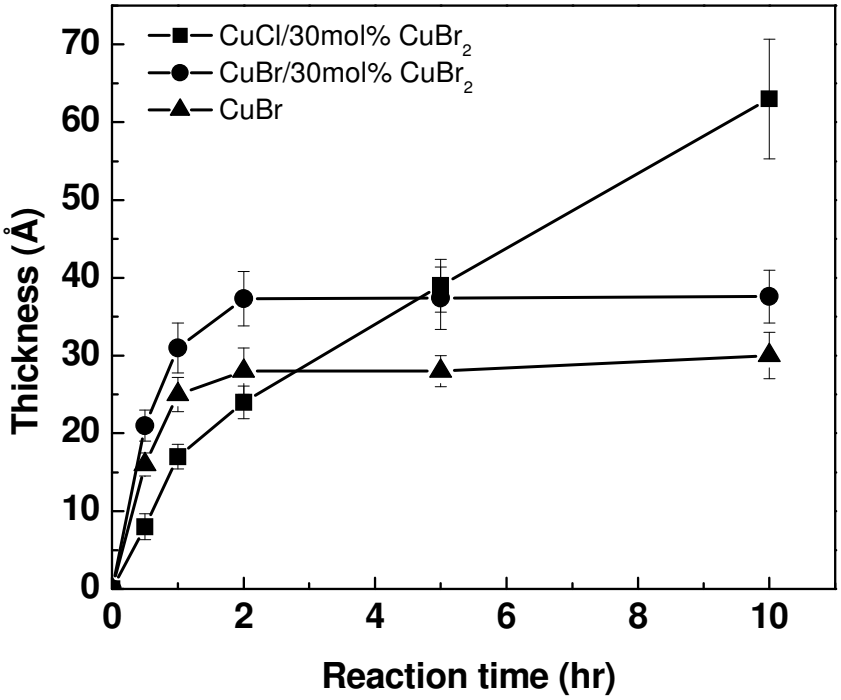

Figure 4.6 Plots of PHEMA film thicknesses as a function of polymerization time from **1**-coated substrates using different halide catalyst systems. The background from nonspecific absorption was subtracted. The reaction conditions are HEMA/H_2O=1:1 (v/v), [CuCl] (or [CuBr]) = 69mM and room temperature.

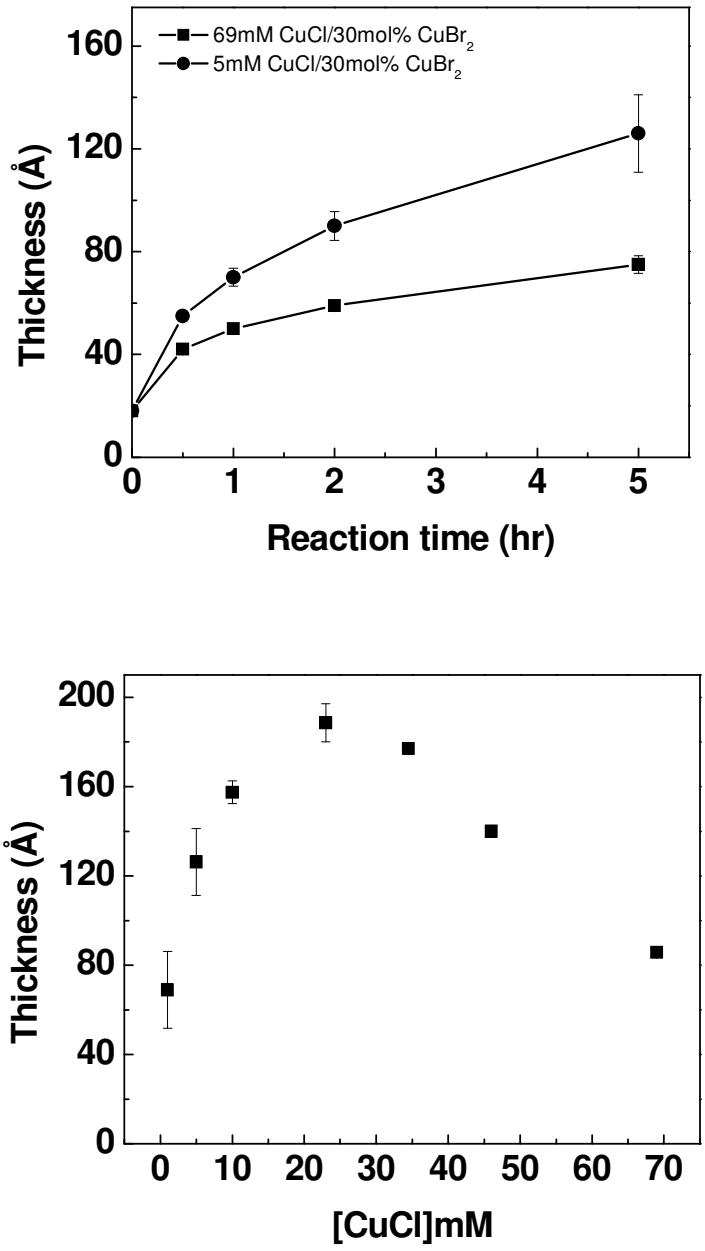

Figure 4.7 (Top) Plots of PHEMA film thicknesses on ssDNA-coated surfaces as a function of polymerization time using 5mM (●) and 69mM (■) of CuCl/30%$CuBr_2$ as the catalyst mixture. (Bottom) Plots of PHEMA thicknesses as a function of CuCl concentration in a 5hr reaction. The catalyst ratio of CuCl:$CuBr_2$:bpy =1:0.3:2.9 was maintained, but the absolute concentrations of each component were varied. ATRP was performed in a 1:1 HEMA/ H_2O mixture at room temperature.

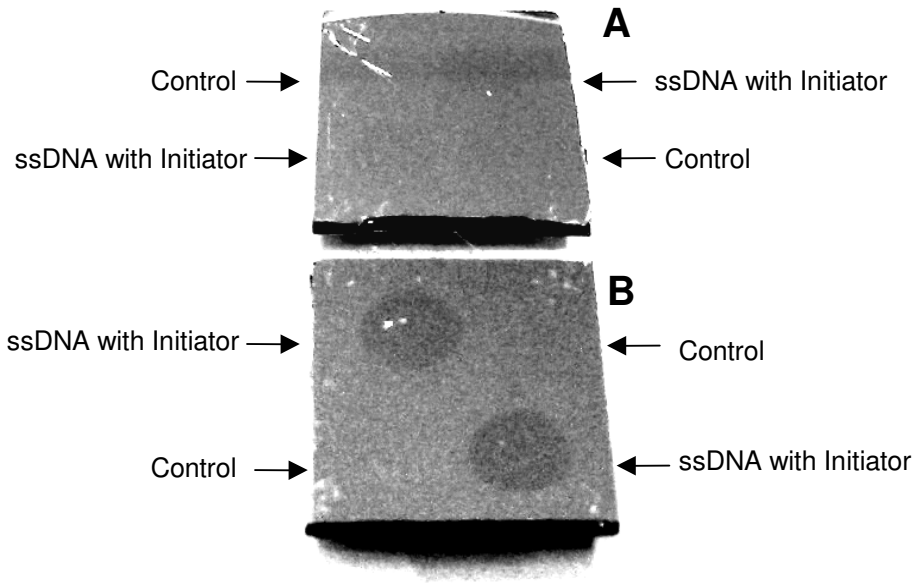

Figure 4.8 A photograph showing two substrates in which PHEMA was formed atop ssDNA molecules using (A) CuBr/bpy = 1:2.2 and [CuBr] = 69mM and (B) CuCl/$CuBr_2$/bpy = 1:0.3:2.9 and [CuCl] = 23mM. ATRP was performed in a 1:1 HEMA / H_2O mixture at room temperature.

References

(1) Matyjaszewski, K.; Xia, J. *Chem. Rev.* **2001**, *101*, 2921-2990.
(2) Patten, T. E.; Matyjaszewski, K. *Adv. Mater.* **1998**, *10*, 901-915.
(3) Sawamoto, M.; Kamigaito, M. *J. Macromol. Sci.* **1997**, *A34*, 1803-1814.
(4) Bontempo, D.; Maynard, H. D. *J. Am. Chem. Soc.* **2005**, *127*, 6508-6509.
(5) Mei, Y.; Beers, K. L.; Byrd, H. C. M.; VanderHart, D. L.; Washburn, N. R. *J. Am. Chem. Soc.* **2004**, *126*, 3472-3476.
(6) Wang, X. S.; Jackson, R. A.; Armes, S. P. *Macromolecules* **2000**, *33*, 255-257.
(7) Ma, Y. H.; Tang, Y. Q.; Billingham, N. C.; Armes, S. P.; Lewis, A. L.; Lloyd, A. W.; Salvage, J. P. *Macromolecules* **2003**, *36*, 3475-3484.
(8) Licciardi, M.; Tang, Y.; Billingham, N. C.; Armes, S. P.; Lewis, A. L. *Biomacromolecules* **2005**, *6*, 1085-1096.
(9) Xu, F. J.; Li, Y. L.; Kang, E. T.; Neoh, K. G. *Biomacromolecules* **2005**, *6*, 1759-1768.
(10) Fu, G. D.; Kang, E. T.; Neoh, K. G. *Langmuir* **2005**, *21*, 3619-3624.
(11) Lou, X.; Lewis, M. S.; Gorman, C. B.; He, L. *Anal. Chem.* **2005,** 77, 4698-4705.
(12) Matyjaszewski, K.; Patten, T. E.; Xia, J. *J. Am. Chem. Soc.* **1997**, *119*, 674-680.
(13) Matyjaszewski, K.; Shipp, D. A.; Wang, J. L.; Grimaud, T.; Patten, T. E. *Macromolecules* **1998**, *31*, 6836-6840.
(14) Wang, J.-S.; Matyjaszewski, K. *Macromolecules* **1995**, *28*, 7572-7573.
(15) Huang, W.; Kim, J.-B.; Bruening, M. L.; Baker, G. L. *Macromolecules* **2002**, *35*, 1175-1179.
(16) Kim, J.-B.; Huang, W.; Miller, M. D.; Baker, G. L.; Bruening, M. L. *J. Polym. Sci., Part A: Polymer Chemistry* **2003**, *41*, 386-394.
(17) Ma, H. W.; Hyun, J. H.; Stiller, P.; Chilkoti, A. *Adv. Mater.* **2004**, *16*, 338-+.
(18) Jones, D. M.; Brown, A. A.; Huck, W. T. S. *Langmuir* **2002**, *18*, 1265-1269.
(19) Bontempo, D.; Tirelli, N.; Masci, G.; Crescenzi, V.; Hubbell, J. A. *Macromol. Rapid Commun.* **2002**, *23*, 418-422.
(20) Ziegler, M. J.; Paik, H.-j.; Davis, K. A.; Matyjaszewski, K. *Polymer Preprints* **1999**, *40*, 432-433.
(21) Wang, X. S.; Armes, S. P. *Macromolecules* **2000**, *33*, 6640-6647.
(22) Haddleton, D. M.; Heming, A. M.; Kukulj, D.; Duncalf, D. J.; Shooter, A. J. *Macromolecules* **1998**, *31*, 2016-2018.
(23) Chatterjee, U.; Jewrajka, S. K.; Mandal, B. M. *Polymer* **2005**, *46*, 1575-1582.
(24) Yamamoto, S.; Ejaz, M.; Tsujii, Y.; Fukuda, T. *Macromolecules* **2000**, *33*, 5608-5612.
(25) Matyjaszewski, K.; Miller, P. J.; Shukla, N.; Immaraporn, B.; Gelman, A.; Luokala, B. B.; Siclovan, T. M.; Kickelbick, G.; Vallant, T.; Hoffmann, H.; Pakula, T. *Macromolecules* **1999**, *32*, 8716-8724.
(26) Lou, X.; He, L. *Polymer Preprint* **2004**, *45*, 455-456.
(27) Herne, T. M.; Tarlov, M. J. *J. Am. Chem. Soc.* **1997**, *119*, 8916-8920.
(28) Petrovykh, D. Y.; Kimura-Suda, H.; Whitman, L. J.; Tarlov, M. J. *J. Am. Chem. Soc.* **2003**, *125*, 5219-5226.

(29) Peterlinz, K. A.; Georgiadis, R. M. *J. Am. Chem. Soc.* **1997**, *119*, 3401-3402.
(30) Nakajima, N.; Ikada, Y. *Bioconjugate Chem.* **1995**, *6*, 123-130.
(31) Wang, X. S.; Lascelles, S. F.; Jackson, R. A.; Armes, S. P. *Chem. Commun.* **1999**, 1817-1818.
(32) Brewer, S. H.; Anthireya, S. J.; Lappi, S. E.; Drapcho, D. L.; Franzen, S. *Langmuir* **2002**, *18*, 4460-4464.
(33) Elhadj, S.; Singh, G.; Saraf, R. F. *Langmuir* **2004**, *20*, 5539-5543.
(34) Martensson, J.; Arwin, H. *Langmuir* **1995**, *11*, 963-968.
(35) Teodorescu, M.; Matyjaszewski, K. *Macromolecules* **1999**, *32*, 4826-4831.
(36) Tam-Chang, S.-W.; Biebuyck, H. A.; Whitesides, G. M.; Jeon, N.; Nuzzo, R. G. *Langmuir* **1995**, *11*, 4371-4382.
(37) Steel, A. B.; Levicky, R. L.; Herne, T. M.; Tarlov, M. J. *Biophys. J.* **2000**, *79*, 975-981.
(38) Zhang, H.-L.; Chen, M.; Li, H.-L. *J. Phys. Chem. B* **2000**, *104*, 28-36.
(39) Li, L.; Chen, S.; Jiang, S. *Langmuir* **2003**, *19*, 3266-3271.
(40) Ulman, A. *Chem. Rev.* **1996**, *96*, 1533-1554.
(41) Narain, R.; Armes, S. P. *Biomacromolecules* **2003**, *4*, 1746-1758.
(42) Matyjaszewski, K.; Nakagawa, Y.; Jasieczek, C. B. *Macromolecules* **1998**, *31*, 1535-1541.
(43) Kizhakkedathu, J. N.; Brooks, D. E. *Macromolecules* **2003**, *36*, 591-598.
(44) Hettich, R. L. *Int. J. Mass Spectrom.* **2001**, *204*, 55-75.
(45) Acar, A. E.; Yagci, M. B.; Mathias, L. J. *Macromolecules* **2000**, *33*, 7700-7706.
(46) Nanda, A. K.; Hong, S. C.; Matyjaszewski, K. *Macromol. Chem. Phys.* **2003**, *204*, 1151-1159.

CHAPTER 5 Applications of ATRP-Based DNA Detection In Single Nucleotide Polymorphisms (SNPs) Detection and Human Gender Determination

5.1 Introduction

After finishing the concept proof experiment of the ATRP-based DNA detection method (see Chapter 2), the optimization of this method for improving sensitivity (see Chapter 3) and the kinetic study of ATRP reaction initiated from ssDNA (see Chapter 4), the focus of my research turned to the applications of this detection method: single nucleotide polymorphisms (SNPs) detection and human gender determination.

5.1.1 Single Nucleotide Polymorphisms (SNPs) Detection

A Single Nucleotide Polymorphism (SNP) is a single nucleotide change, or variation within a DNA sequence. For example, a nucleotide, such as A (adenine), is replaced by another nucleotide, C (cytosine), T (thymine), or G (guanine). On average, SNPs are estimated to occur at a frequency of approximately one per 1000 nucleotides[1-4]. SNPs can be found in different regions of the genome, such as coding or non-coding sections, with or without any effects on the gene product. Most SNPs are found outside of "coding sequences". However, SNPs found within a coding sequence are of particular interest to researchers because they are more likely to alter the biological function of a protein. Synonym SNPs do not change the encoded amino acids, but non-synonym SNPs induce new amion acids. The mutated proteins could possess different conformations that eventually could lead to a change in enzyme activities[5].

The genetic variability is the key to resolve different biological problems. One important role of SNPs is its application in biological evolution research: since most SNPs occur in highly recombination regions, evolutionary alterations and the trait of selection can be followed.[6] Another important role of SNPs is in pharmacology. As we know, individuals tolerate drugs and environmental effects differently. The knowledge of SNPs in metabolic genes could result in better formulation of medicines.[7,8] The third role of SNPs is to greatly improve disease diagnosis. Many believe that SNPs in the coding sections are related with many diseases directly or indirectly since individuals with defined SNPs suffer from a disease more frequently compared to the healthy population.

Because of the potential importance of SNPs in understanding the causes of disease, National Center for Biotechnology Information (NCBI) created a database to track known SNPs in 1998, with the hope of accelerating disease association efforts and providing insights for locating candidate gene targets for disease diagnosis and treatment. With the establishment of such public and private SNP database, researchers in the field of bioanalytical chemistry immediately launched efforts in utilizing the gained knowledge to develop effective SNP detection methods. A large variety of different techniques have been developed for SNP analysis (see Chapter 1).

In this chapter, the fidelity of the ATRP-based DNA single base mismatch detection was tested and the ATRP amplification step exhibited the required specificity. The perfectly matched DNA targets were distinctively differentiated from those with mutations.

5.1.2 Human Gender Determination

Evaluation of the ATRP-based DNA detection method in complex genetic samples where high concentration of unrelated DNA molecules are present is also important In this chapter, an assay of human gender determination was used as a simple model to evaluate the fidelity of ATRP-based DNA detection method.

Human gender determination is part of the important human identification systems in forensic and archaeological work.[9,10] It is also essential in prenatal identification of unborns. The amelogenin genes (AMEL X and AMEL Y) present on both the X and the Y chromosomes are routinely used for sex discrimination based on their size difference. The most commonly utilized sex test method based on a 6bp deletion on the AMEL X was developed by Sullivan *et al* in 1992. In their method males are differentiated from females by the presence of both 106bp and 112bp products.[11] However, the reliability of this amelogenin gene-based sex test method has been argued since 1998 by three research groups from England, India, and Austria.[12-14] According to their research, 2 unrelated males from Sri Lanka out of 350 males, 6 out of 29,432 males with European and 5 out of 270 Indian males were all found the deletion of AMEL Y gene and the presence of SRY, the male sex-determining gene at the same time. Another research group from Australia also found that a mutation in the annealing region of the amelogenin primers led to the failure of amplification of the amelogenin Y-homolog.[10] Even though these phenomena occur with a low frequency, it is still necessary to solve these problems considering the serious implications for the forensic community.

It has been suggested to add one Y specific marker, such as SRY, STR or 50f2, for gender determination, which makes the PCR amplification for gender determination more complicated. Another gender determination method based on a 90bp deletion on the human X chromosome in an X-Y homologous region has recently been described by Batzer *et al*.[15] This X deletion was first discovered by the same group and tested on 593 DNA samples with 100% accuracy.[16]

In this chapter, the ATRP-based DNA detection method described in Chapter 2 was applied for human sex test by monitoring the presence of the 90bp deletion on X chromosome.

5.2 Experimental Section

5.2.1 Materials

Single stranded DNAs for SNP detection, oligonucletide PCR primers and gender determination probes were purchased from Integrated DNA Technologies, Inc. (Coralville, IA) (**Table 5.1-5.2**). Male and female genomic DNA was purchased from Promega at 150ng/μL and 159ng/μL concentration respectively. Hot start PCR amplification was performed using HotStarTaq® DNA polymerase from Qiagen (Valencia, CA) and routine PCR amplification was performed using PCR core systems from Promega Corporation (Madison, WI). Single stranded DNA product after PCR was prepared with Strandase ™ ssDNA preparation kit from Novagen. SYBR® gold nucleic acid gel stain was purchased from Molecular Probes for double- and single-stranded DNA detection in electrophoresis gel. Monodispersed low molecular weight PEG thiol

OEG_7, $[CH_3\text{-}(OCH_2CH_2)_7\text{-}S\text{-}]_2$, was from BioVectra Targeted Biopharmaceutical Solutions (Prince Edward Island, Canada). Phenol saturated with Tris at pH6.6-7.9 and chloroform/isoamyl alcohol 24:1 (v:v) were generously provided by Dr. Wendy Boss' group in the Department of Botany at NCSU. 2-hydroxyethyl methacrylate (HEMA, 98%) was purchased from Sigma-Aldrich. HEMA was purified using an inhibitor remover column to remove methyl hydroquinone inhibitor. The inhibitor remover was purchased from Aldrich and the column was packed in house. Acrylamide (electrophoresis grade), N, N'-methylenebisacrylamide, ammonium persulfate, N,N,N',N'-tetramethylenediamine, urea, N-hydroxysuccinimide acid (NHS), bromoisobutyryl bromide, 3- hydroxypicolinic acid (3-HPA), diammonium citrate, dioxane, dithiothreitol (DTT), triethylamine (TEA), copper (I) chloride (CuCl), copper (II) bromide ($CuBr_2$), 2,2'-bipyridine (bpy), and diethyl ether were purchased from Sigma-Aldrich and used as received. Gold substrates (50Å Chromium followed by 1000Å gold on float glass) were purchased from Evaporated Metal Films (Ithaca, NY). Micro Bio-Spin® 30 Columns were bought from Bio-Rad Laboratories, Inc. for single stranded DNA purification. A NAP™-5 column was purchased from Amersham Pharmacia Biotech for DNA purification. C_{18}ZipTip™ was bought from Millipore for DNA desalting before MALDI measurements.

5.2.2 Single Nucleotide Polymorphisms (SNPs) Detection

Capture Probe Immobilization; *Initiator Coupling to Detection Probe (**D**)*; *Three-strand DNA Hybridization*; *DNA Ligation* and *ATRP Reaction for DNA Detection* are all as

described in Chapter 2 including all the ssDNA used. Three separate substrates were prepared with the same DNA probes immobilized in four spots: two spots of the capture DNA probes (**C**), and the other two of non-complementary probes (**NC**) for inter-substrate comparison. After surface passivation, three substrates were exposed to the solutions containing perfectly matched DNA target (**C'D'**), one base-mismatch (**C1'D'**), and three-mismatch DNA (**C3'D'**) solutions, respectively. All three substrates were treated with the same DNA detection probe, followed by DNA ligation. A 5hr one step ATRP reaction was conducted, followed by initiator coupling.

The Optimization of Salt Stringency Wash Conditions after Hybridizations. The salt stringency wash conditions were optimized by monitoring SPR intensity changes in situ. The probe C and NC were immobilized onto the same SPR substrate with their duplicates, following the protocol in *Capture Probe Immobilization*. Probe **C** and **NC**-attached SPR surface was installed into the SPR sample cell and incubated with 1M NaCl TE until baseline was stable. After the baseline was stabilized, the real-time SPR hybridization and dehybridization experiment was started. Firstly, the surface was continuously washed with 1M NaCl TE buffer for 2min, then an aqueous solution of 1μM target DNA **C'D'** in 1M NaCl TE buffer was passed through the cell for 5min, followed by the wash step using 1M NaCl TE buffer for 2min. The surface was subsequently washed with 8mM NaCl PBS buffer for 2min, then 1M NaCl TE buffer until stable, followed by water for 2min, and 1M NaCl TE buffer until stable. 8M urea solution was then flowed through the cell for 10min to denature the duplex formed in the first step, then the surface was

again washed with 1M NaCl TE buffer until the SPR signal was stable. 1μM one mismatched target DNA **C1'D'** in1M NaCl TE buffer was then passed through the SPR sample cell for 5min, followed by the wash step using 1M NaCl TE buffer for 2min. The surface was again subsequently washed by 8mM NaCl PBS buffer for 2min, 1M NaCl TE buffer until stable, water for 2min, and 1M NaCl TE buffer until stable.

5.2.3 Human Gender Determination

PCR primer and probe design. The human gender determination assay was designed according to a 90bp deletion on the human X chromosome in an X-Y homologous region first discovered by Batzer and his colleagues in 2003 (**Figure 5.1**).[15] Primers are shown in bold font and probes are shown in different colors. We took advantage of a specific deletion region, starting at X position 89810740, to differentiate X and Y chromosomes and determine patient genders. The same 24bp forward primer and reverse primer (phosphorylated at 5' end) as shown in **Figure 5.1, A** were used to PCR amplify a 79bp fragment on the human X chromosome and a 169bp fragment on the human Y chromosome. Female PCR amplification product should contain only the 79bp fragment and male PCR product both 79bp and 169bp fragments. The binding specificities of the primers were confirmed using the BLAST program (http://www.ncbi.nl.nih.gov/blast/). The assay surface was prepared using three different capture probes, negative control probe **Neg**, probe **XY** and probe **Y**. Probe XY has the sequence complementary to the common region of X and Y chromosome that can specifically recognize X and Y chromosomes. Probe Y has the sequence only complementary to the region on

chromosome Y, and will only show positive response from male sample. Negative control probe will be used to evaluate the nonspecific adsorption. Both 79bp and 169bp fragments can specifically hybridize with probe XY and only 169bp fragment can specifically hybridize with probe Y. The expected sensor response is shown in **Figure 5.1, C.**

Routine PCR Amplification Using Taq DNA Polymerase. The PCR amplifications were performed using Taq DNA polymerase from Promega. Two sets of reverse primers and forward primers with different length were used in PCR amplification (**Table 5.2**). PCR cycling conditions consisted of an initial 2-5min preheating at 95°C, followed by 30 amplification cycles of denaturation at 95°C for 1min, annealing at 50-56°C for 30s and extension at 72°C for 20s. Each PCR tube contains 80-1200ng human genomic template, 30-50pmol forward primer, 30-50pmol reverse primer, 200μM dNTPs, 1.5mM $MgCl_2$ and 2.5U Taq DNA polymerase in a 100μL 1 x PCR buffer.

Hybrid PCR Amplification and Strandase Exonuclease Reaction. Hybrid PCR amplification was performed using HotStarTaq DNA polymerase from Qiagen. A 5' end phosphorylated reverse primer and a regular forward primer was used in PCR amplification (**Table 5.2**). PCR cycling conditions consisted of an initial 15min at 95°C to activate the HotStarTaq DNA polymerase, followed by 30 amplification cycles of denaturation at 95°C for1min, annealing at 56°C for 30s and extension at 72°C for 20s. Each PCR tube contains 700ng human genomic template, 30pmol forward primer,

30pmol reverse primer, 200μM dNTPs, 1.5mM $MgCl_2$ and 5U HotStarTaq DNA polymerase in a 100μL 1 x PCR buffer.

After PCR amplification, the PCR product was purified by ethanol precipitation to concentrate the DNA product and remove primers and other reaction components. Briefly, 1μL glycogen, 9μL 3M sodium acetate at pH5.2 and 60μL isopropanol were added into each 100μL PCR reaction mixture, vortexed and left at room temperature for 5min. The mixture was centrifuged for 10min at 13,000rpm at room temperature and the supernatant was removed. 250μL of 70% ethanol was used to rinse the DNA pellet and the solution was centrifuged for 2min, followed by removal of supernatant with a pipette. The DNA pellet was then washed again with absolute ethanol. After centrifugation the DNA pellet was allowed to dry in air (usually 5-10min) and resuspended in 10μL of sterile water. The amount of purified DNA was quantified by the UV-vis absorbance at 260nm (A_{260} of 1=50μg/mL).

After PCR product purification, exonuclease reaction was performed using the Strandase ssDNA Preparation Kit from Novagen. 8μL amplified and purified primer-free DNA, 1μL 10x Strandase buffer and 1μL Strandase λ Exonuclease (5U/μL) were mixed at 37°C for 20min, followed by heating at 75°C for 10min to stop reaction.

Capture Probe Immobilization. The protocol that was published was used to reduce three capture probes and immobilize them on gold surface.[17] The gold substrates were cleaned in a piranha solution (70% H_2SO_4, 30% H_2O_2) prior to the use. The oligonucleotide probes, probe XY, probe Y, and negative control probe Neg (**Table 5.2**),

had disulfide bonds at the 3'-end for surface attachment. To generate free thiol groups for surface immobilization, 3μL stock oligonucleotide solution (probe (XY), probe (Y) or negative control probe (Neg)) at 100μM was mixed with 25μL DTT (0.1M in H_2O), 21μL H_2O and 1μL TEA at room temperature for 20min. After reduction, the excess amount of DTT was removed using a Micro-Bio-Spin column. The concentrations of the reduced oligonucleotides were determined by the UV absorbance at 260 nm. Freshly reduced capture probes at 1μM in a KH_2PO_4 buffer (1M, pH 4.4) were spotted onto Au substrates at room temperature and incubated in a humid chamber overnight. The surfaces were then incubated with 1mM OEG_7 in absolute ethanol solution for 1hr, followed by copious rinsing with ethanol and were dried under compressed air.

Initiator Coupling to Detector. Initiator-coupled DNA detection probe(**HGD-D-IN**) was prepared as previously described.[18] Briefly, 100μL of detector DNA (**HGD-D**) (**Table 5.2**) at 100μM and 15μL of 10 x conjugation buffer (1.0M $NaHCO_3/Na_2CO_3$, pH9.0) were added into a 1.5mL centrifuge tube, followed by the addition of freshly prepared bromoisobutyryl NHS ester solution (10mg/mL in DMF, 35μL). Bromoisobutyryl NHS ester was also synthesized according to previous published protocol.[18] After 30min reaction at room temperature, the excessive NHS ester was removed through NAP-5 column gel filtration. MALDI-TOF MS was used to confirm the successful coupling by measuring the relative peak intensities of the detector DNA and initiator coupled detector.

Three-strand DNA Hybridization. Before hybridization with the three probe attached gold surfaces, the PCR products after exonuclease reaction were purified by phenol extraction and ethanol precipitation, followed by incubation under alkaline conditions. 100μL PCR reaction mixture (female or male) after exonuclease reaction was added into a 1.5mL centrifuge tube along with 100 μL phenol, vortexed 30s and centrifuged at 2000rpm for 5min and 8000rpm for 1min. The aqueous phase at the top layer was transferred with care to a fresh centrifuge tube and an equal volume of 24:1 (v:v) chloroform-isoamyl alcohol (85μL) was subsequently added into the same tube, centrifuged and the aqueous layer which contained DNA was transferred to a fresh centrifuge tube. 6.5μL of 3M Na_2AC and 143μL of absolute ethanol were added into the tube with DNA solution and incubated at -70°C for 1.5hr. DNA was then precipitated out by centrifugation at 13000rpm for 15min. The pellet was further washed with 200μL 70% ethanol and dried in air for 30min. The purified DNA was resuspended into 10μL of Millipore water and quantified by UV absorption at 260nm.

The purified PCR products were subsequently treated under alkaline, formamide and thermal conditions. The 30μL DNA containing mixture contained 0.3M NaOH, 20% formamide, 0.15M PBS buffer and purified PCR product. The mixture was incubated at 42°C for 30min, then 0.74μL of 12.1M HCl was added to neutralize the mixture.

The Probe-attached Au surface was then incubated with 2μL the alkaline treated PCR product (female or male) for each probe spot for 2hr in a humid chamber at room temperature. After hybridization, a stringency wash (50mM NaCl, 10mM phosphate buffer) was performed to selectively denature the imperfect duplexes. An additional

hybridization with 1μM initiator-modified detection probes, **HGD-D-IN**, was conducted for 2hr in 0.5M PBS buffer afterwards. After hybridization, the surface was briefly rinsed with the ligation buffer containing 50mM Tris-HCl (pH7.5) and 7mM $MgCl_2$ with the absence of DTT to eliminate possible replacement of thiol-labeled DNA probes) and water.

DNA T4 Ligation. After hybridization, the surface was then reacted with 2μL per probe spot of a solution containing 4U T4 DNA ligase and 15% PEG 8000 in a 1 x T4 DNA ligation buffer. The reaction was allowed to proceed for 2hr at room temperature before rinsing with water. The surface was subsequently incubated in 8.3M Urea for 15min and rinsed with water.

ATRP Reaction for DNA Detection. In a typical surface-initiated ATRP reaction, a solution of HEMA (40mL) and DI water (40mL) was purged by Ar for 30min to reduce the amount of O_2 present in the reaction system, followed by another 15min purging upon the addition of the catalyst mixture of CuCl (183.5mg), $CuBr_2$ (120mg) and 2,2'-bipyridyl (813.5mg). The flask containing the DNA-immobilized substrate was also purged with Ar for 5min. The monomer/catalyst solution was then injected into the flask where the substrate was located. The polymerization was stopped after 2hr by the removal of the substrate, followed by the subsequent rinse with methanol. The subsequent derivatization of the hydroxyl groups of the side chains of PHEMA was carried out by immersing

PHEMA-coated substrate in 10mL DMF containing 2-bromoisobutyryl bromide (0.08M) and TEA (0.1M) for 20min at room temperature.

5.3 Results and Discussion

5.3.1 Single Nucleotide Polymorphisms (SNPs) Detection

Target DNAs of single or three mismatches were used to evaluate the fidelity of ATRP-assisted SNP detection (**Table 5.1**). After the ATRP reaction, the growth of PHEMA was visible on the substrate incubated with both the perfectly matched target sequences **C'D'** and one mismatched target sequences **C1'D'**. No discernable patterns could be recognized for the substrates incubated with **C3'D'**, and the same low backgrounds were observed from the control spots across all three substrates (**NC**) (**Figure 5.2**). The contact angle measurements could also only differentiate the perfect matched and one mismatched surface from three mismatched and non-complementary surfaces. The increase of the contact angles after initiator coupling resulted from the stronger hydrophobicity of the bromoisobutyryl groups compared to the hydroxyl groups. As shown in **Table 5.3**, the ellipsometric measurements demonstrated that the PHEMA film formed from perfectly matched surface and one mismatched surface were 100.1±0.7Å and 74.9±0.7Å, respectively. Those values were significantly higher than those measured from three mismatched and non-complementary surfaces. Even through the perfectly matched and one mismatched surface were capable of being differentiated by ellipsometric measurements, only the three base mismatched sample can be directly differentiated from matched and one mismatched samples by the naked eye.

The low specificity of single mismatch detection of this method (about (100.1-38.9)/(74.9-38.9)=1.7 according to the ellipsometric measurements) was mainly due to the low specificity of T4 ligase (see Chapter 7). Under current assay conditions, it is necessary to either conduct salt stringency wash to dehybridize one mismatched target DNA from probe C before T4 ligation or use high specificity ligation conditions, such as optimized probe mismatch locations, using high NaCl concentration or using thermostable DNA ligase with high fidelity. In this chapter, salt stringency wash was simply applied to enhance the specificity of the SNP detection. In Chapter 7, the direct comparison of CNBr chemical ligation with high specificity and T4 ligation was conducted.

The salt stringency wash conditions for one mismatch detection were optimized by in-situ SPR measurements. The perfect matched and one mismatched target DNA C'D' and C1'D' were subsequently hybridized with the same substrate attached with probe C and NC. As shown in **Figure 5.3**, the in situ kinetic curve demonstrated that a washing protocol consisting of a 2min 8mM NaCl PBS buffer wash and 2min water wash effectively de-hybridized more than 93% of the one mismatched dsDNA (relative SPR intensity from 7.0pixels to 0.5pixel) while still kept matched dsDNA up to 94% hybridized (relative SPR intensity from 8.0pixels to 7.5pixels).

By adding the salt stringency wash step in the DNA sensing protocol, perfect matched and one mismatched samples were able to be distinguished by the naked eye after ATRP. As shown in **Figure 5.4**, after the ATRP reaction, the growth of PHEMA was only visible on the substrate incubated with the perfectly matched target sequences

(**C'D'**). No discernable patterns could be recognized for the substrates incubated with **C1'D'**, **C3'D'**, and the same low backgrounds were observed from the control spots across all three substrates (**NC**).

5.3.2 Human Gender Determination

Sample Preparation. PCR amplification of human gene (**Figure 5.1**) was originally conducted using TaqDNA polymerase with varied success. Specifically, the first experiment was performed with 80ng template and 25pmol primers in 50μL reaction volume, 50°C annealing remperature, and 2min preheating step at 95°, resulting in no formation of expected PCR products for both female and male sample. The most likely reason for the failed experiment is non-sufficient preheating time. Due to the long length of human chromosomes (genome of 3.3 x 10^9bp), 2min preheating step might not be sufficient to dehybridize the double strand DNAs and 5min preheating step was used afterwards. Higher amount of templates were also used to favor the formation of the products. By using 5min preheating step in the second experiment, the expected PCR products for both male (77bp and 167bp) and female (77bp) were formed after 30 cycles. However, for the female sample, the primer-dimmers were still formed as the dominant product along with the 77bp product. The primer-dimmer would compete with the PCR products in the later hybridization step since the primer-dimmer was not short enough to be effectively removed by PCR clean-up kit (about 25% left over when Wizard® SV gel and PCR clean-up stystem was used). In order to prevent the formation of primer-dimmers, several factors including annealing temperature (experiment 3), template

amount (experiment 4 and 6), and primer length (experiment 5), have been tested. No acceptable reproducibility was achieved and the formation of primer-dimmers remained a major problem (**Table 5.4**).

The problem was solved by the use of hot start PCR amplification to significantly enhance the specificity of amplification and avoid the formation of primer-dimmers compared with the routine PCR amplification. The HotStarTaq DNA polymerase has no polymerase activity at ambient temperature, which prevents the formation of misprimed products and primer-dimmers at low temperatures. As shown in **Figure 5.5**, the expected PCR products for both female and male sample were amplified with the evidence from denatured PAGE gel electrophoresis. Single bright band at 79bp for female sample and two bright bands at 79bp/169bp were observed after 30 cycles.

The exonulease reaction was then conducted to digest one strand of duplex DNA from 5' phosphorylated end and left the non-phosphorylated single strand ready for surface hybridization in gender determination assay. Before the exonuclease reaction step, PCR amplification was conducted using the 5'phosphorylated reverse primer (P24) and non-phosphorylated forward primer (24) under optimized conditions as mentioned in the experimental section. The successful digestion was confirmed by PAGE gel electrophoresis analysis under non-denaturing conditions in **Figure 5.6**. Single-stranded DNA migrated faster than the double-stranded counterpart. As shown in **Figure 5.6**, the exonuclease reaction of female and male PCR products was quite efficient and only traces amount of double- stranded DNA was left after the 20min reaction. After exonuclease reaction, the reaction mixture containing single stranded PCR products were

diluted into 1M NaCl TE buffer at the concentrations of 0.5μM for 79bp and 0.25μM for 169bp strands, respectively. The SPR in situ hybridization experiment exhibited that the relative hybridization efficiencies with probe (XY) were 25±6% for female PCR products and 19±6% for male PCR products, in which shorter synthetic linker (XY) (**Table 5.2**) was used as reference target DNA of 100% hybridization efficiency to calculate relative hybridization efficiency using the following formula:

$$\%= \frac{[(\text{SPR intensity changes from PCR sample}) \times \text{MW of linker XY}]}{[(\text{SPR intensity changes from linker XY}) \times \text{MW of PCR products}]} \times 100\%$$

The molecular weight of linker XY and PCR products were listed underneath the **Table 5.5**.

Additional improvement in hybridization efficiency using a treatment condition including alkaline and formamide at elevated temperature was achieved by minimizing the formation of the secondary structures of female and male PCR products.[19] Specifically, DNA molecules were purified by phenol extraction and ethanol precipitation. The purified single stranded PCR products were then treated under alkaline conditions as described in the experimental section and subsequently hybridized with the probe attached surface. This combination condition significantly improved the hybridization efficiencies for both female and male PCR products up to the level similar to short synthetic DNA (**Table 5.5**). In addition, the detectable SPR signal changes were observed at the probe (Y) positions for male PCR product (data not shown here).

Sample Detection. Gender determination was then carried out following a similar protocol similar to the one described in Chapter 2.[17] First, the detector (HGD-D) was pre-coupled with the ATRP initiator, an isobromobutyl group, at the end of it. The successful coupling was confirmed by MALDI-TOF mass spectra before and after initiator coupling. A mass increase of 148.6 was clearly observed, corresponding well to the addition of bromoisobutyroyl group at the end of probe HGD-D (**Figure 5.7**). The negligible residual peak at the original position confirmed the coupling reaction was near completion in less than 30 min.

After PCR products successfully hybridized on the surface, the initiator labeled detector DNA (HGD-D-IN) was subsequently hybridized with the PCR product to form three component dsDNA, followed by T4 liagtion. ATRP amplification was then conducted under optimized conditions.[20] 2hr ATRP and 20min initiator coupling rendered the visibility of the polymer spots on the substrates by the naked eye. As shown in **Figure 5.8,** the substrate (a) that experienced the hybridization with female PCR sample showed two white spots at the positions of probe (XY), and the substrate (b) that hybridized with the male PCR sample showed four white spots at the locations of probe (XY) and probe (Y).

5.4 Conclusions

ATRP-based detector-free DNA detection method has been successfully applied for single nucleotide polymorphisms (SNPs) detection. The perfectly matched DNA targets were distinctively differentiated from those with mutations. Similarly, human X

and Y chromosomes were successfully differentiated based on the 90bp deletion on X chromosome.

The demonstrated capability to detect DNA mutation and real genetic samples with direct visualization laid the groundwork for the future development of detector-free testing kits in specific gene screenings.

Tables

Table 5.1 DNA Sequences Used in SNPs Detection.

Name	Sequence	Description
C	5'-pTAA CAA TAA TCC CTC AA A_{18}-C_3-S-S-C_3	Capture probe partially complementary to **C'** portion of target **C'D'**
D	5'-NH_2-C_6-A_{18} AAA TCC TTA TCA ATA TT	Detection probe partially complementary to **D'** portion of target **C'D'**
D-IN	5'-Br$(CH_3)_2$CCONH -C_6-A_{18} AAA TCC TTA TCA ATA TT	Initiator-coupled **D**
NC	5'-pGGC AGC TCG TGG TGA AA A_{18}-C_3-S-S-C_3	Non-complementary capture probes to target **C'D'**
C'D'	5'-GAG GGA TTA TTG TTA AAT ATT GAT AAG GAT	Perfectly matched target DNA complementary to probes **C** and **D**.
C1'D'	5'-GAG GGA **A**TA TTG TTA AAT ATT GAT AAG GAT	Single-mismatch target, with the mutation site shown in the bold and underline letter.
C3'D'	5'-GAG GGA **AAG** TTG TTA AAT ATT GAT AAG GAT	Three-mismatch target, with the mutation sites shown in the bold and underline letters.

Table 5.2 Primers and Probes for Human Gender Determination Assay.

Oligonucleotide	Sequence	Size(bp)
Forward primer(28)	5'CCACGAACTTTAATTAGTCACCTACTGT3'	28
Reverse primer (28)	5'ATTCCTCTCTCCATTATGTTCAATTACA3'	28
Forward primer(24)	5'CACGAACTTTAATTAGTCACCTAC3'	24
Reverse primer (24)	5' TTAATTCCTCTCTCCATTATGTTC3'	24
Reverse primer (P24)	5'Phos-TTAATTCCTCTCTCCATTATGTTC3'	24
Probe (XY)	5'Phos-CACATTGTCTGGCACT$_{20}$ –C$_3$-S-S-C$_3$3'	35
Probe (Y)	5'Phos-CACATCGTATCCTAGT$_{20}$ –C$_3$-S-S-C$_3$3'	35
Negative Control Probe (Neg)	5'NH$_2$-C$_6$-T$_{20}$-C$_3$-S-S-C$_3$3'	20
Detector (HGD-D)	5'NH$_2$ –C$_6$ –T$_{20}$ AATTACACCATTTAT 3'	35
Detector (HGD-D-IN)	5'Br(CH$_3$)$_2$CCONH–C$_6$–T$_{20}$ AATTACACCATTTAT3'	35
Linker (XY)	5'TGCCAGACAATGTGATAAATGGTGTAA3'	27

Table 5.3 Ellipsometric and Contact Angle Measurements in SNPs by ATRP-Assisted DNA Detection.

Linker	C'D'	C1'D'	C3'D'	Non-complementary
Film thickness after ATRP(Å)	100.1±0.7	74.9±0.7	37.2±0.7	38.9±0.6
Contact angle after ATRP (°)	54±2	54±2	49±2	47±2
Contact angle after initiator coupling (°)	68±3	67±3	48±2	47±2

Table 5.4 Optimization of PCR Using TaqDNA Polymerase.

Exp #	Template (ng/50µl)	Primers (pmole/50µl)	Annealing Temp. (°C)	Preheating time (min)	Results
1	80	primers(28), 25	50	2min/95°C	Primer-dimmer
2	250	primers(28), 25	50	5min/95°C	F (primer-dimmer & 77bp) M (77bp/167bp/ >200bpunknown)
3	250	primers(28), 15	50-60	5min/95°C	F(77bp when >=58°C) M(primer-dimmer/77bp/167bp; when>=58°C, low amplification)
4	300, 600	primers(28), 15	50-60	5min/95°C	F(primer-dimmer/ 77bp) M(primer-dimmer/77bp/167bp; when>=58°C, low amplification)
5	250	primers(24), 15	56	5min/95°C	F(primer-dimmer or 79bp) M(primer-dimmer/79bp/169bp; when>=58°C, low amplification)
6	50-500	primers(24), 15	56	5min/95°C	F (some primer-dimmer and 79bp, some only primer-dimmer) M(primer-dimmer major product except 350ng template only desired two products)

Table 5.5 SPR Intensity Changes From Hybridization.

Target DNA	SPR intensity changes at probe (XY) (ΔPixel)	Relative hybridization efficiency
Linker (XY)	5.5±1.0	100%
PCR-F(ds), high temperature	0±1.0	0%
PCR-M(ds), high temperature	0±1.0	0%
PCR-F(ss), after exonuclease reaction	4.0±1.0	25±6%
PCR-M(ss), after exonuclease reaction	3.0±1.0	19±6%
PCR-F(ss),after alkaline condition treatment	16±1.0	100±6%
PCR-M(ss),after alkaline condition treatment	16±4.0	100±25%

M.W. of linker (XY): 8371.5;
M.W. of 79bp single stranded PCR product: 24484.0;
M.W. of 169bp single stranded PCR product: 52418.1.

Figures

A)

X chromosome A C T G A A G A G T C **C A C G A A C T T T A A T T A G T C A C**
Y chromosome A C T G A A G A G T C **C A C G A A C T T T A A T T A G T C A C**

X chromosome **C T A C** T G T G C C A G A C A A T G T G - - - - - - - - - - - -
Y chromosome **C T A C** T G T G C C A G A C A A T G T G C T A G G C T C T A G

X chromosome -
Y chromosome G A A T A C A A A A G A G A G T A T G A C A A A C A T G G C A

X chromosome -
Y chromosomeT G G G C C T C T T T G A G C C A T G A C A C T C T T A T A G A

X chromosome - A T A A A T G G T G T A A T T **G**
Y chromosome T C T A G G A T A C G A T G T G A T A A A T G A T G T A A T T **G**

X chromosome **A A C A T A A T G G A G A G A G G A A T T A A** T T T T T G T T
Y chromosome **A A C A T A A T G G A G A G A G G A A T T A A** T T T T T G T T

B)

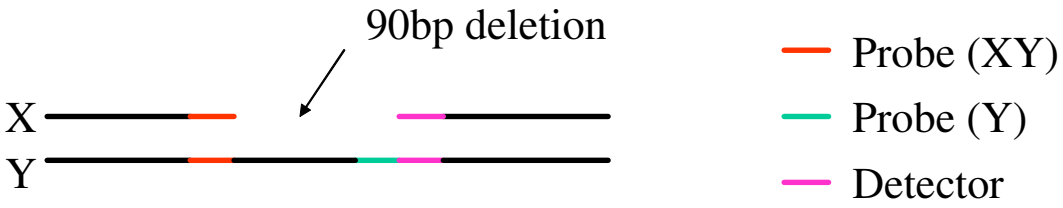

C)

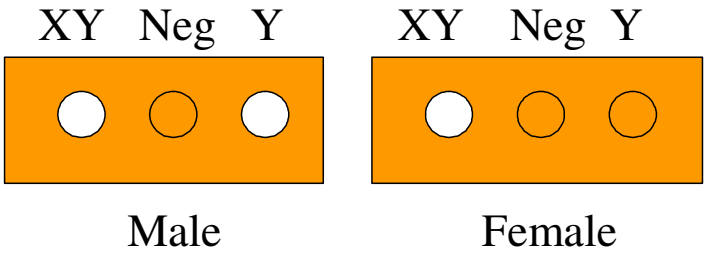

Figure 5.1 **A)** Sequence alignment of a portion of the homologous region of the human sex chromosomes. The dashes represent a 90bp deletion specific to the human X chromosome. Primers are shown in bold font. **B)** Probe design of gender determination. **C)** Gender determination assay. White circle represents positive results and yellow circle represents negative results.

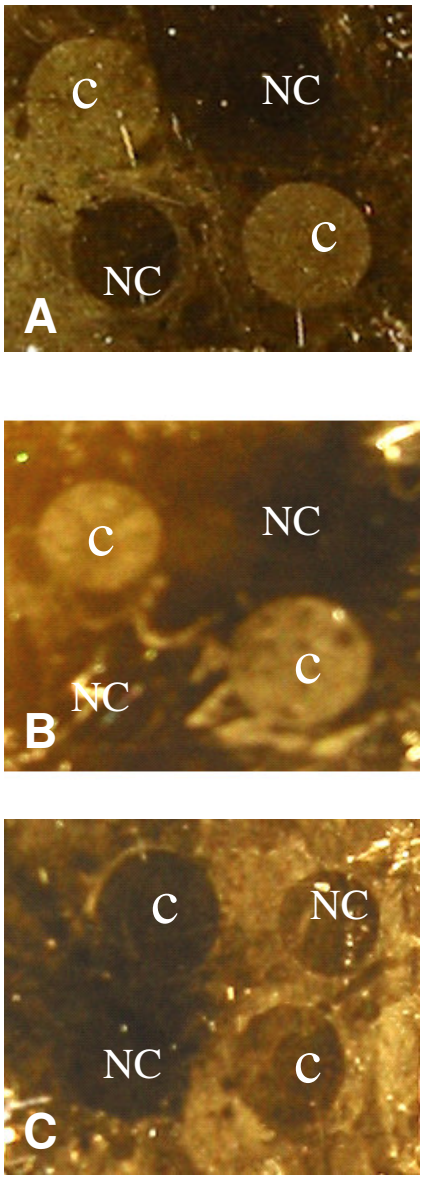

Figure 5.2 Photos of ATRP-assisted DNA amplification in DNA point mutation detection. Both perfectly matched target DNA (**Image A**, spots **C'D'**) and 1-mismatch (**Image B**, spots **C1'D'**) are visible to the naked eyes, whereas 3-mismatch (**Image C**, spots **C3'D'**) and non-complementary sequences (spots **NC** in **Image A-C**) show negative responses. The dotted circles are guides to the eye.

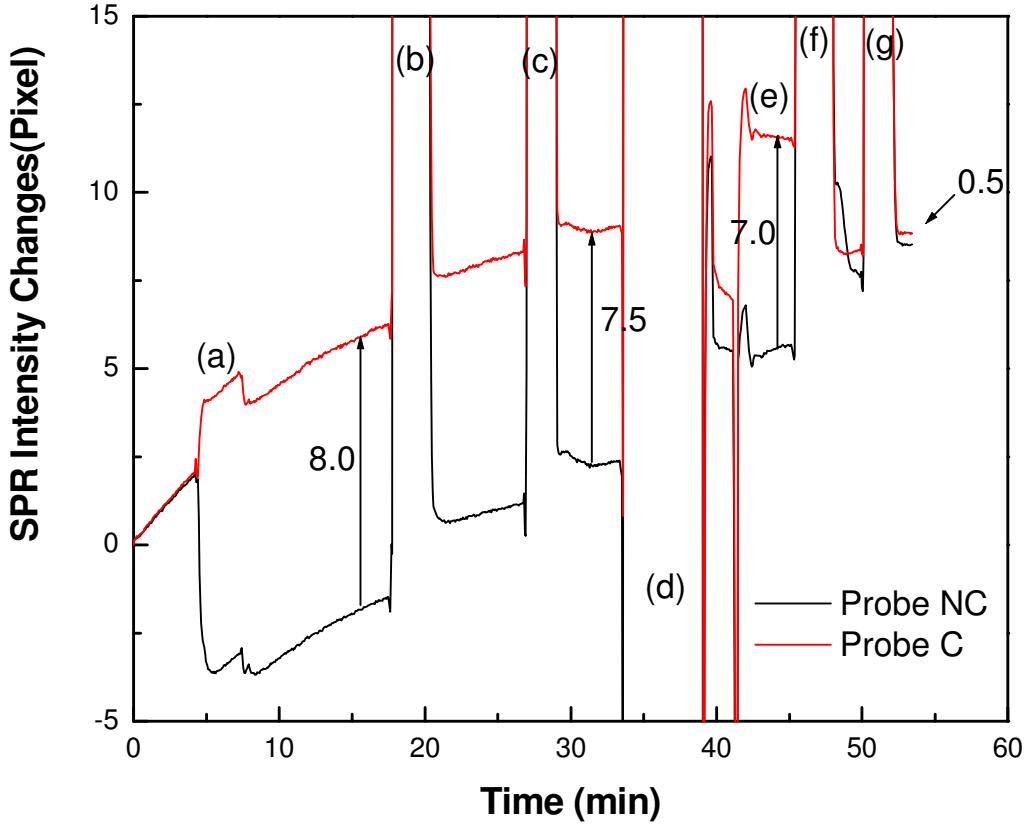

Figure 5.3 Hybridization and salt stringency wash for C'D' complementary DNA and C1'D' one mismatched DNA on the same surface. The experiment was conducted in the following steps: (a) hybridization with C'D'; (b) 8mM NaCl PBS buffer wash; (c) H_2O wash; (d) dehybridization with urea; (e) hybridization with C1'D'; (f) 8mM NaCl PBS buffer wash; (g) H_2O wash. 1M NaCl TE buffer washed the surface betwee steps. Black lines correspond to probe NC and red lines correspond to probe C.

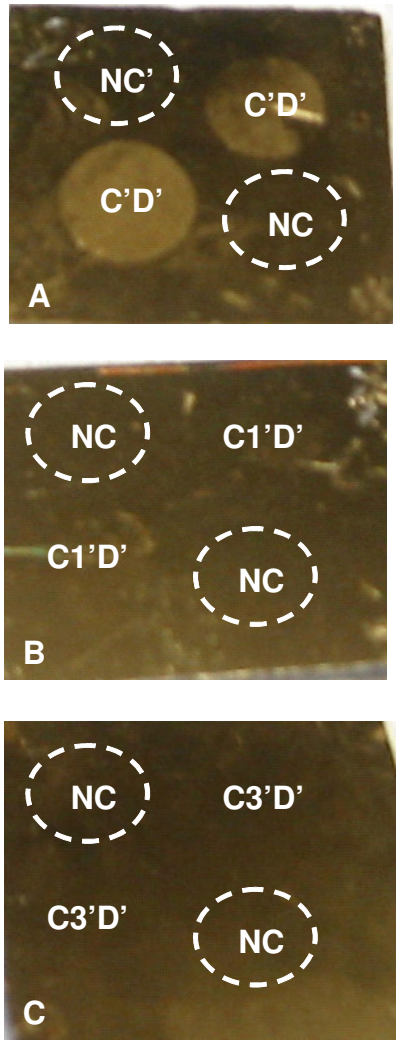

Figure 5.4 Photos of ATRP-assisted DNA amplification in DNA point mutation detection. Only perfectly matched target DNA is visible to the naked eyes (**Image A**, spots **C'D'**), whereas 1-mismatch (**Image B**, spots **C1'D'**), 3-mismatch (**Image C**, spots **C3'D'**) and non-complementary sequences (spots **NC** in **Image A-C**) show negative responses. The dotted circles are guides to the eye.

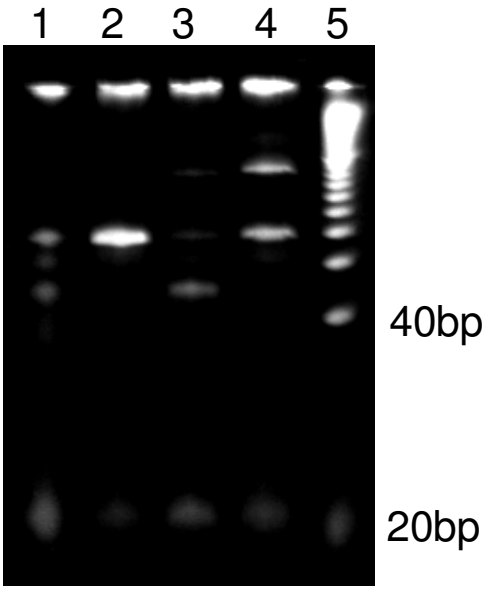

Figure 5.5 15% denatured PAGE gel image of PCR amplification of human genomic DNA. Lane 1 contains female template and TaqDNA polymerase; lane 2 contains female template and HotstarTaqDNA polymerase; lane 3 contains male template and TaqDNA polymerase; lane 4 contains male template and HotstarTaqDNA polymerase and lane 5 contains 20bp single stranded DNA ladder. The gel was stained by SYBR-gold for 10min in 1x TBE buffer.

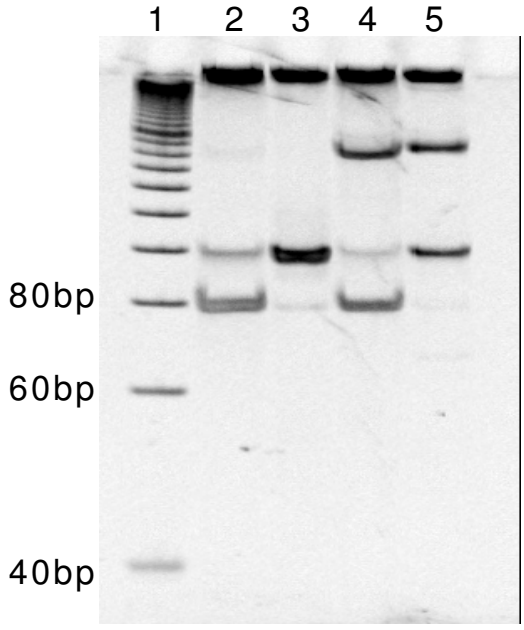

Figure 5.6 15% non-denatured PAGE gel image of hybrid PCR amplification of human genomic DNA and ssDNA preparation by exonuclease reaction after PCR amplification. Lane 1 contains 20bp single stranded DNA ladder; lane 2 contains female hybrid PCR reaction mixture after exonuclease reaction; lane 3 contains female hybrid PCR reaction mixture before exonuclease reaction; lane 4 contains male hybrid PCR reaction mixture after exonuclease reaction and lane 5 contains male hybrid PCR reaction mixture before exonuclease reaction. The gel was stained by SYBR-gold for 10min in 1x TBE buffer.

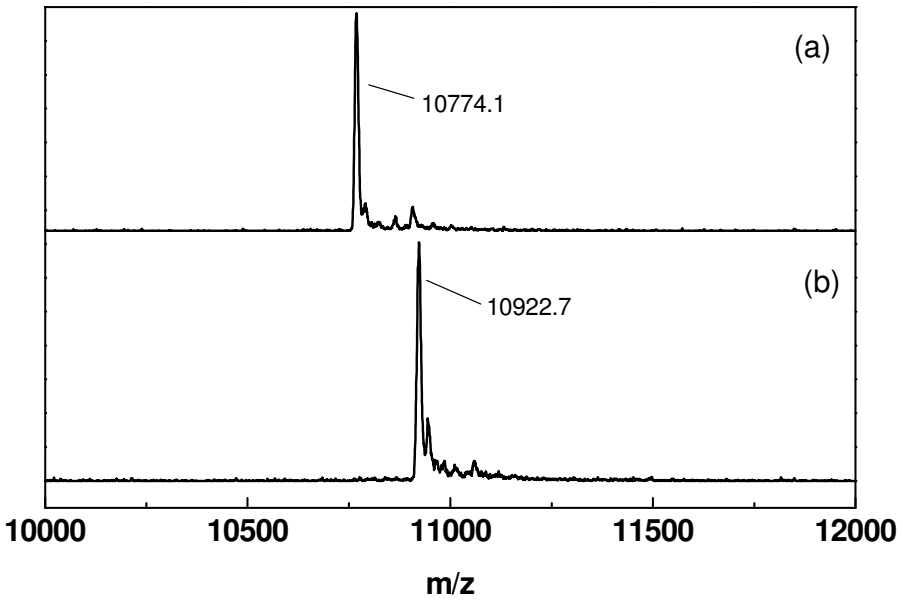

Figure 5.7 MALDI spectra of detection probe **D** (**a**) before and (**b**) after the coupling of the ATRP initiator (ΔMW=148.6). MALDI-MS conditions: accelerating voltage 25kV, grid voltage 90%, positive mode detection, delay time 300ns, and 100 laser shots collected per spectrum, 35mg/mL 3-HPA as the matrix.

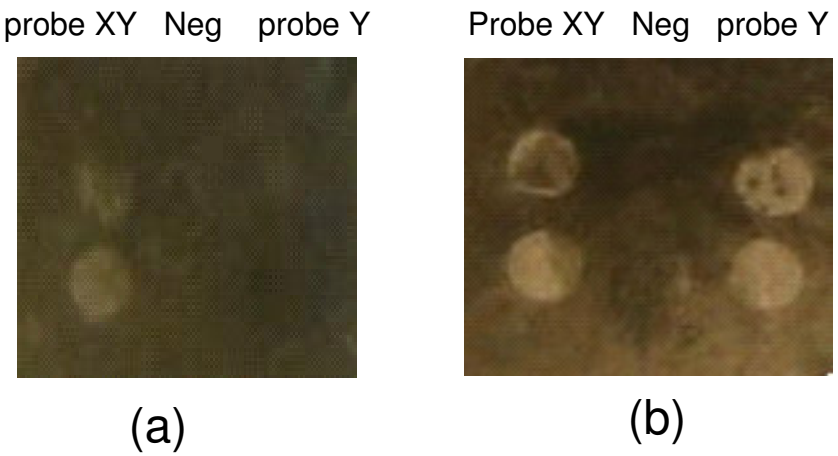

Figure 5.8 Photos of ATRP-assisted DNA amplification in human gender determination. For female PCR sample, two spots at probe (XY) locations are visible to the naked eyes (**Image a**), whereas for male PCR sample, four spots at probe (XY) and probe (Y) locations are visible to the naked eyes (**Image b**). Negative control probes show negative responses.

References

(1) Wang, D. G.; Fan, J. B.; Siao, C. J.; Berno, A.; Young, P.; Sapolsky, R.; Ghandour, G.; Perkins, N.; Winchester, E.; Spencer, J.; Kruglyak, L.; Stein, L.; Hsie, L.; Topaloglou, T.; Hubbell, E.; Robinson, E.; Mittmann, M.; Morris, M. S.; Shen, N. P.; Kilburn, D.; Rioux, J.; Nusbaum, C.; Rozen, S.; Hudson, T. J.; Lipshutz, R.; Chee, M.; Lander, E. S. *Science* **1998**, *280*, 1077-1082.

(2) Schafer, A. J.; Hawkins, J. R. *Nat. Biotechnol.* **1998**, *16*, 33-39.

(3) Landegren, U.; Nilsson, M.; Kwok, P. Y. *Genom. Res.* **1998**, *8*, 769-776.

(4) Brookes, A. J. *Gene* **1999**, *234*, 177-186.

(5) Bessenyei, B.; Marka, M.; Urban, L.; Zeher, M.; Semsei, I. *Biogerontology* **2004**, *5*, 291-303.

(6) Schmidt, P. S.; Duvernell, D. D.; Eanes, W. F. *Proc. Natl. Acad. Sci. U. S. A.* **2000**, *97*, 10861-10865.

(7) Bell, P. A.; Chaturvedi, S.; Gelfand, C. A.; Huang, C. Y.; Kochersperger, M.; Kopla, R.; Modica, F.; Pohl, M.; Varde, S.; Zhao, R. B.; Zhao, X. J.; Boyce-Jacino, M. T. *BioTech.* **2002**, 70-+.

(8) Marsh, S.; Kwok, P.; McLeod, H. L. *Hum. Mut.* **2002**, *20*, 174-179.

(9) Faerman, M.; Kahila, G.; Smith, P.; Greenblatt, C.; Stager, L.; Filon, D.; Oppenheim, A. *Nature* **1997**, *385*, 212-213.

(10) Roffey, P. E.; Eckhoff, C. I.; Kuhl, J. L. *J. Forensic Sci.* **2000**, *45*, 1016-1019.

(11) Sullivan, K. M.; Mannucci, A.; Kimpton, C. P.; Gill, P. *BioTech.* **1993**, *15*, 636-&.

(12) Santos, F. R.; Pandya, A.; Tyler-Smith, C. *Nat. Genet.* **1998**, *18*, 103-103.

(13) Thangaraj, K.; Reddy, A. G.; Singh, L. *Int. J. Legal Med.* **2002**, *116*, 121-123.

(14) Steinlechner, M.; Berger, B.; Niederstatter, H.; Parson, W. *Int. J. Legal Med.* **2002**, *116*, 117-120.

(15) Walker, J. A.; Hedges, D. J.; Perodeau, B. P.; Landry, K. E.; Stoilova, N.; Laborde, M. E.; Shewale, J.; Sinha, S. K.; Batzer, M. A. *Anal. Biochem.* **2005**, *337*, 89-97.

(16) Callinan, P. A.; Hedges, D. J.; Salem, A. H.; Xing, J. C.; Walker, J. A.; Garber, R. K.; Watkins, W. S.; Bamshad, M. J.; Jorde, L. B.; Batzer, M. A. *Gene* **2003**, *317*, 103-110.

(17) Lou, X.; Lewis, M. S.; Gorman, C. B.; He, L. *Anal. Chem.* **2005**, *77*, 4698-4705.

(18) Lou, X.; He, L. *Polymer Preprint* **2004**, *45*, 455-456.

(19) Giakoumaki, E.; Minunni, M.; Tombelli, S.; Tothill, I. E.; Mascini, M.; Bogani, P.; Buiatti, M. *Biosens. Bioelectron.* **2003**, *19*, 337-344.

(20) Lou, X.; He, L. *Langmuir* **2006**, *22*, 2640-2646.

CHAPTER 6 Homogeneous DNA Detection Using Polymer-Coated Core-shell Nanoparticles

6.1 Introduction

Particle-based colorimetric biosensing is based on a simple concept in which molecules of interest (target analytes) are detected by monitoring the absorption changes of metallic nanoparticles. In particular, the nanoparticles used in the assays are pre-coated with different capture probes that recognize the same target analyte but of different binding sites. Molecular recognition between the target analytes and the capture probes leads to the formation of particle aggregates and subsequently red-shifts the surface plasmon absorption (λ_{max}) of the particles due to electromagnetic coupling. Mirkin and his coworkers demonstrated this concept in DNA sensing in which 3 strands of DNA sequences formed DNA duplexes during hybridization and brought Au nanoparticles into a close proximity which resulted in the precipitation of Au particle aggregates. Their unoptimized system can detect about 10 femtomoles of an oligonucleotide.[1,2] Tan *et al* combined isothermal DNA amplification with gold nanoparticle-based colorimetric detection to push the detection limit down to 1 atomole. This isothermal amplification method provides $>10^6$-fold amplification in 5min.[3] Storhoff *et al* have improved the detection limit of the colorimetric detection method to zeptomole range by monitoring scattered light rather than reflective light from gold nanoparticles.[4] Rothberg *et al* have made a twist of the concept by taking advantage of the different affinity of single stranded DNA and double stranded DNA to citrate-coated gold nanoparticles. DNA duplexes

couldn't absorb onto citrate coated gold nanoparticles and the particles aggregated at increased salt concentration, whereas the absence of hybridization (i.e. no detectable target DNA sequences present) prevented the particles from salt-induced aggregation. The assay they developed can detect less than 100 femtomoles of target DNAs in 5min.[5]

A reverse-colorimetric detection scheme in which the presence of target DNA molecules leads to the immobilization of an initiator molecule on the Au nanoparticle surface through DNA hybridization and ligation reactions was reported here (**Scheme 6.1**). This small molecule is capable of initiating radical polymerization that prompts polymer growth and forms a thin yet stable polymer layer outside of the particles. Exposing the DNA-coated particles to an extremely high salt condition or centrifugation the particles at high speed rate results in particle aggregation, and subsequently changes the optical absorption of the particles. In contrast, the polymer-DNA coated particles are stable and no surface plasmon shift is observed.

For this study, atom transfer radical polymerization (ATRP), a controlled/"living" free radical polymerization process, is used to grow DNA-hybrid polymer outside of nanoparticle surface.[6-8] It is a robust polymerization reaction based on the repetitive addition of monomers to radicals in a reversible redox process. By maintaining a low yet stationary concentration of radicals through the establishment of equilibrium between the active and dormant species, a steady growth of polymer chains on the surface is achieved till the complete consumption of monomers or forced radical termination. Compared with free radical polymerization, ATRP limits the growth of polymer chains at where the reaction initiators are located, i.e. a point-initiated polymerization reaction.

ATRP has been used to grow polymer chains from the surface, including both flat surface, such as silicon, silica, gold, and carbon black, and curved surface of spherical particles, such as silica particles and polystyrene particles.[9] Among them, polymer/silica and polymer/polystyrene latex core shell nanoparticles are the most popular type of hybrid studied.[10-13] One major reason behind this is the relatively good stability and versatile solubility of modified silica and latex particles. The syntheses of polymer/gold hybrids have been conducted only in organic solvents by ATRP because hydrophobic initiator monolayer coated gold nanoparticles do not dissolve well in an aqueous solution.[14,15] Herein for the first time the growth of polymers atop a DNA layer in a core-shell particle format was demonstrated in aqueous ATRP due to the good solubility of DNA coated gold nanoparticles in water. The immobilization of DNA outside of gold nanoparticles greatly enhanced the stability of gold nanoparticles in aqueous solution at high ionic strength. This improved stability opens a door for the synthesis of polymer/gold nanoparticles using aqueous ATRP. This polymer/gold hybrid has wide potential applications in many fields such as biosensing and drug delivery. The application in DNA biosensing as an example has been illustrated.

6.2 Experimental Section

6.2.1 Materials

Single stranded DNAs used in this study were purchased from Integrated DNA Technologies, Inc. (Coralville, IA) and are listed in **Table 6.1**. Monomethoxy-capped oligo (ethylene glycol) methacrylate (OEGMA, mean degree of polymerization of 7-8)

was a gift from Laporte Specialties (Hythe, UK). 2-hydroxyethyl methacrylate (HEMA, 98%) was purchased from Sigma-Aldrich. OEGMA and HEMA were both purified to remove methyl hydroquinone inhibitor using an inhibitor remover column packed in house. N-hydroxysuccinimide acid (NHS), bromoisobutyryl bromide, 3-hydroxypicolinic acid (3-HPA), diammonium citrate, dioxane, dithiothreitol (DTT), triethylamine (TEA), CuCl, $CuBr_2$, 2, 2'-bipyridine (bpy), trissodium citrate dihydrate, $HAuCl_4 \cdot 3H_2O$ and diethyl ether were purchased from Sigma-Aldrich and used as received. Bis(p-sulfonatophenyl)phenylphosphine dihydrate dipotassium (BSPP) was purchased from Strem Chemicals Inc. (Newburyport, MA). NAP-5 columns (Sephadex G-25 Medium, DNA grade) were purchased from Pharmacia Biotech. For all experiments, Millipore H_2O purified with a Millipore ultra-pure water system was used. The 300 mesh copper grid with formvar/carbon supportive films (prod# 01753-F) were purchased from Ted Pella Inc. (Redding, CA).

6.2.2 Preparation of Au Nanoparticle Conjugates Prior to ATRP Reactions

A solution of 13nm Au nanoparticles was prepared according to previously published protocols.[16] In particular, an aqueous solution of $HAuCl_4$ (1mM, 250mL) was heated and refluxed for 10min. A solution of trisodium citrate (38.8mM, 25mL) was quickly added to the refluxed $HAuCl_4$ solution, resulting in a rapid color change from pale yellow to deep red that indicated the formation of gold nanoparticles. After a continuous reflux for an additional 15min the solution was slowly cooled down to room temperature and the particle solution was filtered through a 0.22μm cellulose nitrate filter

to remove any floating aggregates. The quality of the particles was monitored with UV-vis and transmission electron microscopy (TEM). All glassware and the stir bar used in the preparation was cleaned in aqua regia (3:1 HCl:HNO_3), rinsed with Millipore water, and then dried in an oven.

A solution of citrate-coated nanoparticles (10mL) was then mixed with 25mg BSPP to replace the citrating coating with BSPP.[17] The mixture was stirred vigorously for an overnight reaction. The resulting colloidal particles were precipitated by adding NaCl powder to the stirred solution until the colloidal suspension turned gray/brown. The gray/brown solution was centrifuged for 15min at 13,000rpm until a black pellet was formed at the bottom. After the removal of the supernatant, the pellet was resuspended in 250mg/mL BSPP solution for storage.

DNA-particle conjugates were prepared through direct thiol-Au interaction using either a dual-labeled ssDNA (**Nano-A-IN**) or 3'-thiolated capture DNA probe (**Nano-B-SH**). For example, in the preparation of **Nano-A-IN** DNA conjugates, ATRP initiators were first coupled to **Nano-A** DNA probes by mixing 40μL 10 x conjugation buffer (1.0M $NaHCO_3/Na_2CO_3$, pH9.0), 280μL disulfide bond-protected **Nano-A** (100μM), and 80μL bromoisobutyryl NHS ester [18] in a DMF solution (10mg/mL) for 30min. 480μL of 0.1M DTT and 19.2μL of triethylamine (TEA) were then added into the same tube for 20min to cleave the disulfide bonds. The reaction mixture of **Nano-A-IN** was purified in a phosphate buffer (10mM) using a desalting NAP^{TM}-10 column. The concentrations of the DNA solutions were determined by the UV-vis absorption at 260nm. The initiator coupling and disulfide reduction efficiencies were monitored using MALDI mass

spectrometry. **Nano-B-SH** was simply prepared by mixing 100μL ssDNA **Nano-B**, 100μL 0.1M DTT, 5μL TEA and 45μL water for 20min for disulfide cleavage, followed by column purification and UV-vis quantification. Both reduced DNA probes (**Nano-A-IN** or **Nano-B-SH**) were mixed with BSPP-coated Au nanoparticle solution (~122nM) at a molar ratio of 500:1. After 16hr incubation, the final solution salt concentration was gradually increased to 0.3M NaCl by stepwise adding 1M NaCl phosphate buffer in 2 days to increase DNA loading. The conjugates were washed with 0.1M NaCl or 0.3M KCl 20mM tris-HCl (pH7.5) and stored in water for **Nano-A-IN**, in 0.3M KCl 20mM tris-HCl for **Nano-B-SH** at 4°C till the next experiments.

Initiator-coupled DNA detection probe (**Nano-D-IN**) was prepared as previously described by incubating oligonucleotide **Nano-D** with bromoisobutyryl NHS ester solution for 30min reaction, followed by the removal of unreacted NHS ester by gel filtration. MALDI-TOF MS was again used to monitor the coupling efficiency by measuring the amount of oligonucleotides before and after the coupling reaction.

During DNA hybridization, a mixture of **Nano-B**-coated GNPs (35nm), complementary target DNA **B'D'** (or non-complementary DNA target **Non-B'D'**, concentrations in text), and 0.1-1μM detection probe (**Nano-D-IN**) were prepared in 0.3M KCl 20mM tris-HCl (pH7.5) and incubated for different period of times at room temperature. The solution was then diluted with T4 ligation buffer containing 0.09U/μL T4 ligase and incubated for 1hr. After 1hr incubation, the reaction mixture was centrifuged at 10000rpm for 30min, washed twice by 0.3M KCl 20mM tris-HCl and resuspended into the same buffer.

6.2.3 Au Nanoparticle Conjugates during ATRP Reactions

A 25μL solution of initiator-coated GNPs was mixed with 6.25μL OEGMA and 50μL H_2O, and degassed for 5min under Ar. The ATRP reaction was then initiated by introducing 3μL freshly purged catalyst stock solution (CuCl/30%$CuBr_2$/bpy, 100mM). The reaction was terminated by introducing fresh air into the system to quench radicals and the particles was purified by centrifugation at 13000rpm for 30min. Similarly, a 50μL GNP solution was also used to react with 25μL of 2-hydroxyethyl methacrylate (HEMA) as the polymerization monomers in 100μL H_2O/75μL DMF to improve PHEMA solubility. After the ATRP reaction, the gold nanoparticles were cleaned and re-dispersed in H_2O or methanol for POEGMA-coated and PHEMA-coated particles, respectively.

6.2.4 Instrumentation

A Voyager^{TM} DE-STR matrix-assisted laser desorption/ionization mass spectrometry (MALDI-MS) was used to monitor the coupling reaction between amino-labeled DNA and bromoisobutyryl NHS ester, and the reduction of disulfide bonds on DNA. A linear positive detection mode was used; each spectrum was collected by averaging 100 laser shots. The best detection was achieved at 90% grid voltage of 25,000V and 300ns delay time. The MALDI matrix solution contained 35mg/mL 3-HPA, 7mg/mL diammonium citrate, and 10% acetonitrile. DNA solutions were desalted using C_{18} ZipTips (Millipore) before the MALDI measurements.

We used an Agilent 8453E UV-visible Spectrophotometer to characterize the optical properties of citrate, BSPP, DNA, and polymer coated gold nanoparticles. The prepared gold nanoparticles were diluted with appropriate buffers before transfering them to the sample sell. The scanning wavelength was set from 400 to 900nm for all the measurements of Au nanoparticle conjugates.

For the light scattering measurements, a Malvern 1000HSa light scattering instrument from Malvern Instruments (Worcestershire, UK) operating with 5mW He-Ne laser at 633nm and a fixed scattering at 90° was used to measure particle size. For all samples, data was collected at room temperature and was averaged from 3 runs.

The agarose gel electrophoresis experiments were conducted in 1% agarose gel and were run in 1 x TBE buffer (89mM Tris-borate, 2mM EDTA), at a voltage of 96V. 10μL sample and 4μL glycerol was mixed and loaded into each well. The gels were scanned in a HP scanner.

Transmission electron microscopy (TEM) was performed with a Hitachi 8100 transmission electron microscope. A typical sample was prepared by dropping 10μL of the nanoparticle solution onto a copper TEM grid with formvar/carbon supportive films, followed by wicking the solution away. The grid was subsequently dried in the air and imaged.

AFM images were captured in tapping mode utilizing a Digital Instruments Nanoscope IIIa controller and multimode base. The following protocol was used for imaging all POEGMA or PHEMA coated particles. A solution with a nanoparticle concentration of circa 1nM was diluted using deionized water by a factor of

approximately 10:1. The solution was then placed upon a freshly cleaved mica substrate and allowed to rest for between 10-15min. The solution was then wicked dry using capillary action with a Kimwipe. After this step the sample was washed 3-4 times with a total of 300μL of DI water, using a Kimwipe after each wash to wick away the water. Once the last wash and wick cycle was completed the sample was then blown dry under a gentle nitrogen stream. The BSPP particles were prepared using a nanoparticle solution with a concentration of circa 1nM which was diluted by a factor of 25:1. The solution was placed upon freshly cleaved mica and allowed to rest for 10-15min. The sample was then wicked dry with a Kimwipe and imaged without any further modifications. The purpose of the extra steps with the POEGMA or PHEMA particles was to remove free polymer from the surface.

The data points were generated by measuring a collection of particles from various images and determining their heights utilizing the Digital Instruments software. The images were flattened before entering the line scan portion of the software. A three way line scans was measured for each particle and the highest number for each particle was taken to be its true height. The numbers were then transferred to an Excel spreadsheet where the average and standard deviation were calculated. The error bars for the data points are the 95% confidence interval for that point.

6.3 Results and Discussion

6.3.1 Polymer Growth on DNA-coated Nanoparticles

For the study, a solution of 13nm Au nanoparticles (GNPs) was prepared according to the previously published protocol using trisodium citrate as the reducing reagent. A typical solution of 13nm diameter gold particles exhibited a characteristic surface plasmon band centered at 520nm (**Figure 6.1, a**). The TEM image collected also confirmed the synthesis of uniformed GNPs (**Figure 6.2, A**). The citrated –coated gold nanoparticles are well known for their relative low stability in high ionic strength. Enhanced nanoparticle stabilization is essential to prevent colloidal aggregation during ATRP polymerization.

To further improve the particle stability, bis(p-sulfonatophenyl)phenylphosphine dihydrate dipotassium (BSPP) was used to replace the citrate coating.[17] The resulting particle solution showed a slight surface plasmon shift from 520nm to 523nm (**Figure 6.1, b**) and no changes were observed from TEM image (**Figure 6.2, B**). The successful replacement of citrate by BSPP outside GNPs was confirmed by the significantly improved stability of gold nanoparticles. The NaCl titration experiment illustrated that citrate-coated gold nanoparticles were not stable when the concentration of NaCl is higher than 5mM (**Table 6.2**). BSPP coated gold nanoparticles stayed suspended until NaCl concentration was higher than 90mM (**Table 6.3**). This increased stability was also observed in the gel electrophoresis experiment (**Figure 6.3**). When 13nm citrate-coated GNP (lane **a** and **g**) was loaded onto the agarose gel the GNP immediately aggregated

into the well, as indicated by the color change from red to blue. However, no color change was observed for BSPP-coated GNP (lane **b** and **h**) on the same gel.

DNA gold nanoparticle conjugates were synthesized following the procedure developed by the Mirkin group.[19] The ssDNAs with disulfide bond at one end were reduced by DTT to form free thiol group. MALDI-TOF was used to routinely monitor the coupling of initiators onto DNAs and disulfide bond reduction. As shown in **Figure 6.4**, the successful two-step synthesis **Nano-A-IN** was confirmed by the molecular ion peak shifts in corresponding MALDI-TOF spectra. A single MS peak at *m*/*z* 6446.4 was observed before the coupling reaction, corresponding to the molecular ion peak of **Nano-A**. The MS peak shifted to *m*/*z* 6596.6 upon coupling of the bromoisobutyryl group. The observed mass increase of Δ*m*/*z* 150.4 corresponded well to the expected structural addition of the bromoisobutyryl moiety (theoretical Δ*m*/*z* 148.9). The disappearance of the *m*/*z* 6446.4 peak suggested that the coupling reaction was close to completion in 30 min. A subsequent reduction of disulfide bonds at the 3'-end of **Nano-A** led to the back shift of the MS peak to *m*/*z* 6507.6, along with the disappearance of the MS peak at *m*/*z* 6596.6.

The λ_{max} of UV-vis absorption of purified DNA-coated gold nanoparticles was sightly higher than that of citrate-coated GNPs, but similar to that of BSPP-coated GNPs (**Figure 6.1, c**). The TEM image showed clusters of individual Au nanoparticles, which were formed during the drying process of sample preparation on the TEM grid (**Figure 6.2, C**). The formation of clusters was not observed for either citrate-coated or BSPP-

coated Au nanoparticles. The driving force of the formation of clusters for DNA coated gold nanoparticles might be the strong hydrogen bonding among DNA molecules.

To demonstrate the feasibility of polymer growth on the DNA-coated particles using ATRP, a ssDNA molecule of dual functional groups (**Nano-A-IN**) was used to mimic the ligation product. The 5'-termini of DNAs were modified with primary amines that were pre-coupled with bromoisobutyryl NHS ester, the ATRP initiator. The 3'-thiol groups were used for DNA attachment to bring the ATRP initiators close to the particle surface. **Scheme 6.2** shows the chemical reaction in ATRP. 50μL GNP solution was used to react with 25μL of 2-hydroxyethyl methacrylate (HEMA) in H_2O/DMF. 30% (volume percentage) DMF was used to improve PHEMA solubility and prevent particle aggregation. The UV-vis spectra of PHEMA-coated particles demonstrated the shift of surface plasmon from previous 523nm to 535nm (**Figure 6.1, d**), a strong evidence of the polymer shell formation with an increase in local dielectric constant surrounding the particles. By comparison, the DNA (**Nano-A**) coated GNPs under the same reaction conditions were aggregated as indicated by the broad absorption in UV-vis (**Figure 6.1, e)**. The similar phenomenon was also observed when OEGMA was used as the monomer (**Figure 6.5, A**).

To further confirm the growth of the polymer shell on DNA-coated nanoparticles, gel electrophoresis was used to examine the mobility change on the particles (**Figure 6.3**). BSPP-coated GNPs with increased particle stability migrated towards the cathode inside of the porous gel upon the use of electric field. A similar charge density was measured from ssDNA-coated GNPs to BSPP-coated ones. The long DNA strands

loosely bound on the particles in comparison to a close-packed BSPP layer, however, significantly increased the particle solvation diameter and increased the particle movement friction. Subsequently, the DNA-coated GNPs lagged behind BSPP-coated particles (**Figure 6.3**, lane **c** and **i**).[20, 21] The POEGMA-DNA coated GNPs were even further behind (**Figure 6.3**, lane **j**), a combined result of successful shielding of the negative charges on the DNA backbones with neutral polymer chains and significantly increased particle sizes. The POEGMA –DNA coated GNPs instead of PHEMA-coated were selected in this gel electrophoresis experiment for their good solubility and stability in the gel electrophoresis buffer.

Further evidences on the core-shell formation are shown in the light scattering measurements in which the particle dynamic sizes changed from 30nm of DNA-coated particles to 120nm of PHEMA-DNA-coated particles (**Figure 6.6**).[20] The formation of polymers around the particles was also directly visualized in the TEM images (**Figure 6.2, D-F**): most particles remained isolated from each other after ATRP, which was significantly different from DNA coated-Au nanoparticles **(Figure 6.2, C)**. The average diameter of GNP-PHEMA hybrids was 90-100nm, slightly smaller than the value from light scattering measurements. This difference is in agreement with the fact that TEM measurements were conducted on dried samples and light scattering measured the hydrodynamic size of the samples. The high energy electron beam used in TEM partially cachinnated the attached polymer shells. Therefore, the layer changed into an opaque color and deformed during imaging (**Figure 6.2, D** and **6.2, E**). With extended TEM imaging, the polymer films were completely vaporized with only GNPs left behind,

making the actual size measurement a challenging task. Nevertheless, a careful examination of the TEM results showed that the polymeric materials were only presented around GNPs, qualitatively confirming the polymer attachment. Images in **Figure 6.2, D** and **6.2, E** were collected from the unpurified PHEMA-coated sample. Similar results were seen in **Figure 6.2, F** from POEGMA-coated GNPs.

6.3.2 Polymer-DNA-Coated GNPs in DNA Detection

An interesting color change phenomenon was observed after ATRP was conducted on gold nanoparticles. The color change was clearly observed from **Nano-A**-coated particles either immediately or overnight after the ATRP reaction**,** whereas the polymer-DNA-coated GNPs remained unchanged with the original burgundy color (**Figure 6.5**). The original stability of ssDNA-coated GNPs in solution was attributed to the highly charged backbones of DNA molecules that electrostatically repelled each other. A mild increase in ionic strength of the particle environment, e.g. 0.3M KCl hybridization buffer, was not sufficient to neutralize all the charges on the GNPs; therefore the DNA-coated GNPs did not precipitate during DNA hybridization. The stability and solubility of DNA-coated GNPs in the ATRP reaction solution was decreased due to the decreased polarity of the solution containing less polar components such as monomers (OEGMA or HEMA) and catalyst ligands. It was observed that the DNA-coated GNPs changed into purple color when HEMA was added into the aqueous solution of GNPs before ATRP. In order to increase the solubility of GNPs, 30% DMF was added into the reaction mixture.

However, the formation of the polymers outside of GNPs during ATRP could enhance the stability of GNPs provided that the polymers have good solubility in the reaction mixture. The polymer shells behaved as a cushion to separate GNPs away from each other and prevent the aggregation during ATRP.[22,23] The free polymer formed in solution either from free initiators left over (calculated concentration 3-30pM) or from auto polymerization also improved the stability of even uncoated GNPs to the certain level. However, the polymer formed in solution couldn't permanently prevent the aggregation of GNPs. The DNA-coated-only GNPs slowly aggregated overnight as shown in **Figure 6.5, C**. In comparison the GNPs with polymer covalently coated outside remained stable after an extended period of time.

The difference in particle stability was confirmed by an accelerated means to differentiate surface bound polymers and free polymers in solution by centrifugation. The surface attached polymer was still bounded to the GNPs after 30min centrifugation at a high spinning rate and the resulting red pellet was able to be resuspended into the appropriate solvents. The free polymers were separated from GNPs after centrifugation and the resulting black pellet of aggregated particles can not be resuspended into the appropriate solvents even by sonication.

Considering the polymer shell only forms when there is the ATRP initiator immobilized on the GNP surface, a DNA sensing method can be derived by building a direct correlation between DNA hybridization and initiator attachment, and taking advantage of this stability difference to signal the occurrence of DNA hybridization in a reversed colorimetric detection.

Scheme 6.1 illustrates the concept of the formation of core-shell particles in DNA sensing. Specifically, the assay was conducted in four stages: **I**: the attachment of capture DNA probes (**Nano-B**) that recognized the target sequences (**B'D'** or **Non-B'D'** as the control); **II**: DNA recognition through conventional DNA hybridization by forming three-strand DNA duplexes with the target DNA **B'D'** and detector **Nano-D-IN**. A ligation experiment was also carried out to permanently affix the ATRP initiators at the GNP surfaces**.** The stage **III** was the ATRP reaction that formed a polymer shell to stabilize the particles, followed by the last stage (**IV)** of solution centrifugation to differentiate the GNPs with polymer shells from those without.

The result of the proof of concept experiment was shown in **Figure 6.7**. When complementary target DNA **B'D'** and detector **Nano-D-IN** was mixed with **Nano-B** coated Au nanoparticles, followed by T4 ligation, dsDNA (**Nano-B-D-IN**) was formed outside of GNPs. In contrast, **Nano-B** coated Au nanoparticles kept unchanged when incubated with the mixture of non-complementary target DNA **Non-B'D'** and **Nano-D-IN**, followed by ligation. When dsDNA was formed outside the GNPs, the size of GNPs was larger than that of the corresponding ssDNA-coated GNPs and the mobility of GNPs was smaller than that of the corresponding ssDNA-coated GNPs. The gel electrophoresis data clearly demonstrated the successful formation of dsDNA outside GNPs under the right conditions (**Figure 6.3, d**). Lane **d** moved slower than lane **c**, which resulted from the successful hybridization with **B'D'**. As contrast, lane **e** moved at the same rate as lane **c** did due to the absence of hybridization with **Non-B'D'**.

Regardless of the success of the hybridization and ligation steps, the gold colloid solutions still maintained the same red color for both reaction conditions. However, after 1.5hr ATRP and centrifugation the two reaction mixtures showed distinctively different colors: red color for the colloid mixed with matched **B'D'** and the blue color for the one mixed with non-complementary target **Non-B'D'** (**Figure 6.7,** bottom). The blue color was from the oxidized copper catalyst where the aggregated particles precipitated at the bottom. UV-vis spectra were taken after ATRP (**Figure 6.7,** top). The plasmon band of the colloid mixed with matched **B'D'** red shifted to 529nm due to the polymer growth outside GNPs. By comparison, the gold nanoparticle plasmon band of the one mixed with non-complementary target **Non-B'D'** disappeared and only broad absorption from copper catalyst was observed. All these experimental data positively supported the potential application of this method in DNA detection.

After the success of the proof of concept experiment, the detection limit of this method was tested. **Figure 6.8** illustrated the successful detection of target DNA (**B'D'**) with the concentrations ranging from 1μM, 1nM, 1pM, 1aM and 0. The colors of the solutions varied from the most stable GNPs in red, to a slight purple color of little aggregation, to the blue of complete aggregation of the control. It was astonishing to note the significant color difference between the sample containing only 1fM target sequence and the tube without any target DNAs, regardless both tubes went through the same experimental steps, including ATRP (while the 1aM tube also showed color difference, to err on the conservative side, the detection limit was estimated at the fM level). AFM height measurements showed significant height increase after the ATRP reaction, even

for the particles incubated with 1aM target DNA (**Figure 6.8,** bottom). The heights of the particles increased with the increase of the target DNA concentrations, as expected. Considering the concentration of GNPs in solution was approximately 10nM, 1fM target DNA in solution suggested that less than three in 10^8 GNPs were hybridized with a single copy of DNA. It is difficult to comprehend that the growth of POEGMA from three copies of DNA molecules was sufficient to stabilize 10^8 particles in solution, with the assumption that the hybridization efficiency was 100% and the ATRP initiator was 100% active. However, the phenomenon was observed several times, which eliminated the possiblility of operator error. The possibility of nonspecific polymer growth was also eliminated since no GNP stabilization was observed from the control system. A careful examination of GNP stability with its double-layer potential and the possible radical transferring with rapid binding kinetics among particles is in process.

Further improvement in detection sensitivity was achieved by extending the polymerization time. For example, by merely doubling the reaction time to 2hr resulted in a more stable GNP solution for the detection of 1aM target sequence with improved confidence (**Figure 6.9**). Extending the ATRP reaction time from 1hr to 12hr, a large λ_{max} shift was observed in the UV-vis spectrum, suggesting the formation of a thicker polymer film and the possibility of further lowering of the detection limit.

6.4 Conclusions

A homogeneous DNA detection method using polymer-Au core-shell nanoparticles was reported here. In particular, poly-monomethoxy-capped oligo (ethylene

glycol) methacrylate (POEGMA) was selectively grown on Au nanoparticles where DNA hybridization occurred. The formation of the polymer shell stabilized the particles in solution against aggregation under high ionic strengths and strong centrifugation forces. UV-vis absorption spectroscopy, dynamic light scattering (DLS), gel electrophoresis, transmission electron microscopy (TEM) and atomic force microscopy (AFM) were used to characterize the formed core-shell particles. This amplification-at-will platform was shown to be flexible and sensitive. Despite the limited knowledge on the rationale behind this extremely high sensing sensitivity obtained, the profound impacts of its realization can not be ignored.

Schemes

Scheme 6.1: Colorimetric DNA Sensing Using Core-Shell Particles Formed in ATRP.

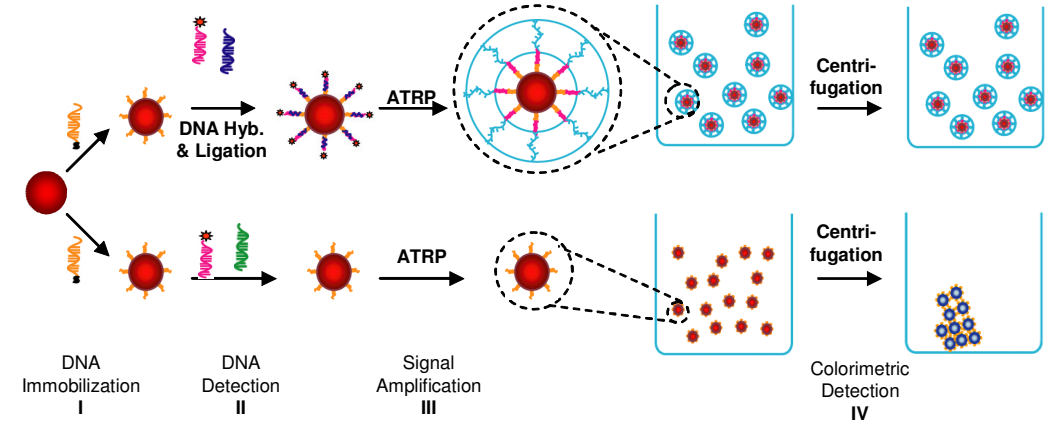

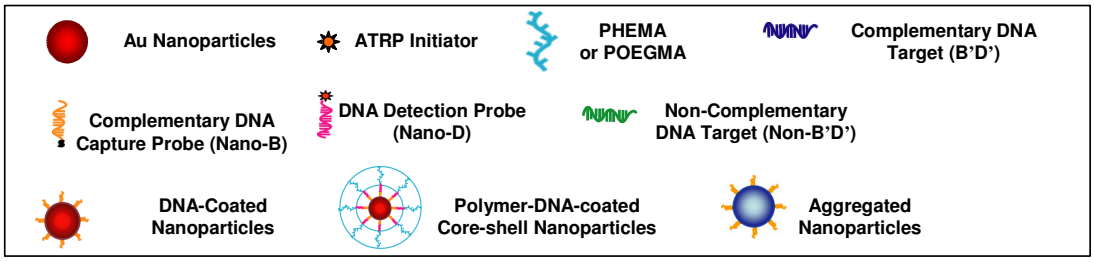

Scheme 6.2: PHEMA and POEGMA Formation in ATRP.

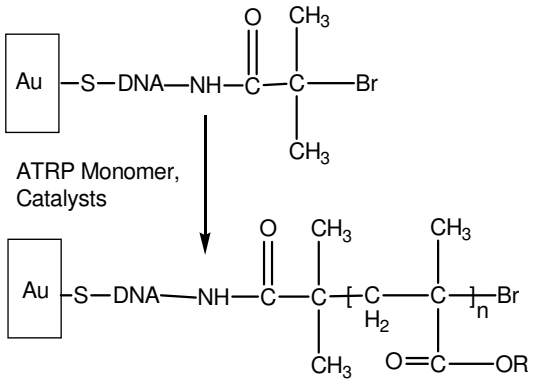

R=CH_2CH_2OH (as in PHEMA)

or = $(CH_2CH_2O)_7CH_3$ (as in POEGMA)

Tables

Table 6.1 Summary of the DNA Sequences Used.

Name	Sequence	Description
Nano-A	5'-NH_2-C_6-T_{20}- C_3-S-S-C_3	Dual-Labeled DNA Sequence
Nano-A-IN	5'-Br$(CH_3)_2$CCONH-C_6-T_{20}-C_3-S-S-C_3	Initiator-Labeled DNA Sequence
Nano-B	5'Phos-CAC ATT GTC TGG CAC T_{20}- C_3-S-S-C_3	Capture Probe for Solution-Based DNA detection
B'D'	5'TGC CAG ACA ATG TGA TAA ATG GTG TAA	Complementary Target DNA to Probes **Nano-B** and **Nano-D**
Non-B'D'	5'GGA TTA TTG TTA AAT ATT GAT AAG GAT	Non-Complementary Target DNA to probes **Nano-B** and **Nano-D**
Nano-D	5'NH_2-C_6-T_{20}AAT TAC ACC ATT TAT	Detector Probe for Solution-Based DNA detection with Amino Groups for the coupling of ATRP Initiators

Table 6.2 NaCl Titration of Citrate-Capped Gold Nanoparticles (13nm).

Volume NaCl(1.0M) added(µl)	$[Na^+]$ in solution (mM)	λ_{max}(nm)	Abs(OD)
0	0	522	0.862
5	9.9	524	0.873
10	19.6	524	0.832
15	29.1	524	0.772
20	38.5	526	0.725
25	47.6	528	0.666
30	56.6	531	0.575
35	65.4	536	0.498
40	74.1	630	0.468

[citrate-coated GNP] = 1nM. 500µL.

Table 6.3 NaCl titration of BSPP-Capped Au Nanoparticles (13nm).

Volume NaCl(1.0M) added(μl)	$[Na^+]$ in solution (mM)	λ_{max}(nm)	Abs(OD)
0	0	526	0.849
5	9.9	526	0.848
10	19.6	526	0.838
15	29.1	525	0.835
20	38.5	526	0.826
25	47.6	526	0.817
30	56.6	526	0.808
35	65.4	525	0.801
40	74.1	526	0.796
45	82.6	526	0.790
50	90.9	528	0.774
55	99.1	528	0.757
60	107.1	528	0.745
65	115	532	0.726
70	122.8	537	0.714

[BSPP-coated GNP] = 1nM. 500μL.

Figures

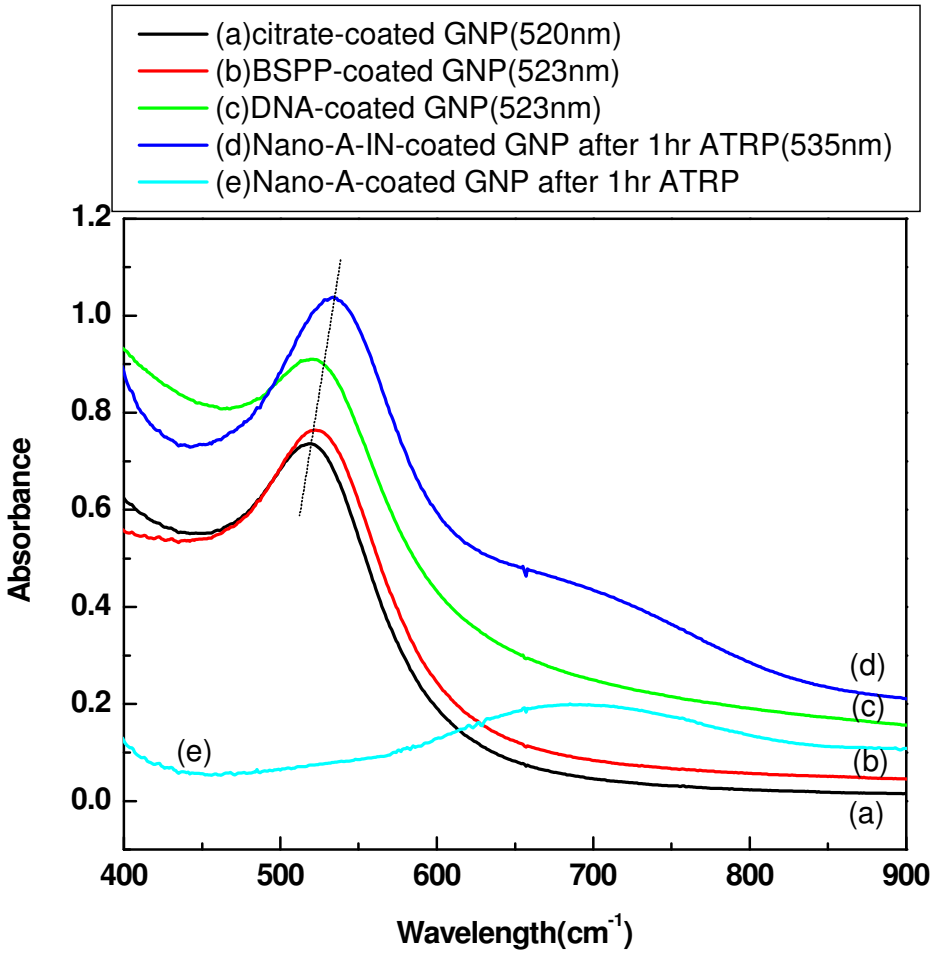

Figure 6.1 *Polymer-coated particle characterization:* UV-vis spectra of (a) citrate-coated 13nm Au nanoparticles (λ_{max}520nm), (b) BSPP-coated Au nanoparticles(λ_{max} 523nm), (c) DNA (Nano-A-IN)-coated Au nanoparticles(λ_{max}523nm), (d) DNA (**Nano-A-IN**)-coated Au nanoparticles after 1.5hr ATRP (λ_{max}535nm) and (e) DNA (**Nano-A**)-coated Au nanoparticles after 1.5hr ATRP.

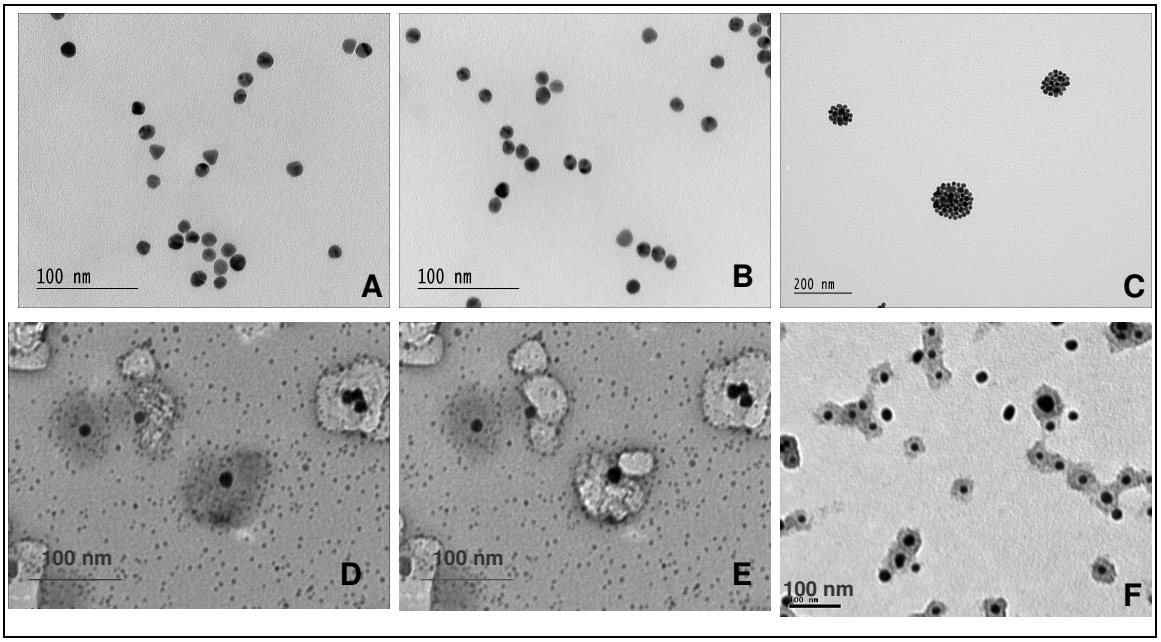

Figure 6.2 *TEM images of Gold particle conjugates:* (A) citrate-coated Au nanoparticles, (B) BSPP-coated Au nanoparticles, (C) DNA-coated Au nanoparticles, (D) and (E) DNA-coated Au nanoparticles after a 1.5hr ATRP reaction using HEMA as the monomers, and (F) DNA-coated Au nanoparticles after 7hr ATRP reaction using OEGMA as the monomers.

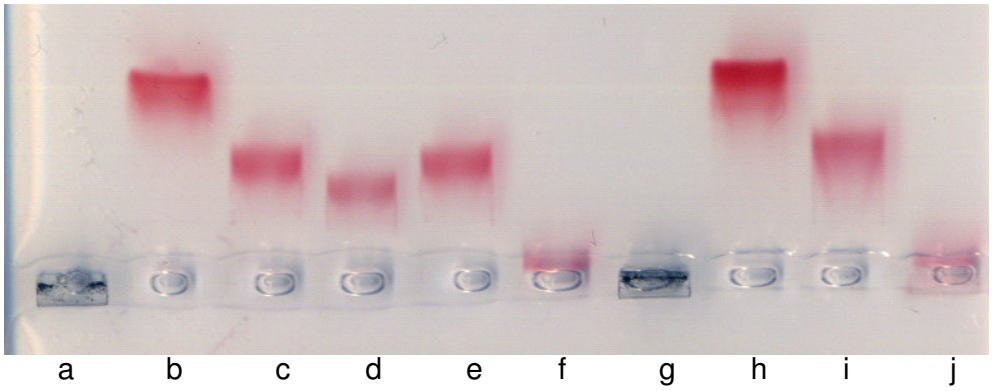

Figure 6.3 *Au particle conjugates characterization:* Nondenaturing 1% agarose gel of gold nanoparticles: (a) and (g) citrate-coated Au nanoparticles (13nm), (b) and (h) BSPP-coated Au nanoparticles, (c) DNA (Nano-B)-coated Au nanoparticles, (d) DNA duplex (Nano-B-B'D'-D-IN)-coated Au nanoparticles, (e) DNA (Nano-B)-coated Au nanoparticles after mixing with non-B'D' and D-IN, followed by ligation, (f) DNA duplex (Nano-B-B'D'-D-IN)-coated Au nanoparticles after 1hr ATRP, (i) DNA (Nano-A-IN)-coated Au nanoparticles and (j) DNA (Nano-A-IN)-coated Au nanoparticles after 3hr ATRP.

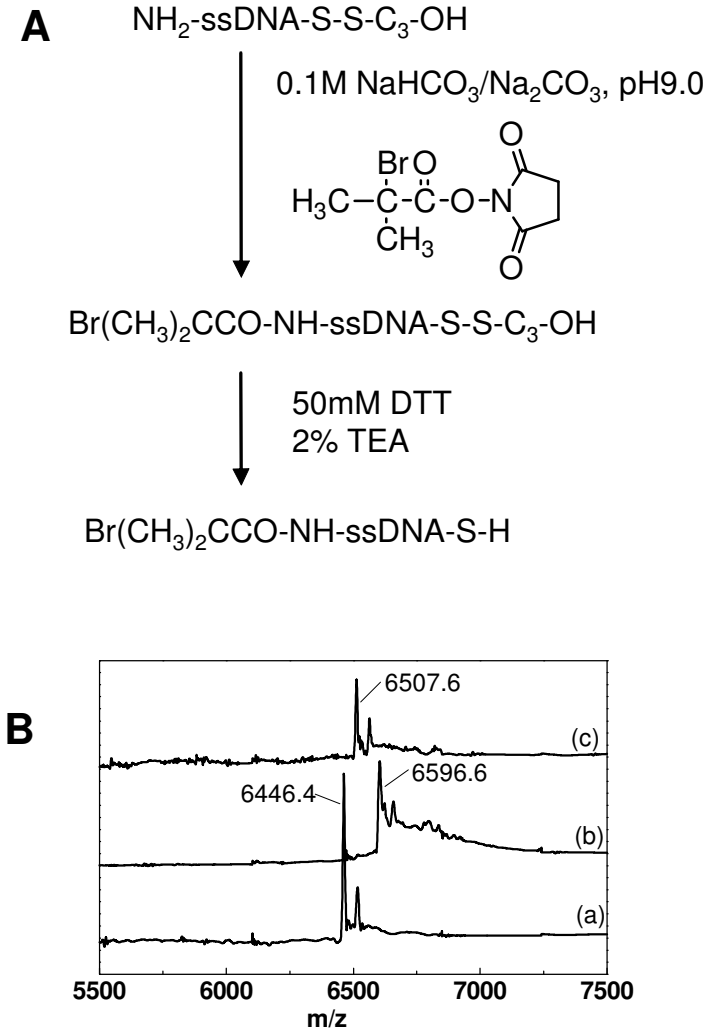

Figure 6.4 (A) Chemical pathway to prepare initiator-coupled ssDNA(**Nano-A-IN**) molecules to be used as the model molecule in the study; (B) MALDI spectra of (a) **Nano-A**, (b) initiator-coupled **Nano-A**, and (c) initiator-coupled **Nano-A** after DTT reduction. Details of the measurements see the Experimental Section.

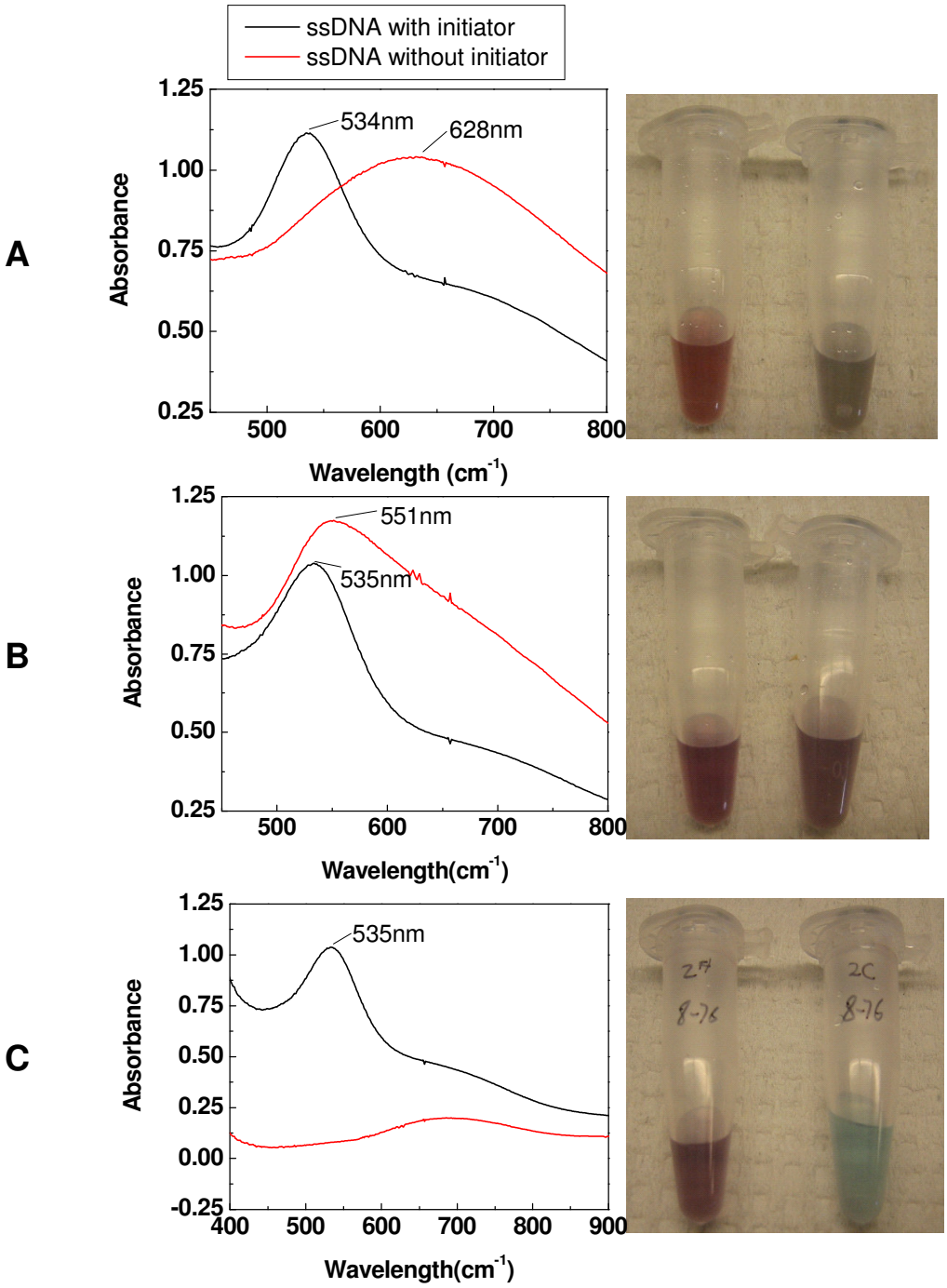

Figure 6.5 UV-vis spectra and photo images of DNA conjugates (**Nano-A** red line and **Nano-A-IN** black line) immediately after 1.5hr ATRP when (A) OEGMA and (B) HEMA used as monomers, and (C) overnight after 1.5hr ATRP when HEMA used as monomers. All UV-vis spectra were collected without sample purification.

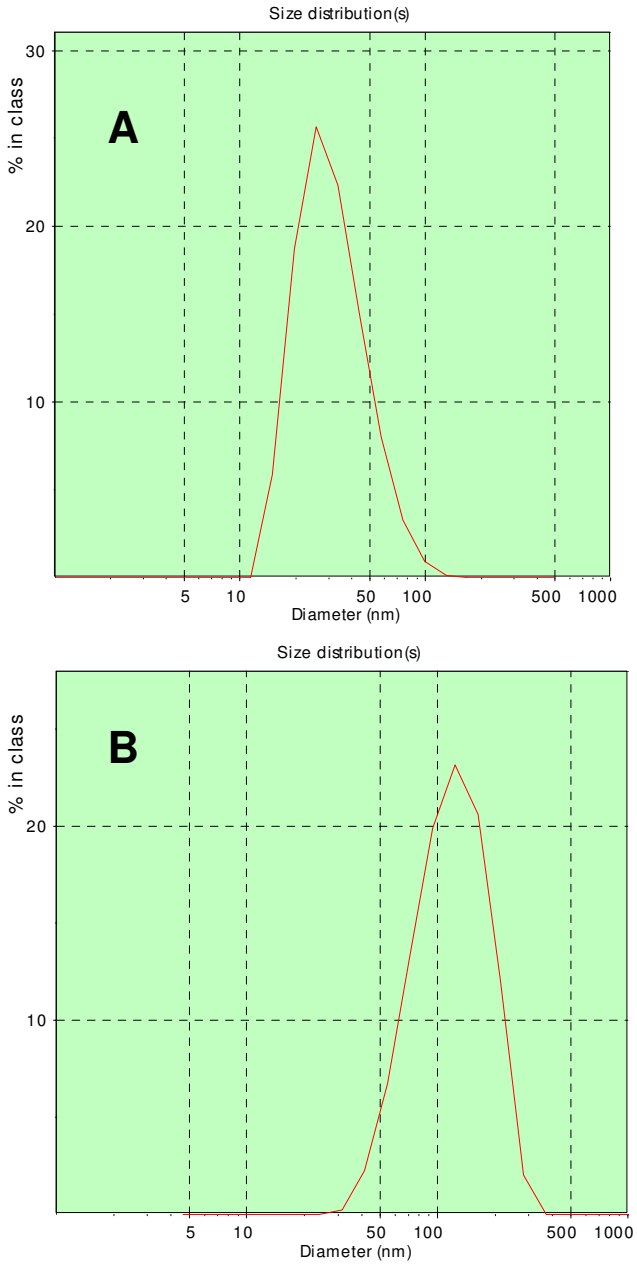

Figure 6.6 Light scattering measurements of DNA (Nano-A-IN) GNP conjugates (A) before and (B) after 1.5hr ATRP. ATRP reaction conditions were mentioned in Experimental section. HEMA was used as monomer in this case.

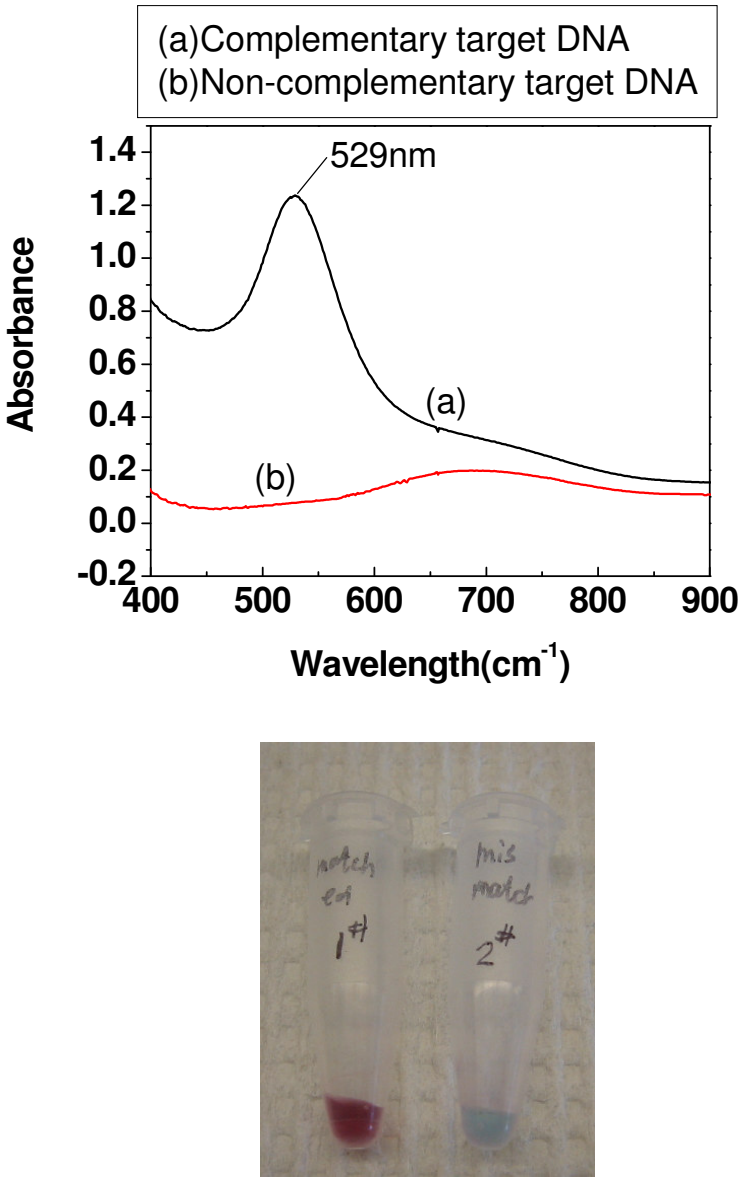

Figure 6.7 *Concept-proof in DNA sensing* (Top) UV-vis spectra of Au nanoparticles in the detection of 1μM complementary DNA (B'D') (a) and the detection of 1μM non-complementary DNA (Non-B'D') in the control experiment (b) after an 1.5hr ATRP reaction using OEGMA as the monomers. (Bottom) The corresponding photo image of Au nanoparticle solution for the detection of 1 μM complementary DNA (B'D') (a) and the control experiment (b). The red-colored particle solution turned into a blue color, suggesting the aggregation of the particles.

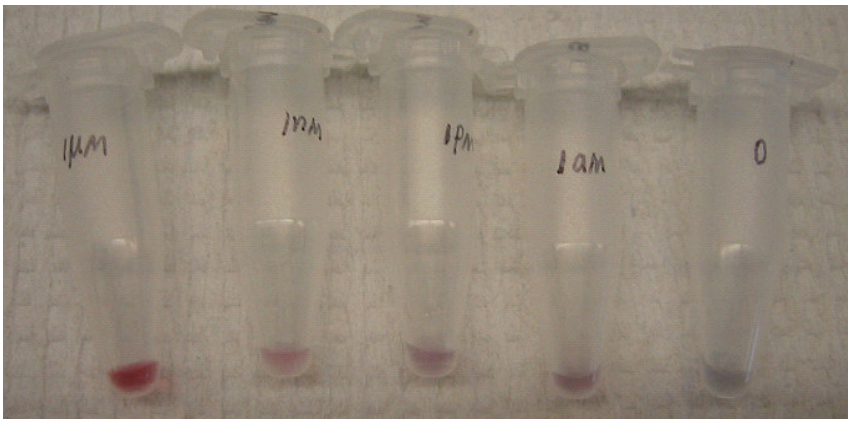

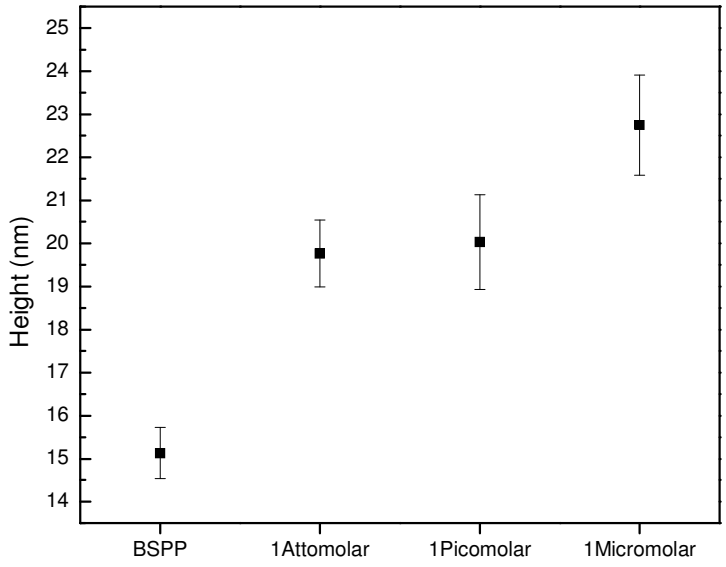

Figure 6.8 *Concept-proof in DNA sensing:* (Top)The photo image of the Au nanoparticle solutions for the detection of complementary DNA (0-1μM) after 1.5hr ATRP reaction using OEGMA as the monomers. The red-colored particle solution visibly turned into a blue color with the decreasing target DNA concentrations. (Bottom) AFM height measurements of Au particles. Detailed instrumental and experimental conditions were described in experimental section.

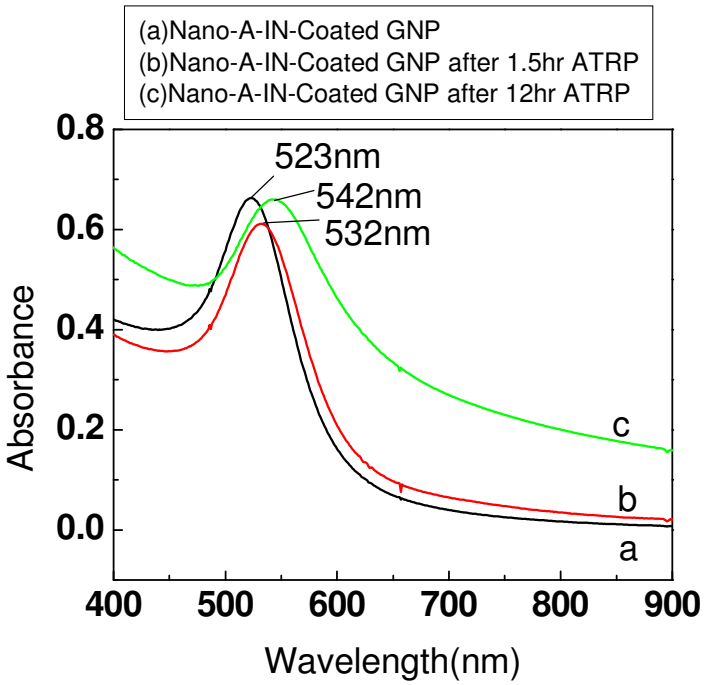

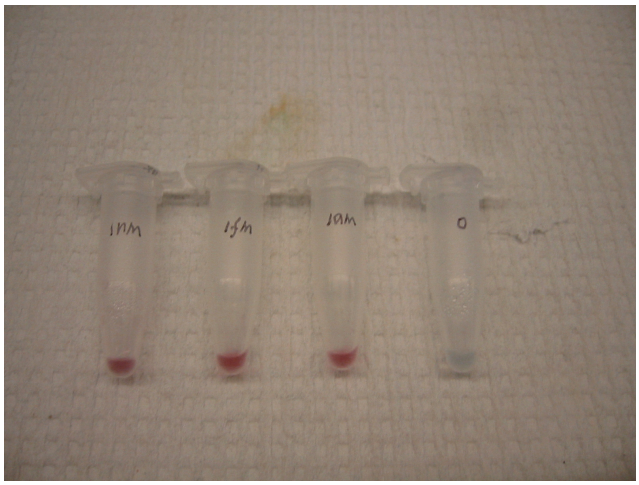

Figure 6.9 *DNA detection of increasing ATRP times* (Top) UV-vis spectra of Nano-A-IN-coated Au nanoparticles (a) in ATRP after a 1.5hr (b) and a 12hr (c) ATRP reaction using HEMA as the monomers. (Bottom) The photo image of the Au nanoparticle solutions for the detection of complementary DNA (0-1nM) after 2hr ATRP. The red-colored particle solution turned into a blue color, suggesting the aggregation of the particles.

References

(1) Mirkin, C. A.; Letsinger, R. L.; Mucic, R. C.; Storhoff, J. J. *Nature* **1996**, *382*, 607-609.
(2) Elghanian, R.; Storhoff, J. J.; Mucic, R. C.; Letsinger, R. L.; Mirkin, C. A. *Science* **1997**, *277*, 1078-1081.
(3) Tan, E.; Wong, J.; Nguyen, D.; Zhang, Y.; Erwin, B.; Van Ness, L. K.; Baker, S. M.; Galas, D. J.; Niemz, A. *Anal. Chem.* **2005**, *77*, 7984-7992.
(4) Storhoff, J. J.; Lucas, A. D.; Garimella, V.; Bao, Y. P.; Muller, U. R. *Nat. Biotechnol.* **2004**, *22*, 883-887.
(5) Li, H. X.; Rothberg, L. *Proc. Natl. Acad. Sci. U. S. A.* **2004**, *101*, 14036-14039.
(6) Kato, M.; Kamigaito, M.; Sawamoto, M.; Higashimura, T. *Macromolecules* **1995**, *28*, 1721-1723.
(7) Wang, J.-S.; Matyjaszewski, K. *Macromolecules* **1995**, *28*, 7572-7573.
(8) Patten, T. E.; Xia, J.; Abernathy, T.; Matyjaszewski, K. *Science* **1996**, *272*, 866-868.
(9) Pyun, J.; Matyjaszewski, K. *Chem. Mat.* **2001**, *13*, 3436-3448.
(10) Von Werne, T.; Patten, T. E. *J. Am. Chem. Soc.* **2001**, *123*, 7497-7505.
(11) Chen, X.; Armes, S. P. *Adv. Mater.* **2003**, *15*, 1558-1562.
(12) Bontempo, D.; Tirelli, N.; Masci, G.; Crescenzi, V.; Hubbell, J. A. *Macromol. Rapid Commun.* **2002**, *23*, 418-422.
(13) Kizhakkedathu, J. N.; Norris-Jones, R.; Brooks, D. E. *Macromolecules* **2004**, *37*, 734-743.
(14) Nuss, S.; Bottcher, H.; Wurm, H.; Hallensleben, M. L. *Angew. Chem. Int. Ed.* **2001**, *40*, 4016-4018.
(15) Ohno, K.; Koh, K.; Tsujii, Y.; Fukuda, T. *Macromolecules* **2002**, *35*, 8989-8993.
(16) Frens, G. *Nature-Physical Science* **1973**, *241*, 20-22.
(17) Schmid, G.; Lehnert, A. *Angew. Chem. Int. Edit. Engl.* **1989**, *28*, 780-781.
(18) Lou, X.; Lewis, M. S.; Gorman, C. B.; He, L. *Anal. Chem.* **2005**, *77*, 4698-4705.
(19) Storhoff, J. J.; Elghanian, R.; Mucic, R. C.; Mirkin, C. A.; Letsinger, R. L. *J. Am. Chem. Soc.* **1998**, *120*, 1959-1964.
(20) Parak, W. J.; Pellegrino, T.; Micheel, C. M.; Gerion, D.; Williams, S. C.; Alivisatos, A. P. *Nano Lett.* **2003**, *3*, 33-36.
(21) Zanchet, D.; Micheel, C. M.; Parak, W. J.; Gerion, D.; Alivisatos, A. P. *Nano Lett.* **2001**, *1*, 32-35.
(22) Sato, T.; Ruch, R. *Stabilization of Colloidal Dispersions by Polymer Adsorption*; Marcel Dekker: New York, 1980.
(23) Mangeney, C.; Ferrage, F.; Aujard, I.; Marchi-Artzner, V.; Jullien, L.; Ouari, O.; Rekai, E. D.; Laschewsky, A.; Vikholm, I.; Sadowski, J. W. *J. Am. Chem. Soc.* **2002**, *124*, 5811-5821.

CHAPTER 7 Comparison Between CNBr Chemial Ligation And T4 Enzymic Ligation

7.1 Introduction

Joining linear DNA fragments together with covalent bond is called DNA ligation. Specifically, DNA ligation is a process to create a phosphodiester bond between two DNA strands, which has been found to be an essential component of DNA repair[1], replication[2] and recombination.[3] *In vivo* DNA ligation is catalyzed by DNA ligases that carry out the covalent linkage of the 3'-hydroxyl and 5'-phosphate ends of DNA strands generated by different DNA processes. Typically, two types of ligation reactions occur at the presence of DNA ligases: connection of two double stranded DNA strands having blunt or compatible cohesive ends and linkage of two single stranded DNA at the nick position at the presence of template DNA. DNA ligases are found in all organisms, and divided into two general categories based on the cofactor required, ATP or NAD^+.[4,5] Despite the big differences in amino sequences, size and properties among those DNA ligases, all DNA ligases share a common three-step mechanism. **Scheme 7.1** is the three-step mechanism of DNA ligase catalyzed ligation at nick position. The first step is the formation of the covalent enzyme-adenylate intermediate through the transfer of an adenylyl group (AMP) from ATP or NAD to the amino group of a lysine residue in the enzyme. In the second step, the adenylyl group is transferred from the enzyme to the 5'-phosphate of the ssDNA substrate to activate the phosphate group. Finally, a phosphodiester bond is formed by nucleophilic attack of the 3'-hydroxyl group of the

other ssDNA substrate on the activated 5'phosphate group with the release of AMP at the same time.[4]

DNA ligases have been widely used in all fields of biotechnology including DNA point mutation detection assays, construction of novel nanostructures and DNA computing.[6-11] Landegren *et al* first used a ligase in a DNA sensing assay,[9,10] since then numerous ligase –mediated DNA detection assays, such as ligase chain reaction (LCR)[12] and ligase detection reaction (LDR),[13] have been developed.[11,14,15] The recent developments in ligase-mediated detection methods have been reviewed.[16] Most ligase-mediated DNA detection assays are based on the ability of two oligonucleotides to anneal together at the presence of a complementary target DNA molecule. The specificity of those ligase-mediated detection methods is attributed to the inherent specificity of ligases against the presence of mismatches in the ligation reaction. Among various ligases, T4 ligase has been most widely used to date due to its commercial availability, well documented scientific information available, and mild reaction conditions.

However, the relative low specificity of T4 DNA ligase just like most other ligases has been noticed for quite long time.[10,17-20] The mismatched nick sealings such as 3' and 5' A-A or T-T mismatches,[17] 5' G-T mismatches,[20] and 3' C-A, C-T, T-G, T-T, T-C, A-C, G-G or G-T mismatches[10] were reported. The fidelity of T4 DNA ligase may be improved in the presence of high NaCl concentration, spermidine, or low ligase concentrations, but the ligation of nicks with T-G or G-T mismatches are still unavoidable.[10,17]

In our previous DNA single base mismatch detection study (see Chapter 5), similar to what other researchers have observed, we have also observed the limited ligation specificity of T4 ligase on a gold surface. Only when salt stringency wash was conducted after hybridization and before T4 ligation to denature mismatched duplexes, would the ligation occur on the positions where perfect matched target DNA was present. Finding the suitable wash conditions including salt ionic strength, wash time and sometimes buffer temperature is quite time consuming. The suitable condition has to be tested from case to case since different DNA duplexes have quite different melting profiles.

In addition to optimizing ligation conditions, different ligation method such as using thermal stable ligases or chemical ligations could be used to improve ligation specificity. For example, Even though some ligases, such as thermal stable *Thermus thermophilus* ligases (T*th* DNA ligase), have much higher specificity compared to T4 ligases.[14] The ligation reactions are conducted under high temperature (e.g. 65°C) at which mismatched double strands wouldn't survive. However, the Au-S bonds between capture ssDNA probes and gold surface also might dissociate from the surface at elevated temperature. More importantly, higher ligation temperature requires a longer hybridization oligonucleotide length to acquire high ligation efficiency, which is not suitable for our system where the target DNA complementary oligonucleotide length is only 15bp for both anchor and detector.

Non-enzymatic methods of ligating DNA oligonucleotides with their wide applications in fabrication of nanostructures,[21-24] evolution of amplified small molecule

libraries[25-28] and DNA detection[29, 30] have been studied recently by several laboratories.[28, 29, 31-33] Most studies have been focused on exploring the feasibility of various chemical reactions for ligating modified oligonucleotides. Not limited to the phosphodiester bonds,[34] many types of bonds including pyrophosphates, phosphorothiolates,[31] phosphoroselenoates,[35] phosphoamides,[36] secondary amines,[37] amides,[38] salenes,[39] and metal complexes were formed between oligonucleotides through different types of reactions such as condensations, alkylations, cycloadditions and Wittig reactions.[25-27, 40]

Among those reactions, direct condensation between a hydroxyl group of one oligonucleotide and a phosphate group of another oligonucleotide using condensing reagents like EDC or cyanogens bromide is the most convenient technique of chemical ligation since no further modifications of oligonucleotides is needed and only bench top reaction conditions are required.[29,33] Major drawbacks of EDC condensation, however, are its slow reaction rate (several hours to several days) and relative low ligation efficiency compared to ligases. It was reported that when CNBr was used as condensing reagent, the ligation reaction was able to finish in a minute with quite high ligation efficiency and mismatch specificity.[34, 41]

Scheme 7.2 shows the reaction mechanism of CNBr chemical ligation.[42] First, CNBr reacts with 4-morpholineethane sulfonic acid to form the stable quaternary ammonium base in aqueous solution. Secondly, the phosphate group either at 5' or 3' ends of the DNA substrates was activated by the quaternary ammonium base, followed by the formation of phosphodiester bond by nucleophilic attack of the 5' or 3'-hydroxyl group of the other ssDNA substrate on the activated phosphate group.

This efficient ligation method is quite attractive for the applications in DNA sensing with the potencials in decreasing assay time and increase sensing specificity against mismatches. However, compared to T4 ligase, very little data has been reported about the sequence specificity of template-directed CNBr ligation reaction, which is a critical requirement for its applications in DNA detection. In addition, there is no direct comparison available between T4 ligation and CNBr ligation using same ssDNA stands and templates.

In this chapter, a systematic comparison of CNBr-assisted chemical ligation and T4 ligation was conducted. For both ligation methods, reaction conditions, such as temperature, pH, template length, and $MgCl_2$ concentration, ligase concentration, NaCl concentration as well as the number and position of mismatches in the templates, are optimized to achieve the best specificity of the reaction against mismatches and ligation yield. Under optimized conditions, CNBr ligation showed improved performance than T4 ligation in regard to the ligation specificity and efficiency. This chemical ligation method has been successfully used in ATRP-based DNA sensing assays (see Chapter 3).

7.2 Experimental Section

7.2.1 Materials

Dithiothreitol (DTT), triethylamine (TEA), bromoisobutyryl bromide, N-hydroxysuccinimide (NHS), PEG8000, 4-morpholine ethane sulfonic acid (MES), $MgCl_2$ and CNBr (5M in CH_3CN) were all purchased from Sigma-Aldrich (St. Louis, MO). T4 DNA ligase was purchased from Stratagene (La Jolla, CA) or Promega. All

oligonucleotides were purchased from Integrated DNA Technologies (Coralville, IA). The sequences of DNA used in this report are listed in **Table 7.1**. A NAP^{TM}-5 column from Amersham Pharmacia Biotech was used for DNA purification. C_{18}ZipTip^{TM} was purchased from Millipore for DNA desalting before MALDI measurements. All the chemicals for gel electrophoresis experiments including Urea, acrylamide (gel electrophoresis grade), N,N'-methylenebisacrylamide, tris base, EDTA, boric acid and ammonium persulfate were all purchased from Sigma-Aldrich or Fischer Scientific. SYBR® gold nucleic acid gel stain was purchased from Molecular Probes for single-stranded DNA detection in electrophoresis gel.

7.2.2 Initiator Coupling to Detection Probe (D)

Initiator-coupled DNA detection probe was prepared as previously described in Chapter 2. Briefly, 70μL of oligonucleotide **D** solution at 100μM and 10μL of 10 x conjugation buffer (1.0M $NaHCO_3/Na_2CO_3$, pH9.0) were added into a 1.5mL centrifuge tube, followed by the addition of freshly prepared bromoisobutyryl NHS ester solution (10mg/mL in DMF, 20μL). After 30min reaction at room temperature, unreacted NHS ester was removed by gel filtration. MALDI-TOF MS was used to monitor the coupling efficiency by measuring the amount of oligonucleotides before and after the coupling reaction.

7.2.3 T4 DNA Ligation

A typical T4 ligation was conducted by mixing 50pmole anchor oligonucleotide, 50pmole detector-IN, 50pmole of one of the templates (**Table 7.1**) and T4 ligase in 1 x ligation buffer with or without DTT in a final volume of 10μL. The incubation time was 2hr at room temperature and the T4 ligase from Stratagem was used if not otherwise mentioned. After ligation, the reaction was inactivated at 65°C for 10min.

7.2.4 CNBr Chemical Ligation

A typical CNBr ligation was conducted by mixing 50pmole anchor oligonucleotide, 50pmole detector-IN and 50pmole one of templates (**Table 7.1**) in 0.25M MES buffer at different pH values and different $MgCl_2$ concentrations in a final volume of 10μL containing 0.5M CNBr. The incubation time was 1min at 0°C if not otherwise mentioned. After ligation, the reaction was quenched by adding 200μL absolute ethanol. The reaction mixture was then dried in SpeedVac and the solid was redissolved in 10μL water.

7.2.5 Gel Electrophoresis Analysis of Ligation Products

4μL of the ligation reaction mixture of either T4 liation or CNBr ligation was loaded onto a 15% denaturing PAGE (10cm x 8cm x 0.8mm) with 1μL 10 x TBE, 1μL loading dye (phenol blue in formamide) and 4μL H_2O. The same amount of anchor DNA and detector DNA as used in the ligation reactions, without the template DNA, were loaded on the same gel for ligation yield calculations. The 20bp single stranded DNA

ladder was also loaded on the same gel to indicate the approximate molecular weight of the sample components. The running voltage was set as 200V. After the dye moved to the bottom of the gel, the gel was stained in 1 x SYBR ® gold nucleic acid gel stain in 1 x TBE for 15min. Gel images were scanned using KODAK gel logic 200 imaging system and the quantitative analyses of the images were done with KODAK 1D 3.6 Image Analysis Software. Specifically, the ligation product band, the anchor DNA band and the detector DNA band in each lane on the gel were selected manually as regions of interest (ROIs). Then the net intensities (the sum of the background-subtracted pixel values with the ROIs) of those ROIs were displayed in the ROI information windows. The yield of each ligation reaction was calculated by dividing the net intensity of the ligation product by the total net intensities of the ligation product, the anchor DNA and the detector DNA. The total net intensities of the standard anchor band and detector band on the same image were used for calculations in the case that anchor band (and/or detector band) overlapped with the template band. The standard deviations of all the values reported in this chapter are 2±5%. The specificity of matched against mismatched template was calculated by dividing the ligation efficiency at the presence of matched template by the ligation efficiency at the presence of mismatched template.

7.2.6 MALDI-TOF Mass Spectrometer Analysis of Ligation Products

A Voyager^{TM} DE-STR matrix-assisted laser desorption/ionization mass spectrometry (MALDI-MS) was used to characterize the ligation product. After gel electrophoresis separation, the ligation product band was cut off from the PAGE gel and

the piece of gel containing the ligation product was crushed into small pieces and incubated with water at 94°C for 15min, at -70°C for 15min and 94°C for another 2min. Then the gel pieces were centrifuged to the bottom of the centrifuge tube. The supernatant was concentrated in Speedvac and then analyzed by MALDI-TOF mass spectrometer. 35mg/mL 3-hydroxypicolinic acid (3-HPA) in 7mg/mL diammonium citrate and 10% acetonitrile in water was used as the MALDI matrix. Two-layer deposition method was used here: the first layer was 3-HPA matrix and the second layer was DNA sample. DNA solutions were desalted using C_{18}ZipTip^{TM} (Millipore). MALDI-MS was conducted under the following conditions: accelerating voltage 25kV, grid voltage 90%, positive mode detection, delay time 300ns, and 100 laser shots collected per spectrum.

7.3 Results and Discussions

7.3.1 Optimization of T4 ligation

Substrate DNA Design. Wallace *et al* reported the enhanced ligation specificity of T4 ligation at elevated temperature and high NaCl concentration (200mM). They also found that mismatch ligation had lower ligation efficiency when the mismatch occurred at the 5' side of the junction (refer to template) rather than at the 3'side of the junction.[17] This different ligation specificity was attributed to the fact that the single base mismatch on the shorter 5' DNA stand destabilized the duplex to a much greater extent than the mismatch on the longer 3' DNA strand. Another possible reason is that the enzyme has more stringent requirement for the 3' substrate than for the 5' substrate.[43] According to

literature reported results, we have designed the single mismatches either on the 3' side of the nick when two DNA substrates have the same length or on the shorter DNA substrates side (**Table 7.1**). The mismatch bases are printed in red and the nick positions are in green in the table.

Effect of DTT Concentration. DTT commonly exists in the T4 ligation buffer and enzyme storage to prevent the oxidization of enzyme. The final concentration of DTT in T4 ligation solution is in the range of 1-10mM for T4 enzymes purchased from various companies. DTT at millimolar concentrations is quite efficient to replace ssDNA probes attached on the gold surface through ligand exchange. For our ATRP-based DNA detection method both on surface and in solution, ssDNA probes all attached onto gold surface through Au-S interaction. We have observed significant loss of DNA probes after incubation with a gold surface with DTT containing buffers for 2hr at room temperature in surface plasmon resonance measurements. In order to minimize the loss of DNA probes on the surface during T4 ligation, it is necessary to minimize the DTT concentrations in the ligation reaction mixture and still keep acceptable enzyme activity at the same time. For this purpose, we conducted T4 ligation reactions at different DTT concentrations by using ligation buffer with and without DTT. Two different T4 ligases have been tested, one from Stratagene and another from Promega. The reaction conditions tested and ligation efficiencies are listed in **Table 7.2**. The experimental data showed that the ligation efficiencies were much lower at the decreased DTT concentrations for both ligases. However, the presence of 50μg/mL BSA or

12%PEG8000 significantly improved the ligation efficiencies (80.0% and 69.2%) and compensated the absence of 2mM DTT (55.3%). Longer incubation time did result in higher ligation efficiencies for both ligases, especially the one from Stratagene. However, longer incubation time can also cause more DNA probes on the gold surface to be replaced by DTT, which would eventually decrease the detection sensitivity. In addition, shorter ligation time is always preferred with aim to shorten the total array time. Therefore, a 2hr ligation using the buffer containing 1mM DTT, 12%PEG8000, and T4 ligase from Stratagene was used for the further studies. PEG8000 instead of BSA was chosen because PEG 8000 would cause less background noise in the repetitive ATRP amplification steps as described in Chapter 3.

MALDI-MS was used to confirm the formation of the correct ligation product (**Figure 7.1**). A mass charge ratio of 22145.6 was clearly observed, corresponding well to the calculated molecular weight of the ligation product- 22144.6. The peaks at m/z 11072.9 and m/z 7382.0 are the double and triple charged ions of the ligation products, respectively.

NaCl Concentration. The relaxed ligation specificity of T4 ligases is well known. The presence of 200mM NaCl has been found to improve the ligation efficiency up to 10 and 26 times when the mismatch located on the 5' and 3' side of the nick, respectively.[17] From our experimental results (**Figure 7.2**), the presence of 200mM NaCl did not improve the specificity of T4 ligation as expected with significant amount of ligation products formed when one mismatched or even three mismatched template was used.

Specifically, the specificity against T-C mismatch slightly increased from 1.05 to 1.08 and the specificity against three mismatches increased from 1.14 to 1.29 at the presence of 200mM NaCl. All the values were calculated according to the method described in experimental section.

Template Length. Theoretically, the shorter template should offer better specificity since the mismatch on the shorter template destabilizes the duplex more compared to the one on the longer template. For this reason, we have designed shorter complementary one and three mismatched templates. While the shorter templates significantly improved the ligation specificity of 3-mismatch from 1.29 to 8.73, it was still not sufficient to differentiate 1-mismatched ones with ligation specificity from 1.14 to 1.21 for T-C mismatch (**Figure 7.3)**.

Enzyme Concentration. Landegren *et al* have developed a ligase-mediated gene detection technique based on the enhanced specificity of T4 ligase at higher NaCl concentrations along with using less amount of ligase.[10] Here the NaCl concentration was kept at 200mM and the amount of T4 ligase decreased from 1U to 50mU or 5mU per 10μL reaction. The results demonstrated that lower ligase concentrations combined with high NaCl concentration offered better specificities. The ligation specificity against T-C mismatch was enhanced from 1.14 at the presence of 1U ligase, to 1.79 at the presence of 50mU ligase, and to 2.87 at the presence of 5mU ligase. The ligation specificity against T-G mismatch was enhanced from 1.00 at the presence of 50mU ligase to 1.82 at the

presence of 5mU ligase (**Figure 7.4**). But the ligation specificity was still considered low for some stable mismatched templates such as T-G mismatch. In addition, low ligase concentrations disfavor all ligation reactions kinetically no matter what templates were used.

In conclusion, the specificity of T4 ligation was improved to a limited level under optimized conditions, using higher NaCl concentrations (200mM), lower ligase concentrations (5mU) and shorter templates (23bp). The ligation specificity against T-G mismatch still remained low, resulting in a significant amount of ligation product formed. The optimized conditions for T4 liagase to achieve the highest specificity are: 5mU ligase for 10μL reaction, 200mM NaCl, 2hr reaction at 37°C. With ligation efficiency at the presence of matched template 43%, the best specificities achieved for T-C mismatch and T-G mismatch were 2.87 and 1.79, respectively. In order to achieve higher ligation specificity and higher ligation efficiency, it is necessary to utilize other ligation methods with higher specificity.

7.3.2 Optimization of CNBr Chemical Ligation

T4 ligation provided only very limited ligation specificity to differentiate single base mismatched templates according to our experimental data. CNBr chemical ligation was tested here to see if better ligation specificity could be achieved in comparing to the T4 ligation. It has been reported that the efficiency and the specificity of the CNBr activated ligation reaction are also closely related to reaction conditions, such as buffer, $MgCl_2$ concentration, pH value and temperature when a linear template was used.[41] Here

the CNBr ligation system was optimized by varying temperature, buffer pH and $MgCl_2$ concentration.

Comparison of Ligation Efficiency at 0°C and 25°C. Temperature plays an important role in reagent stability, reaction kinetics and equilibrium. Selvasekaran *et al* reported a totally opposite effect of temperature on the ligation efficiencies at the presence of linear and circular DNA template. Specifically, lower ligation efficiency was observed at the presence of linear template when the temperature was increased from 4°C to 15°C. The reversed trend was observed at the presence of circular DNA template.[41] The phenomena could result from the combinational effects of several factors that are closely related with the reaction temperatures. Firstly, temperature affects the hybridization efficiency, or binding between the substrate and the template, especially for shorter templates. Lower reaction temperature favors the hybridization between the substrate and the template, which leads to a higher ligation yield. Secondly, temperature has a direct influence on the equilibrium of the ligation reaction. Lower temperature thermodynamically disfavors the formation of the ligation product. Thirdly, lower temperature kinetically disfavors the ligation reaction. In addition, higher temperature might also speed up the degradation of CNBr and disfavor the ligation reaction. Considering the extremely high reaction rate of CNBr ligation reaction (reaction is usually finished within 1min), the third factor will not seriously effect the ligation efficiency that much. Based on the facts that CNBr was in excess by a factor of 10^5 and the reaction time was limited in 1min, the degradation of CNBr could be ignored. When the templates are circular DNAs, the effect of the first

factor is weak since the binding between the circular templates and the substrates keeps strong at the increased temperature. As the result, the second factor is dominant and higher ligation efficiency is expected at higher temperature. Together, the final ligation yield is expected to be determined by the first factor for our ligation system, where the templates are short linear DNAs, leading to the decreased ligation efficiency at higher temperature.

The speculation was confirmed in **Figure 7.5**. Similar to Selvasekaran and his coworkers' observation, slightly higher ligation efficiency at 0°C than that at 25°C was observed. This is likely due to reduced hybridization efficiency of the complementary oligonucleotides at 25°C since Tm for the anchor-template complementary region is only 18°C in the 1x ligation buffer. At 0°C the percentage yield at the presence of the complementary template was around 44.9% similar to that achieved by T4 ligase (43%, see **Figure 7.4**) and the ligation specificity against T-C mismatch was about 9.0, which is much higher than the optimized specificity of T4 ligation (2.87, see **Figure 7.4**).

The Effect of $MgCl_2$ Concentration. Salt ionic strength strongly affects the stability of the duplex. It is well known that higher salt concentration increases the stability of both matched and mismatched duplexes. As shown in **Figure 7.6**, at 200mM $MgCl_2$, the ligation efficiency significantly increased to 85% at the presence of matched template, but the specificity against T-C mismatch dropped to approximately 1.2 at the same time. Conversely, at absence of $MgCl_2$ the ligation efficiency decreased to 25% at the present

of matched template. The optimized $MgCl_2$ concentration for both ligation efficiency and specificity was found to be 20mM.

The Effect of pH value of the buffer. It is anticipated that lower pH would result in optimal substrate/template binding to offer higher yield. As shown in **Figure 7.7**, the yield of ligation and the specificity against single mismatches were decreased at pH8.0, compared to those at pH7.5. This phenomenon might come from the fact that CNBr is unstable at the high pH where it reacts quickly with hydroxide ions in solution.

The Effect of Template length. The length of the templates also affects the specificity of the CNBr ligation reactions like T4 ligation. **Figure 7.8** demonstrated a significantly increased specificity at the presence of 23bp templates compared to 30bp templates. Specifically, the specificity against T-C mismatch and T-G mismatch was increased from 8.9 to 31.3 and from 4.5 to 12.5, respectively.

The Effect of Nick Position. CNBr ligation has shown much better ligation specificity than T4 ligation, but the ligation efficiency of CNBr ligation is still not satisfactory when 5' phosphate group and 3' hydroxyl group are present at the nick positions. It has been found that CNBr can even more effectively ligate a nick with 5' hydroxyl group and 3' phosphate group.[34] The higher reactivity of primary hydroxyl group than the secondary hydroxyl group to attack positive charged phosphate center is the major reason of the higher ligation efficiency. A simple comparative experiment was conducted using CNBr to ligate two types of nicks: one with 5' hydroxyl group and 3' phosphate group and the

other with 3' hydroxyl group and 5' phosphate group. As shown in **Figure 7.9**, the ligation efficiency of the nicks with 5' hydroxyl group and 3' phosphate group was 97.3% at the presence of complementary template, which was 3.9 times higher than the ligation efficiency of the nicks with 3' hydroxyl group and 5' phosphate group under the same reaction conditions. The ligation specificity of the nick ligation with 5' hydroxyl group was 3.5, which is similar to the specificity of the nick ligation with 5' phosphate group (3.3). Since this comparative experiment was not conducted under optimized conditions (pH 8.0 for this experiment), a better ligation specificity is expected according to the data shown in **Figure 7.7**.

In conclusion, the data demonstrated that CNBr chemical ligation had higher specificity and ligation efficiency compared to T4 ligase under optimized conditions.

7.4 Conclusions

T4 ligation and CNBr chemical ligation have been optimized respectively using the same ssDNA substrates and templates as those used in ATRP-based DNA detection experiments in Chapter 2. The effects of DTT concentration, salt and ligase amount have been examined in T4 ligation. The optimal specificity against T-C mismatch was 2.87 at 200mM NaCl, 5mU/10μL ligase for 2hr reaction at room temperature. In parallel, the effects of temperature, pH, salt, template length and functional group were examined in CNBr ligation. The optimal specificity against T-C mismatch was 31.3 at pH 7.5, 0°C, in 0.25M MES buffer containing 20mM $MgCl_2$ and 23bp templates for 1min reaction. The ligation efficiency was significantly improved to 97% at the presence of matched

template when the DNA fragments are with 5’ hydroxyl group and 3’ phosphate group at the nick position, without the loss of the specificity at the same time. With the demonstrated fast reaction, high specificity and ligation yield, CNBr chemical ligation showed great potential applications in ligation-based DNA detection methods.

Scheme 7.1: T4 Ligation Mechanism.[4]

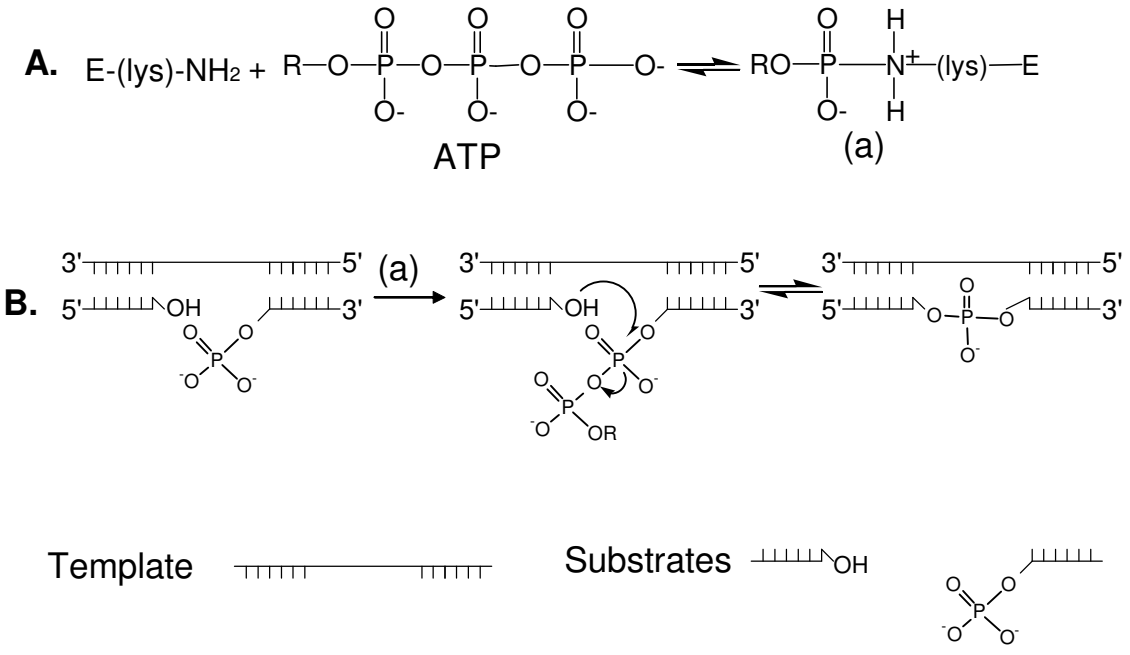

Scheme 7.2: CNBr Ligation Mechanism.

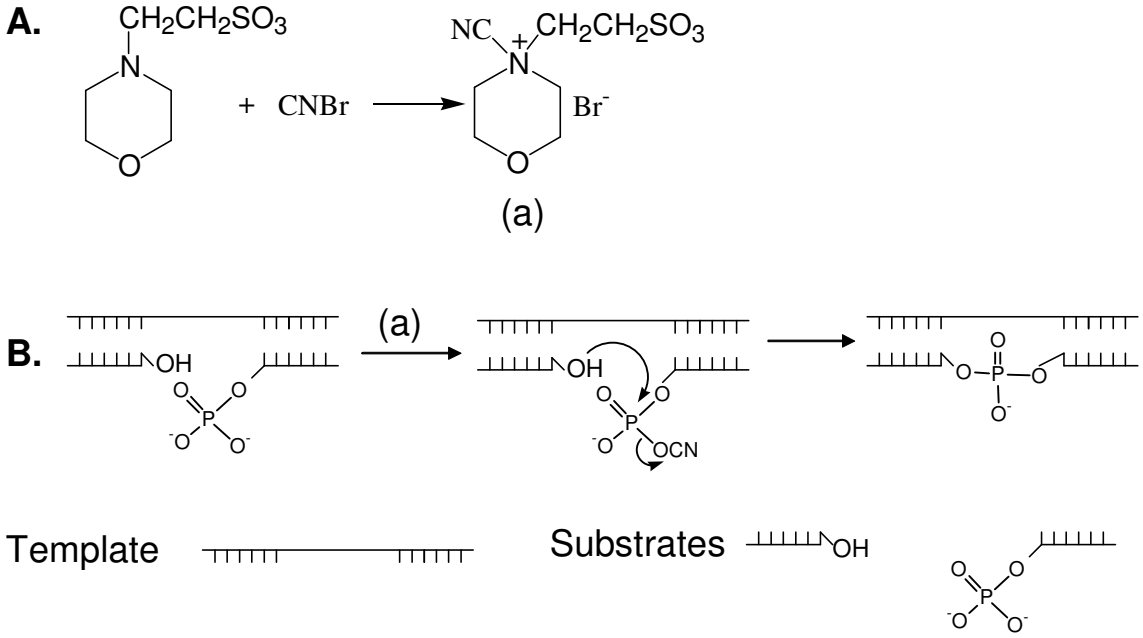

Table 7.1 Oligonucleotides Used in This Report.

Oligonucleotide	Sequence	Size(bp)
Anchor	5'Phos-TAA CAA TAA TCC CTC A_{20}-C_3-S-S-C_3	35
Anchor-5'OH	5'TAA CAA TAA TCC CTC A_{20}	35
Detector	5'NH_2-C_6-A_{18} AAA TCC TTA TCA ATA TT	35
Detector-IN	5'Br$(CH_3)_2$CCONH -C_6-A_{21} TCC TTA TCA ATA TT	35
Detector-3'Phos	5'A_{18} AAA TCC TTA TCA ATA TT-Phos	35
Template (30)	5'GAG GGA TTA TTG TTA AAT ATT GAT AAG GAT	30
Template (30)-1C	5'GAG GGA TTA TTG TTA CAT ATT GAT AAG GAT	30
Template (30)-1G	5'GAG GGA TTA TTG TTA GAT ATT GAT AAG GAT	30
Template (30)-3	5'GAG GGA AAG TTG TTA AAT ATT GAT AAG GAT	30
Template (23)	5'TA TTG TTA AAT ATT GAT AAG GAT	23
Template (23)-1C	5'TA TTG TTC AAT ATT GAT AAG GAT	23
Template (23)-3	5'TA AGC TTA AAT ATT GAT AAG GAT	23

Table 7.2 The Effect of DTT Concentrations on Ligation Efficiency.

T4 Ligase	DTT Final Con.(mM)	BSA(μg/mL)	PEG8000(%)	Incubation Time/Temp	Ligation Yield(%)
Strategen	1	0	0	2h, rt	31.4
Strategen	2	0	0	2h, rt	55.3
Strategen	2	0	0	Overnight,4°C	83.1
Strategen	1	50	0	2h, rt	80.0
Strategen	1	0	12	2h, rt	69.2
Promega	0.1	0	0	2h, rt	36.9
Promega	10	0	0	2h, rt	53.6
Promega	10	0	0	Overnight,4°C	62.4

rt: room temperature.

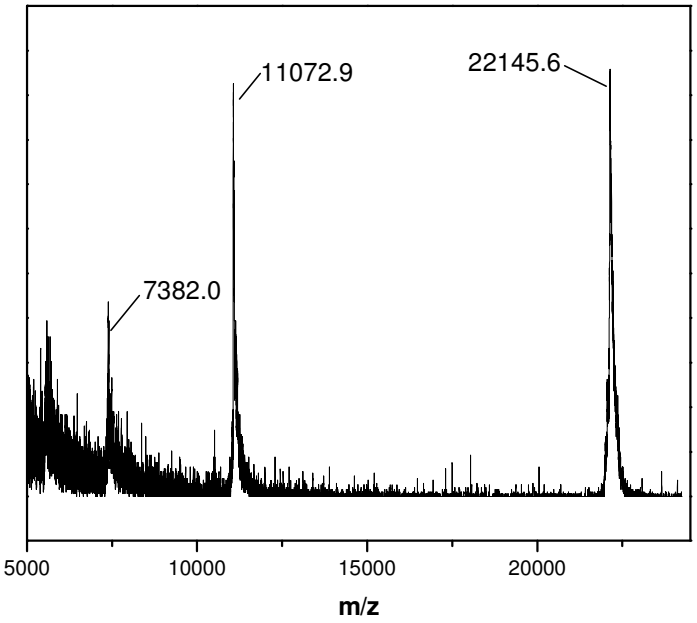

Figure 7.1 MALDI-TOF mass spectrum of T4 ligation product.

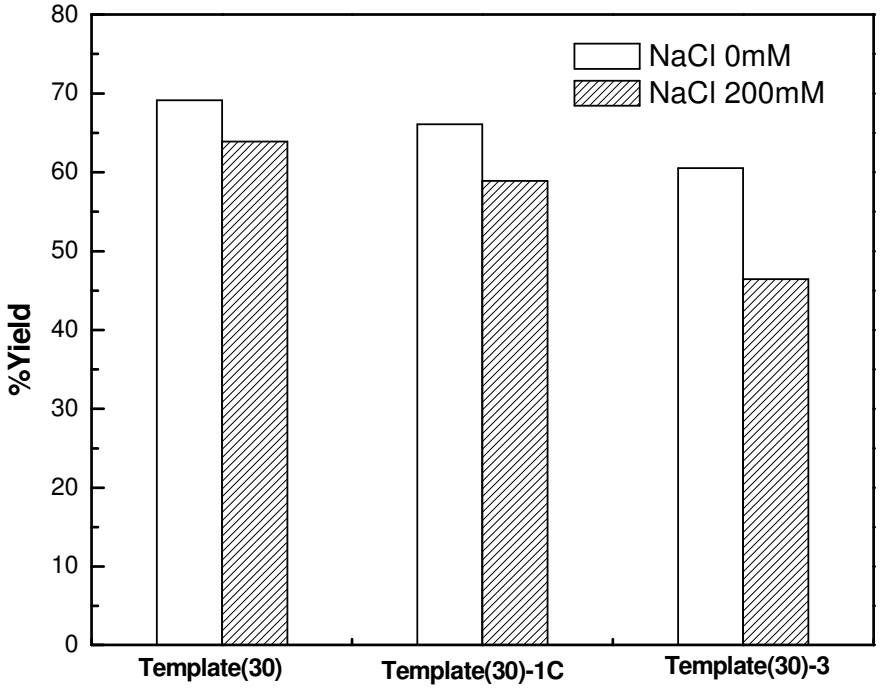

Figure 7.2 Effect of NaCl on T4 ligation efficiency. All the reactions contained 12%PEG8000.

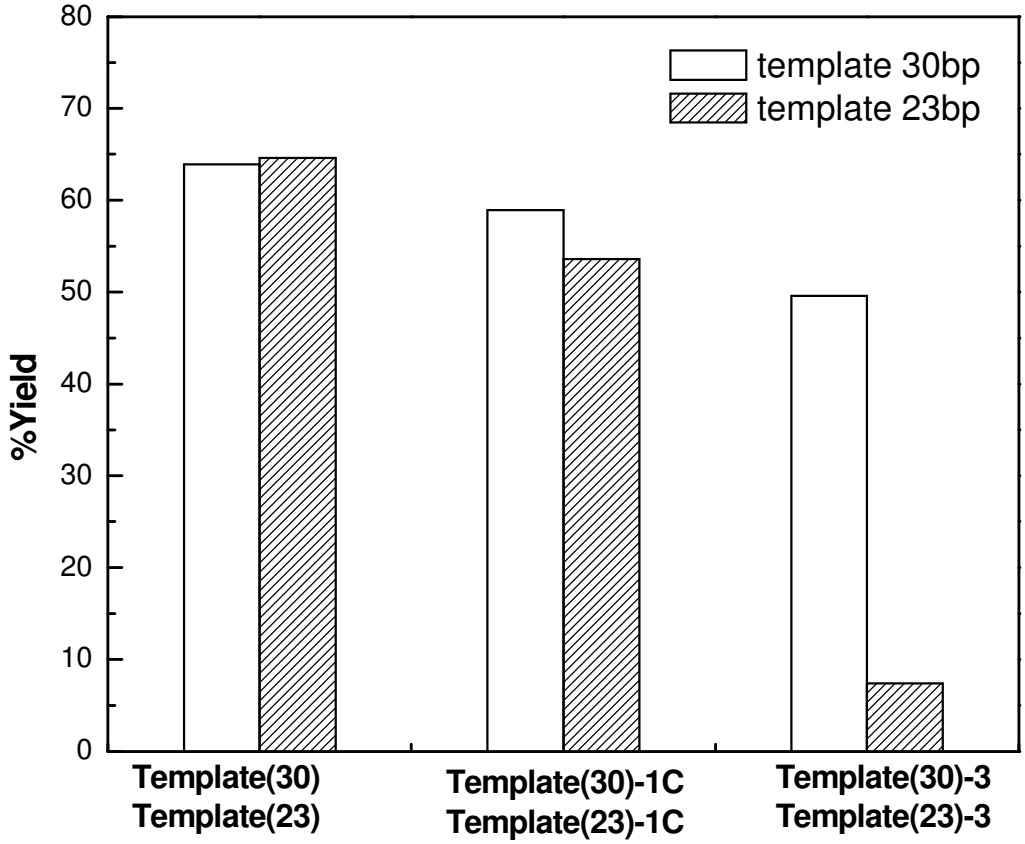

Figure 7.3 Effect of template length on T4 ligation efficiency. All reactions contained 200mM NaCl.

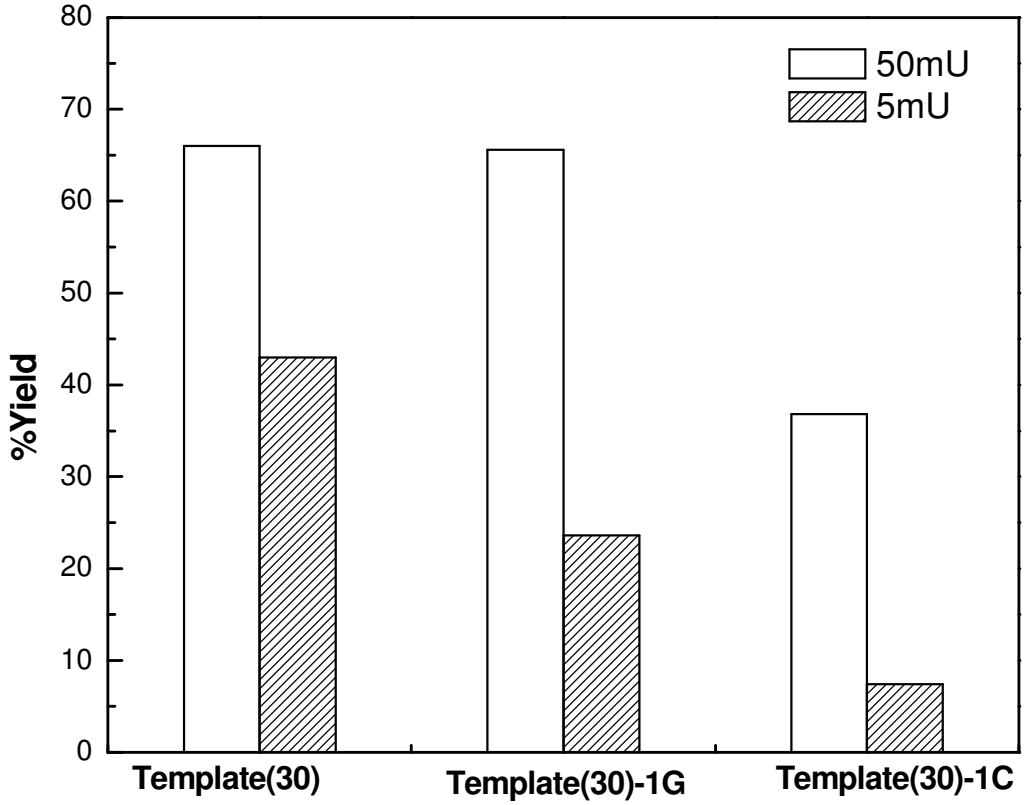

Figure 7.4 Effect of the amount of T4 ligase on T4 ligation efficiency. All reaction mixtures contained 200mM NaCl and 12%PEG8000 and were incubated at37º for 2hr.

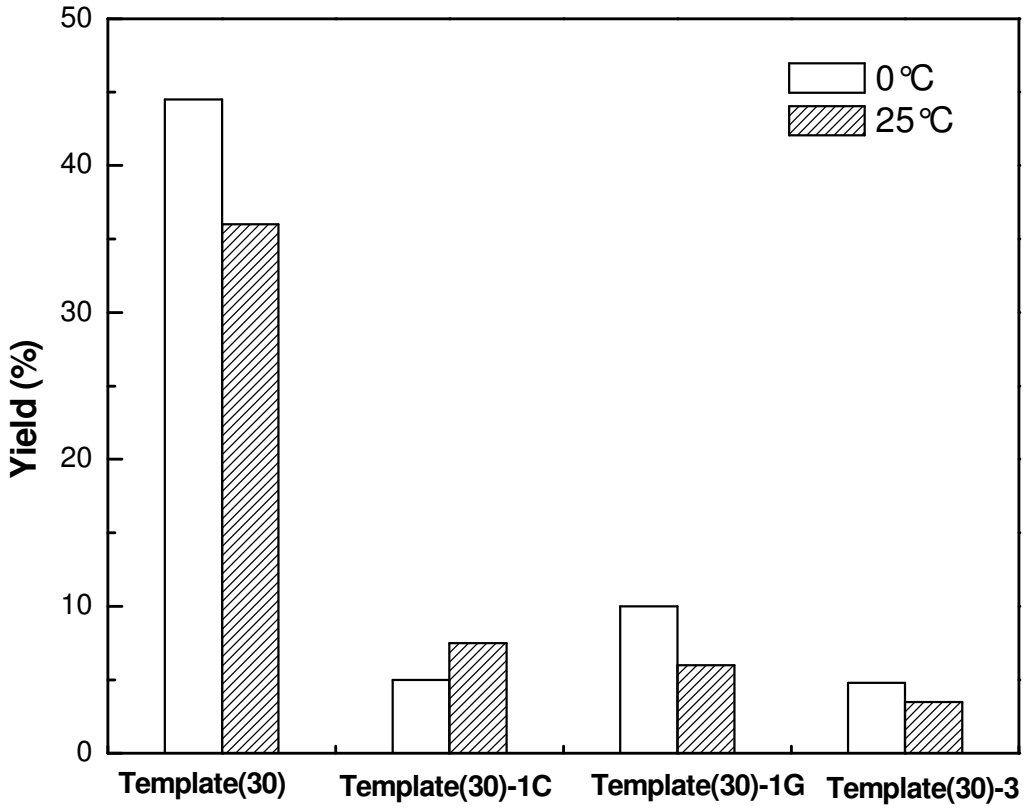

Figure 7.5 CNBr chemical ligation at 0°C and 25°C. Reactions were conducted in 0.25M MES, 20mM $MgCl_2$buffer at pH7.5, 1min.

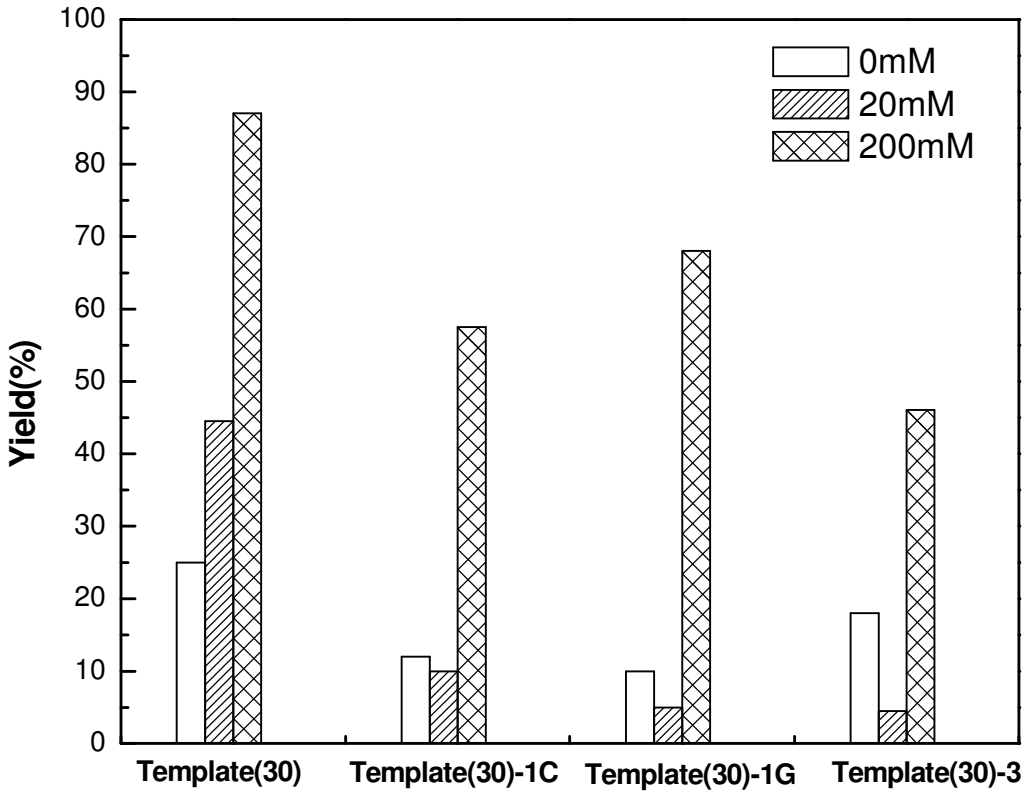

Figure 7.6 CNBr chemical ligation at different $MgCl_2$ concentrations. Reactions were conducted in 0.25M MES buffer at pH7.5, 1min at 0°C.

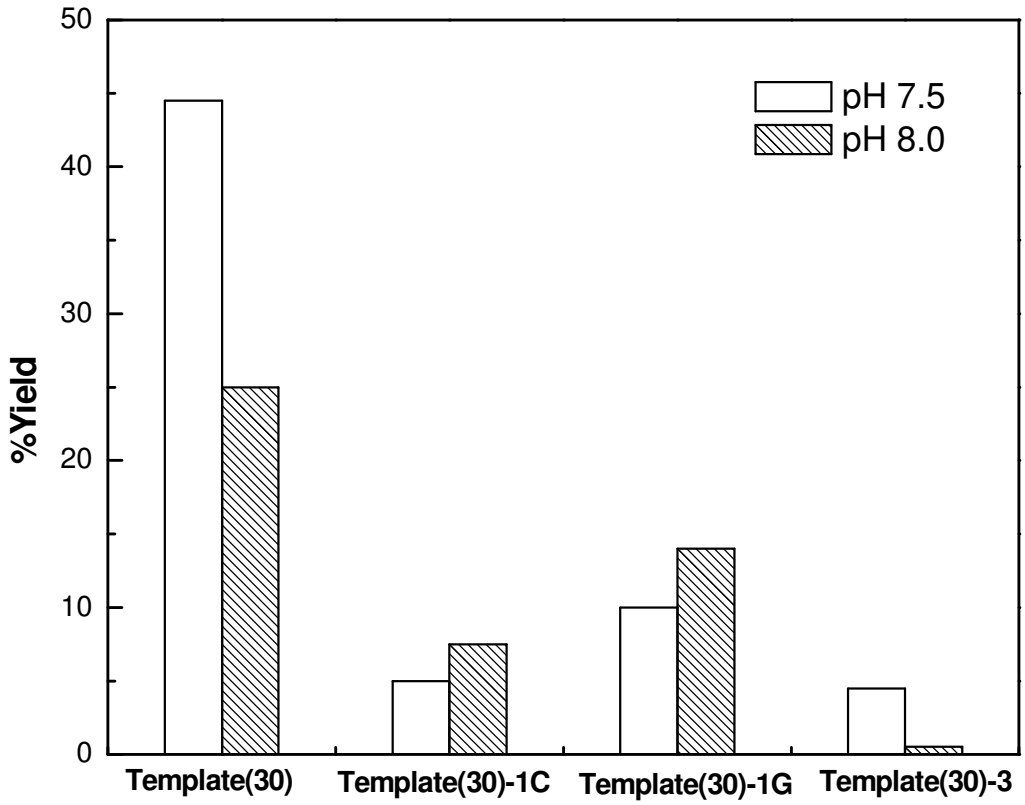

Figure 7.7 CNBr chemical ligation at different buffer pH. Reactions were conducted in 0.25M MES buffer (20mM $MgCl_2$), 1min at 0°C.

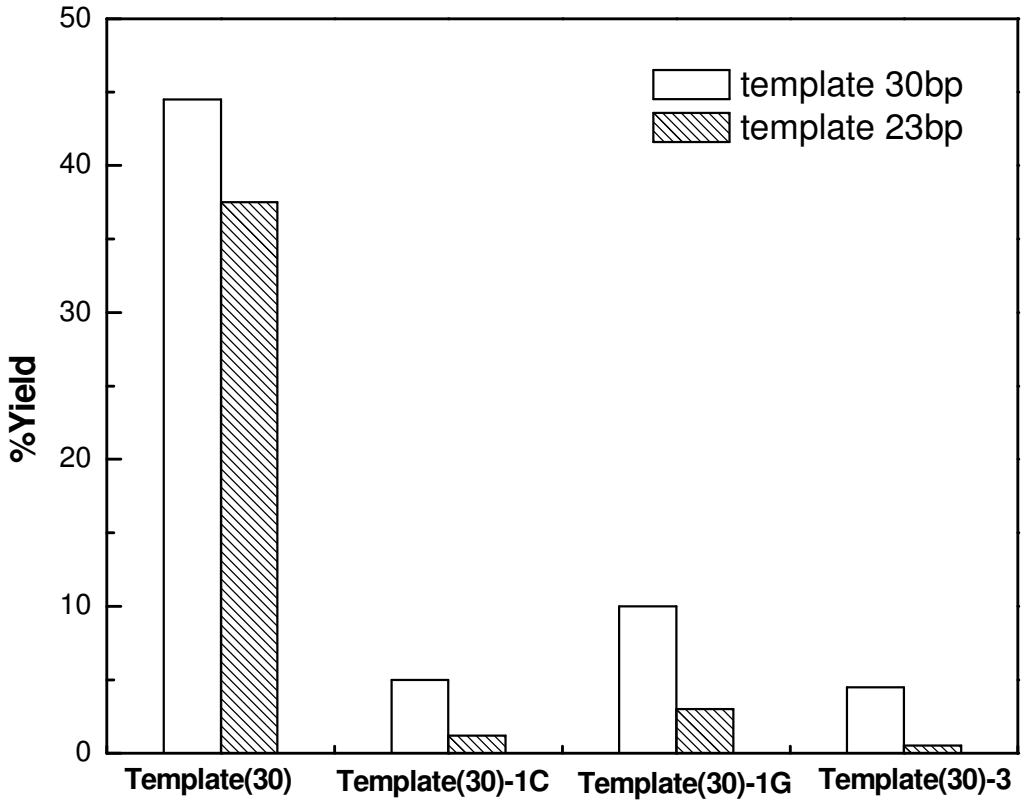

Figure 7.8 CNBr chemical ligation at the presence of templates with different lengths. Reactions were conducted in 0.25M MES buffer (20mM $MgCl_2$), pH7.5, 1min at 0°C.

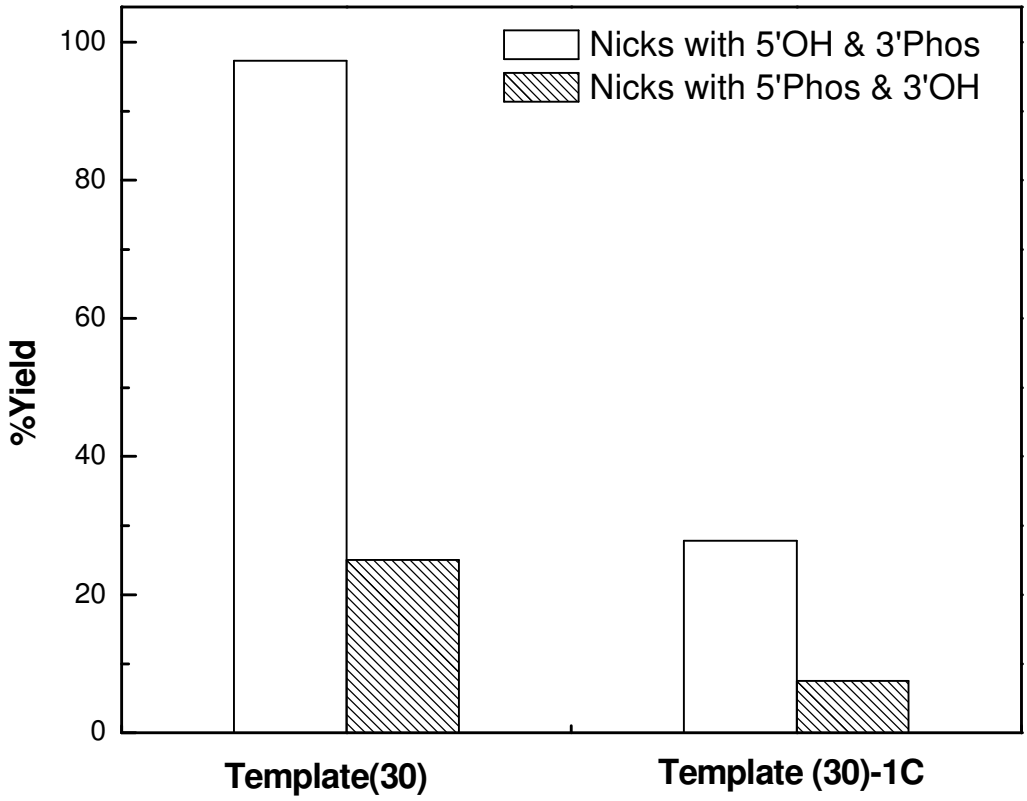

Figure 7.9 CNBr chemical ligation at different types of nicks. Reactions were conducted in 0.25M MES buffer (20mM $MgCl_2$) at pH8.0, 1min at 0°C.

References

(1) Gellert, M. *Proc. Natl. Acad. Sci. U. S. A.* **1967**, *57*, 148-155.
(2) Okazaki, R.; Okazaki, T.; Sakabe, K.; Sugimoto, K.; Sugino, A. *Proc. Natl. Acad. Sci. U. S. A.* **1968**, *59*, 598-601.
(3) Meselson, M.; Weigle, J. J. *Proc. Natl. Acad. Sci. U. S. A.* **1961**, *47*, 857-862.
(4) Lehman, I. R. *Science* **1974**, *186*, 790-797.
(5) Doherty, A. J.; Suh, S. W. *Nucleic Acids Res.* **2000**, *28*, 4051-4058.
(6) Frutos, A. G.; Smith, L. M.; Corn, R. M. *J. Am. Chem. Soc.* **1998**, *120*, 10277-10282.
(7) Braun, E.; Eichen, Y.; Sivan, U.; Ben-Yoseph, G. *Nature* **1998**, *391*, 775-778.
(8) Kim, J. H.; Hong, J. A.; Yoon, M.; Yoon, M. Y.; Jeong, H. S.; Hwang, H. J. *J. Biotechnol.* **2002**, *96*, 213-221.
(9) Nickerson, D. A.; Kaiser, R.; Lappin, S.; Stewart, J.; Hood, L.; Landegren, U. *Proc. Natl. Acad. Sci. U. S. A.* **1990**, *87*, 8923-8927.
(10) Landegren, U.; Kaiser, R.; Sanders, J.; Hood, L. *Science* **1988**, *241*, 1077-1080.
(11) Zhong, X. B.; Reynolds, R.; Kidd, J. R.; Kidd, K. K.; Jenison, R.; Marlar, R. A.; Ward, D. C. *Proc Natl Acad Sci U S A* **2003**, *100*, 11559-11564.
(12) Barany, F. *Proc. Natl. Acad. Sci. U. S. A.* **1991**, *88*, 189-193.
(13) Barany, F.; Gelfand, D. H. *Gene* **1991**, *109*, 1-11.
(14) Luo, j.; Bergstrom, D. E.; Barany, F. *Nucleic Acids Res.* **1996**, *24*, 3071-3078.
(15) Gunderson, K. L.; Huang, X. H. C.; Morris, M. S.; Lipshutz, R. J.; Lockhart, D. J.; Chee, M. S. *Genom. Res.* **1998**, *8*, 1142-1153.
(16) Cao, W. *Trends Biotechnol.* **2004**, *22*, 38-44.
(17) Wu, D. Y.; wallace, B. R. *Gene.* **1989**, *76*, 245-254.
(18) Shuman, S. *Biochemistry* **1995**, *34*, 16138-16147.
(19) Husain, I.; Tomkinson, A. E.; Burkhart, W. A.; Moyer, M. B.; Ramos, W.; Mackey, Z. B.; Besterman, J. M.; Chen, J. W. *J. Biol. Chem.* **1995**, *270*, 9683-9690.
(20) Harada, K.; Orgel, L. E. *Nucleic Acids Res.* **1993**, *21*, 2287-2291.
(21) von Kiedrowski, G.; Eckardt, L. H.; Naumann, K.; Pankau, W. M.; Reimold, M.; Rein, M. *Pure Appl. Chem.* **2003**, *75*, 609-619.
(22) Lovrinovic, M.; Seidel, R.; Wacker, R.; Schroeder, H.; Seitz, O.; Engelhard, M.; Goody, R. S.; Niemeyer, C. M. *Chem. Commun.* **2003**, 822-823.
(23) Winssinger, N.; Harris, J. L.; Backes, B. J.; Schultz, P. G. *Angew. Chem. Int. Ed.* **2001**, *40*, 3152-3155.
(24) Gothelf, K. V.; Thomsen, A.; Nielsen, M.; Clo, E.; Brown, R. S. *J. Am. Chem. Soc.* **2004**, *126*, 1044-1046.
(25) Gartner, Z. J.; Kanan, M. W.; Liu, D. R. *Angew. Chem. Int. Ed.* **2002**, *41*, 1796-1800.
(26) Gartner, Z. J.; Kanan, M. W.; Liu, D. R. *J. Am. Chem. Soc.* **2002**, *124*, 10304-10306.
(27) Gartner, Z. J.; Liu, D. R. *J. Am. Chem. Soc.* **2001**, *123*, 6961-6963.

(28) Gartner, Z. J.; Tse, B. N.; Grubina, R.; Doyon, J. B.; Snyder, T. M.; Liu, D. R. *Science* **2004**, *305*, 1601-1605.
(29) Ficht, S.; Mattes, A.; Seitz, O. *J. Am. Chem. Soc.* **2004**, *126*, 9970-9981.
(30) Xu, Y. Z.; Karalkar, N. B.; Kool, E. T. *Nat. Biotechnol.* **2001**, *19*, 148-152.
(31) Xu, Y. Z.; Kool, E. T. *Tetrahedron Lett.* **1997**, *38*, 5595-5598.
(32) Gryaznov, S. M. *Nucleosides & Nucleotides* **1995**, *14*, 1019-1022.
(33) Carriero, S.; Damha, M. J. *J. Org. Chem.* **2003**, *68*, 8328-8338.
(34) Sokolova, N. I.; Ashirbekova, D. T.; Dolinnaya, N. G.; Shabarova, Z. A. *FEBS Lett.* **1988**, *232*, 153-155.
(35) Xu, Y. Z.; Kool, E. T. *J. Am. Chem. Soc.* **2000**, *122*, 9040-9041.
(36) Dolinnaya, N. G.; Sokolova, N. I.; Gryaznova, O. I.; Shabarova, Z. A. *Nucleic Acids Res.* **1988**, *16*, 3721-3738.
(37) Li, Z. Y.; Zhang, Z. Y. J.; Knipe, R.; Lynn, D. G. *J. Am. Chem. Soc.* **2002**, *124*, 746-747.
(38) Koppitz, M.; Nielsen, P. E.; Orgel, L. E. *J. Am. Chem. Soc.* **1998**, *120*, 4563-4569.
(39) Czlapinski, J. L.; Sheppard, T. L. *J. Am. Chem. Soc.* **2001**, *123*, 8618-8619.
(40) Fujimoto, K.; Matsuda, S.; Takahashi, N.; Saito, I. *J. Am. Chem. Soc.* **2000**, *122*, 5646-5647.
(41) Selvasekaran, J.; Turnbull, K. D. *Nucleic Acids Res.* **1999**, *27*, 624-627.
(42) Shabarova, Z. A.; Fedorova, O. A.; Dolinnaya, N. G.; Gottikh, M. B. *Orig. Life Evol. Biosph.* **1997**, *27*, 555-566.
(43) Olivera, B. M.; Lehman, I. R. *J. Mol. Biol.* **1968**, *36*, 261-266.